Aeroelastic stability analysis and certification of wind turbine blades

by
Panagiotis N. Schinas
A Thesis Submitted to the Graduate Faculty of
NATIONAL TECHNICAL UNIVERSITY of ATHENS
in Partial Fulfillment of the
Requirements for the degree of
DOCTOR OF PHILOSOPHY
Major Subject: Wind Energy

Approved by the
Examining Committee:

Bouris Demetri__________________
Member
Papadakis George ________________
Member
Philippidis Theodoros _____________
Member
Riziotis Vasilios __________________
Member
Saravanos Dimitris ________________
Member
Spiliopoulos Konstantinos __________
Member
Voutsinas Spyros_________________
Thesis Adviser

NATIONAL TECHNICAL UNIVERSITY of ATHENS

January, 2022

CONTENTS

LIST OF TABLES

LIST OF FIGURES

Abbreviations

a.o.a.		Angle of Attack
Btsp	:	Bootstrap method
CDF	:	Cumulative distribution Function
CoV		Coefficient of Variation
DOFs	:	Degrees of Freedom to the global coordinate's system
FRP	:	Fiber reinforced plastics
FTM	:	Floquet's transition matrix
GM	:	global maxima peak method
K-S	:	Kolmogorov-Smirnov test
LN	:	Lognormal distribution
ML	:	Maximum Likelihood method
N	:	Standard normal distribution
POT	:	Peak over threshold method
RefMP		Reference Material Properties
StoMP		Stochastic Material Properties
STD		standard deviation
W/T		Wind Turbine
2pW	:	Weibull distribution with 2 parameters
3pW	:	3 parameter Weibull distribution

Nomenclature for wind turbine composite material properties

E_1 : Tensile modulus of elasticity parallel to composite fibers

E_2 : Tensile modulus of elasticity transverse to the fibers

G_{12} : In-plane shear modulus of elasticity

v_{12} : Major Poisson ratio

v_{21} : Minor Poisson ratio

Nomenclature for wind turbine certification

I : Turbulence intensity

I_{ref} : Expected value (reference) of turbulence intensity at 15 m/s at the hub height

V_{bin} : Wind speed bin

V_{ave} : Scale parameter of V_{hub} for the Rayleigh distribution

V_{ref} : Reference wind speed average over 10 min at the hub height

V_{hub} : 10 min mean wind speed at the hub height

V_{rated} : Rated 10 min mean wind speed

Nomenclature for ROM (Reduced Order Model) (Latin)

a, a' : Induction coefficients

$C_{L0}(r)$: Lift coefficient

∂C_{L0} : Slope of lift coefficient

$C_{D0}(r)$: Drag coefficient

∂C_{D0} : Slope of drag coefficient

$C_{M0}(r)$: Moment coefficient

∂C_{M0} : Slope of moment coefficient

C : Damping matrix of the structural part

F : Vector of flap and edge forces with respect to the global system coordinates

$H_{fltower}$: Distance from floater to the beginning of tower (m)

H_{towALL} : Height of the tower (m)

H_{shaft} : Length of the shaft (m)

H_{offset} : Offset of center of hub to the center of nacelle mass (m)

H_{hub} : Distance of hub to blade (m)

I_{ni} : 2nd Moment of inertia of the nacelle to the tilt direction ($kg.m^2$)

I_{shaft} : 2nd Moment of inertia of the shaft ($kg.m^2$)

J_k : Integer factor of the imaginary part for each mode

K : Stiffness matrix of the structural part

K_{aer} : Additional stiffness matrix from linearization of the aerodynamic loads

K_β : Stiffness of the blade to the flapwise direction (Nm/rad)

K_ξ : Stiffness of the blade to the edgewise direction (Nm/rad)

K_{sh} : Stiffness of the shaft (Nm/rad)

K_f : Stiffness of the tower for the for – aft motion (Nm/rad)

K_l : Stiffness of the tower for the lateral motion (Nm/rad)

K_t : Stiffness of the nacelle for the tilt motion (Nm/rad)

K_{yaw} : Stiffness of the nacelle for the yaw motion (Nm/rad)

K_{tl} : Stiffness of the nacelle for the tilt lateral motion (Nm/rad)

local_dofs_wu : Degree of freedom, to the local blade element coordinates system

M : Mass matrix of the structural part

M_{aer} : Additional mass matrix from linearization of the aerodynamic loads

M_{blade} : Mass of the blade (kg)

M_{nac} : Mass of the nacelle (kg)

M_{flap} : Moment of forces to flapwise direction

M_{edge} : Moment of forces to edgewise direction

M_{tow} : Mass of tower (kg)

M_{hub} : Mass of hub (kg)

Q : Forces, contain gravity, buoyancy and the aerodynamic part

Q_j : Generalized loads corresponding to the external loads f_i

q_j : Degrees of freedom, DOFs

q_{tilt} : Tilt angle of nacelle for the forward backward motion

q_f : Forward - backward motion along axis X of the nacelle

q_{yaw} : Yaw angle to axis Y of the nacelle

q_{tl} : Tilt lateral angle of nacelle for the side to side motion of the nacelle

q_l : Side to side motion along axis Z of the nacelle

$q_k(0)$: Modal content in the initial condition, to a pure excitation of mode k

r : Radial, position of any material point

THY : Local blade pitch angle

Ueff : Effective velocity

Ueffx : Local effective velocity to X direction

Ueffz : Local effective velocity to Z direction

Ub : Local blade velocity to edgewise direction

Uw : Wind velocity

Wb : Local blade velocity to flapwise direction

$u_{p,j,i,k}$: Fourier coefficients

$u_{p,k}(t)$: Principal periodic mode shape

u_k (t) : Periodic mode shape of mode number k

x_m : Rotating DOFs of the m-th blade

x_0 : Transformed coordinate designated as collective, cyclic cosine and cyclic sine expressed in the non-rotating frame

Nomenclature for ROM (Greek)

α : Effective angle of attack

$\alpha_0(r)$: Effective angle of attack (a.o.a.) for the reference state at a specific radial position

$A_{imaginary ,p ,k}$: Imaginary part of the maximum magnitude

A_{pk} : Maximum value of magnitude

$A_{real,p ,k}$: Real part of the maximum magnitude

$\beta 1,2,3$: Flap-wise deflection angle to axis Z of blade 1,2,3

$\delta\alpha = a - \alpha_0$: Perturbation (small) of the a.o.a. due to other motions

$\delta Ua, \delta Uc$: Extra velocity contribution to the X and Z axis of system coordinates

ζ : Damping ratio

Λ_C : Eigenvalue matrix

Λ_B : Eigenvalues vector

$\lambda_{p,\kappa}$: Eigenvalue solution of matrix

λ_i : Eigenvalues

$\xi_{1,2,3}$: Edge-wise deflection angle to axis X of the blade 1,2,3

σ_κ : Damping, real part of $\lambda_{p,\kappa}$

Φ : Modal matrix

φ_i : Eigenvectors

$\Phi(2\pi)$: Floquet transition matrix (FTM)

$\omega_{p,k}$: principal periodic eigenvalue , imaginary part of $\lambda_{p,\kappa}$

ω_k : periodic eigenvalue

Ω, Ωr : Rotational speed of the rotor in cycles/sec

Ορολογία στα ελληνικά

Flapwise	Κατεύθυνση πτερύγισης (παράλληλη στον άξονα περιστροφής & κάθετη στο δίσκο)
Edgewise	Κατεύθυνση στο επίπεδο του δρομέα (στη κατεύθυνση της περιστροφής & κάθετη στον άξονα του πτερυγίου)
Torsion	Στρεπτική κίνηση (για τα πτερύγια και εν γένει τους φορείς που προσομοιώνονται ως δοκοί)
Pitch	Γωνία βήματος πτερυγίου
Roll -	Γωνιακή κίνηση διατοίχησης στο κάθετο επίπεδο του πύργου
Yaw	Γωνιακή κίνηση εκτροπής του πύργου στο οριζόντιο επίπεδο
Tilt - angle motion	Εγκάρσια γωνιακή κίνηση του πύργου
Fore- aft motion	κίνηση του πύργου και της ‘nacelle’ στο οριζόντιο επίπεδο στην εμπρός πίσω κατεύθυνση
Side to side	κίνηση του πύργου και της nacelle στο οριζόντιο επίπεδο στην πλευρική κατεύθυνση κίνησης
Roll floatter	Γωνιακή κίνηση διατοίχησης γύρω από τον οριζόντιο άξονα του πλωτήρα κατά την κατεύθυνση του κύμματος
Pitch Floatter	Γωνιακή κίνηση πρόνευσης γύρω από τον άξονα Y του πλωτήρα
Yaw	Γωνιακή κίνηση εκτροπής γύρω από τον κατακόρυφο άξονα του πλωτήρα
Surge	Κίνηση στην κατευθυνση του κύμματος του πλωτήρα
Sway	Κίνηση στην κατευθυνση της ταλάντευσης, κάθετα στο κύμμα, του πλωτήρα
:Heave	Κίνηση στην κατεύθυνση πάνω κάτω, κατά μήκος του κατακόρυφου άξονα του πλωτήρα

ACKNOWLEDGMENT

Acknowledgements (in Greek)

Αρχικά θα ήθελα να ευχαριστήσω τον επιβλέποντα καθηγητή μου Σπύρο Βουτσινά, για την ουσιαστική στήριξη που μου παρείχε αυτά τα χρόνια, σε όλα τα επίπεδα που απαιτεί η εκπόνηση μίας διδακτορικής διατριβής. Επίσης ευχαριστώ τους καθηγητές μου Θεόδωρο Φιλιππίδη, αναπληρωτή καθηγητή στο Πανεπίστήμιο της Πάτρας και τον Βασίλη Ριζιώτη αναπληρωτή καθηγητή στο Εθνικό Μετσόβιο Πολυτεχνείο. Ακόμα ευχαριστώ τον φίλο και συνάδελφο Δημήτρη Μανωλά που με στήριξε και συνέδραμε ουσιαστικά, καθόλη την πορεία της διδακτορικής μου διατριβής.

Ένα μεγάλο ευχαριστώ στην αδελφή μου Ελένη και την σύζυγο μου Πηνελόπη που στάθηκαν με κατανόηση δίπλα μου.

Ευχαριστώ όλους τους φίλους και συνεργάτες οι οποίοι με την στήριξή τους είτε έμμεσα είτε άμεσα συνέβαλαν στο να ολοκληρωθεί αυτή η εργασία.

Summary (in Greek)

Το παρόν διδακτορικό πραγματεύεται θέματα αεροελαστικής ανάλυσης ανεμογεννητριών αλλά και θέματα πιστοποίησης βάση του προτύπου IEC και των σύγχρονων ερευνητικών τάσεων.

Τα πρώτα κεφάλαια αυτού του διδακτορικού, ασχολούνται με την πιστοποίηση ανεμογεννητριών και πιο συγκεκριμένα με την έρευνα στο ζήτημα του ακριβούς προσδιορισμού των ακραίων φορτίων 50ετίας. Πρόκειται για στοιχείο της διαδικασίας πιστοποίησης που παραμένει ανοικτό στην βιβλιογραφία.

Τα πτερύγια των μηχανών είναι μεγάλες κατασκευές από σύνθετα υλικά τα οποία λειτουργούν σε ένα τελείως στοχαστικό περιβάλλον. Εξαιτίας της τυχαιότητας της ταχυτήτας του αέρα, τα φορτία που ασκούνται στο πτερύγιο και κατ'επέκταση οι αναπτυσσόμενες εσωτερικές αντιδράσεις σε οποιαδήποτε διατομή κατά μήκος του πτερυγίου είναι στοχαστικά μεγέθη. Επιπλέον, στοχαστική συμπεριφορά παρατηρείται και στις μηχανικές ιδιότητες των συνθέτων υλικών. Η ποσοτικοποίηση της μεταβλητότητας που παρουσιάζουν οι βασικές μεταβλητές (φορτία, μηχανικές ιδιότητες υλικών κ.τ.λ.) καθώς και η θεώρησή τους στον τελικό σχεδιασμό του πτερυγίου επιτυγχάνεται μονάχα με την χρήση στατιστικών μεθοδολογιών.

Για το σκοπό αυτό χρησιμοποιήθηκαν ως δεδομένα εισόδου της στοχαστικής μεθοδολογίας τα στοιχεία της βάσης δεδομένων OptiDAT, με πειράματα και στατιστικά δεδομένα για τον προσδιορισμό των μηχανικών ιδιοτήτων του συνθέτου υλικού. Τα στοχαστικά μοντέλα των ιδιοτήτων του υλικού αναπαριστούν τόσο την φυσική όσο και τη στατιστική αβεβαιότητα η οποία προκύπτει από την ανομοιόγενεια των συνθέτων υλικών.

Επίσης η στοχαστικότητα του ανέμου προσεγγίστηκε με 10-λεπτές αεροελαστικές προσομοιωμένες χρονοσειρές. Οι προσομοιώσεις αυτές αντιστοιχούν στην αναπαραγωγή της φόρτισης της όλης κατασκευής με είσοδο χρονοσειρές ανέμου που αντιστοιχούν σε φάσμα ανέμου Kaimal και που δημιουργούνται με κατάλληλο λογισμικό που έχει αναπτυχθεί στο Εργαστήριο Αεροδυναμικής.

Όσον αφορά την ακραία φόρτιση, η 10-λεπτη μακροπρόθεσμη κατανομή συμπληρωματικής πιθανότητας ακραίας φόρτισης, δηλαδή των εσωτερικών αντιδράσεων σε οποιαδήποτε διατομή κατά μήκος του πτερυγίου, εκτιμάται υλοποιώντας την τεχνική της προεκβολής των φορτίων - Load Extrapolation – κατ εφαρμογή του κανονισμού IEC 61400-1 ed. 3. Σύμφωνα με το πρότυπο IEC, οι σχεδιαστές υποχρεούνται σε μία από τις περιπτώσεις φορτίων, να κάνουν χρήση μεθόδων στατιστικής προβολής, που να ορίζουν τα φορτία σχεδιασμού. Οι απαραίτητοι αεροελαστικοί υπολογισμοί πραγματοποιήθηκαν για το 63 m Glass-epoxy πτερύγιο που αναπτύχθηκε από το ερευνητικό κέντρο NREL στα πλαίσια του ερευνητικού έργου UPWIND για την μηχανή αναφοράς του NREL των 5MW.

Δύο μέθοδοι εξαγωγής μεγίστων εξετάστηκαν και 3 κατανομές προσαρμόστηκαν στα διάφορα δείγματα των εξαγόμενων μεγίστων. Έγινε έλεγχος για το ποιές είναι οι κατάλληλες επιλογή συνάρτησης και μέθοδος συλλογής μεγίστων. Υλοποιήθηκε μελέτη σύγκλισης της μεθόδου προεκβολής για τον καθορισμό του απαραίτητου αριθμού αεροελαστικών χρονοσειρών. Η μελέτη αυτή έγινε απευθείας στην παραγόμενη μακροπρόθεσμη κατανομή συμπληρωματικής πιθανότητας ακραίας φόρτισης. Στην τελική κατανομή της ακραίας φόρτισης ελήφθη υπόψη η στατιστική αβεβαιότητα εξαιτίας του περιορισμένου αριθμού διαθέσιμων αεροελαστικών χρονοσειρών. Επίσης έγινε σύγκριση της απόδοσης μεταξύ διαφορετικών εναλλακτικών τεχνικών για την συλλογή

σημείων και εν συνεχεία τη στατιστική προεκβολή των φορτίων του δρομέα. Αυτές οι μέθοδοι ήταν η μέθοδος του ενός μεγίστου σημείου και η μέθοδος της συλλογής επάνω από ένα όριο. Το ζητούμενο φορτίο υπολογισμού ήταν το φορτίο σχεδιασμού των 50 ετών.

Σύμφωνα με την σειρά των προσομοιώσεων, αρχικά παρουσιάζεται η πρόβλεψη των μεγίστων φορτίων υπό την επιρροή στοχαστικού ανέμου. Το επόμενο βήμα είναι η πρόβλεψη του φορτίου σχεδιασμού και της αβεβαιότητας των προβλέψεων ωςσυνάρτηση των ιδιοτήτων των συνθέτων υλικών που χρησιμοποιούνται για την κατασκευή της πτέρυγας. Έτσι η μεθοδολογία που ακολουθείται είναι ο υπολογισμός του μεγίστου φορτίου που προκύπτει από τον στοχαστικό άνεμο με σταθερές τις ιδιότητες του σύνθετου υλικού και μετά οι αντίστοιχες προβλέψεις με χρήση λογαριθμικής κανονικής κατανομής για τις κατανεμημένες ιδιοτήτες του σύνθετου υλικού. Οι ιδιότητες που θεωρούνται στοχαστικές για το υλικό είναι το E_1 μέτρο ελαστικότητας κατά μήκος των ινών του συνθέτου υλικού, το E_2 μέτρο ελαστικότητας κάθετα στις ίνες του συνθέτου υλικού, το G_{12} μέτρο διάτμησης και τέλος ο λόγος Poisson v_{12}. Ενώ ο άνεμος παραμένει πάντα στοχαστικός εξ ορισμού. Από αυτές τις δύο ξεχωριστές προβλέψεις, προκύπτουν συμπεράσματα αναφορικά με το αποτέλεσμα στο φορτίο σχεδιασμού αλλά και για την ανάλυση τάσεων διατομής της πτέρυγας με στατιστική προεκβολή.

Επίσης αναπτύχθηκε κώδικας στατιστικής επεξεργασίας στο περιβάλλον του λογισμικού Matlab, βάσει του κώδικα πιστοποίησης ανεμογεννητριών IEC [18] και ειδικότερα του παραρτήματος, annex F, που αναφέρεται στην πρόβλεψη του μεγίστου φορτίου σχεδιασμού. Με αυτόν τον τρόπο έγινε επεξεργασία των αποτελεσμάτων και εκτιμήθηκαν τα ακραία φορτία σχεδιασμού. Επίσης προέκυψαν συμπεράσματα για τα ακραία φορτία σχεδιασμού, τις μεθόδους στατιστικής ανάλυσης και την αβεβαιότητα που υπεισέρχεται στους αεροελαστικούς υπολογισμούς.

Επειδή η μελέτη κάνει χρήση των αεροελαστικών προσομοιώσεων στην πρόβλεψη στατιστικών φορτίων προεκβολής, τα συμπεράσματα των οποίων θα είναι χρήσιμα και σε άλλες περιπτώσεις. Δηλαδή σε περιπτώσεις προσομοιώσεων, όπου για την πρόβλεψη των φορτίων σχεδιασμού και την ανάλυση τάσεων διατομής της πτέρυγας αντίστοιχα ερωτήματα αναδεικνύονται αναφορικά με τις τεχνικές προεκβολής, την επιλογή κατανομών και το μέγεθος των δεδομένων που χρειάζονται.

Σε κάθε περίπτωση, για τις ανάγκες της διαδικασίας πιστοποίησης, είναι απαραίτητη η ύπαρξη κώδικα γρήγορου και ακριβή ώστε να υπάρχει δυνατότητα πολλών αεροελαστικών υπολογισμών, σε ρεαλιστικό υπολογιστικό χρόνο. Για αυτό το λόγο αναπτύχθηκε ένα μειωμένης τάξης πρότυπο (R.O.M.) για την προσομοίωση της δυναμικής συμπεριφοράς ανεμογεννήτριας, με περιορισμένο αριθμό βαθμών ελευθερίας (είκοσι δύο (22) συνολικά). Η διατύπωση των δυναμικών εξισώσεων του προβλήματος βασίστηκε στην αρχή του Hamilton. Στην συνέχεια προγραμματίστηκε υπολογιστικός κώδικας για τη δυναμική ανάλυση πλωτής ανεμογεννήτριας, βασισμένος στο προαναφερθέν πρότυπο. Ακολούθως πιστοποιήθηκε η ορθότητά του προτύπου σε σύγκριση με αποτελέσματα που δίνει η πλήρης και λεπτομερής προσομοίωση πεπερασμένων στοιχείων.

Επίσης αναπτύχθηκε κώδικας που προσομοιώνει την αεροελαστική συμπεριφορά λαμβάνοντας υπόψη την επίδραση των ελαστικών παραμορφώσεων στα αεροδυναμικά φορτία του δρομέα. Για το σύστημα αυτό πραγματοποιήθηκε ανάλυση αεροελαστικής ευστάθειας βασισμένη στη μέθοδο μετασχηματισμού Coleman, για την άρση των περιοδικών όρων. Ο μετασχηματισμός Coleman χρησιμοποιείται για την εύρεση των ιδιοσυχνοτήτων, της απόσβεσης και των περιοδικών ιδιομορφών μιας περιστρεφόμενης ανεμογεννήτριας από την περιγραφή των βαθμών ελευθερίας στο αρχικό σύστημα συντεταγμένων. Η προσέγγιση Coleman είναι ακριβής μονάχα για ισότροπα συστήματα (συστήματα με περιφερειακή συμμετρία).

Σε ανομοιογενή συστήματα, για παράδειγμα σε δρομείς με ανισοκατανομή βάρους, η διαχείριση γίνεται με τη γενική προσέγγιση της ανάλυσης Floquet, που ορίζει ένα μοναδικό σύστημα αναφοράς για την εποπτεία των ιδιοσυχνοτήτων, στις οποίες προστίθεται κάθε πολλαπλάσιο της γωνιακής ταχύτητας του ρότορα. Η εν λόγω ασάφεια, επιλύεται με την απαίτηση πως η περιοδική ιδιομορφή είναι τόσο σταθερή όσο στο αρχικό σύστημα συντεταγμένων. Η ιδιοσυχνότητα αναγνωρίζεται ως η κυρίαρχη συχνότητα στην απόκριση μίας απλής διέγερσης της ιδιομορφής που παρατηρείται στο αρχικό σύστημα συντεταγμένων.

Έτσι αναπτύχθηκε κώδικας και εφάρμοστηκε η μέθοδος Floquet για την ανάλυση ευστάθειας συστήματος με περιοδικούς συντελεστές και αναπτύχθηκε υπορουτίνα για την εύρεση των ιδιοσυχνοτήτων του συστήματος. Έγινε διερεύνηση της επίδρασης των περιοδικών φορτίσεων στην ευστάθεια ανεμογεννήτριας, όπως η διαφορά μάζας στις πτέρυγες και η περίπτωση ανέμου με κατεύθυνση υπό γωνία απόκλισης 20 μοιρών, με χρήση του υπολογιστικού εργαλείου. Το εργαλείο πιστοποιήθηκε ως προς την ακρίβεια και την ορθότητά του σε σύγκριση με τον κώδικα FEM hGAST για την ανεμογεννήτρια NREL 5MW.

Αναφορικά με την διαδικασία αναγνώρισης ιδιοσυχνοτήτων, σε ισοτροπικές συνθήκες οι περιοδικές ιδιομορφές περιέχουν μέχρι 3 αρμονικές, ενώ σε ανισότροπές συνθήκες περιέχουν άπειρο αριθμό αρμονικών με ιδιοσυχνότητες που είναι πολλαπλάσια της συχνότητας περιστροφής. Αυτές οι αρμονικές εμφανίζονται σε υπολογισμένες συχνότητες απόκρισης της μηχανής. Με στόχο την αναγνώριση των σωστών ιδιοσυχνοτήτων από όλα τα πολλαπλάσια της γωνιακής ταχύτητας περιστροφής χρησιμοποιείται κατάλληλη μέθοδος ταυτοποίησης.

Summary

The present thesis is related with the key issue of wind turbines aeroelastic stability and the modern research developments of the certification processes analyzed to IEC certification code.

The first chapters deal with certification issues of wind turbines. The certification process is essential for the designers, especially the evaluation of fifty years design load base target.

W/T rotor blades are large composite structures operating in a completely stochastic environment. Hence, the applied wind loads and further the developed stress resultants in the rotor blade sections are stochastic themselves. Moreover, stochastic behaviour is also exhibited by composite materials showing great scatter both in their fatigue and static mechanical properties. A rational way to quantify the variability in the basic variables and take into account these uncertainties in the final design of the structure is provided by probabilistic methods.

Towards this, it was used as data input for the stochastic methodology an already known database of experimental data for the evaluation of composite mechanical properties. The stochastic models of composite material properties reproduce the statistical uncertainty of the blade beam properties, which resulted from the heterogeneity of composite materials.

In terms of wind inflow, its stochasticness is reproduced with 10 minute aeroelastic simulations. The simulations represent the loading over the whole structure with Kaimal wind spectrum. This spectrum is calculated with the relevant simulation software INWIND which was developed in the laboratory of aerodynamics.

Concerning the extreme loading, the long-term probability distribution for the extreme load is evaluated using load extrapolation technics according to IEC 61400-1 certification code. After the introduction of the 3rd edition of the IEC Standard 61400-1, designers of wind turbines are now required, in one of the prescribed load cases, to use statistical extrapolation techniques to determine nominal design loads.

For the present thesis, a series of data simulation made for the NREL 5MW turbine, in order to compare the performance of several alternative techniques for statistical extrapolation of rotor loads. The methods are the GM and the POT method. Using each one of those, fifty-year return loads are estimated for the selected wind turbine.

Two methods for extracting maximum values from time series and three cumulative distribution functions (CDFs) to these maxima data are analysed and compared between each other, in order to find out which is the correct choice for collecting data and which CDF is the appropriate one to extrapolate data gathered. Also, a convergence analysis has been made for the evaluation of the extrapolation method and the necessary number of aeroelastic time series in particular. This study was made directly to the long term distribution of the extreme values. To the final CDF of the extreme values, the statistical uncertainty due to the limited number of aeroelastic simulations was accounted for. Also, the different alternative techniques of data collection and statistical extrapolation methods for the rotor loads prediction were compared. These methods are: the method of collecting one maximum value from the whole time simulation and the method of selecting all values above a threshold. Finally at the end of the process, the 50 year design load value is estimated.

Also, the selection of parametric distribution used for fitting is analyzed. Firstly, the prediction of extreme loads under turbulent wind input is presented. Then the uncertainty for the composite

material properties used in the blade construction is introduced. So, initially the extreme loads are calculated for the case of fixed composite material properties, and then similar estimates are obtained for lognormally distributed material properties. The properties considered are: the E_1, the E_2, the G_{12} and the ν_{12}. The E_1 is the tensile modulus of elasticity along the fibers of the composite. The E_2 is the tensile modulus of elasticity vertical to the fibers. The G_{12} is the shear modulus and finally the ν_{12} is the Poisson ratio. In both sets of estimated extreme loading the wind is turbulent. From these separate estimates, conclusions are made regarding what is the effect of the material properties on the design load estimations and the stress analysis of a blade section with statistical extrapolations.

A statistical code has been also developed with the commercial software Matlab, for the IEC code of W/T certification and especially for Annex F. Annex F refers to the extreme design load forecast. While this study makes use of aero-elastic simulations data in addressing statistical load extrapolation issues, the findings should also be useful in other ways. For example, the results are useful in similar questions regarding extrapolation techniques, distribution choices, and the amount of data that are needed.

In any case, for the needs of the certification process, it is important to have a fast and precise code in order to have as many as possible aeroelastic calculations under realistic computation cost. For these needs a reduced order model has been developed for the simulation of the dynamic response of a W/T with twenty-two (22) DOFs in total. The formulation of the dynamic equations of the problem is based on the Hamilton's theorem. A simulation code was also programmed for the dynamic response and the analysis of a floating wind turbine, based on the aforementioned model, which was verified with the results from the finite element analysis code hGAST.

Similarly, a code was developed to simulate the aeroelastic behavior and taking into account the effect of aeroelastic deflections to the aerodynamic loads of the rotor. For the system of equations, aeroelastic stability analysis was made with Coleman's transformation, in order to eliminate the periodic terms. Coleman's transformation is used to enable extraction of modal frequencies, damping, and periodic mode shapes of a rotating W/T by describing the rotor DOFs in the inertial frame. The Coleman approach is valid only for a homogeneous system. Disparate systems, e.g. an unbalanced rotor, are treated with the general approach of Floquet analysis. Floquet does not provide a unique reference frame for observing the modal frequencies, to which any multiple of the rotor speed can be added. This indeterminacy is resolved by requiring the periodic mode shape to be as constant as possible in the inertial frame. The modal frequency is thus identified as the dominant frequency in the response of a pure excitation of the mode is observed in the inertial frame. The corresponding code and the Floquet method were developed for the stability analysis of balanced and unbalanced W/T systems. A separate routine was programmed for the eigenvalue identification of the system. The effect of the periodic terms on the stability of the wind turbine was examined assuming mass difference for the blades, wind yaw etc. The tool was validated against system identification with results from the hGAST FEM tool for the NREL 5MW wind turbine.

Concerning the eigenvalue identification process, in homogeneous conditions the periodic mode shape contains up to three harmonic components, but in disparate conditions it can contain an infinite number of harmonic components with frequencies that are multiples of the rotor speed. These harmonics appear in calculated frequency responses of the turbine. In order to identify the right eigenvalues from all multiples of the rotor speed, the appropriate identification method has been implemented.

So, the specific ROM can be used for fast aeroelastic calculations in order the design – certification process to be as fast as possible for the cases that the model is accurate and covers important part of the aeroelastic calculations.

1. Introduction

1.1 General

The need for environmentally friendly and sustainable sources of energy turned the interest of the global community in the renewable sources. Thus, an entire industrial sector has been developed, the wind energy industry. During the last decades, wind energy has become one of the most important sources of renewable energy. Climate agreements have convinced governments to implement policies that have favored the construction of wind farms all over the world. The continuous improvement of Wind Turbine (W/T) technology has dramatically lowered the cost of energy to the point that, the energy produced with onshore wind is cheaper than coal, gas and nuclear energy. This improvement resulted in wind turbines of progressively larger size, with the last ones having a diameter of higher than 200 m, and capable of producing 12-15 MW of power. Due to the continuous increase in rotor diameter and the related increase in blade flexibility, aeroelastic stability analysis has become an important aspect of W/T design.

During operation, W/Ts are subjected to loads from a variety of sources. The wind deflects the blades and the tower, and the rotation produces strong centrifugal forces on the blade. The wind is, however, not constant, it varies spatially (e.g. with the height due to wind shear) and temporally due to turbulence. The highly flexible blades of modern W/Ts are subject to a complex wind profile that interacts with active and passive control systems, causing complex aero-servo-elastic phenomena.

Additionally, the composite materials used to construct the blades have inherently stochastic properties. These aforementioned factors generate a dynamic loading scenario. In the design process this scenario is determined by a standard suite of time simulations of the response to the varying loading. Time simulations yield details of important design loads, but they disclose little of the underlying phenomena causing the loads. The assessment of the loads and the design of control algorithms require a thorough understanding of the turbine dynamics. A decomposition of the turbine dynamic response into modal contributions, which is one of the issues of the present thesis, is indeed an effective way to gain this understanding of the dynamics and the factors contributing to the loads.

1.2 Certification issues

The first three chapters of the present thesis deal with the certification process of W/Ts and the calculation of the design loads. Given a limited amount of simulation data, our goal is to use statistical extrapolation techniques to predict 50-year return levels of W/T components. This is essentially the same task that is currently required in the Design Load Case 1.1 of the IEC Standard 61400-1, 3rd edition 1 [17]. In the IEC, extrapolation to max values is applied to simulated loads data.

W/Ts operate in a completely stochastic environment. Further, uncertainty arises in the material mechanical properties due to the inherent variability of the disparate fibre reinforced plastics (FRP) as well as due to the manufacturing process of the composite laminates. The variabilities, both on the aerodynamic loads and the material properties imply that various uncertainties are involved in the design process.

Rotor blades are mainly manufactured by glass/carbon-epoxy/polyester composites. It is worth mentioning that there is high annual failure rate of rotor blades not specifically recorded in open literature, compared to the respective rates of other mechanical components of W/Ts e.g. mechanical breaks, rotor hub, tower, drive train etc. This implies that the rotor blade design is still an open issue.

In order to assure a safe design, standards and certifications must be followed. According to the IEC 61400-1 ed.3 standard, W/Ts are designed for various design load cases. These design load scenarios (cases DLCs) are defined by combining relevant loading situations, W/Ts may experience in their design life different external conditions. DLCs are divided into operational and temporary states, such as power production states and transportation/installation ones respectively. The external conditions are classified as normal or extreme.

Particularly, statistical analysis to the experimental data of the material properties as well as to the load simulations is performed by determining representative (characteristic) values. Safety and reduction factors are further applied to these values to account for uncertainties that were missed. These missing uncertainties may be both in the experimental procedure on the material property characterization as well as on load response evaluation performed by means of aero-elastic simulators. The resulting design values are used in the loop described previously.

Although Annex F of the IEC guidelines make reference to the methods of peaking maxima values by using several different distributions, details of the extrapolation procedure are left to the designer. In the present thesis, the simulation data were obtained and extrapolated using two different peaking maxima methods, three different distributions and finally two different set of initial stochastic conditions. All these cases are compared with each other. The goal is to assess how the design load depends on the stochastic nature of wind input and the variability of the composite material properties. The best suited peaking method and fitting function to the data are proposed along with the best suited procedure for determining the extreme loads.

In this respect, the following two peak extraction methods are compared:

- The Method of Global Maxima (GM) - In this method, only the single largest data point (load) from each ten-minute load file is used, and statistical distributions for these ten-minute maxima are estimated directly.
- Peak-Over-Threshold (POT) Method – In this method, multiple peaks are extracted from each file. Specifically, the largest value between every successive up-crossing of the threshold is extracted. Distributions are fitted to load exceedances over the selected threshold.

The question of which parametric distribution may be most appropriate, is explored both on theoretical and practical grounds. Also, the variability of long-term load predictions as a function of the amount of data included in the analyses is checked. Then, conclusions are drawn regarding the length of the dataset needed to produce reliable statistical extrapolation of loads for design. Another relevant implementation issue is to assess the effect of the variability of the blade structural properties on the extreme blade moments and loads, the blade tip deflections, the maximum stresses and the Tsai-Wu failure criterion, in the context of the IEC standard.

1.3 Reduced order modeling and modal analysis

For the needs of the certification process, it is important to have fast but still reliable aeroelastic solvers. So, in the present thesis, a reduced order model of 22 DOFs for the whole floating W/T is combined with a rigid-body description of a floater defined by its corresponding 6 (rigid) DOFs of motion.

The problem is formulated in the context of Hamiltonian dynamics. External loading includes aerodynamic loading on the rotor, hydrodynamic loading on the support structure and gravitational loading. The formulation allows stability analysis of the system which involves three basic items: the selection of a reference (steady or periodic state) operating condition, the linearization of the equations of motion about this state and finally the modal decomposition of the linearized system providing modal frequencies, modal damping, and mode shapes.

Structural and aerodynamic imbalances, caused for example by the ice accretion, can be detected by identifying the mode shapes. The ability of a numerical model to accurately predict the loads is important. System identification techniques can be used to measure the modes, and hence validate the numerical model. Mode measurement of a rotating blade is a very challenging analysis. Identifications are not only necessary to do model validation, but they are also used to perform continuous monitoring, as it is well known that the aerodynamic properties of the blades degrade with time, and hence the damping level may change in an unpredictable manner.

A W/T in operation that is subjected to steady wind inflow, may experience periodic loads, and therefore the blades will undergo periodic motions. One source of periodicity is gravity, which causes a periodic stiffening of each blade. The vertical and horizontal wind shears cause aerodynamic loads that periodically change their direction and magnitude. For these reasons, stability analysis of W/Ts is conducted within a periodic framework and in particular by employing Floquet's theory. The periodic system assumption has been applied several times to wind turbines, and the main features of a periodic system are the following:

- Each mode is characterized, due to periodic nature of the system, by multiple eigenvalues and damping characteristics, which manifest with more or less strength on different parts of the structure.
- A steady wind causes both constant loads, and loads at frequencies multiple of the rotor speed.

It is well known, that the matrices of a linearized W/T model are periodic functions of the azimuth angle. In order to perform stability analysis, it has been shown that averaging the state matrix and performing eigenvalue analysis on the result leads to erroneous predictions. This is because by neglecting the whole periodic content results in a too raw approximation. Another approach would be to solve the eigenvalue problem for each azimuth angle, to get the time evolution of the frequencies and damping. This is known as the time-frozen approximation, and is valid only for very slowly time-varying systems.

One popular approach to the stability analysis of rotors in general, and of wind turbines in particular, is to use Coleman's multi-blade coordinates (MBC) transformation. Given the dynamical equations of motion, this periodic transformation expresses the model rotating DOFs in a new set of coordinates achieving a significant reduction. This method is not able to cancel the periodic content of the state matrix and the remaining periodicity is typically removed by averaging. The resulting model is finally analyzed using standard time-invariant techniques. This procedure is known as Coleman's approximation and it has been implemented in the hGAST code that is applied in the present work. In principle, there are issues connected with any Coleman-based stability analysis approach. First, the level of approximation implied by the averaging of the remaining periodicity is difficult to assess and quantify a priori. Although, there is no theoretical proof yet that the periodicity that remains after the application of the Coleman is in general negligible, its use is widespread.

The exact stability analysis of a periodic system is performed by employing Floquet's theory. If the model has only a few dozens of DOFs, then a continuous-time Floquet analysis can be carried out with standard computer hardware. On the other hand, high-fidelity W/T models have thousands of DOFs, and hence the computational cost of a full Floquet analysis is overwhelming. The elevated computational cost of Floquet theory is not only caused by the high number of DOFs, but also from the integration of the equations of motion along the period.

1.4 Objectives

The main objective of the present thesis is to propose new insights in the certification process and in stability analysis. Also, the work aims at a thorough understanding of ROMs, for onshore and offshore wind turbines in cases of homogeneous and disparate rotors.

Concerning the certification processes of wind turbines, according to modern research developments the IEC code does not necessarily fully cover all certification issues. So, the certification process is revised by assuming much more data sets of simulations for every wind speed bin, besides the 15 simulations that are proposed by the IEC. Additionally, stochastic values are assumed for all material properties of the blade composites. So, another set of calculations is performed with the same set of turbulent winds but with lognormally distributed material properties. Comparisons are made and presented for these two data sets and final conclusions are drawn for the certification process in the IEC code. The final goal is to assess the effect of the variability of the blade structural properties on the extreme blade moments and loads, the blade tip deflections, the maximum stresses and the Tsai-Wu failure criterion.

Concerning fast aeroelastic simulations and stability, the Stab-code is an accurate model of offshore W/T with a fast ROM code. The necessity for such kind of fast codes instead of codes including FEM calculations has emerged in connection to application of Floquet's theory.

1.5 Outline

In chapter 2 the inherent stochastic material properties (StoMP) for composite W/T blades are discussed and analyzed, in order to understand their nature and their influence to load calculations. The parameter estimation is presented together with the selection of the most accurate distribution that can describe the stochastic nature of StoMP. Different experimental databases are presented and the OptiDAT database is finally selected to describe the material properties of the composites that are used in aeroelastic calculations. Uncertainties are mentioned for the model of material properties that is used. Lognormally distributed material properties E_1, E_2, G_{12} and ν_{12}, as well as the relevant beam properties of the blade are presented.

In chapter 3, the certification process for wind turbines is analyzed in detail. Current issues on certification are mentioned, as well as the late additions of the certification code IEC. Recent papers and reviews are analyzed in order to drive our research effort to open issues. The nature of turbulent wind inputs is analyzed and the way to calculate the wind input for the aeroelastic simulations is presented. All calculation results are presented with the GM and the POT peak methods that select maxima data from time simulations. The issue of convergence is also analyzed according to the IEC. Additionally, short-term distribution fittings and long-term distributions for the extrapolation and the calculations for the fifty-year design load base target are presented. Finally, statistical uncertainty and conclusions concerning certification process are presented in order to propose best practices.

In chapter 4, all certification processes and calculations are presented for all moments, loads, deflections and stress resultants. These include the flapwise, the edgewise and the torsion moments and loads. Also, the relevant blade tip deflections are analysed. From these calculations the fifty years design loads, moments and blade tip deflections are evaluated. The presentation is for different data sets per wind speed bin and for both RefMP input with standard material properties, as well as for blade data input with lognormally distributed material properties. The certification process is presented also for the data sets proposed by the IEC code. Additionally, the different methods of selection maxima and different blade data inputs are compared in terms of design load base targeting.

A thorough analysis is presented for the wind speed bin of 14 m/s in order to better assess the differences in loads and deflections caused by the uncertainty in the material properties. Towards this purpose an additional set of simulations is defined and processed. Twenty different sets of material properties, defining 20 different blade datasets, are randomly selected from the OptiDAT database (fitted LN distributions). For each one of them 24 DLC1.1 servo-aero-elastic simulations are performed at the wind speed of 14m/s (wind speed at which maximum flapwise bending moment occurs) using different turbulence seeds. POT extreme values extraction is applied to each of the 24 simulations per material set and then a 3pW CDF is fitted to the collected extreme values per material set. Finally, extrapolated values at the 1e-4 probability threshold are recorded in all cases. The same procedure is also applied to the reference blade data using the same 24 wind seeds, in order to compare reference against StoMP on the same basis.

Furthermore, an analysis of the cross-section stresses is also performed. A cross-sectional analysis tool based on full stiffness matrix is adopted for the calculation of the cross-sectional stresses along the blade span. The tool provides the stress distribution and the Tsai-Wu failure criterion, over the cross section, based on an input set of resultant loads applied at a reference point over the section (i.e. ultimate resultant forces and moments estimated through the servo-aero-elastic analysis). The Tsai – Wu failure criterion is based on the theory of material failure for disparate composite materials with different strengths in tension and compression. The criterion predicts failure when the strength ratio is below 1.

In chapter 5 a formulation is illustrated for the fast aeroelastic calculations code, formulated with a ROM. The analysis begins with aerodynamic modeling and dynamic definition of the mechanical system, up to the procedure of linearization. The chapter finally concludes to the results of the general formulation for the ROM which will be used in the next chapter.

In chapter 6 the ROM formulated in chapter 5 is used for a model with 22 DOFs for the whole offshore W/T. Validation is carried out against FEM based simulations of hGAST and concerns: the eigenvalue analysis and predicted time signals of loads. The ROM aeroelastic stab-tool results are presented and the periodic parts of the matrices due to rotation, are resolved with Coleman transformation. The code is validated for the homogeneous rotor with Coleman transformation and the eigenvalue analysis compared to the FEW version of hGAST. In case there are anisotropies, the analysis uses Floquet's theory. The method results to an infinite number of possible eigenvalues. An identification method is used to solve this indeterminacy and is validated for its accuracy.

Finally, in chapter 7, the general conclusions from all chapters are compiled and suggestions for future research are given.

2. Inherent stochastic composite material properties

2.1 Structural reliability of W/T rotor blades and state of the art issues

W/T rotor blades are huge composite structures working in a completely stochastic environment due to turbulent wind. So, the applied wind loads and the stress resultants developed on the rotor blades are stochastic. In addition to the excitation, also stochastic are the mechanical properties of the blade materials because of their inherent inhomogeneity and the manufacturing uncertainty. Therefore, reliability assessment for the W/T rotor blades begins with quantification of the uncertainty of the composite mechanical properties and of the exciting loads.

A lot of work ([1], [2], [3], [5], [6] and [7]) has been published on the stochastic modeling of strength and elastic properties of fiber reinforced composites. Depending on the starting scale at which uncertainties are built up in the composite materials, three main approaches appear in the literature. In the first approach, the uncertainties are modeled at micro-scale level while the macroscopic material properties of the laminates are obtained using various micro-mechanical models.

The second approach deals with uncertainties of modeling at the meso-scale or ply level. These uncertainties originate from the thermo-mechanical properties of the lamina. Such a property is the tensile strength in the fiber direction of a UD laminate, which is usually stochastically modeled. A lot of research has been carried out in the ply level [58] – [62] mainly due to the well- established confidence in conducting such experimental tests as they form the main experimental procedure in various standards. A comparison of the probabilistic models of material properties for FRP laminates, as derived from the micro and ply level approaches, has been carried out in [63], [64]. In this respect, a useful conclusion for the present thesis is that stiffness properties agree with the corresponding strength variables.

In this ply level context, Bacharoudis and Philippidis in [14] presented the estimation of the reliability level of an existing rotor blade design according to IEC 61400-1 ed.3. The analysis performed at the ply level using a detailed 3D shell FE model in the probabilistic design system (PDS) of ANSYS. The stochastic nature of material mechanical properties and loads was taken into account. Blade loading consisting of the flap, edge bending moment and the axial force distributions was derived from aero-elastic simulations. A procedure was developed to convert the sectional beam stress resultant time series into statically equivalent concentrated force time series acting on the FE blade model. Correlation both in the material properties and the extreme loads was taken into account. Reliability analysis was addressed by implementing efficiently the Response Surface Method combined with direct Monte Carlo simulation (RSM/MC). Statistical uncertainty and their influence on the blade failure or buckling probability were investigated.

Also in the meso-scale level, Bacharoudis and Philippidis introduced an integrated probabilistic tool in [15] for the reliability and structural analysis of composite rotor blade sections under ultimate loading. The exhaustive exercise in [14] revealed the considerable CPU time needed when reliability analysis of detailed 3D shell FE models was implemented. Therefore, the code in [1], introduced by Lekou and Philippidis was further enhanced with (i) a buckling analysis module based on the finite strip method, (ii) a procedure for the stochastic representation of the extreme loads directly from the aero-elastic time series implementing the IEC 61400-1 ed. 3 [17], (iii) additional reliability methods (iv) more flexible material models compatible with JCSS uncertainty patterns and (v) numerical statistical procedures that account for uncertainty and correlation of the basic design variables. Physical and statistical uncertainty of the basic variables was taken into account while several model uncertainties related to the material properties were further introduced and quantified in the light of appropriate test results. To prove the efficiency of the code as a design tool, the effect of various probabilistic assumptions concerning the material properties was directly investigated on the estimated reliability β-index values for two rotor blade design cases typical of stall- and pitch-regulated wind turbines.

The third and last approach is carried out at the macro scale level involving uncertainties determined by experimental tests similar to those required for ply characterization. Experimental data however, concern composite components or laminates with more generic lay-ups, subcomponents or full-scale blade tests which contain ply drops or adhesive joints. In any of the above considered scales, different types of uncertainties are introduced.

Correlation between mechanical properties can be quantified starting from any of the above-mentioned scales. Considering the macro scale as starting point, correlation between nine material properties, was recently evaluated in [13] based on experimental data. Assessment of the probabilistic models of FRP material properties may be performed using classical statistical analysis.

All the above analyses concerning the structural properties of the composite materials, contribute to the design process of wind turbines. One of the main issues of the design process is the extreme loading forecast. In order to estimate the extreme loading of a W/T, the state of art aero-elastic tool hGAST is used. The code hGAST is used for the prediction of the loading on the rotor blades as well as for the loads assessment of the whole wind turbine. The tool models the blades by means of beam theory specifically adapted for more accurate predictions of the wind turbine response, and uses the Finite Element Method. In order to take advantage of the available aero-elastic code, but also accurately represent the mechanical properties of the full three-dimensional blade in the one-dimensional beam element, the computational tools PRE-THIN and THIN have been used. They have been presented in a review by Lekou and Philippidis [1], [2] which details that THIN is based on the Euler-Bernoulli beam theory for thin wall multi-cellular sections, like those of wind turbine blades. Results from 'THIN' are used as input in the aero-elastic code for the needs of the present thesis.

2.2 Material properties

Stochastic characterization of material properties is a vital ingredient of structural reliability analysis. The composite laminates of a typical blade section consist of many layers. The material properties for fibers and matrix are stochastic variables. For material properties, the physical and statistical uncertainties must be quantified. Uncertainty arises mainly due to, a) the inhomogeneous nature of the FRP material, b) manufacturing processes and c) the limited number of experimental tests [4].

The measurement of material properties on small coupons, may give significantly different values from the respective ones on a 63m long real rotor blade, as is the blade in the present thesis. In addition to uncertainties driven by the manufacturing process itself, environmental conditions such as temperature, humidity and UV radiation are also uncertainty contributors.

2.2.1 Material characterization

The OptiDAT database has been used in order to select values for the E_1, E_2, G_{12} and v_{12} material properties of the composite. The engineering constants of interest are listed in Table 1, and the measured material properties in [Appendix 1].

The material properties E_1, E_2, G_{12} and v_{12} are assumed random variables and the reliability level of the rotor blade, is investigated.

Symbol	**Description**
E_1	Tensile modulus of elasticity parallel to the fibers
E_1C	Compressive modulus of elasticity parallel to the fibers
E_2	Tensile modulus of elasticity transverse to the fibers
E_2C	Compressive modulus of elasticity transverse to the fibers
v_{12}	Major Poisson ratio
v_{21}	Minor Poisson ratio
G_{12}	In-plane shear modulus of elasticity
XT	Tensile strength parallel to the fibers
XC	Compressive strength parallel to the fibers
YT	Tensile strength transverse to the fibers
YC	Compressive strength transverse to the fibers
S	In-plane shear strength

Table 1: Tensile moduli and strength properties considered in the OptiDAT database

2.2.2 Parameter estimation and distribution model selection

A lot of parametric distributions have been proposed to probabilistically model the material properties. Some of them are rather arbitrary while others possess a certain level of theoretical background. The most frequently used functions are the Normal (N), the Lognormal (LN) and the Weibull (W) distributions. The descriptive statistics of the cumulative distribution functions are given in [Appendix 2] and [Appendix 3]. Several research works [5], [6] have been published employing the aforementioned models, while these models have been also proposed and used by certification bodies and standards e.g. [8].

In order to fit/choose a certain probabilistic model, the parameters of every distribution have to be estimated from the samples, and an appropriate distribution test (or visual inspection) has to be applied. The 4-point estimation methods are proposed for computing the parameter values of the candidate distributions. These are: the method of moments, the maximum likelihood (ML) method, the least square fit as well as visual inspections of the data plotted on special probability paper.

It must be mentioned however, that ML estimators exhibit a number of desirable statistical properties. For samples of large size (Obs. >30), the ML estimators are approximately unbiased. They produce variances that are nearly as small as they could be obtained with any other point estimation method, while they asymptotically follow a lognormal distribution function. Taking into account that the ML method has been implemented in several statistical toolboxes, ML estimators are favored. So, in the present thesis the ML estimators are used for the OptiDAT database.

Many fitting tests are available to judge the quality of the distribution fitting to data. According to JCSS [9] and DNV [10], the K-S test may be applied. All possible distributions that may be fitted to data are mentioned in Table 2, even if the K-S test suggests the lognormal CDF distribution. The properties mentioned are E_1, E_2, G_{12} and v_{12}. The p-value of K-S test is the Observed Significance Level (OSL). This OSL is defined as the smallest significance level that would result in rejection of the null hypothesis for a set of given data and a selected distribution. The null hypothesis indicates whether or not a specific CDF describes the data identically. The p-values of the K-S test for the material properties of the OptiDAT database are presented in Table 21 of [Appendix 3] and indicate which of the CDFs describes better the data gathered, the LN, the Normal or the Weibull function**.** So, the LN parametric distribution is proposed since the p-value of the K-S test is above 0.95 for all material properties, although Normal distribution would be accepted with p-value 0.93.

Material property	Present statistical analysis CDFs	JCSS [9]	DNV [10]	MIL-HDBK-17-1F
E_1	LN	LN, W	LN, N	N
E_2	LN	LN, W	LN, N	W
G_{12}	LN	LN, W	LN, N	W
v_{12}	LN	LN, W	LN, N	W

Table 2: Parametric distributions for the E_1, E_2, G_{12} and v_{12} material properties

Concerning correlation issues, there are two major points of concern on material properties: the correlation between material properties at a point of a blade and the spatial correlation of every property. Very few 1_point correlation experimental data on FRP composites with continuous fibers are found in the literature that allows investigating possible correlations between mechanical properties. In spatial correlations, there are large uncertainties in terms of material properties.

Especially for the case of strength, there is lack of experimental results in the macro-scale level (coupons). So, the validation of estimated correlations is difficult. For the OptiDAT database used herein, out of the thirty-six correlation coefficients between nine material properties (E_1, E_2, v_{12}, G_{12}, XT, XC, YT, YC, S), only five of them are/can be estimated. It is mentioned clearly to the Thesis of Bacharoudis [13]. The analysis indicates that E_1 is fairly correlated with XT. This could have been anticipated, since these properties are both fiber dominated. On the other hand, no significant correlation was found between the shear properties.

2.2.3 Comparison between existing composite material databases

Prior to the OPTIMAT project [16], two databases were built. The first was connected to the MEGAWIND project in the late 90's and concerned Glass/Polyester FRP while the other was related to the UPWIND project and concerned Glass/Epoxy FRP. The third one OptiDAT which was created within OPTIMAT BLADES project (2005), [12] and [16] concerned a Glass/Epoxy FRP material. Descriptive statistics and analysis of the OptiDAT database can be found in [Appendix

3]. In the sequel, these databases will be referenced by the name of the project in which they were created.

The stiffness property E_1 for the three databases is compared in Figure 1 in terms of minimum and maximum values, as well as the mean and the STD of E_1. The error bars in the plot have a range of two STDs in each case. It may be concluded that new age materials and manufacturing processes maintain advanced mechanical properties compared to the older generations. The oldest database is MEGAWIND that reports lower values for both stiffness and strength properties. This fact certainly lies on the different constituent of the unidirectional ply and the manufacturing methods of constructing the respective test coupons. The same reason explains high spread of MEGAWIND data compared to the other sets, despite the fact that testing procedure was quite similar in all sets. MEGAWIND coupons were made with wet hand lay-up. It is already recognized that this method introduces a lot of uncertainty in the final product and thus great variability to the material properties. The lowest spread of the data can be seen in OptiDAT material properties. This is due to the fact that specimens were cut and tested from few plates and thus the variability in the manufacturing process of the plates essentially was not significant.

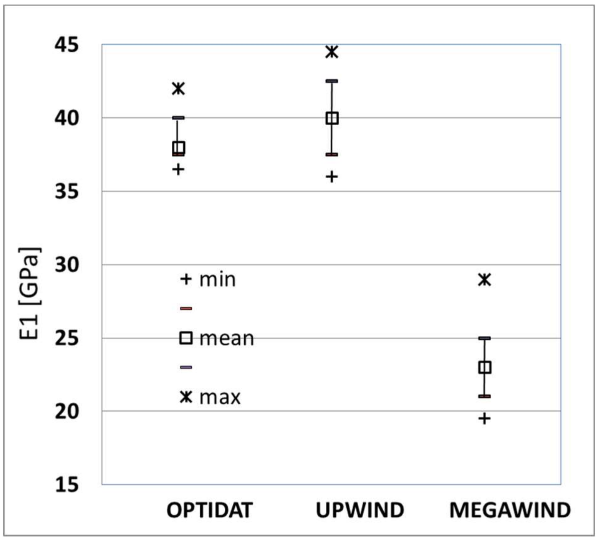

Figure 1: Descriptive statistics plots of the stiffness property E_1 for the OptiDAT, UPWIND and MEGAWIND databases

	UPWIND	OptiDAT	MEGA WIND
P E_1 - ν_{12}	0.54	0.21	-0.05
P E_1 - XT	0.72	0.55	0.22
P E_2 - YT	0.42	-0.04	0.18
P ν_{12} - XT	0.23	0.15	-0.39
P G_{12} - S	-0.09	-0.24	0.47

Table 3: Correlation coefficients estimated from the UPWIND, OptiDAT and MEGAWIND databases

Comparing OptiDAT and UPWIND databases, UPWIND materials are stiffer and definitely exhibit greater tensile strength in the direction parallel to the fibers. In spite of that the min-max range of the UPWIND materials is greater than that of the OptiDAT one. This means greater STD for the UPWIND database.

Also, in Table 3 it is shown the correlation coefficients between the basic material properties from the OptiDAT, UPWIND and MEGAWIND databases. It was also possible to estimate certain of the correlation coefficients from the OptiDAT, UPWIND and MEGAWIND databases and show them in Table 3. Material properties E_1-XT are dominated by the fiber behavior and are quite well correlated in all three databases. For the properties dominated by the matrix behavior E_2-YT, the databases indicate different trends. UPWIND database exhibits a fair correlation between E_2-YT while in the OptiDAT database this is not the case. This multifold trend is also obvious in the in-plane shear properties. In particular, in UPWIND, G_{12} and S are uncorrelated variables, in MEGAWIND they are positively correlated and finally in OptiDAT they are negatively correlated.

2.2.4 Other Model uncertainties

The geometrical blade complexity (physical and statistical) was evaluated by testing coupons of simple geometry according to international standards. However, it is expected that uncertainties may significantly change when considering the rotor blade structure. This happens mainly due to the complex geometry of the structure and the manufacturing process. In addition, the small coupons have not experienced any ageing effect since the respective tests. Also tests were performed in controlled environmental conditions at room temperature, under low relative humidity and absence of UV radiation. This is not the case for materials on a real wind turbine. All these types of uncertainty are usually accounted for in deterministic design by using partial safety and reduction factors. Random variables should be used instead in a probabilistic structural analysis to quantify each of these sources of variability. Therefore the most general probabilistic model for material properties proposed and used in the current thesis has the form:

$$W = X_{manuf}\ X_{temp}\ X_{age}\, R \qquad (2\text{-}1)$$

Where X_{manuf} stands for a variety of uncertainties, related to the structure and its manufacturing process. It accounts for uncertainties in material property values related to differences between full scale blade structure and coupon tests (size effects). It also includes uncertainties due to the manufacturing process. For example, composite laminates produced by hand lay-up or infusion method, as well as composite laminates which are post-cured or not will be different. Additionally, X_{manuf} is associated with uncertainties due to geometrical parameters of rotor blades as well as uncertainties due to flaws and defects.

X_{temp} denotes the uncertainty due to temperature loads; varies with time and in part can be predicted if the time variation of temperature T(t) is known.

X_{age} stands for the uncertainty due to ageing of the material. Ageing is a time dependent process related to the exposure of the material system to the operating environmental conditions e.g. UV radiation, snow, salty water etc. Thus, the corresponding uncertainty should be defined with respect to a certain period of time. Estimation details are given in [13], where quantification of the respective uncertainties was based on appropriate experimental data. It was found that extreme conditions i.e. high temperature values (thermal effect) and the presence of salt water (ageing effect), greatly influence the strength properties of glass FRP materials. This is especially true for the compressive and shear strength properties.

Finally, R is the physical and statistical uncertainty as evaluated from small coupon experimental tests. The aforementioned model uncertainties, which are variables themselves, are modelled as lognormally distributed material properties having mean values and variances estimated from tables that are made by engineering judgement and experimental data. It should be mentioned that defects were not considered herein (for recent contributions towards the probabilistic modeling of defects, see [65]).

2.3 Inherent stochastic material properties to simulations

The OptiDAT composite material database consists of about 3000 records of tests on Glass-fiber/epoxy coupons with a wide range of material characteristics, various lay-ups and laminate orientations all representative of W/T blade application. The database contains extensive material properties and load data from static/strength and dynamic/fatigue tests. Besides standard flat coupons, bi-axial test geometries like cruciform and tubular shape geometries are included in the database, as well as repaired and thick laminate coupons. The properties considered are stochastic and include the modulus of elasticity E_1 along the direction of the fibers, the tensile modulus of elasticity E_2 vertical to the direction of the fibers, the major Poisson ratio v_{12} and the in-plane shear modulus of elasticity G_{12}. In Table 4 minimum, maximum and mean values of the above-mentioned properties are provided, along with parameters of their statistical distributions CoV, skewness and kurtosis, as extracted from the OptiDAT database.

The variability of beam equivalent properties for a composite blade is estimated with PRETHIN and THIN [1], [2] that were mentioned in paragraph 2.1. These codes transform the material properties of the composite and of the stacking sequence of plies, into beam properties of the blade. For all material properties E_1, E_2, v_{12} and G_{12}, LN distributions are assumed and a CoV of 10% was specified at the stage of data generation. The values for the material properties that were generated and selected from the LN with random selection are presented in Figure 2.

material properties	Minimum	Maximum	mean	CoV %	skewness	kurtosis
E_1 (Gpa)	36.74	41.38	39.042	2.644	0.018	3.099
E_2 (Gpa)	13.54	14.73	14.077	2.307	0.392	2.428
G_{12} (Gpa)	4.032	4.396	4.239	2.340	-0.562	2.803
v_{12}	0.240	0.346	0.291	9.339	0.054	2.443

Table 4: Statistics of the composite material properties extracted from the OptiDAT database

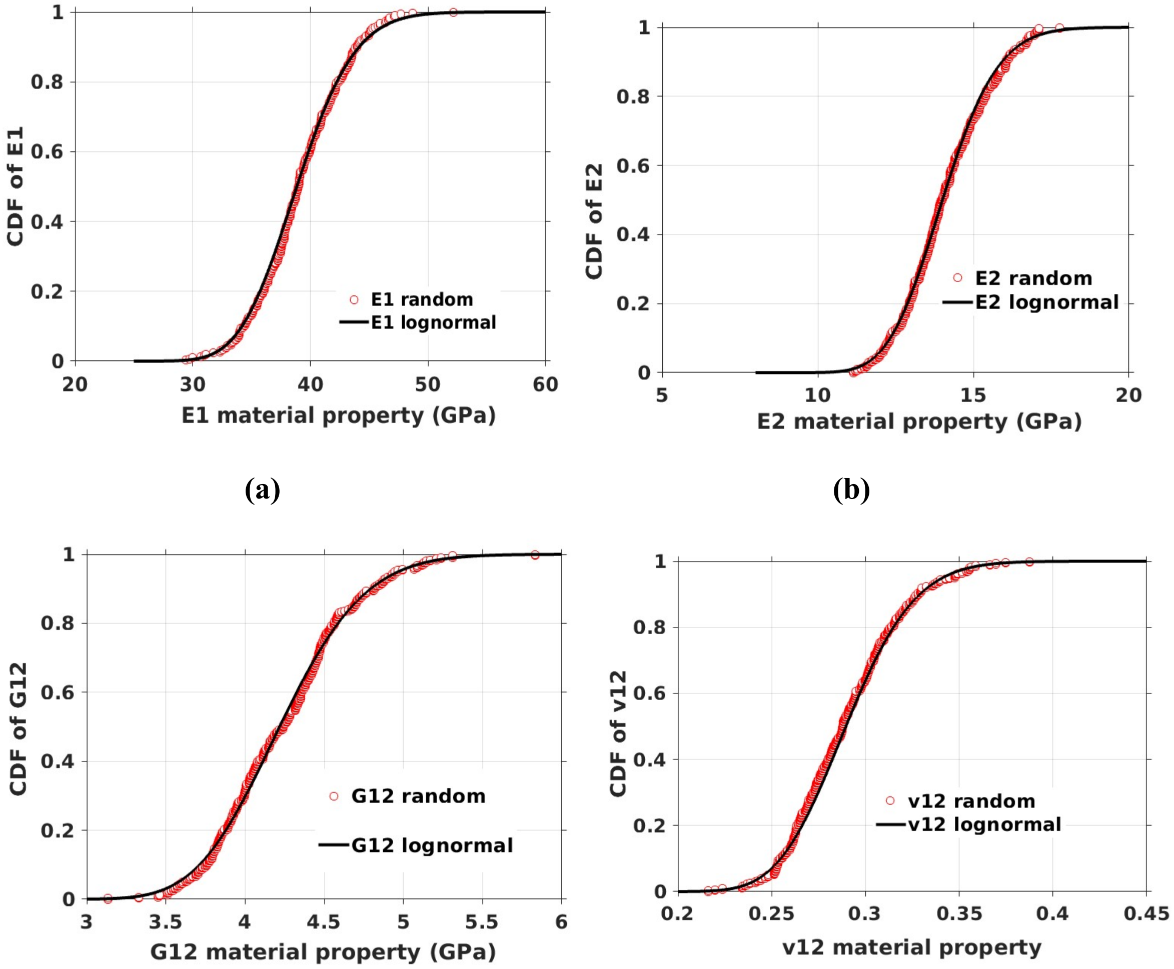

(a) (b)

(c) (d)

Figure 2: Log-normally distributed properties: (a) E_1 tensile elastic modulus parallel to the fibers, (b) E_2 tensile modulus of elasticity vertical to the fibers, (c) G_{12} the shear modulus and (d) ν_{12} the Poisson ratio

The W/T considered in the present work is the NREL 5MW Reference Wind Turbine. The main parameters of the turbine are presented in Appendix 4, while detailed data regarding the structural and aerodynamic properties and the control system can be found in [31].

In Figure 2 the quality of the fitting of LN to the OptiDAT database is shown. On the plot, the taken samples are selected randomly and also randomly combined to produce the random beam properties of the whole blade. These random blade properties are presented in Figure 3 and they are also fitted by a lognormal distribution similarly to the initial description of the composite properties E_1, E_2, G_{12} and ν_{12}.

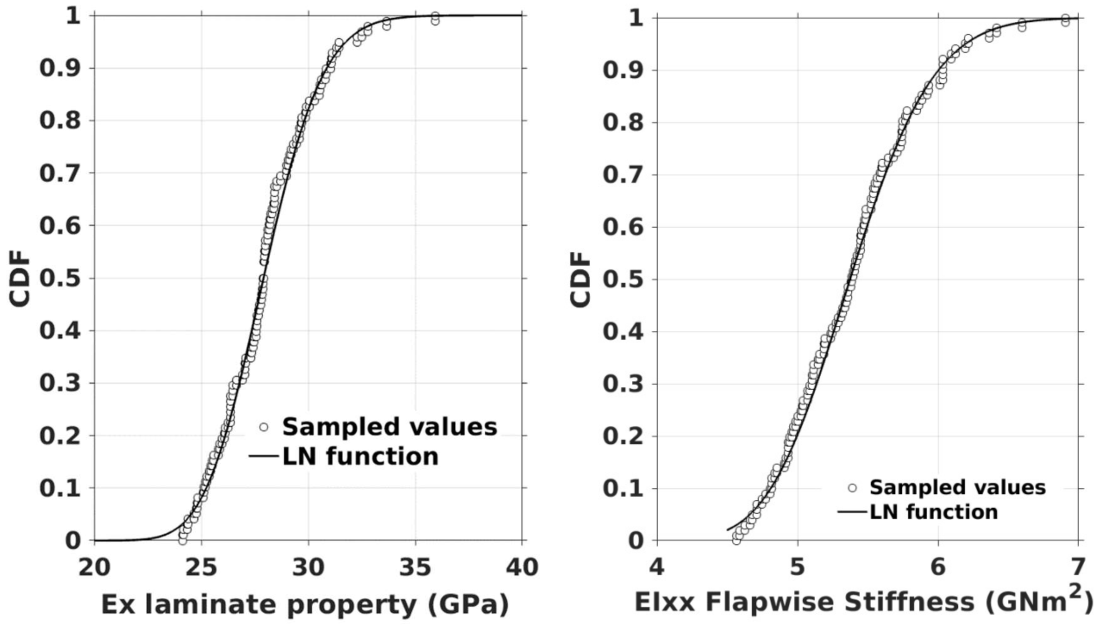

(a) **(b)**

Figure 3: (a) E_x effective laminate modulus of the spar cap at the suction side of the cross-section at r=14m, (b) EIxx flapwise bending stiffness sectional beam property at r=14m

Integrated sectional property	Min	Max	Mean	STD	CoV
Extensional stiffness EA	7.24E+09	1.07E+10	8.47E+09	7.25E+08	8.56%
Flapwise bending stiffness EIxx	4.57E+09	6.90E+09	5.39E+09	4.76E+08	8.82%
Edgewise bending stiffness EIzz	6.77E+09	9.87E+09	7.87E+09	6.52E+08	8.28%
Cross bending stiffness EI_{xz}	-1.02E+09	-7.27E+08	-8.35E+08	6.39E+07	-7.65%
Torsional stiffness GJ	7.54E+08	9.85E+08	8.78E+08	4.59E+07	5.23%
E_x effective laminate modulus of the spar cap	2.41E+10	3.59E+10	2.8E+10	2.22E+09	7.9%

Table 5: Statistics of the derived beam properties at section 7 (r=14m) and for the E_x effective laminate modulus of the spar cap.

Equivalent integrated beam properties for the NREL 5 MW blade are generated using the tools PRE-THIN [1] and THIN [2]. Specifically, PRE-THIN is using the detailed input for the material properties and the data for the lamination sequences used at each location on the section, and the effective properties of each laminate are calculated using Classical Lamination Theory (CLT) approach. The next analysis step is the basic processor, THIN based on thin wall beam theory, taking into account the in-homogeneity and the elastic anisotropy of the cross-sectional elements. The processor, estimates for each section of the blade the mass centre, the elastic centre, the shear centre and the sectional properties, through the input of the effective laminate properties derived through PRE-THIN. These might then be used with the aero-elastic FEM hGAST to simulate the behaviour of the wind turbine.

In this respect and in view of clarifying the specifics of the coordinate systems defined for the blade and beam, a short description follows. In this description the following are also included:

- the stress-strain relations for the sections and the equations for the stresses,
- the normal and shear stress definition
- the integrated stresses over any cross section of the beam structure, that resulted to the internal forces and moments
- the sectional stiffness properties and the inertial/mass properties that are integrated over the beam cross section

Let [**Oxyz**] denote the coordinate system with respect to which the beam axis in the un-deformed state coincides with the *y*-axis Figure 4. Axes *x, z* correspond to the two lateral bending directions. A beam structure subjected to combined bending in the two lateral directions *x* and *z* including shear and torsion and tension in *y* direction is considered.

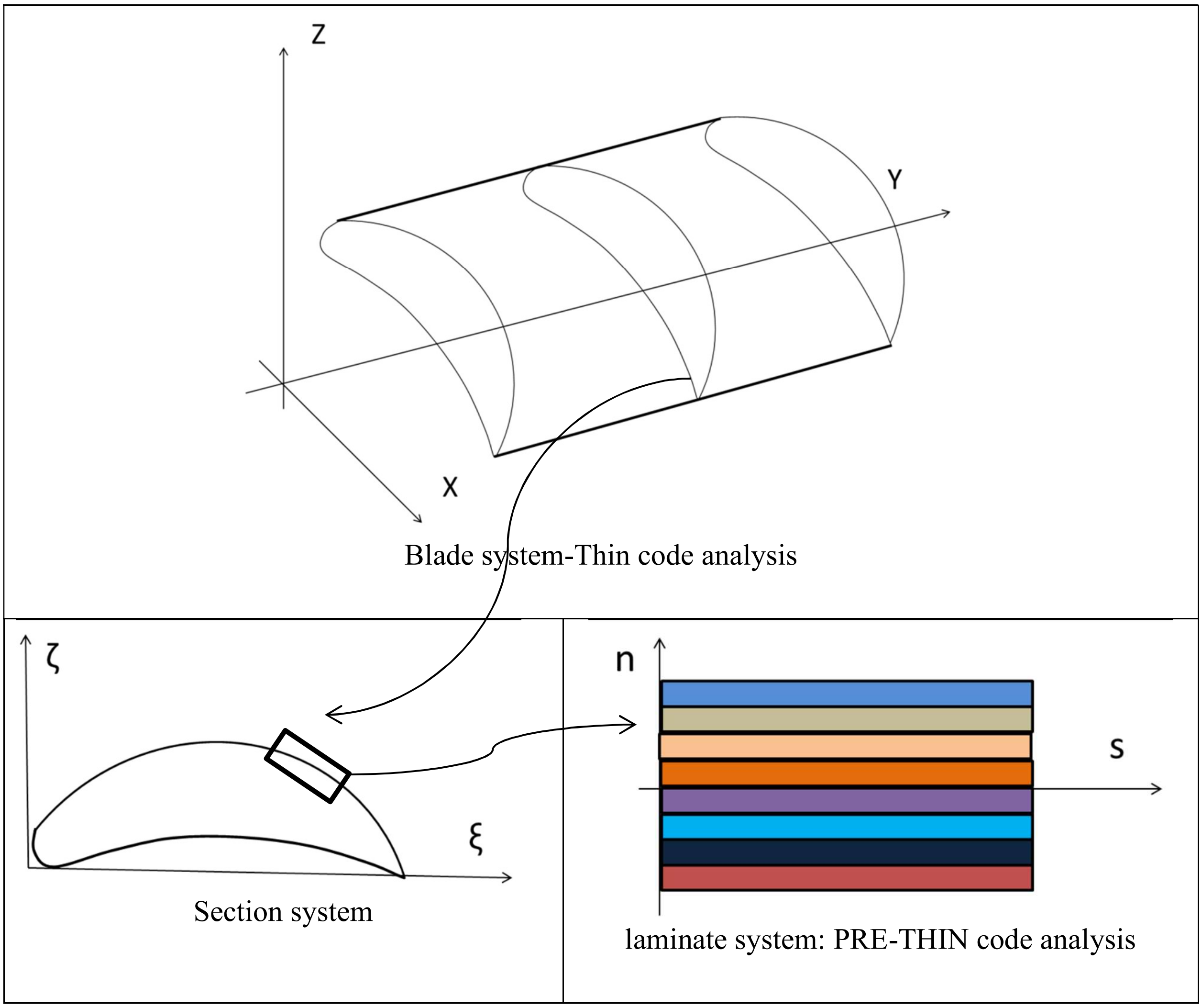

Blade system-Thin code analysis

Section system

laminate system: PRE-THIN code analysis

Figure 4: Coordinate systems definition of the beam

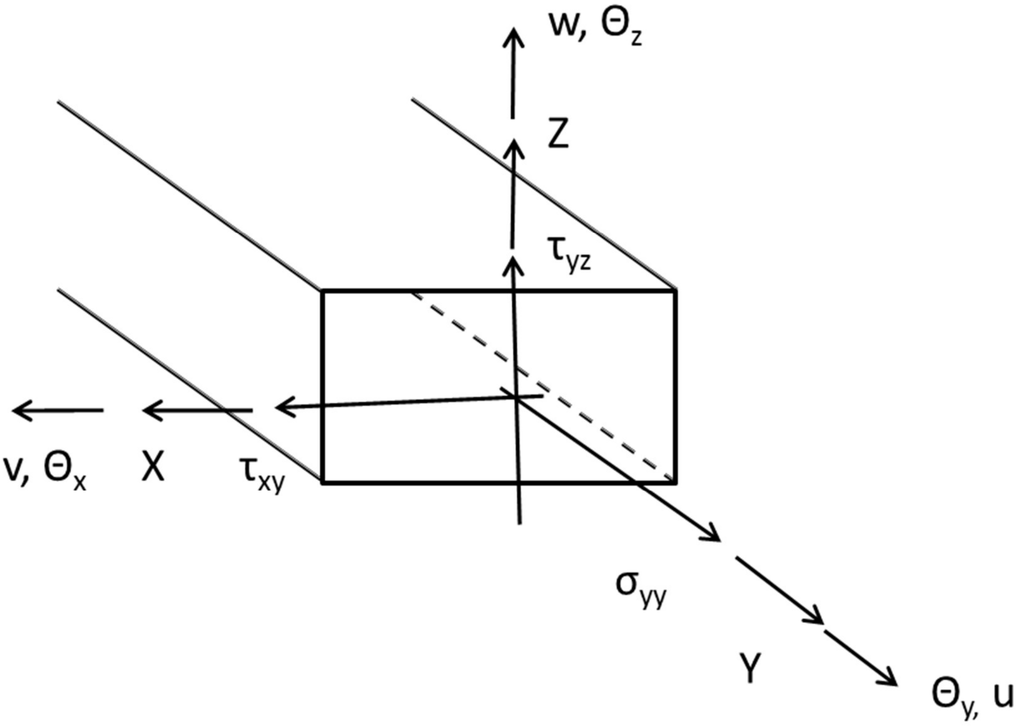

Figure 5: Coordinate system stress-strain definition of the beam section

In Figure 5, the two bending displacements *u*, *w*, the axial displacement *v*, the torsion angle θ_y and the bending rotation angles θ_x, θ_z which include the shear deflections, are defined. So, the displacement field $\mathbf{U} = (U, V, W)^T$ with respect to which strains are defined, is expressed.

$$\begin{pmatrix} U \\ V \\ W \end{pmatrix} = \begin{bmatrix} 1 & 0 & 0 & 0 & z_0 & 0 \\ 0 & 1 & 0 & -z_0 & 0 & x_0 \\ 0 & 0 & 1 & 0 & -x_0 & 0 \end{bmatrix} \cdot \begin{pmatrix} u \\ v \\ w \\ \vartheta_x \\ \vartheta_y \\ \vartheta_z \end{pmatrix} \tag{2.2}$$

Using the definition of Green's strains and Hooke's law for the stress-strain relation of an isotropic material, the following equations for the stresses are derived:

$$
\begin{aligned}
\sigma_{yy} &= E \cdot \varepsilon_{yy} = E \cdot \frac{\partial V}{\partial y_0} = E \cdot v' - E \cdot z_0 \cdot \vartheta'_x + E \cdot x_0 \cdot \vartheta'_z \\
\tau_{xy} &= G_x \cdot \gamma_{xy} = G_x \cdot \left(\frac{\partial U}{\partial y_0} + \frac{\partial V}{\partial x_0} \right) = G_x \cdot u' + G_x \cdot z_0 \cdot \vartheta'_y + G_x \cdot \vartheta_z \\
\tau_{yz} &= G_z \cdot \gamma_{yz} = G_z \cdot \left(\frac{\partial V}{\partial z_0} + \frac{\partial W}{\partial y_0} \right) = G_z \cdot w' - G_z \cdot x_0 \cdot \vartheta'_y - G_z \cdot \vartheta_x
\end{aligned}
\tag{2.3}
$$

where ε_{yy}, y_{xy}, γ_{yz} denote the Green's strains and σ_{yy}, τ_{xy} and τ_{yz} the corresponding stresses [Figure 5], E is the Young's modulus and G_x, G_z the shear modulus in x and z directions respectively.

By integrating the stresses over any cross section of the beam structure, the internal forces and moments are obtained which will be later on introduced in the dynamic equilibrium equations,

$$
\begin{aligned}
F_x &= \int_A \tau_{xy} dA = \int_A \left(G_x u' + G_x z_0 \vartheta'_y + G_x \vartheta_z \right) dA = GxA \cdot u' + GxAx \cdot \vartheta'_y + GxA \cdot \vartheta_z \\
F_y &= \int_A \sigma_{yy} dA = \int_A \left(Ev' - Ez_0 \vartheta'_x + Ex_0 \vartheta'_z \right) dA = EA \cdot v' - EAx \cdot \vartheta'_x + EAz \cdot \vartheta'_z \\
F_z &= \int_A \tau_{yz} dA = \int_A \left(G_z w' - G_z x_0 \vartheta'_y - G_z \vartheta_x \right) dA = GzA \cdot w' - GzAz \cdot \vartheta'_y - GzA \cdot \vartheta_x \\
M_x &= -\int_A \sigma_{yy} z_0 dA = \int_A \left(Ez_0 v' - Ez_0{}^2 \vartheta'_x + Ex_0 z_0 \vartheta'_z \right) dA = EAx \cdot v' - EIxx \cdot \vartheta'_x + EIxz \cdot \vartheta'_z \\
M_y &= \int_A \left(\tau_{xy} z_0 - \tau_{yz} x_0 \right) dA = \\
&= \int_A \left[\left(G_x z_0{}^2 + G_z x_0{}^2 \right) \vartheta'_y + G_x z_0 u' + G_x z_0 \vartheta_z - G_z x_0 w' + G_z x_0 \vartheta_x \right] dA = \\
&= GJ \cdot \vartheta'_y + GxAx \cdot u' + GxAx \cdot \vartheta_z - GzAz \cdot w' + GzAz \cdot \vartheta_x \\
M \; &= \int_A \sigma_{yy} x_0 dA = \int_A \left(Ex_0 v' - Ez_0 x_0 \vartheta'_x + Ex_0{}^2 \vartheta'_z \right) dA = EAz \cdot v' - EIxz \cdot \vartheta'_x + Ezz \cdot \vartheta'_z
\end{aligned}
\tag{2.4}
$$

The sectional stiffness properties of the beam structure are defined as,

$$
\begin{array}{lll}
EA=\int\limits_A EdA, & EAx=\int\limits_A Ez_0dA, & EAz=\int\limits_A Ex_0dA \\
EIxx=\int\limits_A Ez_0^2dA, & EIxz=\int\limits_A Ex_0z_0dA, & EIzz=\int\limits_A Ex_0^2dA \\
GJ=\int\limits_A\left(G_xz_0{}^2+G_zx_0{}^2\right)dA & & \\
GxA=\int\limits_A G_xdA, & GzA=\int\limits_A G_zdA, & \\
GxAx=\int\limits_A G_xz_0dA, & GzAz=\int\limits_A G_zx_0dA, &
\end{array}
\tag{2.5}
$$

Similarly, to the stiffness sectional stiffness properties obtained in (2.17), integration over the beam cross section *A* will give the following inertial/mass properties,

$$
\begin{array}{lll}
m=\int\limits_A \rho dA, & mx=\int\limits_A \rho z_0dA, & mz=\int\limits_A \rho x_0dA \\
mIxx=\int\limits_A \rho z_0^2dA, & mIxz=\int\limits_A \rho x_0z_0dA, & mIzz=\int\limits_A \rho x_0^2dA \\
Ip=\int\limits_A \rho\left(z_0{}^2+x_0{}^2\right)dA & &
\end{array}
\tag{2.6}
$$

In Table 5, the minimum, maximum and mean values of the main beam properties at a representative section located at r=14m are presented. Also, the STD and the CoV are presented in [Table 5]. The software tools PRE-THIN [1] and THIN take as input the composite material properties with a certain statistical distribution and information about the stacking sequence of the composite plies, over different cross sections of the blade. They output distributions of integrated beam equivalent properties along the blade span. In generating beam-like property distributions for the NREL 5 MW blade, the stacking sequence information defined in the framework of the UPWIND project [3] and the above reported material properties from the OptiDAT database [5] have been considered. Figure 3 presents the modulus E_x of a [0/45/90] laminate of the spar cap on the suction side of a cross-section. Specifically, the material properties needed as input are the mass density and the elastic properties of each orthotropic layer used in any lamination sequence in the section. These are the elasticity modulus in the two main directions of the orthotropic medium, the in-plane Poisson ratio and the in-plane shear modulus of the layer. These are used to estimate the homogenized multi-layer construction effective properties: the total thickness of the laminate, the mass density and the elasticity and shear moduli on the primary laminate axis which is usually the blade axis. Also Figure 3 presents the sectional bending stiffness in the flapwise direction, EA and EIxx. The latter are both located at a radial distance r=14m from the blade root. The stochastic nature of the material characteristics assumed for the laminate effective mechanical properties is also reflected on the integrated properties per laminate and on the overall cross-sectional beam properties as indicated by the fitted LN distribution function.

The usual first step in performing a dynamic analysis for a W/T structure is to determine the natural frequencies and mode shapes of the W/T. They characterize the basic dynamic behavior of the structure and identify how the structure will respond to the external dynamic loading. For the rotating wind turbine, it is important to determine if the operating frequencies of the W/T rotor come close to one of the natural frequencies of the whole structure. In such a case, structural damage or failure due to resonance may occur.

The effect of the beam material properties on the eigenvalues of the W/T is shown in Figure 6 together with the corresponding CoVs. By randomly combining the different material properties, 96 different blades are defined. These blades have different concentrated structural properties which result in different natural frequencies for the combined wind turbine structure. These different frequencies are illustrated in Figure 6 a) for all the 96 different blade structures. Also, in Figure 6 b) the coefficient of variation for every frequency is compared to the natural frequency of the reference blade. The list includes the tower longitudinal mode (fore-aft) and lateral (side-to-side) bending, the drive train torsion, the flapwise and edgewise yaw, the flapwise and edgewise pitch and the collective flapwise mode. In Figure 6(a) the eigenvalues of the reference and of all the 96 sets of material properties with CoV between 2.5% and 4.5%, are drawn while in Figure 6(b) the coefficient of variation for every eigenvalue is given. The tower longitudinal frequency does not change that much (CoV = 1%), but all the other eigenvalues exhibit coefficients of variation above 2.5%. So, the eigenvalues of the W/T are not affected seriously from the stochastic variability of the material properties of the blade.

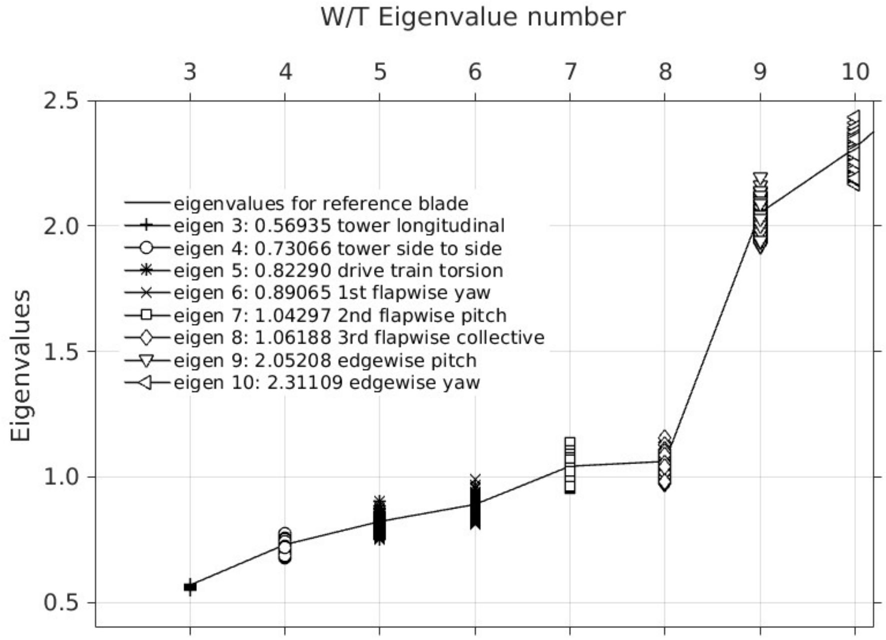

(a)

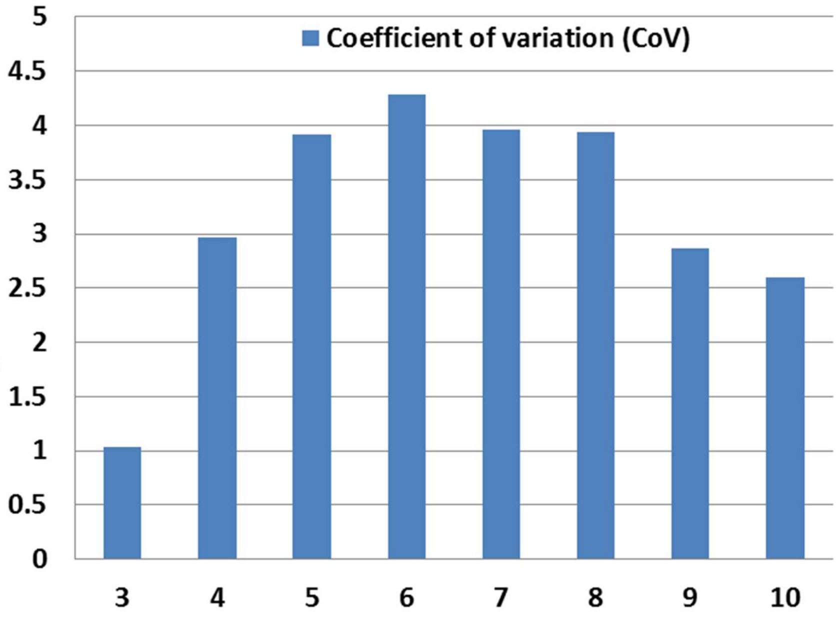

(b)

Figure 6: (a) Onshore NREL W/T eigenvalues of blade with reference and StoMP (b) table with CoV (STD/mean*100) for the first 10 eigenvalues of the blade with StoMP

In Figure 7, all the beam properties of section 7, at r=14m from the blade root are presented for all the different material sets including the reference ones, indicated by the vertical lines that are the mean values of the different blade properties selected.

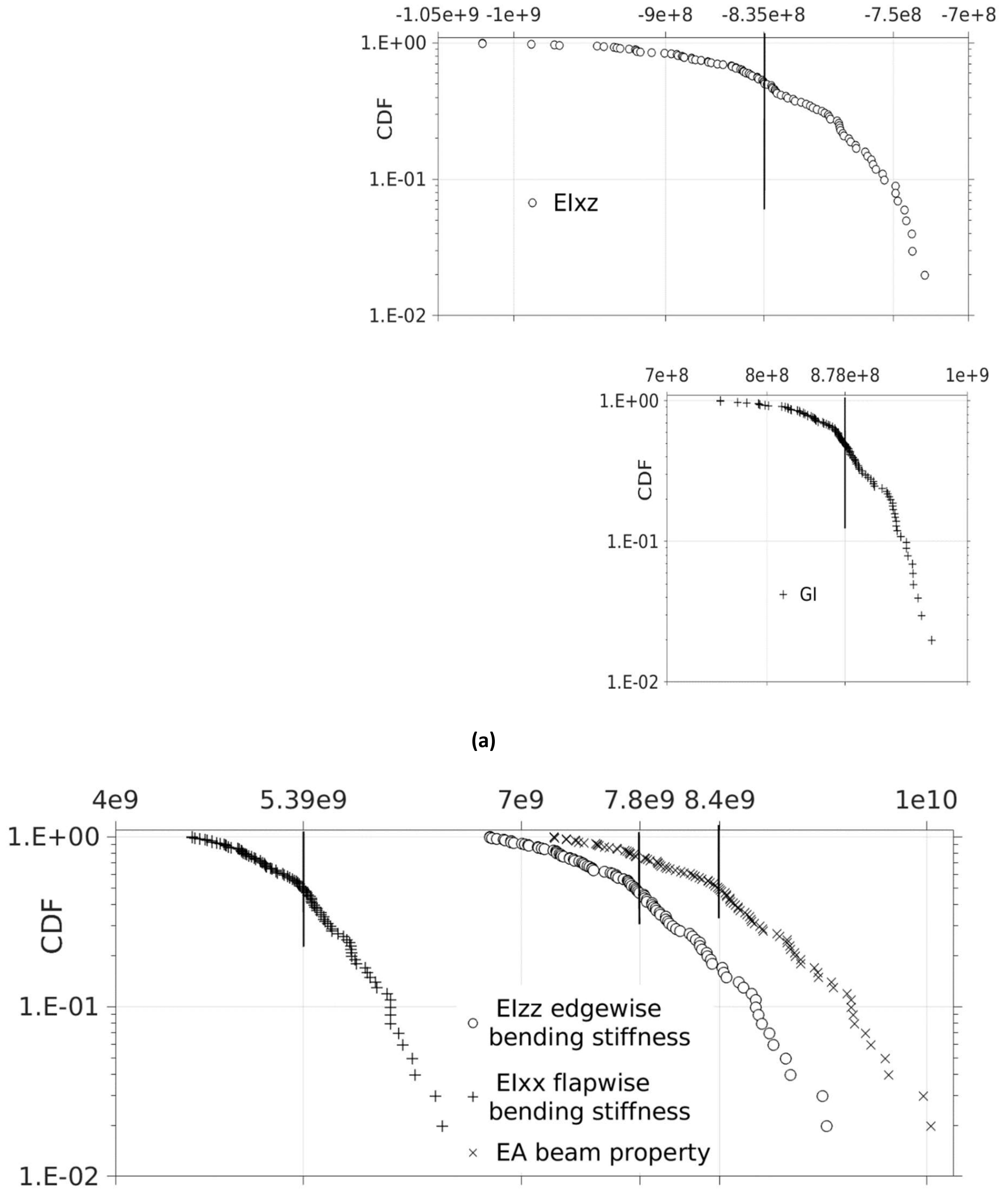

Figure 7: Beam properties for section 7, 14m from the blade root with the reference blade data and the StoMP for the NREL W/T (a) EIxz cross bending stiffness and GIt torsional stiffness (b) EIzz edgewise bending stiffness, EIxx flapwise bending stiffness and EA extensional stiffness beam properties

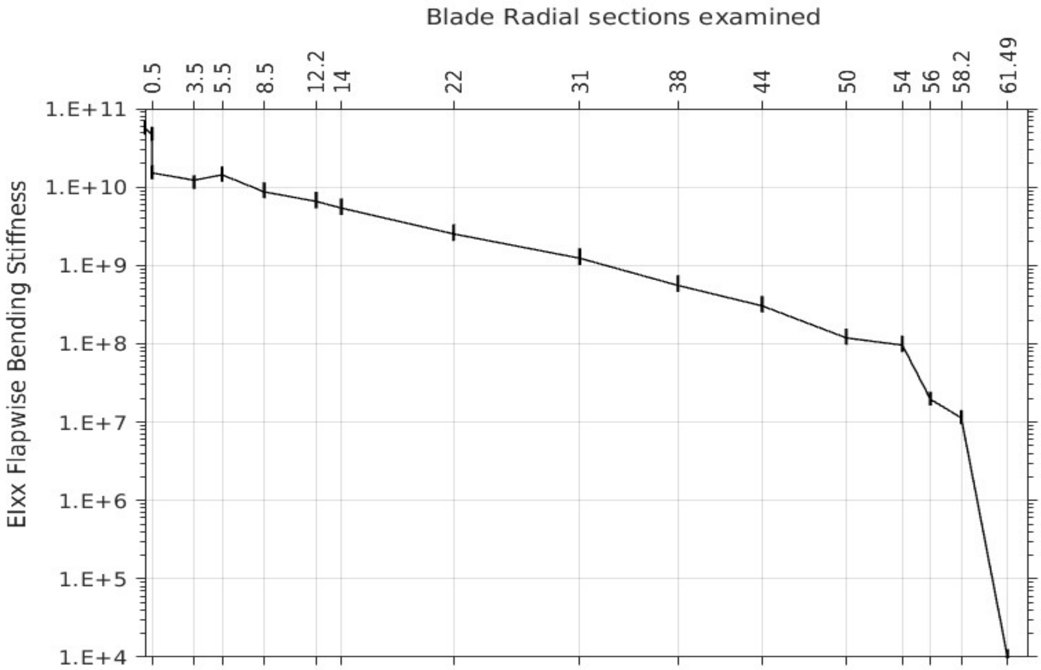
Blade Radial sections examined
0.5
3.5
5.5
8.5
12.2
14
22
31
38
44
50
54
56
58.2
61.49
EIxx Flapwise Bending Stiffness
1.E+11
1.E+10
1.E+9
1.E+8
1.E+7
1.E+6
1.E+5
1.E+4

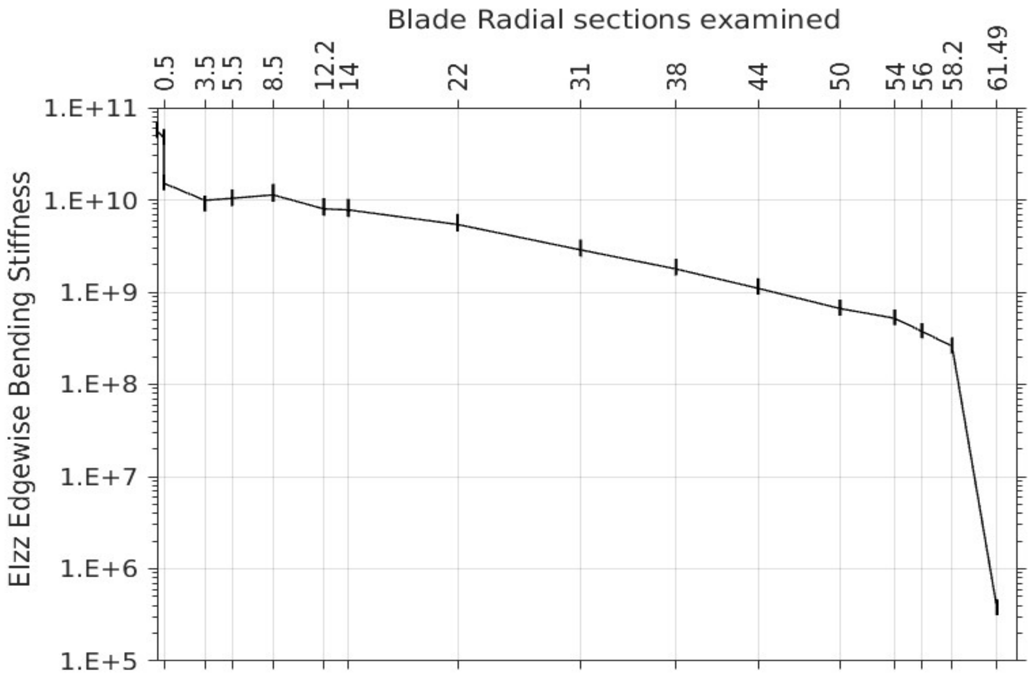
Blade Radial sections examined
0.5
3.5
5.5
8.5
12.2
14
22
31
38
44
50
54
56
58.2
61.49
EIzz Edgewise Bending Stiffness
1.E+11
1.E+10
1.E+9
1.E+8
1.E+7
1.E+6
1.E+5

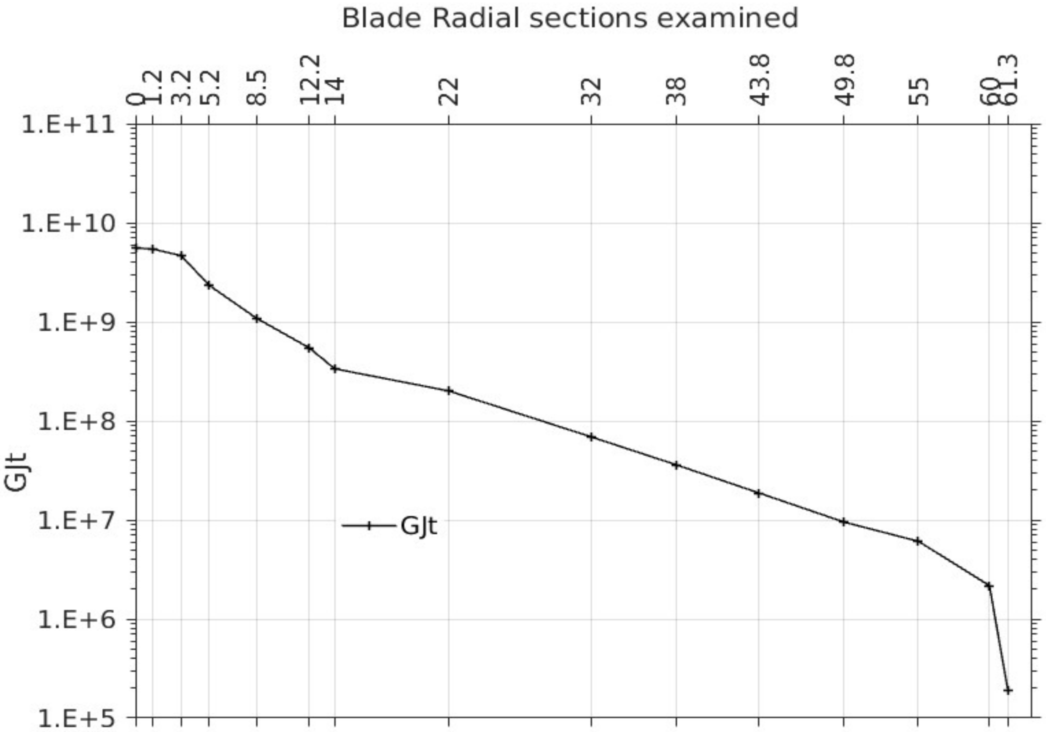
Blade Radial sections examined
0
1.2
3.2
5.2
8.5
12.2
14
22
32
38
43.8
49.8
55
60
61.3
1.E+11
1.E+10
1.E+9
1.E+8
1.E+7
1.E+6
1.E+5
GJt
GJt

(a)

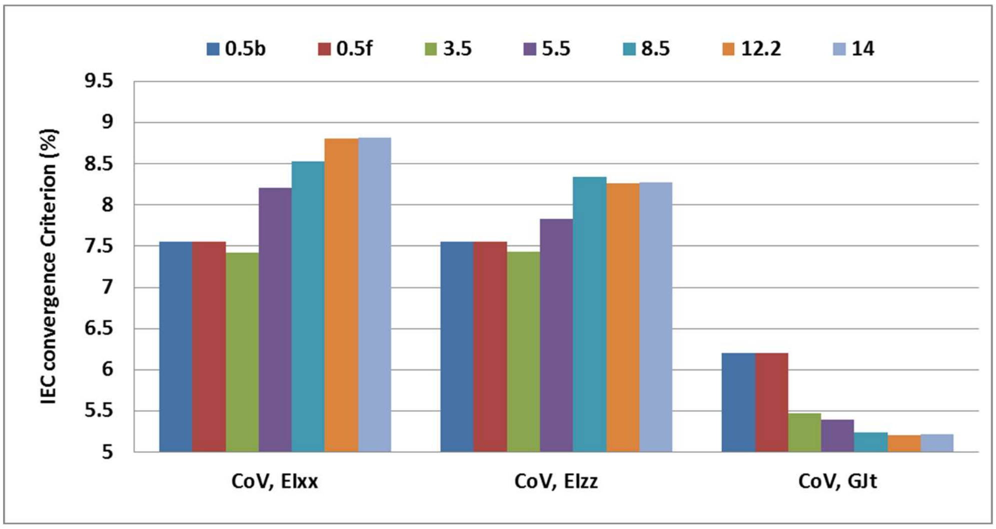
0.5b
0.5f
3.5
5.5
8.5
12.2
14
9.5
9
8.5
8
7.5
7
6.5
6
5.5
5
IEC convergence Criterion (%)
CoV, EIxx
CoV, EIzz
CoV, GJt

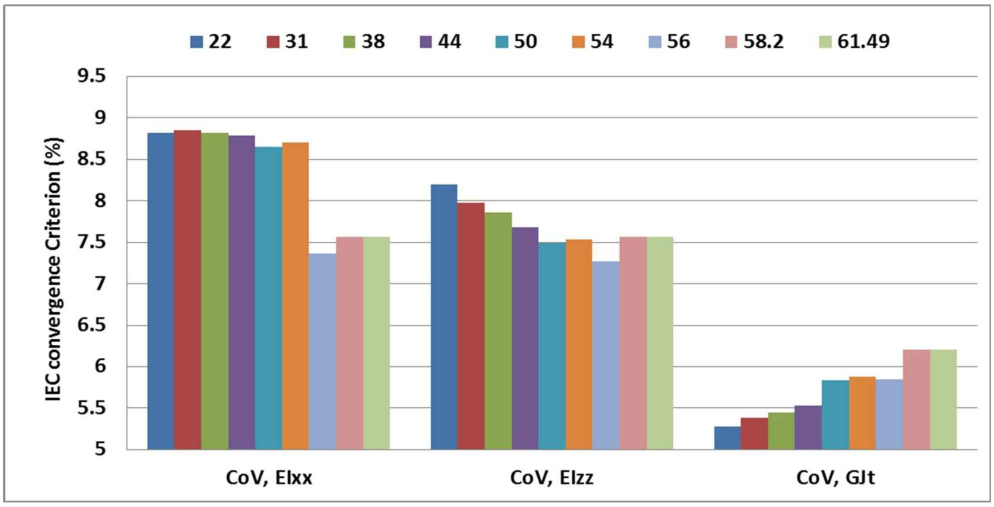

(b)

Figure 8: (a) EIxx, bending stiffness of the blade to the flapwise direction, EIzz to the edgewise direction and GJ to the shear direction for all sections of the blade examined to hGAST FEM code for the NREL W/T (b) table with CoV of the EIxx, EIzz and GJ beam properties with the StoMP along the Blade radial sections

In Figure 8 the flapwise bending stiffness EIxx, the edgewise bending stiffness EIzz and the shear bending stiffness GJ are illustrated along the blade span for the stochastic blade material properties with dots for all different blades, while the reference continuous lines stand for the blade with RefMP, which are the mean values of the OptiDAT database. The shape of the beam properties for all sections is the expected one. All properties reduce their magnitude from root to tip which is consistent with the chord reduction. Also, the edgewise bending stiffness EIzz is expected higher than that in the flapwise direction EIxx, due to the small thickness/chord ratio. Finally, the distribution of the torsional stiffness property resembles to the other beam properties, as it is reduced from the blade root to tip but with a faster pace.

Additionally, the CoV for EIxx, EIzz and GJt are included in tabular form. CoV (EIxx) is between 7.3% and 8.8%, CoV (EI$_{zz}$) is between 7.2% and 8.3% which is a narrow range compared to EIxx. CoV (GJ) is also in a narrow range of 5.2% - 6.2% which is lower compared to the range of the other properties. All the beam equivalent properties of the blades with StoMP have CoV values in between 5.2% and 8.8% for the E_1, E_2, G_{12} and ν_{12} composite materials with CoV equal to 10%, which was the value initially assumed from the mean values of the OptiDAT database.

Blade radial section	CoV, EIxx	CoV, EIzz	CoV, GJ	Blade radial section	CoV, EIxx	CoV, EIzz	CoV, GJ
0.5b	7.56	7.56	6.2	22	8.82	8.2	5.28
0.5f	7.56	7.56	6.2	31	8.85	7.98	5.38
3.5	7.42	7.43	5.47	38	8.82	7.86	5.45
5.5	8.21	7.83	5.39	44	8.79	7.68	5.53
8.5	8.53	8.34	5.24	50	8.65	7.49	5.84
12.2	8.81	8.26	5.21	54	8.70	7.53	5.88

14	8.82	8.28	5.22		56	7.36	7.27	5.85
					58.2	7.56	7.56	6.2
					61.49	7.56	7.56	6.2

Table 6: CoV of the EIxx, EIzz and GJ beam properties with the StoMP along the Blade radial sections

2.4 Conclusions from the stochastic composite material properties chapter

By comparing the OptiDAT database which was created from a sufficient number of experiments and is the most recent one, against the UPWIND and MEGAWIND ones, the following conclusions can be drawn regarding the statistical characteristics of composite material properties:

- The LN is one of the most efficient choices for most of the properties and therefore its selection is made in the present thesis – next comes N
- Out of the various property correlations, only the E_1-XT correlation was found to be significant and positive in sign. For the positively correlated properties E_1-XT, when any of the values E_1 are increased, then the corresponding value of XT is increased for the specific composite material compared to another. The correlations between E_2-YT and shear G_{12}-S properties depict a rather multifold trend.
- New materials (OptiDAT, UPWIND) present on average, higher strength and upgraded elastic properties compared to the older ones (MEGAWIND). This was attributed to different constituents of unidirectional plies as well as to improved manufacturing processes that were followed to construct the coupons.
- Amongst the various sources of uncertainty, extreme conditions (e.g. high temperature – thermal effect) and salinity as a contributor to ageing should be added since they greatly influence the strength properties of glass FRP materials [13]. This is especially true for the compressive and shear strength properties.

Specifically, the blade material properties, namely the tensile modulus of elasticity E_1 along the direction of the fibres, the tensile modulus of elasticity E_2 vertical to the direction of the fibres, the major Poisson ratio ν_{12} and the in-plane shear modulus of elasticity G_{12}, are varied according to the composite databases following a log-normal distribution. The estimated blade extreme load, the deflection results as well as the stress resultants obtained for the different material properties, are compared to those corresponding to the RefMP. The E_1, E_2, G_{12} and ν_{12} properties vary with CoV 10% for all, the laminate properties and the beam properties of the blade vary with CoV between 5% and 9%, as shown in Table 5.

3. Certification process of wind turbines

3.1 Modern issues on certification process

Part of wind turbines’ certification concerns the estimation of extreme loads corresponding to a 50-year return period. Because ultimate loading is usually driving the blade design, estimation of extreme loads is a decisive step in the design verification process. Due to the stochastic nature of the wind inflow, W/T extreme loads can only be obtained through statistical processing, and thus the resulting values of loads depend strongly on the applied method.

Substantial research efforts ([8], [12], [19]-[22], [24]-[30], [32]) were directed towards load uncertainty investigation. The point was to represent efficiently the turbulent wind conditions, meaning wind speed and turbulence, and by that estimate extreme wind loads. Statistical load extrapolation techniques were used to take into account the aforementioned uncertainties and further build probabilistic models for the developed extreme design values at a section. Research results were already adopted in IEC 61400-1, 3rd edition [17] while further enrichment was followed in its amendment [18].

In the current version of the IEC Standard 61400-1, 3rd edition [18], the statistical process for deriving extreme loads is linked to the Design Load Case (DLC) 1.1, which scans the full range of power producing wind speeds and conditions under Normal Turbulent Inflow modeling. The procedure starts by dividing the power producing range of wind speeds into bins and proceeds with the following steps: a) for every wind speed bin a number of 10min aero-elastic simulations are performed, b) peak loads are extracted from these 10min simulations and c) a probability distribution function is fitted to the above peak-load data, which by extrapolation provides an estimate of the extreme load for the 50 years specific period.

Although Annex F of the standard makes reference to the work by NREL [8], in which different distribution functions are fitted to POT data, a degree of flexibility is provided to the designer to freely choose the details of the statistical procedure to be followed in deriving extreme load values. Besides that, the minimum number of required simulations for reliable extreme value estimations is not strictly specified. In addition to the work by NREL [8], several research and review papers have addressed the issue of load extrapolation and statistical extreme load value estimation.

The extrapolation methods can be divided into three main categories: the peak methods, the process method and the inverse first order reliability method. The peak methods category includes the most used and studied load extrapolation methods namely the GM, the block maxima (BM) and the POT method. The difference between these methods lies on the amount of extracted data from a single simulation (time series). It is important to mention that the load time series are usually obtained either by performing intensive aero-elastic calculations or directly as measured data from operating wind turbines. Several reviews can be found using both types of data. In most of the research efforts ([8], [12], [19]-[22], [24]-[30], [32]) aeroelastic simulations have been used. Although in [19] measured were used, a comparative study highlighted great discrepancy on the estimated extreme loads [20].

Concerning the peak methods, of major concern is the accumulation of a sufficient number of local maxima, saving as much as possible computational time [8]. For the GM method, only one value, the maximum load value, is extracted from an entire 10 min simulation. Thus, a lot of simulations may be required in order to get sufficient samples. On the other hand, in the POT method, a threshold is defined and the maxima are collected between successive up-crossing of the respective threshold. A considerable number of local peaks are gathered from every simulation instead of the one only maximum of the GM method.

However, attention on the threshold selection must be given. A too low threshold value would yield a great number of data making dubious whether these data belong to the extremes [8]. Alternative methods of getting maxima have been also proposed e.g. in [21] where one maxima was extracted per blade revolution. A requirement for all the aforementioned methods is that the extracted maxima must be statistically independent. For this reason, a separation interval of 10-15 sec between successive maxima is often introduced for the POT method to ensure further independence, see e.g. [22]. However, in [19], minor effect is mentioned by positively correlated local maxima, on the characteristic load values that are estimated when performing load extrapolation.

The issues that are related to the necessary number of aeroelastic simulations and to the selection of the appropriate threshold for the POT methods are constantly investigated. Also, the choice of a parametric distribution in order to perform load extrapolation is of vital importance for the certification process. Accordingly see e.g. [26] for the simulations number, [19] for the threshold selection and [19]-[27] for the appropriate model of the cumulative distribution function.

Using the extracted maxima for several wind conditions, a parametric distribution is fitted to the data and short-term distributions of the extreme load are estimated. These short-term distributions are conditioned by both environmental conditions and reference period. The long-term probability of the extreme load for a specified time period is estimated with extrapolation. Each short-term distribution participates into the resulting probability according to the occurrence in the specific wind speed bin. Finally, all of the long-term predictions are gathered in one bin to build the total long-term distribution. That whole method is called fitting first and aggregation afterwards. In addition, an alternative method has been proposed in [18]. According to that, the sufficient number of 10 min simulations for every wind condition is calculated according to the probability of occurrence for the specific wind conditions. So, the empirical long-term distribution is formed by aggregating all the extracted maxima. A parametric distribution is fitted to the aggregated data and extrapolation is next performed. So, this method is called aggregation first and fitting afterwards. A comparative study is presented between the two distinct approaches in [22]. It is proposed that better estimations are acquired when parametric distributions are fitted to the extracted maxima firstly and the distributions are aggregated afterwards.

Research effort has been also put on the process model approach; see e.g. [21], [24]. Accordingly, the distribution of the extreme loads for a reference period of 10 min may be estimated by relating a W/T load (like the flapwise moment) to an associated Gaussian process. The flapwise moment of a 10 min simulation is a non-Gaussian process, which is associated to a Gaussian one via Hermite polynomials and up to four higher order moments.

Another category under the name ‘inverse first order reliability method’ IFORM constitutes a totally different approach compared to the other extrapolation methods. In this method, turbulence and W/T response simulations are carried out for Normal Turbulence Model (NTM) conditions. A minimum of 15 simulations should be carried out for wind speeds ranging from $V_{rated} - 2$ m/s to the cut-out. Firstly, wind conditions with higher blade loads are identified. While the environmental conditions are given, the extrapolation of the short-term load distribution is performed for the probability level of the desired fifty years return period. The convergence criteria for IFORM should be the same as for the other extrapolation methods, except that the designer needs only to estimate confidence intervals for the load distributions from already identified important wind speeds, which is often only one. Further information can be found in [25], [12], [13], and [14].

In [19], field data from a utility-scale 1.5MW turbine operating at Lamar, Colorado were used in comparing the performance of several alternative techniques for statistical extrapolation of rotor and tower loads. The method of GM, the POT method, and a four-moment process model approach were used and then fifty-year return loads were estimated. The conclusion is that the peak-over-threshold method is better, and important details are examined for this method. These details include the selection of the threshold level to be employed, the parametric distribution used in the fitting, and the assumption of statistical independence between successive peaks. While the prediction of extreme loads is of high interest, also vital is the assessment of the uncertainty in the predictions as a function of the amount of data used. Towards this end, estimations of extreme loads associated to target reliability levels based on all of the available data, were presented together with similar estimates obtained with subsets of the data. From these estimates, conclusions are drawn regarding the sufficient amount of data in order to make a reliable statistical extrapolation so the uncertainties on extrapolated results decrease gradually with increasing size of dataset. The peak-over-threshold method yields far superior results in comparison to the other methods. The use of an “optimal” threshold leads to better fits in comparison to the fit obtained with threshold “mean” ± 1.4STD. The Weibull 3-parameter distribution performed consistently well for peak-over-threshold (POT) data. The Generalized Pareto distribution for use with POT data was unstable in some cases, particularly for tower bending moment. The requirement of a minimum time separation between peaks in the POT method has a slight impact on extrapolated long-term load predictions, and has the disadvantage of significantly reducing the available amount of data. Uncertainties on extrapolated results decrease gradually as the size of dataset increases. Additional studies with different field datasets and/or using simulated loads data are necessary to verify the conclusions from limited field data. Especially, in the case of studies based on simulated loads data, useful recommendations can be gained for statistical loads extrapolation.

In [20] the data from load and meteorological recordings obtained at a test site with five 2.5 MW turbines were considered. Extreme load extrapolation was applied on the flap-wise bending moment at blade root and the fore-aft tower bottom bending moment. Attention was paid to the selection of the extreme value probability distribution and the amount of data needed. This study offers the unique opportunity to compare simulations against measured data, with respect to extreme loads, using on both data series, the same statistical methods. The selection method used one maximum per time series, which is the global maximum approach. It is concluded that fifty maxima per wind speed bin are sufficient to estimate the extreme load distribution.

The calculated flap blade root bending moment was found smaller than the measured one while the calculated fore-aft tower bottom bending moment was found larger. It is noted that differences appeared in free, partial and full wake effect conditions, suggesting the need for a deeper insight in wind, wake and aeroelastic modeling for explaining the differences between calculations and measurements.

In [21] a procedure for determining the extreme response distribution of an offshore 3 MW W/T was presented. The statistical description of the offshore environment was described with hind cast data. In order to determine the distribution of the extreme responses, the GM, the POT and the process model approaches were applied. The processing model uses statistical properties to predict the extremes. All three methods led to similar conclusions, but POT and the processing model required fewer simulations than GM. The 100-year responses obtained with these reliability-based models were compared to results from a deterministic model. It was found that the deterministic model predicts smaller maximum flapwise moment for the W/T but higher the maximum overturning moment of the support structure as compared to the reliability-based methods.

In [22], methods of statistical processing and load extrapolation were assessed. Simulation data were produced by means of a Gaussian model, having spectral characteristics that resemble those of the flapwise bending moment of a W/T blade. The maximum values of Gaussian models follow an analytic expression given by the Rice equation [23] which constitutes a good basis for comparing maximum value extraction methods. In [22], the methods of GM, the Block Maxima and the POT with load limits equal to the mean plus 1.4 and 2.0 times the STD were compared. The POT with the 'mean' + 1.4 STD threshold was found to have the smallest deviation (+0.5%) from the analytic solution, which increased to -6.1%, when the 2.0 STD threshold was used, indicating the significant influence threshold may have. Next, fitting before and after collection of all the peak values from all twelve wind speed bins was compared. It was found that 'fitting before aggregation' gives characteristic loads with smaller deviations from the analytic solution and therefore is preferable. The Maximum Likelihood Estimation method was used for the parameter estimation in the statistical analysis of the data, while the two and three parameter Weibull (2pW and 3pW), the Normal, the Rayleigh and the Gumbel probability functions were applied as fitting distributions. Finally, the 3pW was chosen as the most appropriate. The importance of the number of data sets was investigated by considering 25, 50, 75 and 100 simulations per wind speed bin each of 10min duration. Overall, it was concluded that the larger the number of simulations is, the better convergence of the extreme load value is.

In [26] questions concerning the minimum number of required ten-minute turbine simulations were addressed. Also, the question of whether only a single (global) maximum load from each simulation should be saved instead of several time-separated (block) maxima. Regarding the data processing, since all turbine loads are not influenced by each wind speed between cut-in and cut-out to the same degree, the simulation effort focused on winds that modulate the largest loads for each load type. Using global and block maxima for four load metrics from aeroelastic simulations on a 5 MW turbine model, the short-term load distributions were presented as a function of wind speed. Block maxima for different block sizes (time separations) were tested for independence and empirical load distributions were compared. A proposal was presented addressing load extrapolation with focus on efficiency and on how to employ either global or block maxima method. This proposal provides the convergence criteria in order to decide the adequate number of simulations that should be performed for the long-term load prediction extrapolation method.

In [27] the estimation of extreme loads was considered in the context of the new edition of the IEC standard 61400-1:2005 for four new models of multi megawatt wind turbines of different design concepts and different manufacturers. The blade root bending moments and the tip deflection data were analyzed with different extrapolation methods. In terms of loads extrapolation, log-normal and three-parameter Weibull fitting provided more reliable results than GEV and Gumbel, which may lead to too conservative results. This result is supported by comparisons to long-term simulations. Visual tail fitting did not result in significantly improved fits. The extrapolated maximum tip deflection increased by 12–20% for the log-normal and Weibull distributions, in comparison to the IEC 61400-1:1999 loads. The flapwise moment increased by 7–20% and the minimum edgewise bending moment by up to 38%. A significantly increased amount of computation time and pre-/post-processing is required to achieve realistic and reliable results. The judgement of the goodness of fit requires visual inspection. Although the presented methods are mathematically correct, the variability and interpretability of the results require an in-depth analysis for any application case.

Also, in [27], the effect of the Extreme Turbulent Model (ETM) definition on the estimated loads was addressed with respect to turbulence intensity and the resulting system control. Control strategies can introduce non-linearities in the data distribution. It was found that switching from regular to advanced control strategies (active vibration damping and individual pitch) does not significantly change the overall load levels in comparison to IEC 61400-1:1999 load. In order to match the log-normal extrapolated load level, the scaling factor c in the ETM was set to 3.27 and 3.32 (advanced control), while the value is 3.49 for regular control. The final load levels (DLC1.3 loads based on these c values) exceed the IEC 61400-1:1999 levels for the tip deflection by 15 and 20%, and for the flapwise moment by 9 to 25%. The tip deflection was the ‘design driver’ for the advanced control cases and the minimum edgewise moment for the cases of regular control. For the final load levels, there exist no clear tendencies in the results for advanced versus regular control strategies.

In [28], simulations that cover 63 years of the NREL 5MW offshore W/T operation were reported. This by far exceeds the provisions of the IEC code which recommends simulations of one hour and extrapolation to fifty years of lifetime. Such a long period corresponds to an unprecedented amount of load simulations which cannot be carried out routinely. In practice, a much smaller number of simulations are performed and then probabilistic extrapolation techniques are applied in order to extract fatigue and extreme loads. However, such a probabilistic procedure may involve substantial statistical errors. Therefore, the specific data base offers a benchmark set of data against which load extrapolation techniques can be calibrated. It can also be the basis for substantiating answers to practical questions such as “what is an adequate number of simulations needed for reliable extrapolation?”

In [29] the uncertainty of the aerodynamic lift and drag coefficient on extreme loads was assessed. The certification code IEC61400-1, about the extremes recommends a CoV of 10% for the aerodynamic lift and drag polars. The paper indicates that this value of the CoV is appropriate for certain components of the turbine, while conservative for other. The uncertainty in the aerodynamic response was introduced by expressing the polars of the airfoils in parametric form in which the parameters follow a statistical distribution. The CoV of these distributions can be determined through simulations, measurements or even through simple engineering judgment. It is concluded that, although the airfoil aerodynamic characteristics significantly affect the peak loads in power production conditions, they do not affect as much the loads in parked/idling ones.

In [30], the effect of the uncertainty of the turbulence model characteristics on the blade and tower loads is assessed on the basis of different control strategies. Three different controllers were tested; a) a baseline pitch variable speed controller with no load alleviation features, b) a pitch variable speed controller with additional cyclic pitch and static thrust limiter features and c) a pitch variable speed controller with individual pitch control, condition based thrust limiter and active tower vibration damper. It is concluded that the uncertainty of the extreme turbulence model is balanced by the controller when more advanced load alleviation features are added to it. It is also found that the control strategy affects the shape of the Cumulative Distribution Function (CDF) of the load, because the extreme load values are limited by the load management features of advanced controllers.

In [32], it is mentioned that the extrapolation techniques used for predicting long-term W/T loads, have produced highly varying loading estimates depending on the individual designer implementation. In order to test loads extrapolation techniques used in W/T design, two data sets were created. The first data set was collected following the typical process designers use in order to extrapolate loads according to W/T design standards. The second data set consisted of a series of year-long simulations used to quantify the accuracy of extrapolation methods. The wind speeds with the highest loads were identified, for all types of loading. For the in-plane loads and deflections the dominant speeds were found near cut-out while for the out - of plane loads and deflections wind speeds around rated conditions dominated. The other loads were influenced by a wide range of wind speeds. It is concluded that the loads that are dominated by higher wind speeds exhibit higher variability in their extreme values. This reflects the highly varying wind and also the greater sensitivity to higher wind energy content.

There are also simplified methods described to obtain design loads without extrapolation in order to reduce the effort for post processing and simulations. Such simplified methods are the scaling factor and the STD Multiplier method alternative to extrapolation process. Concerning the Scaling Factor, the characteristic load obtained from IEC DLC1.1 is multiplied by an additional scaling factor. The STD Multiplier method assumes that the scaling factor method can be modified by taking the STD of the characteristic loads into account. A new factor is calculated from the multiplier for the STD. The DLC1.1 characteristic load with the corresponding STD factor calculates the 50-year design loads.

In the above-mentioned works, various aspects of the ultimate load estimation procedure are discussed without accounting for the uncertainty of the structural properties. This is particularly relevant for the components made of composite materials (i.e. the blades) and mainly attributed to the manufacturing process. In the present work, the effect of the manufacturing uncertainty (chapter 2) on the estimation of the ultimate loads is assessed. To this end, two databases of simulated loads are generated and the corresponding ultimate load estimations are compared. The first database refers to reference blade structural properties, while the second to properties sampled from their log-normal (LN) distribution. In addition, the process for estimating the design values (chapter 3) - (chapter 4) has been assessed in terms of its numerical implementation and selection of appropriate peak extraction method and fitting cumulative distribution function. In this regard a) the GM and POT (with 1.4 threshold) peak extraction methods are used and compared, b) the LN, 2pW and 3pW CDFs for peak data fitting are considered and evaluated on the basis of the K-S test, c) the convergence with respect to the number of simulations per wind speed bin and d) the convergence of the extreme load in connection to the IEC criterion are addressed. The main novelty of the present contribution lies in the investigation of the effect of the variability of the blade structural properties on the extreme blade loads and tip deflections. In addition, the considered time series of loads and deflections have been obtained using a state-of-the-art, fully coupled aero-elastic solver that accounts for geometric nonlinear effects. Consequently, the extracted peak values are of higher accuracy, as compared to those obtained by employing ROMs based on modal truncation as done in previous studies. So, the present work also concerns the verification of the procedure for estimating extreme loads by means of higher fidelity modelling.

3.2 IEC certification code

Certification of wind turbines is described in the IEC code [17] and [18]. One of the main issues examined in the IEC code is the prediction of the maximum design load with a probability of occurrence once for over 50 year of W/T operational life. There is extensive literature on the IEC 61400 certification code. A number of studies were mentioned in section 3.1, that approach the issue of extraction and extrapolation from different perspectives.

The IEC 61400 [17] is suggesting to calculate 10-minute simulations, for wind conditions between V_{in} and V_{out} ($V_{in} < V_{hub} < V_{out}$) according to Normal Turbulence Model (N.T.M.). Concerning turbulence modeling, the Kaimal and the model of exponential consistency are used. Annex F refers to the ‘characteristic design load case’ and to the probability of maximum load 'F_{ext}', in time observation interval 'T' defined as:

$$\mathrm{Prob}\left(F_{ext},F|V,T\right)=1-\left(F_{max}\left(F|V\right)\right)^{E(n|V,T)} \tag{3-1}$$

Where 'F_{max} (F|V)' is the short-term probability distribution of local maximum loads, that appeared. 'E(n|V,T)' is the number of maximum values that were observed in time period 'T'. The long-term probability and obtained from calculations at all wind speed bins and integration over the whole wind speed range. This is expressed as:

$$\begin{gathered}\mathrm{Prob}\left(F_{ext}\geq F|T\right)\equiv P_e\left(F,T\right)= \\ \int_{Vin}^{Vout}\mathrm{Prob}\left(F_{ext}\geq F|V,T\right).p\left(V\right).dV\end{gathered} \tag{3-2}$$

Where 'p(V)' is the distribution of existence probability for the wind speed. It is described in paragraph 6.3.1.1 of the IEC code and corresponds to the Rayleigh distribution as discussed in paragraph 3.3.2 of the present thesis.

Annex F proposes a calculation method for the design load. From every simulation of the wind speed bins, independent maximum values are selected above the threshold of the mean value plus 1.4 times the STD. Afterwards a suitable cumulative distribution function is fitted to the extracted data load values. A guide for fitting is suggested to the IEC code by Moriarty et. al. (2002) [8]. The choice of a distribution function is evaluated keeping in mind the fitting accuracy over the whole data range collected and the tail of the data distribution, where extreme events appeared.

IEC standard [17] recommends a minimum of 300 min long time series distributed over the range of the most significant wind conditions. According to the above, six 10 min simulations per wind speed bin, for a minimum of five wind speed bins, would be sufficient. So, the long-term probability of extreme load existence is given according to the Rayleigh distribution function for every wind speed bin by the following equation:

$$P_e(F)=\sum_j\left(1-\left(F_{\max}\left(F|V_j\right)\right)^{nj}\right)\,[e^{\left(-\pi\frac{\left(V_j-\frac{\Delta V_j}{2}\right)}{2.V_{ave}}\right)^2}-e^{\left(-\pi\frac{\left(V_j+\frac{\Delta V_j}{2}\right)}{2.V_{ave}}\right)^2}] \tag{3-3}$$

V_j is the wind speed bin center value and ΔV_j is the range of the wind speed bin. The maximum design characteristic load is calculated for the 50 year existence probability, which is $P_e(F_k)=3,8.10^{-7}$.

The earlier version of IEC 61400 is the 2009 edition [18]. In paragraph 7.6.2, on ‘Ultimate strength analysis’, it is suggested to procced with 15 10-minute simulations for every wind speed bin between V_{rated} and $V_{cut\text{-}out}$ with a step of 2 m/s and 6 10-minute realizations between V_{in} and V_{rated} with the same step of 2 m/s, between wind speed bins.

Annex F of 2009, on 'statistical extrapolation of loads for ultimate strength analysis', is more analytic compared to that in the 2005 edition. It analyzes the method of data extraction, the method of statistical fitting and the way to check convergence and the confidence intervals. For the confidence intervals, the usage of the Btsp and of the binomial distribution method are suggested. Besides extrapolation technics, the Inverse first order reliability method (IFORM) is suggested in order to find the extreme design load. Annex F also presents the method of parametric fitting called “fitting first and aggregation afterwards”. The following equation describes the long-term probability distribution, like the (3 2) in previous IEC version:

$$F_{\text{longterm}}(s;T)=\int_{Vin}^{Vout}F_{\text{short-term}}(s|V;T).f(V).dV \tag{3-4}$$

where ′s′ is the load, ‘f(V)’ denotes the distribution function of wind speed between the limits of V_{in} and V_{out} of W/T operation. ‘F_(short-term) (s|V;T)’ is the short term distribution function for a specific wind speed bin V and a specific time period T.

So, if the range of wind speeds is divided into distinct wind speed bins, equation (3-4) for the long-term distribution function will become:

$$F_{\text{long-term}}(s;T)\approx\sum_{k=1}^{M}F_{\text{short-term}}(s|V_k;T).p_k \tag{3-5}$$

Where $p_k=f(V_k).\Delta V_k$ is the wind speed bin probability according to the Rayleigh distribution and $V_{in}\le V_1<\ldots<V_M\le V_{out}$ is the range of operational wind speeds.

Additionally, for the so called 'aggregation first and fitting afterwards' method the total number of simulations N_{total} is divided $N_{sims}(V_k)$ for every wind speed bin into groups of:

$$N_{sims}\left(V_k\right) \approx N_{total} \cdot p_k\left(V_k\right)$$

with p_k the wind speed bin probability mentioned before. Therefore, for the 'aggregation first and fitting afterwards' method, maximum values are extracted from all simulations, for all wind speeds bins and one CDF is fitted to the data.

So, it is necessary especially for these high wind speeds, to use the Btsp for generation in order to extract more values. Concerning the fitting integrity of the above-mentioned methods, extra convergence criteria are suggested in order to check if the number of simulations is the appropriate one, in addition to the initial IEC suggestion. The criterion is defined by the confidence interval of the distribution function fitted to the data. The criterion value, in the GM case, is the ratio of the 90% confidence bound loads, at the 84% of the load fractile denoted as 'S0.84', divided by this load fractile. This criterion ratio should be less than 15%. So, the equation of the convergence criterion is expressed as follows:

$$\frac{F_{ext,0.84,0.05} - F_{ext,0.84,0.95}}{F_{ext,0.84}} \leq 0.15 \tag{3-6}$$

When the method of collecting data is the POT method instead of the GM one, there will be 'm' maximum values from every 10-minute simulation and the load fractile will be $p^* = (0.84)^{1/m}$. The load fractile is calculated in the same way for the POT method. The load fractile 'p' is referred to a specific percentage of load existence. The method used to find the confidence bounds, is the Btsp suggested by the IEC code, with 5000 sets for the calculation of bootstrapped bounds.

An alternative method to assume confidence bounds is the binomial method, which is computationally less demanding than the Btsp one. In the binomial method, the parameters are already calculated for the confidence bounds of a given load limit. So, for the load fractile limit of 84% and for the 90% trust interval, from table F1 of Annex F, the correct parameters are given according to the number of simulations.

Finally, another method to estimate design loads, is the Inverse First Order Reliability Method, IFORM. In this method, at least 15 simulations are needed for each wind speed bin from rated Vrated up to Vcut-out with a step of 2 m/s. The wind speed bins of maximum loads are recognized and from these loads the 50-year extreme design load is calculated. The convergence criterion remains the same for all methods estimating extreme design loads. A numerical tool implementing the procedure for estimating the design values of loads and extreme deflections, based on the IEC guidelines has been developed in MATLAB R2017b [42]. It reads a set of loads/deflections time series and provides the estimated design value. The simulation procedures and their theoretical basis are provided in the following sub-sections.

3.3 Simulation procedures

3.3.1 Time domain aero-elastic solver

Time domain simulations are performed using the in-house, hydro-servo-aero-elastic solver hGAST [33], [39]. In hGAST, the full W/T is considered as a multi-component dynamic system having as components the blades, the drive train and the tower. The components are assembled into the full configuration on the basis of the multibody formulation. It consists of considering each component separately from the others, but subjected to specific free-body kinematic and loading conditions, that are imposed at the connection points of the components. The multibody formulation is also extended to the blades, which are divided into a number of sub-bodies connected to each other through similar kinematic and dynamic constraint conditions. In this way geometric non-linearities related to large deflections are taken into account. All flexible components (blades, drive train and tower) are modelled as Timoshenko beam structures subjected to bending, torsion and tension and approximated with the Finite Element Method (FEM). The Blade Element Momentum (BEM) model approximates the aerodynamics of the rotor [35], which may take into account mean inflow characteristics such as yaw, shear, veer and inclination as well as turbulent fluctuations. Viscous effects, unsteady airfoil aerodynamics and dynamic stall are taken into account using the ONERA model [36]. For integration in time, the Newmark 2nd order scheme is used [37] while the output consists of time series of internal loads and deflections on the FEM grid of the W/T components.

3.3.2 Stochastic wind conditions

The simulations have been performed under turbulent wind inflow conditions. By assuming that turbulent wind at the hub height follows the Kaimal spectrum and using an exponential space coherence function, a box of “turbulent wind velocity data” is generated. The dimensions of the cross-wind section of the box, are chosen to cover the rotor swept area, while the third dimension of the box coincides with the direction of the mean wind velocity and is directly associated with time. The frozen turbulence hypothesis (Taylor’s hypothesis) is made which postulates that disturbances due to turbulence travel with the mean wind velocity. By making use of the above hypothesis, time is directly transformed into length which should be equal to the duration of the simulation times the mean wind speed at hub height. The “useful” part of the simulation should last 10 min but in order to allow initial transients to fade out, an extra period of 50 s is added at the beginning of each simulation. Vertical and horizontal shear as well as veer is added to the turbulent fluctuations. The input parameters for the turbulent wind simulations are defined according to the IEC standard [17].

The defining parameters for the turbulent wind conditions are the 10min mean wind speed ‘V_{hub}’ at hub height and the turbulence intensity ‘I’, function of ‘V_{hub}’. As specified in the standards ‘V_{hub}’ follows the Rayleigh distribution:

$$PV_{hub} = 1 - e^{-\pi\left(\frac{V_{hub}}{2.V_{ave}}\right)^{2}} \tag{3-7}$$

'V_{ave}' is the scale parameter of the distribution according to IEC and $V_{ave} = 0.2 \times V_{ave}$

'V_{ref}' is the reference wind speed average, over 10 min time period at hub height.

The STD of turbulence 'sd_1' along the direction of mean wind speed, is determined by the normal turbulence model (NTM) [18] as follows:

$$sd_1 = I_{ref} \times 0.75 \times V_{hub} + b \tag{3-8}$$

where 'I_{ref}' is the expected value of turbulence intensity for 15 m/s at the hub height and b is a parameter equal to 5.6 m/s. For the W/T class of the present case, $V_{ref} = 42.5 m/s$,. In equation (3-7) as well as in equation (3-8), the expected value of turbulence intensity is $I_{ref} = 0.16$ according to IEC.

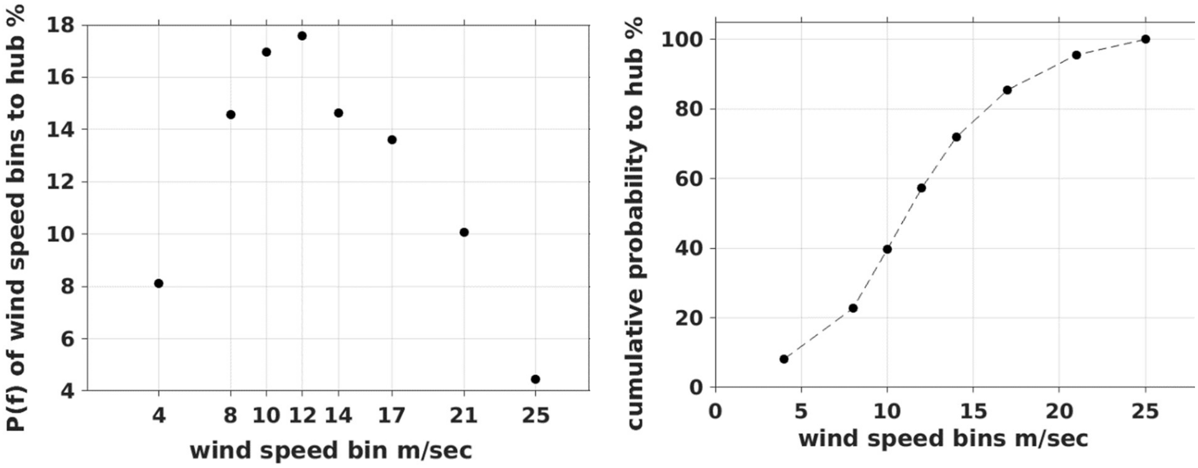

a) b)

Figure 9: Rayleigh distribution for turbulent wind input, a) probability function P(f) for wind speed bins b) cumulative probability function

The Rayleigh distribution describes the contribution of every wind speed bin to the whole wind speed range for the turbulent wind input in Figure 9.

The time series of the turbulent wind speed of a 10-min time simulation, for the 12 m/s mean wind speed bin is presented in Figure 10. Also, in Figure 10, the statistics for all turbulent wind speed bins is illustrated. Evidently the shape of the flapwise moment is dominated by the wind loads fluctuations. Clearly, the min – to – max range increases as the wind speed increases, as expected from equation (3-8).

The stochastic wind speed spectrum is given by the Kaimal [38] spectrum and the exponential space coherence function. The component power spectral densities are given in non-dimensional way by the following equation:

$$\frac{f.S_k(f)}{\sigma^2_k} = \frac{4.f.L_k/V_{hub}}{(1+6.f.L_k/V_{hub})^{5/3}} \tag{3-9}$$

Where:

f: is the frequency in Hertz,

k: is an index referring to velocity component direction (so the index is 1 for longitudinal, 2 for lateral, and 3 for upward),

S

S_k*: is* the single-sided velocity component spectrum,

σ_k: velocity component STD ,

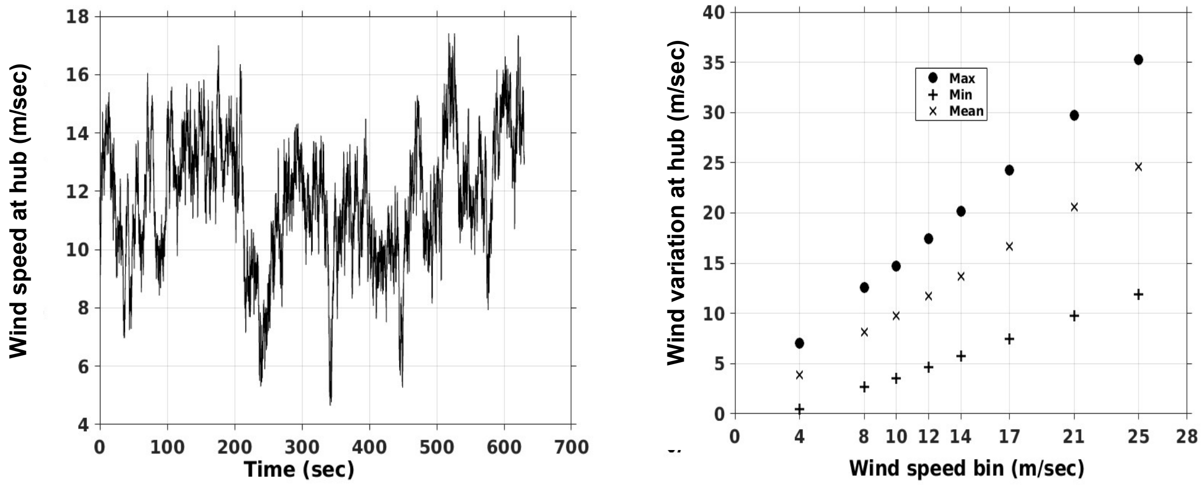

a) **b)**

Figure 10.: Wind speed with respect to time a) u=12m/s , b) Statistics for all turbulent spectrum

L_k*:* velocity component integral scale parameter,

The following equation (3-10) connects velocity and STD components.

$$\sigma^2_\kappa = \int_0^\infty S_k(f).df \tag{3-10}$$

The spectral parameters of turbulence are defined in the IEC code. The exponential coherence model is used with the Kaimal auto spectrum, for the spatial correlation structure of longitudinal velocity component and it is given by the following equation:

$$coh(r,f) = \exp\left[-8,8((f.r/V_{hub})^2 + (0,12r/L_c)^2)^{0,5}\right] \tag{3-11}$$

'Coh(r,f)' is the coherence function that is defined by the complex magnitude of cross-spectral density of longitudinal wind velocity components at two spatially separated points divided by the auto spectrum function,

'*r'* is the magnitude of projection for the separation vector between two points on a plane normal to the average wind direction, and

Lc = 8.1 Λ_1 is the coherence scale length parameter.

3.4 Case study and simulation set-up

Two sets of simulations are performed, one considering the reference blade structural data of the NREL RWT 5MW, and another by considering the blade structural properties as stochastic variables that are allowed to vary as described in chapter 2. The reference data correspond to the mean values of the composite material properties selected from OptiDAT. For the two data sets 10 min servo-aero-elastic simulations are performed under normal turbulence conditions (IEC DLC1.1 (2009:3)) for 8 wind speed bins with central velocities at 4, 8, 10, 12, 14, 17, 21 and 25 m/s. On the inflow side, for every wind speed bin, 96 turbulent wind data sets are generated. On the machine side, 96 different sets of material properties are also defined by randomly selecting their properties from the fitted LN distributions, each corresponding to a structurally different blade. Then every blade is combined with one wind data set. Thus, for every wind speed bin, 96 simulations are carried out, each corresponding to a different blade. In order to assess the effect of the number of simulations per bin on the convergence of the procedure, 24 and 48 simulations have been randomly selected out of the 96 simulations per wind speed, defining two additional datasets.

All time domain simulations were generated using the servo-aero-elastic code hGAST. The present case study is the horizontal, variable speed, pitch controlled onshore W/T (NREL RWT 5MW) with a three - bladed Upwind rotor [40]. The rated power of the turbine is 5 MW while each blade expands to a length equal to 63 m. The operating mean wind speed range is from 3 m/s (cut-in) to 25 m/s (cut-out) with the rated mean wind speed at 12 m/s. The hub height for the rotor is located at 90m. The specific rotor blade design was further modified in [40]. This new design along with material properties of the OptiDAT database were adopted to the present thesis.

Specifically, ninety-six 96 10-min realizations were calculated at 0deg yaw angle per mean wind speed, for eight different wind speed bins. All loads were provided at fifteen sections along the blade length. All data loads were recorded with a sampling frequency of 20 Hz.

All maximum developed sectional loads and all extreme blade tip deflection values were examined for all blade sections. A sample of the derived time series of the flapwise moment load at u=12 m/s is presented in Figure 10 located at r= 14m.

The load extrapolation procedure is presented for blade section 7 located at r= 14m. Also the blade tip deflections extrapolation is presented. All moments and load of that section are further studied and quantified. The long-term extreme design load distributions for a given reference period are specified performing load extrapolation techniques.

3.5 Peak methods

Two methods for extracting peak load values are considered, the GM and the POT peak methods. For every 10 min simulation the GM method outputs the absolute maximum load, while the POT method outputs all load values above a certain threshold. Clearly the GM method provides less data than the POT and hence more simulations are needed in order to establish a well-populated dataset. Besides, having one single value per 10-min simulation implies that high load values appearing in a specific time series are not contributing in determining the exceedance probability function, which can affect the quality of the extrapolation procedure. Therefore, results based on the GM method have only been included in support of the above statement. For the POT method, according to [12] and to IEC code [17], the threshold is chosen to be 1.4 times the STD estimated through all realizations per wind speed bin. Also, a time separation of 10 sec between successive maxima is specified to ensure statistical independence. The way that the maxima are extracted from a 10 min simulation for every peak method is depicted in Figure 10. The biggest circle red marker corresponds to GM method while the smaller ones to POT method.

As maxima data are extracted, it is easy to identify wind speed bins that include the largest turbine loads on average as well as the ones with the greatest variability. According to [8], both of the methods, GM and POT, have a serious impact on the estimation of the long-term distribution of the extremes. Also more effort is needed for the short term extreme distributions of loads that are computed for wind speed bins with more extremes. 'Short' and 'long' term refers to distributions of extreme loads for one or more mean wind speeds accordingly.

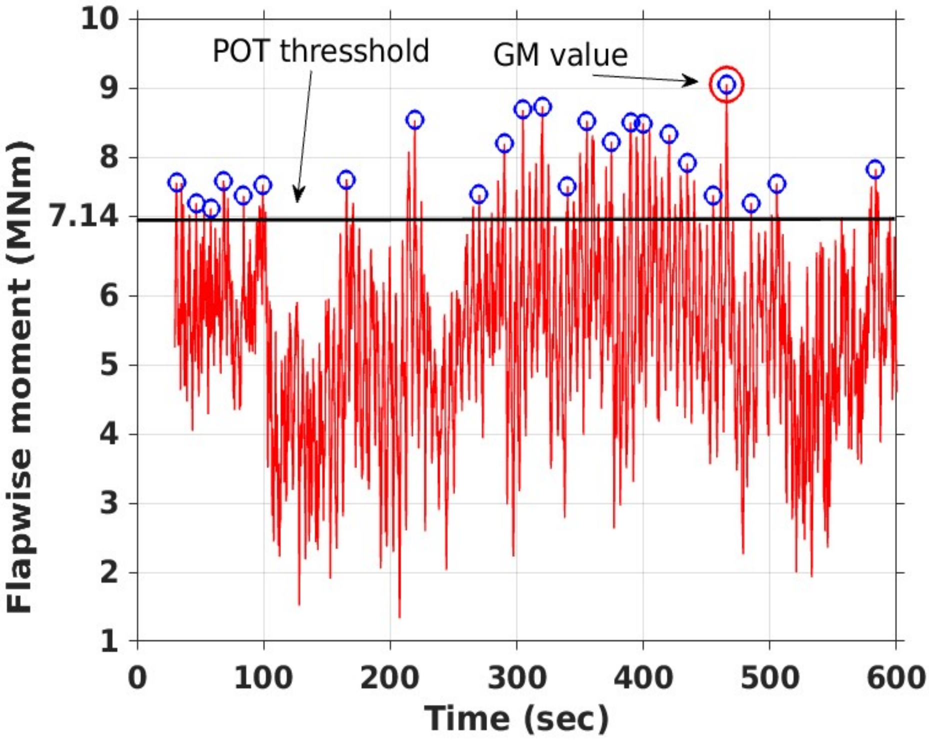

Figure 11: A typical portion of flapwise moment for an aero-elastic simulation at u=12 m/s mean wind speed bin, Flapwise moment with respect to time and selection methods GM (red circle) and POT (blue circle

It is found that the average of extreme loads decreases at all wind speed bins when more and more maxima are extracted from a 10-min simulation as the peak method shifts from GM to POT. At the same time, the range of data as well as their scattering constantly increases. It is easy to conclude that the wind speed bins that are equal or greater to rated speed (u=12 m/s) are the most significant ones, with high average loads and large data scattering.

3.6 Short term parametric distribution fitting

Once the set of peak values is collected, occurrence probability is determined based on the frequency of appearance of the different load/deflection value bins, which is weighted by the corresponding probability of the specific wind speed bin, usually by a Weibull statistical distribution. Then an analytical distribution function is fitted to the discrete one, which estimates the extreme value corresponding to the 50-year return period through extrapolation in time. In the present work, the LN, the 2pW and the 3pW distribution functions are considered for this fitting. The CDFs of the above three distributions are given below:

Log-normal distribution (LN):

$$F(x) = \Phi(\mathrm{lnx\text{-}m} / \sigma), \Phi(\mathrm{x}) = 1/2\left[erf(x/\sqrt{2}) + 1\right], \tag{3-12}$$

$$erf(x) = 2/\sqrt{\pi}\int_{0}^{x} e^{-t^2}\,dt$$

2 parameter Weibull distribution (2pW): $$F(x) = 1 - e^{\left(-\left(\frac{x}{\lambda}\right)^{\kappa}\right)} \tag{3-13}$$

3 parameter Weibull distribution (3pW): $$F(x) = 1 - e^{\left(-\left(\frac{x-\varepsilon}{\lambda}\right)^{\kappa}\right)} \tag{3-14}$$

In the above equations, m and σ are the mean value and the STD, Φ(x) is the standard normal distribution for m=0 and σ =1, erf(x) is the error function and κ, λ, ε are parameters of the Weibull distributions. The defining parameters of the LN and 2pW distributions are determined using the Maximum Likelihood Estimation method [41] (Cousineau, 2009), while those of 3pW using the Method of Moments based on the formulation in NREL [8] of 2004.The selection and fitting of the appropriate CDF to the data is crucial, especially for wind speed bins with higher peak values.

3.7 Distribution model selection

Several goodness-of-fit tests are available to judge the appropriateness of the applied distribution. According to JCSS [9] (2001:40) and DNV [10], the K-S test may be applied. JCSS proposes also a visual judgment of the fitting of the potential parametric distributions to the simulation peak data. Herein the K-S goodness of fit test is performed at a significance level of α=0.05. The K-S test is a non-parametric test, while its statistics quantify the distance between the empirical distribution of the sampled data and the CDF of the reference distribution. In this connection, the p- and h-factor values are used. The p-factor or the observed significance level is defined as the smallest significance level that would lead to rejection of the "null hypothesis" for the given data, which specifies whether the drawn samples follow the assumed distribution. The h-factor is defined as a test decision for the null hypothesis that the data comes from the assumed distribution, against the alternative that it does not. If the test rejects the null hypothesis at the 5% significance level, then h=1. P-values higher than 0.05 and h-factor values equal to zero indicate that the selected CDF fits well the collected data (for details see Smirnov [11] (1948)).

3.8 Long-term exceedance probability for the extreme design load

The long-term exceedance distribution of the extreme load/deflection depends on the extremely low probability values of the short-term exceedance distributions. Typically, the short-term exceedance probabilities of interest are in the range of (1E-04, 1E-08), which means that a much higher number of 10 min aero-elastic simulations would be required in order to construct empirical distributions that contain data points within the above probability range. Because this is computationally prohibitive, load/deflection extrapolation is performed based on fitted distribution models, for long-term periods of e.g. 50 years. Clearly the quality of the evaluation of the long-term design value strongly depends on the successful tail fitting of the short-term empirical exceedance distribution. In this respect, the total probability theorem IEC [17] (2005:78) is applied in estimating the long-term exceedance probability of the extreme value, in reference to a T=10 min period, through partial (short-term exceedance probability) distributions over all operating conditions (wind speed bins):

$$P(F_{ext} \geq F;T) = \int_{Vin}^{Vout} P(F_{ext} \geq F;V,T)p(V)dV \tag{3-15}$$

Where $P(F_{ext} \geq F;V,T)$ is the short-term exceedance probability distribution of the extracted maxima which depends on the wind speed Vat hub-height and period T, while $p(V)$ is the probability density function of the wind speed. The extreme value distribution in a specific reference period of N years (i.e. N=50 in the standards) is derived by assuming independent 10-min intervals and is defined as in IEC [18] (2009:15):

$$P(F_{ext} < F;T = N) = 1 - \left(P(F_{ext} \geq F;V,T = 10min)\right)^{(365\cdot 24\cdot 6\cdot N)} \tag{3-16}$$

The 3pW probability distribution function is used for the reliability calculations as it was earlier proven to be the most appropriate distribution function for fitting short term data.

3.9 Statistical uncertainty

Parameters of probabilistic models were estimated by means of derived simulations data. If other tests were performed, new parameter values for the fitted distributions would be estimated. Thus, ML estimators of distribution parameters can be considered as stochastic variables themselves. This is often called statistical uncertainty. That uncertainty exists due to the limited amount of sample data and can be quantified following the Btsp and by taking advantage of the asymptotic properties of the ML estimators (ap-MLE).

The method relies on generating Btsp samples. The Btsp sample is formed by randomly sampling data from the existing experimental dataset with replacement. Thus, every observation from the experimental database may be arise more than one time in the sample. Also the size of the Btsp sample is equal to the number of observation in this experimental dataset. For every sample, new ML estimators of the hypothesized distribution are evaluated resulted in B set in parameter values. The expected value and the coefficient of variation for derived the samples evaluated. In this way it is introduced variability for the distribution parameters used to perform load extrapolation. In order to quantify that variability, a nonparametric Btsp is implemented. So *B* Btsp samples are generated from the extracted maxima data of each wind speed bin and a certain parametric distribution (LN, 2pW, 3pW) is fitted to the Btsp samples using some point estimation method (ML or MM).

In order to demonstrate the effect of statistical uncertainty on the distribution of the extreme design values, the 10-min long-term exceedance probability was for each sample. Then 5 and 95 percentile levels of probability for a specified load level were evaluated. These are mentioned and depicted in chapter 4 for all loads and deflections. The 3pW is fitted to local maxima derived by means of POT and GM peak methods.

3.10 Conclusions concerning the W/T certification process

Stochastic representation of extreme loads for the NREL reference rotor blade was presented. The proposed methodology involves statistical load extrapolation of extreme loads derived by 10 min time series. The required simulations were derived through aero- elastic calculations. The introduced uncertainties are divided into two different sets. The first set has the turbulent wind input. On top of that, the second set introduces stochastic distributed E_1, E_2, G_{12} and ν_{12} material properties for the composite material, as described in chapter 2.

The analysis showed that a number of issues related to load extrapolation technique should be carefully considered to assure well-established long-term distributions of the extremes. Specifically, two peak methods proposed by the amendment of IEC standard to extract maxima, GM and POT methods. Each led to a different result for the long-term exceedance distribution. Further, several parametric distributions (LN, 2pW, 3pW) were fitted to the extracted maxima.

The current methodology reveals that one must be cautious when selecting peak method as well as the associated probabilistic model. A careless confrontation of these aspects may result in erroneous long-term distributions for the extremes and the design values.

In addition, to better support the findings of the investigation on the uncertainty of the blade structural properties, the process for estimating the design values has been assessed in terms of its numerical implementation and selection of appropriate peak extraction method and fitting cumulative distribution function.

The above research reconfirms the conclusions drawn in previous research studies mentioned in the beginning of the present chapter and verify the consistency of the present implementation for the statistical estimation of the extreme loads and deflections. The combination of POT selection method, with the 3pW probability distribution function and the extended set of 96 simulations per wind speed bin are used for the reliability calculations as it was earlier proven to be the most appropriate for fitting short term data.

4. Certification process results, evaluation of design moments, loads, deflections, stresses and comparisons between different material properties

In the following sections, the short and the long-term fitting will be presented for all design moment and load values of blade section 7 at r=14m of the blade, for two blade data sets: the reference blade and the set with StoMP. Also, the blade tip deflections will be calculated for both blade data sets. Finally, the stress analysis will be given for the load signal containing the maximum flapwise moment and all other relevant loads and moments. The aforementioned moments are the flapwise, the edgewise and the torsion ones, as well as the relevant loads to the blade section at r=14m. Additionally the, deflection values that correspond to the above-mentioned loads are calculated for the blade tip section. Also the stresses to all blade sections are evaluated and the variance between different material properties is calculated. In every section of the chapter, the statistics of the data gathered for the blade and the IEC criteria calculations, the short and the long-term fitting results are presented. Also, the comparison between different methods of collecting data is discussed.

4.1 Short term fitting for all moments and loads of section at r=14m and for the blade tip deflections with reference and stochastic blade data input

4.1.1 Flapwise moment for the blade section at r=14m and blade tip flapwise deflection

Firstly, the case of short-term fitting for the flapwise moment at r=14m section and the blade tip flapwise deflection are presented. The data sets used are 96 per wind speed bin for the reference and the stochastic blade data input cases. In Figure 12 the IEC criterion for all 3 data set cases is illustrated, named 24, 48 and 96. The Btsp with 5000 samples used to calculate the criterion. The same criterion is calculated for all other moments and loads at r=14 m of the blade and for all the corresponding blade tip deflections.

In Figure 12, results of the IEC convergence criterion for the flapwise bending moment at r=14 m and the flapwise deflection at the blade tip are presented for the entire wind speed range, based on the POT peak method. It follows that for both sets of blade material properties and for both signals, the IEC criterion is fulfilled giving an error of less than 15%, except in the flapwise deflections at the wind speed of 21m/s for the reference data and of 25m/s for the stochastic data when 24 simulations are considered. By comparing the reference blade data set with the stochastically defined ones, it follows that the variability of the material properties overall increases the values of the criterion, while this increase is moderated as the number of simulations increases. For the flapwise moment data and for 48 simulations per wind speed bin, the average increase of the criterion (all wind speeds) for the stochastic properties in comparison to the reference properties is 18% while for 96 simulations per bin is 15%. As concerns deflections, the corresponding average rate of increase for 48 and 96 simulations per bin is 65% and 25% respectively. The error level consistently drops as the number of simulations increases and does not exceed 10% for 48 simulations and 5% for 96 simulations for both signals and all wind speed bins.

With all simulations calculated for all wind speed bins, the results were gathered in one diagram presenting the maximum, the minimum and the mean values for the set of maximum values collected with the POT peak method. These statistics for the flapwise deflection at the tip and the flapwise moment at r=14m are presented in Figure 13.

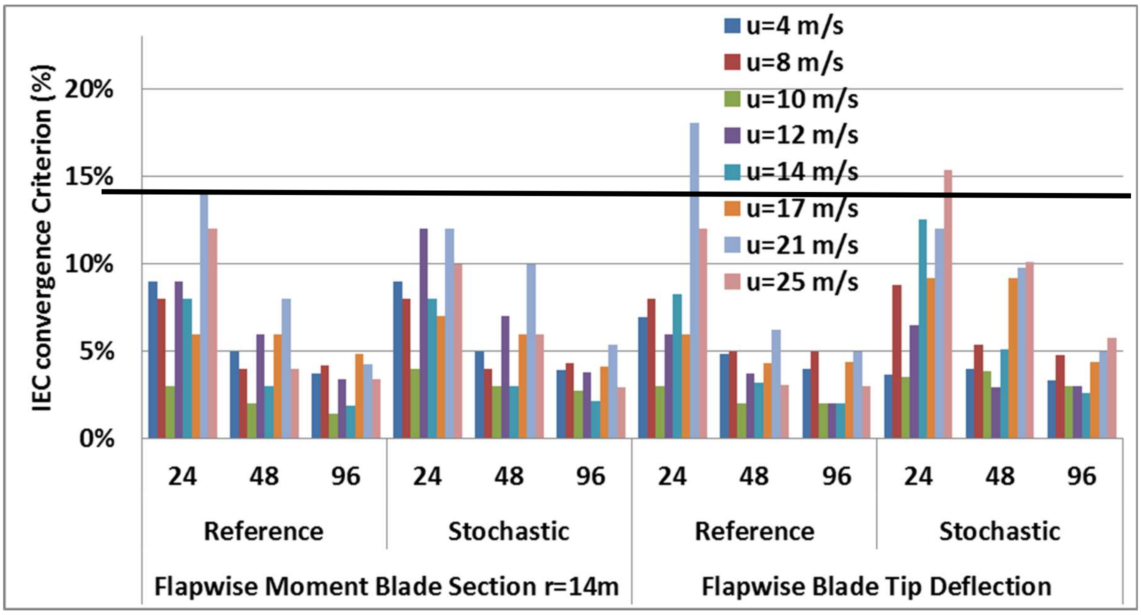

(a)

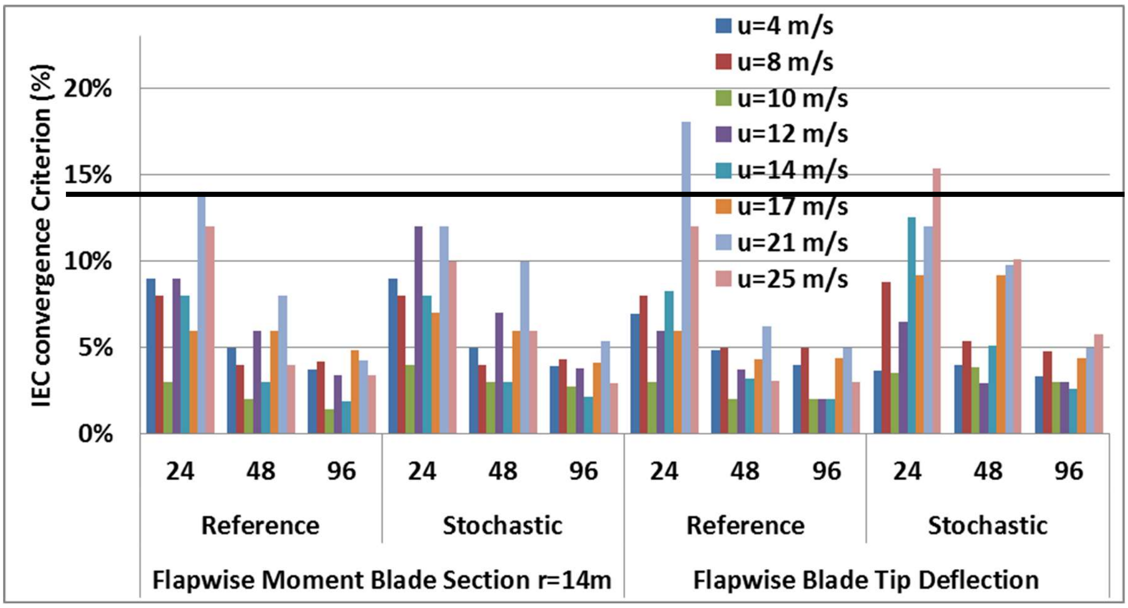

(b)

Figure 12: IEC convergence criterion for the flapwise moment and the blade tip flapwise deflection with reference and stochastic blade data input, with 24, 48 and 96 data sets per wind speed bin and a)POT method, b) GM method

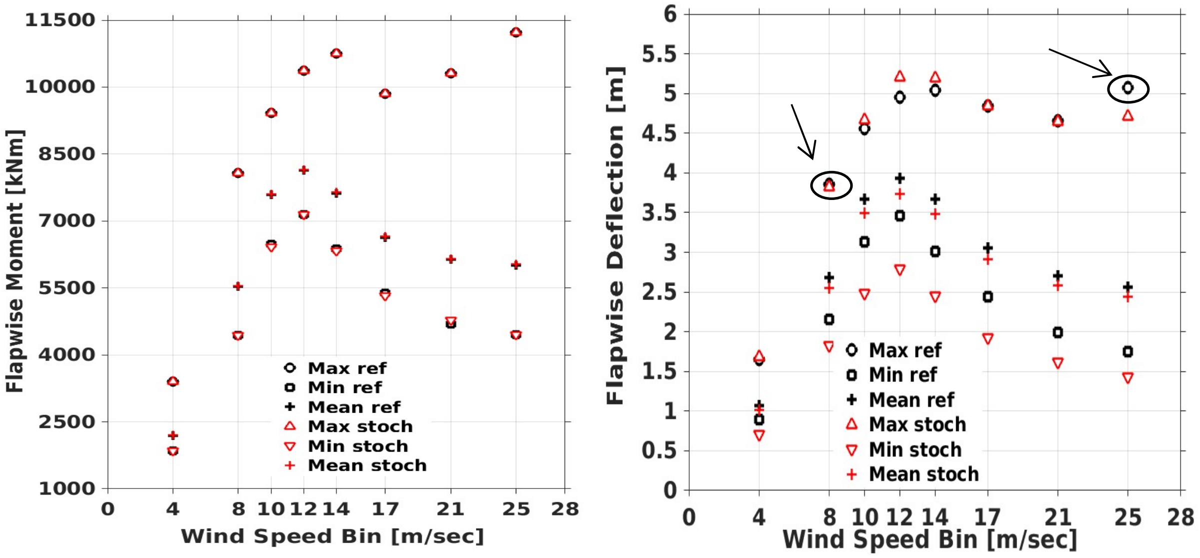

(a) (b)

Figure 13: Statistics of maximum values vs. wind speed. 96 data sets are included for the reference and the StoMP for the POT method (a) for the flapwise moment at r=14m and (b) for the blade tip flapwise deflection

An overall indication of the collected data is given by the statistics of the peak values of the flapwise bending moment and the flapwise deflection shown in Figure 13. The plots compare the reference versus the log-normally distributed blade properties using the POT peak extraction method. The comparison of the different sets of blade properties indicates that the statistics of the load data remain the same, contrary to the blade deflections that change. For example, the maximum difference in load data, is 0.4% for the mean values, at 14 m/s wind speed, while the maximum difference in blade deflection, is -5% at 12m/s wind speed for the mean values and 65% for the min-to-max range. When the uncertainty of the material properties is considered, the maxima as well as the min-to-max ranges of the collected peak deflections increase. Moreover, a larger scatter of the collected load/deflection data is obtained as the wind speed increases.

It is seen that the absolute maximum is reached at the wind speed of 25 m/s, while a local maximum is also obtained at 12-14 m/s. The latter is close to the rated wind speed (11.4 m/s) at which maximum thrust load is obtained, while the former can be attributed to the increased wind speed turbulent fluctuations at higher speeds. Beyond 14 m/s, all statistics (min, max and mean values) of loads/deflections decrease due to the pitching of the blade and then tend to increase again as the cut-out speed is approached.

The STD of the selected values mentioned in Figure 13 is illustrated in Figure 14. These STD values are slightly different for the flapwise moment when the GM method used, which is obvious in Figure 14 at the left column. The main difference is observed in the flapwise deflection for both methods GM and POT of Figure 14. The STD is higher for the stochastic blade data and especially for the GM method. The same conclusion is extracted from all wind speed bins with the POT method and especially for the range from 8m/sec up to 17m/sec.

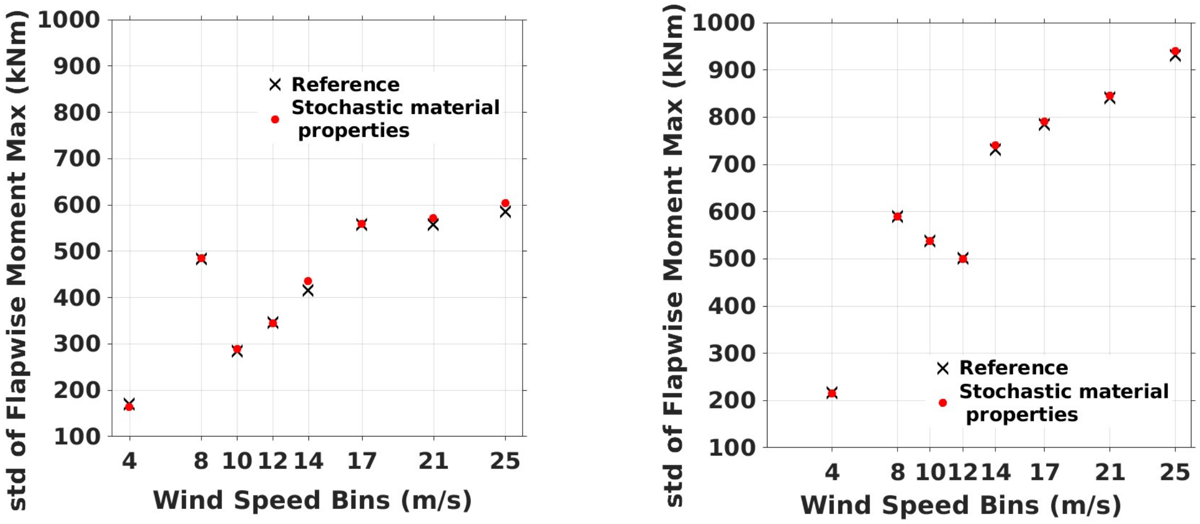

Flapwise moment at r=14m of the blade radial

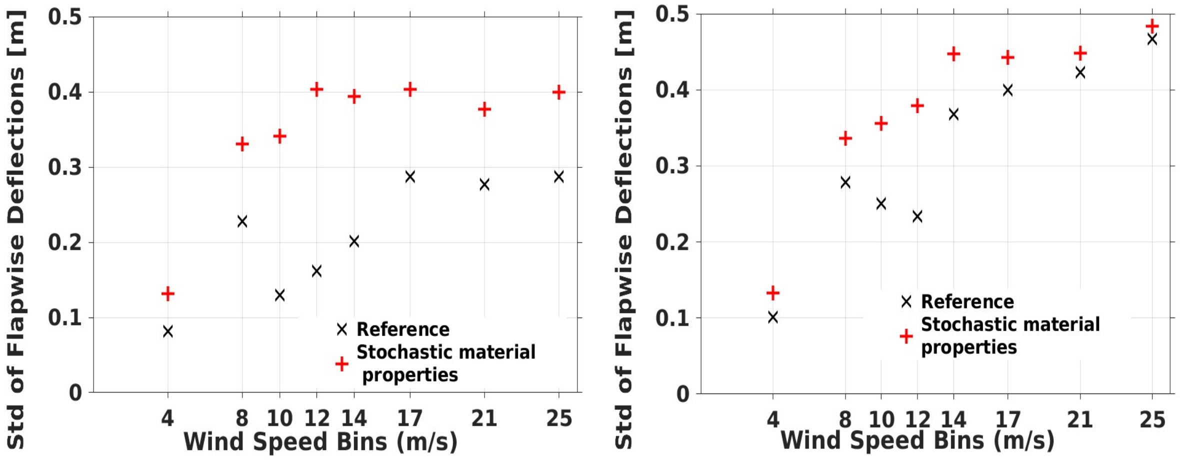

Blade tip flapwise deflection

Figure 14: STD values for Flapwise moment (upper row) and the blade tip Flapwise deflection (lower row). The left columns concern the Peak method GM and the right column concerns the POT method. The results are based on 96 10min simulations and referred to the reference and the log-norm distributed blade properties.

The short-term fittings of flapwise moment and blade tip flapwise deflections data are introduced in Figure 15 using 96, 10 min simulations at the wind speed of 12 m/s. Results are shown for both peak methods (GM and POT), as well as for the reference and log-normally distributed blade data. In every plot, fittings with the three distribution functions (LN, 2pW, 3pW) are displayed. The results indicate that in all cases the 3pW performs better, followed by the LN fitting, while the 2pW fails to fit the tail of the data. Also, in all plots the 3pW fitting is more conservative in comparison to the other two. It is noted that out of the two peak methods, the POT collects and handles more data compared to the GM method, which clearly affects the fitting quality. As regards the two sets of blade data, the comparison indicates that the variability introduced in the case of the StoMP, is insignificant on the moment values.

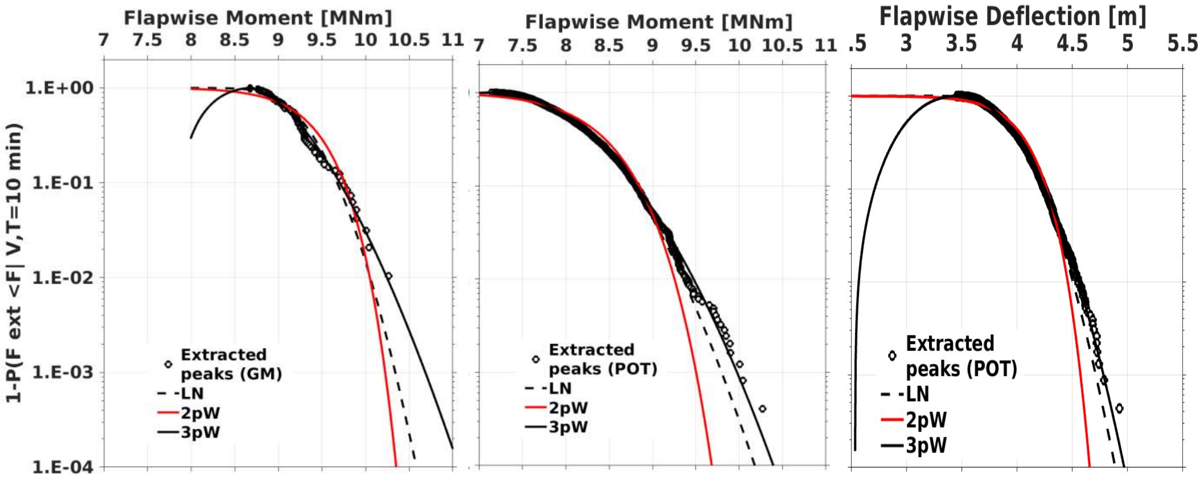

Reference blade properties

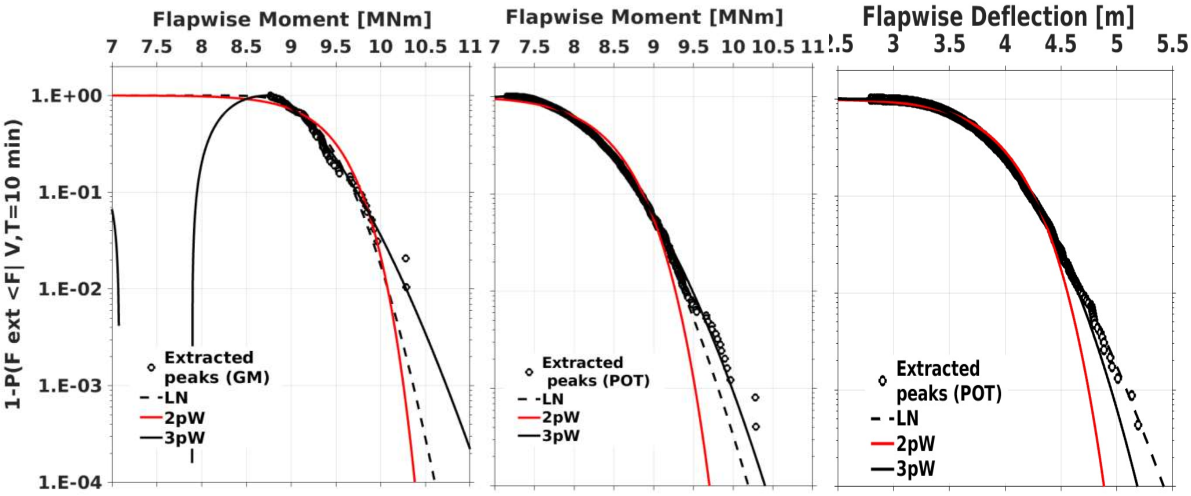

Log normally distributed blade properties

Figure 15: Short term probability fittings for the reference (upper row) and the log-norm (lower row) distributed blade properties. The left and middle columns concern the flapwise moment at r=14m using respectively the GM and POT methods. The right column concerns the flapwise deflection at the blade tip using the POT method. The results refer to a wind speed of 12 m/s and are based on 96 10min simulations. In all plots fittings with (LN, 2pW, 3pW) CDFs are compared.

However, the same does not hold for the flapwise deflection also shown in the same figure, and also based on the POT peak extraction method. The fittings in the case of stochastic blade properties provide higher deflections, while the 3pW is more conservative and forecasts higher values only for the reference blade data. When the stochastic blade data are considered, the LN distribution function provides higher fitted deflections, while the 2pW again fails to fit the tail of the data.

GM POT

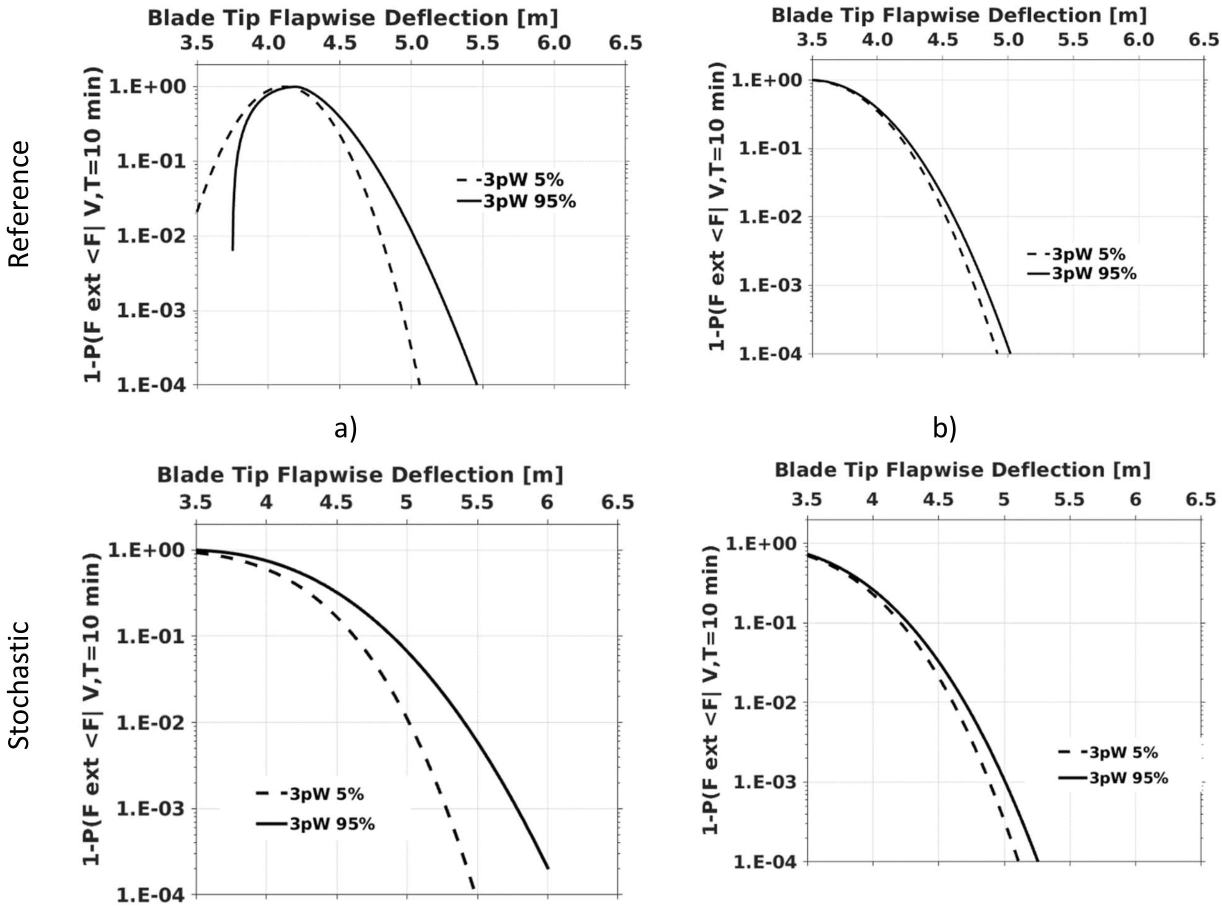

a) b) c) d)

Figure 16: Short term probability and 90% confidence interval of 3pW, for blade tip flapwise deflection, at u=12 m/s with 96 data sets, RefMP (upper row) and StoMP (lower row) for the GM peak method (left row) and POT peak method (right column).

In Figure 16, for the wind speed bin of u=12 m/s, it is apparent that shifting from GM to POT method, the 3 parameter Weibull CDF converges to lower 90% confidence interval values. Also, the confidence interval obtained with POT method is too short compared to that of the GM method for the same number of simulations and for the same wind speed bin. Concerning the choice between material properties, for the stochastic properties the confidence interval becomes wider and the mean value of the range is increased Figure 16 a) vs c) and Figure 16 b) vs d). All results from the visual criterion applied to the short-term fittings, are gathered in [Appendix 5]. The conclusion is that for all wind speeds the 3pW outperforms.

It is mentioned that there are no specific recommendations for the selection of the extrapolations CDF selection in the IEC standard. Great attention must be given to the fitting of the tail of empirical short-term distributions. This is not always an easy task due to load values that are far from the main bulk of the data.

In order to select the precise CDF, the K–S test also used, in chapter 3, besides visual inspection criterion. In this respect, it is mentioned that when the H values of the K-S test are unit (1), the specific CDF is not the correct function to fit the data for the specific wind speed bin. This also means that the specific CDF is not suitable for extrapolating and forecasting the design loads. The K-S test suggests the P factor which proposes the appropriate CDF for data fitting, when the factor is closer to one (1)

The K-S test is applied to all three distributions considered (LN, 2pW, 3pW). The p-values and the h-factor values of the statistical tests are presented in Figure 17 for the flapwise moment at r=14m, considering the stochastic blade data. In these tests, the GM or POT peak method are also compared. According to the K-S test results there is no sufficient evidence to reject the null hypothesis for the 3pW (min p-value=0.9) and the LN (min p-value=0.25) parametric distributions when the GM method is applied. On the contrary the 2pW distribution fails to satisfy the significance level and h-factor criterion at the wind speeds of 4, 12, 21 and 25m/s. When the POT method is used, only the 3pW (min p-value=0.25) complies with the null hypothesis, as a consequence of the significantly higher number of extracted maxima as compared to those obtained with the GM method. Thus, the K-S test qualifies the 3pW distribution as the most appropriate extrapolation function of the maxima collected with either of the two tested peak extraction methods.

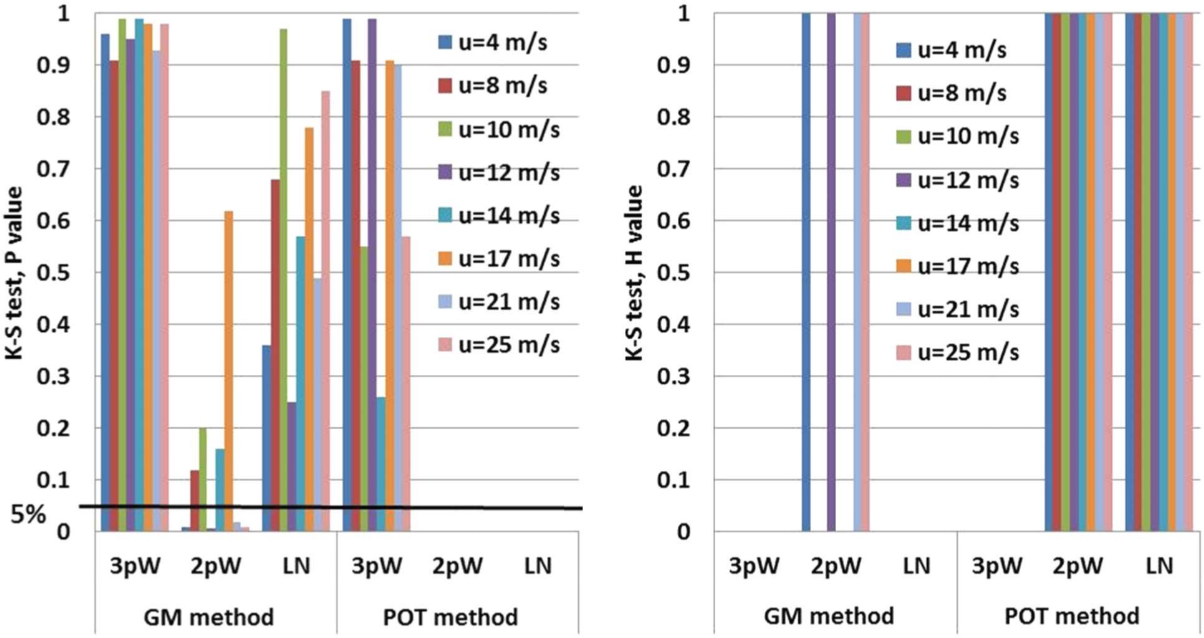

a)

b)

Figure 17: K-S test: P values (left) and H values (right) of the flapwise moment at r=14m considering the log-normally distributed blade data, for all wind speed bins with 3pW, 2pW, LN CDFs. 96 data sets are used per wind speed bin. Results are shown based on the GM and POT peak methods.

The long-term exceedance distribution for extreme load calculation depends on the extremely low probability values of the short-term exceedance distribution presented in this section. Typically, the short- term exceedance probabilities of interest are in the range of 10^{-4} and 10^{-8}. This implies that an even greater number of 10 min aero-elastic simulations should have been realized in order to construct empirical distributions over these ranges. However, that number of simulations is computationally prohibitive and so the load extrapolation is performed based on the fitted distribution models.

4.1.2 Edgewise moment for the blade section at r=14m and blade tip edgewise deflection

From the same aeroelastic simulations for all wind speed bins, the edgewise moment results and the blade tip edgewise deflections are analyzed statistically in Figure 18, following the same way as with the flapwise moment and deflection.

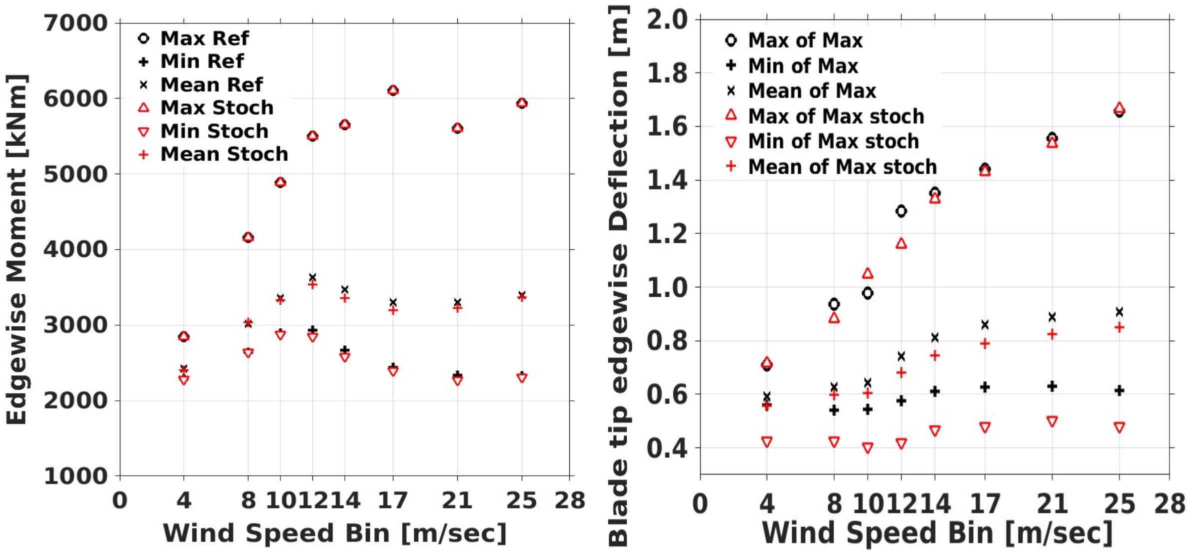

a) b)

Figure 18: Statistics of maximum values vs. wind speed. 96 data sets are included for the reference and the StoMP for the POT method (a) for the edgewise moment at r=14m and (b) for the blade tip edgewise deflection

The Mean values are slightly lower, when, additionally to the turbulent wind input, the material properties of the composite blades are stochastically distributed. This is significant especially for the deflections. The same is observed for the range of the data values collected from every wind speed bin. The minimum deflections are lower, for the stochastic data and the maximum values are generally equal or slightly lower except only for the wind speed bin of 12 m/s. The data values shown in Figure 19 for the STD of the edgewise moment for the StoMP are lower compared to those for RefMP. The opposite happens with the deflection data collected for all wind speed bins. The STD is clearly higher for all wind speed bins, in the case of StoMP. The IEC criterion is calculated and it is accepted being below the limit of 15%.

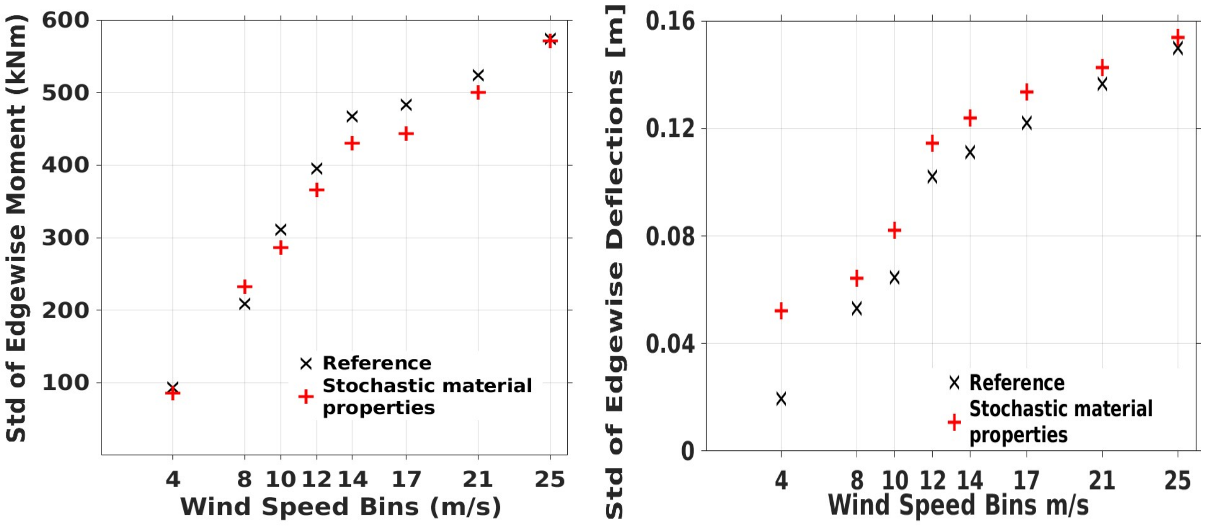

a)

b)

Figure 19: STD of edgewise moment and blade tip edgewise deflection for 96 data sets, POT method, reference and stochastic distributed blade data input (a) edgewise moment (b) blade tip edgewise deflection

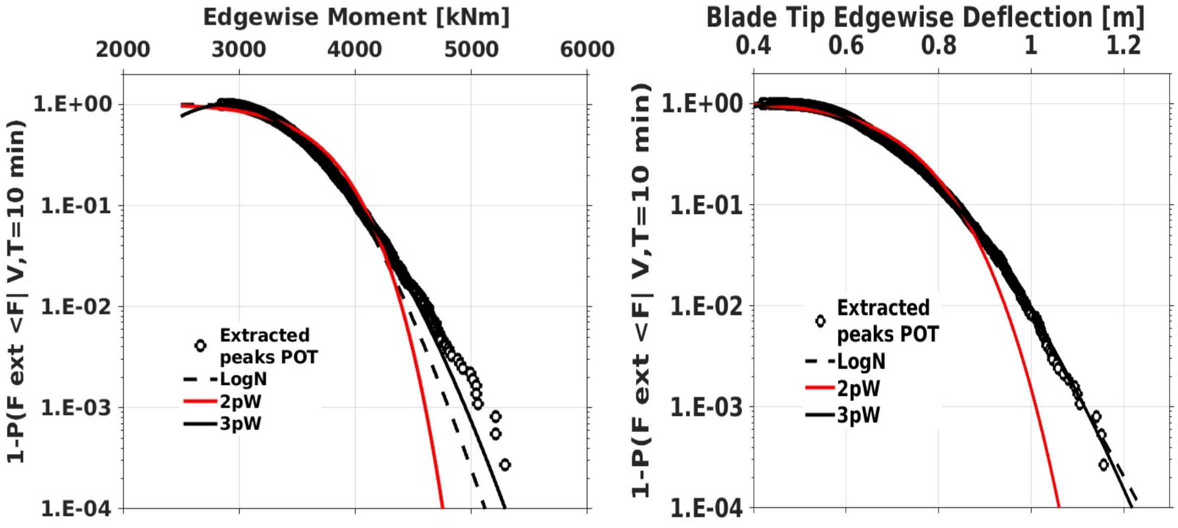

a)

b)

Figure 20: Short term probability for the edgewise moment and the blade tip edgewise deflection at u=12m/s wind speed bin, 3pW CDF fitting, Lognormal and 2pW fitting, 96 data sets, stochastic distributed blade data input

Short term fittings of edgewise moment data are shown in Figure 20 using 96 10 min simulations at the wind speed of 12 m/s. Results are shown for the peak method POT, for the StoMP. In every plot, fittings with the three distribution functions (LN, 2pW, 3pW) are presented. The edgewise deflection results indicate that the 3pW performs better, followed by the LN fitting, while the

2pW fails to fit the tail of the data. Also, in the moment plot the 3pW fitting is more conservative and forecasts higher design value in comparison to the other two.

4.1.3 Torsion moment at r=14m of the blade section and blade tip twist angle

, The collected maxima data and the relevant statistics of the torsion moment of the blade at r=14 m and the blade tip twist angles are gathered in Figure 21. For all wind speed bins and for the POT method, the STD of the data is plotted in Figure 22. The mean values and the range of the torsion moment are the same, for the RefMP and the StoMP. Concerning the blade tip twist angle, the mean values are lower for the stochastic blade data and the range of values is wider. In Figure 22, the STD is higher for the wind speed bins of 4, 17, 21 and 25 m/s. On the contrary, the STD s are equal for the wind speed bins 8, 10, 12 m/s and 14 m/s bin for the data collected with the POT method.

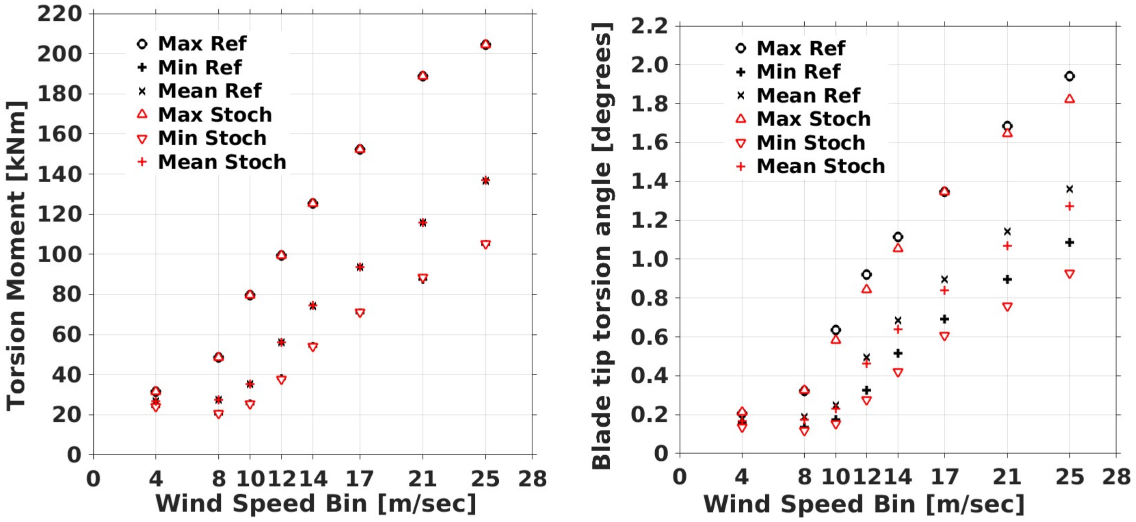

a) b)

Figure 21: Torsion moment at blade section 7 and blade tip torsion angle, maximum values distribution, with 96 data sets per wind speed bin, with reference and stochastic blade data input and peak method POT: a) Torsion moment b) blade tip twist angle

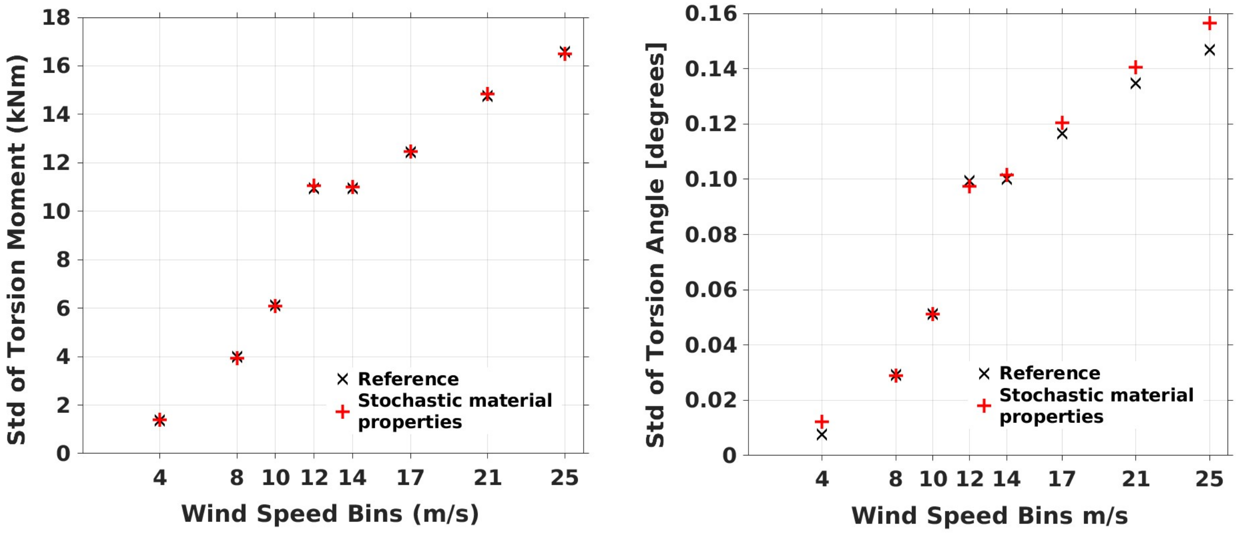

(a) (b)

Figure 22: STD of torsion moment and blade tip torsion angle for 96 data sets, POT method, reference and stochastic distributed blade data input (a) torsion moment (b) blade tip torsion angle

The necessary short-term fittings have been also calculated for the torsion moments and the blade tip torsion angle maximum data with the RefMP and the StoMP as blade data input. In all cases and all wind speed bins the IEC criterion is satisfied and is less than 15**%**, which is the threshold set by the IEC code**.** The conclusion is that the 3pW function is the appropriate CDF for fitting data for the blade tip torsion angle and the torsion moment at section with r=14m according to the visual criterion method and the K-S test.

4.1.4 Flapwise, Edgewise and Axial forces for the blade section at r=14 m

In Figure 23 (a)-(b), the statistics of the maximum collected data are presented, for the flapwise forces, in Figure 23 (c)-(d) the statistics for the edgewise forces and in Figure 23(e)-(f) the maxima axial forces data, for all wind speed bins and for both blade data input. These forces (loads) are defined in equation (2.4) as integrals of the sectional shear and normal stress distributions. The comparison of the different sets of blade properties indicates that the statistics of the flapwise and axial load data remain the same. Moreover, a larger scatter of the collected edgewise load data is obtained as the wind speed increases, from 12 m/s up to 25 m/s. Beyond 12 m/s, the statistics of the min and mean values of edgewise forces increase for the RefMP and so the STDs of the selected values mentioned in Figure 23 (d) are slightly higher for the range from 12m/sec up to 25m/sec.

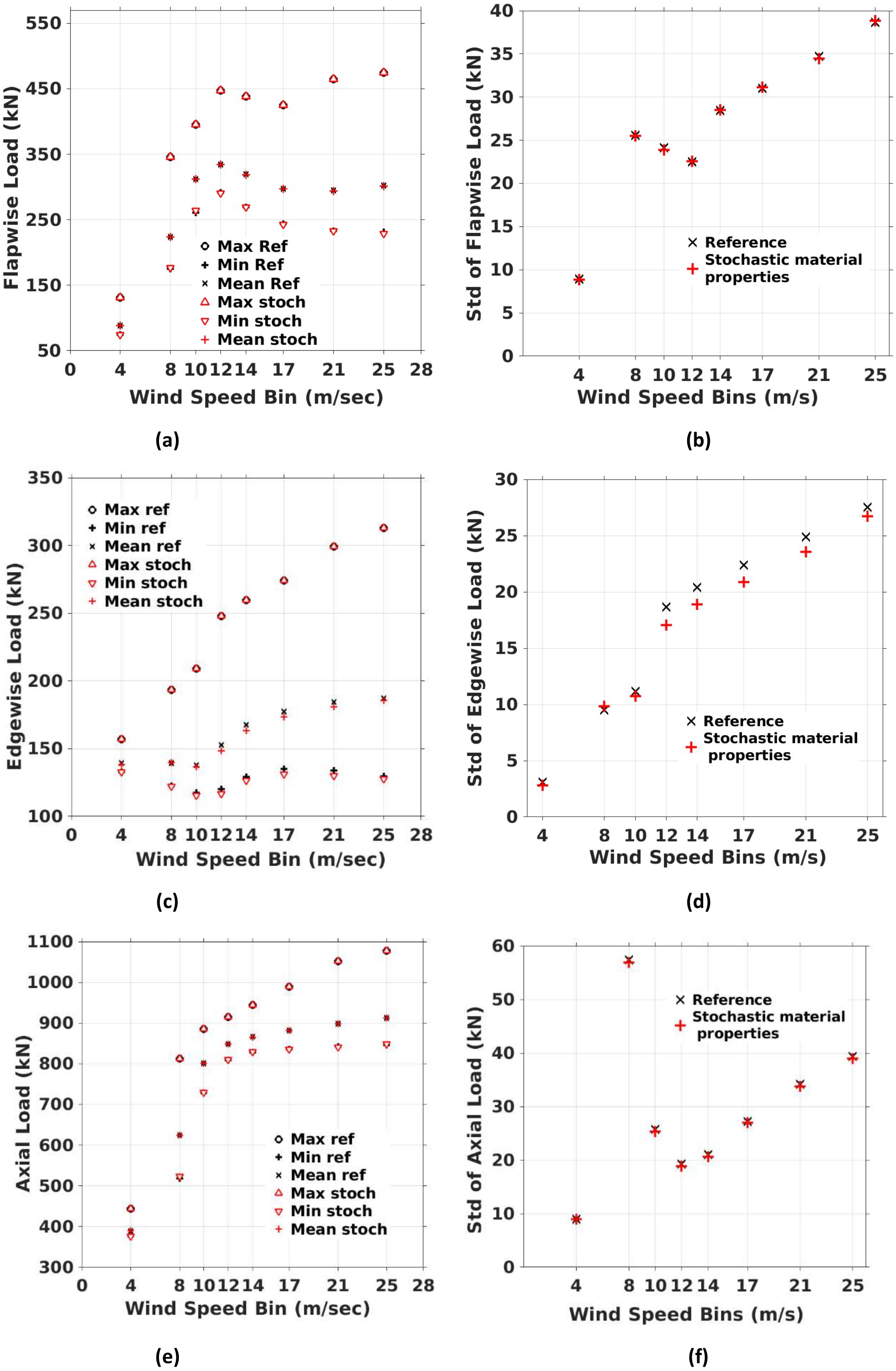

Figure 23: Maximum values distribution (left) and STD (right), with 96 data sets per wind speed bin, with reference and StoMP blade data input and POT peak method, (a)- (b) Flapwise load, (c)- (d) Edgewise load, (e)- (f) Axial load

In all load cases of Figure 23, the IEC criterion is satisfied and found being above 15%. The 3pW function is proposed for the fitting of all forces mentioned, for both peak methods according to the visual criterion method and the K-S test.

4.1.5 Case 2- short term fitting for the 14 m/sec wind speed bin for all material properties

In order to better assess the differences in the deflections in connection to blade material properties, an additional set of results is defined and processed. Twenty different sets of material properties, forming 20 different blade sets, are randomly chosen from the OptiDAT database and for each one of them, 24 DLC1.1 simulations are performed at the wind speed of 14m/s using different turbulence seeds. This forms a total of 480 simulations. POT extraction is applied to each of the 24 simulations per material set and then a 3pW CDF is fitted to the collected extreme data per material set. Finally, extrapolated values at the 1E-4 probability threshold are recorded in all cases. The same procedure is also applied to the reference blade data using the same 24 wind speed sets, in order to compare RefMP against StoMP on the same randomization basis.

Concerning the number of simulations made and mentioned in paragraphs 4.1.1 and 4.1.5, two different set of calculations are carried out. Initially 96 random values have been selected from the lognormal distribution of every one of the composite material properties E_1, E_2, G_{12} and v_{12}. These random values were randomly combined resulting 96 different material combinations for the blade properties. For each one of the different material combinations a simulation with stochastic wind was performed for every mean wind speed bin. So the total number of simulations was 96 for each wind speed bin, with different blade properties and different stochastic wind input for the same mean wind speed bin. In the second set of calculations only the mean wind speed bin of 14 m/s was considered. In this campaign, 20 different blade structures (out of the 96 originally defined), were selected and 24 different stochastic wind speed simulations were performed for each one of them. In the long term probability context, the two sets of simulated results are close in terms of the coefficient of variation resulting from the (stochastic) variation of the material properties of the blades. So, it is considered, that there is no need for more simulations. The choice of 24 simulations for each of the 20 stochastic blades, even for one wind speed bin, resulted to the same variability compared to the reference blade. So, it is considered safe to procceed to certification design results.

Furthermore, in this assessment context, the analysis of the cross-section stresses is also contained. A relevant tool [56] **is** based on the full stiffness matrix formulation of beam cross sections and is applied along the blade span. The tool provides the stress distribution and the Tsai-Hahn failure criterion over a cross section, based on the resultant loads applied at a reference point of the section. The Tsai–Hahn failure criterion which is the special case of Tsai–Wu general equation [57] is based on the theory of material failure for anisotropic composite materials with different strengths in tension and compression. The criterion predicts failure when the strength ratio becomes lower than 1, as stated in equation (4-1),

$$R = \frac{-B+\sqrt{B^2+4A}}{2A} \geq 1 \text{ with} \tag{4-1}$$

$$A=F_{11}\sigma_n\sigma_n + F_{55}\sigma_{nv}\sigma_{nv} + F_{66}\sigma_{ns}\sigma_{ns} \; , \; B = F_1\sigma_n$$

Where F_{11}, F_{55}, F_{66} and F_1 denote strength tensor components of the fourth and second rank respectively that are experimentally determined, while $\sigma_n, \sigma_{nv}, \sigma_{ns}$ denote the stress tensor.

In particular the non zero terms used for the Tsai-Hahn regular failure criterion are the following and the strength properties are mentioned in Table 1

$$F_1 = 1/XT - 1/XC \; , F_{11} = \frac{1}{XT.XC}, F_{55} = \frac{1}{S^2}, F_{66} = \frac{1}{S^2}$$

Also concerning the stress tensor mentioned above, on the laminate local coordinate system the stresses developed in each layer are connected to strains through:

$$\begin{Bmatrix} \sigma_n \\ \sigma_s \\ \sigma_{sv} \\ \sigma_{nv} \\ \sigma_{ns} \end{Bmatrix} = \begin{bmatrix} q_{n11} & q_{n12} & 0 & 0 & q_{n16} \\ q_{n12} & q_{n22} & 0 & 0 & q_{n26} \\ 0 & 0 & q_{n44} & q_{n45} & 0 \\ 0 & 0 & q_{n54} & q_{n55} & 0 \\ q_{n61} & q_{n26} & 0 & 0 & q_{n66} \end{bmatrix} \begin{Bmatrix} \varepsilon_n \\ \varepsilon_s \\ \gamma_{sv} \\ \gamma_{nv} \\ \gamma_{ns} \end{Bmatrix} \tag{4-2}$$

Subscript n reminds that the coordinate system is the local laminate system. The 5x5 **qn** matrix is symmetric. At this point, in the stress software used a matrix reduction is performed, assuming that the in-plane strains in the transverse direction, ε_s, as well as the through-the-thickness shear strains (γ_{sv}) can be neglected. So matrix reduction leads to following relation between layer stresses and strains on the laminate local axis:

$$\begin{Bmatrix} \sigma_n \\ \sigma_{nv} \\ \sigma_{ns} \end{Bmatrix} = \begin{bmatrix} q_{n11} & 0 & q_{n16} \\ 0 & q_{n55} & 0 \\ q_{n61} & 0 & q_{n66} \end{bmatrix} \begin{Bmatrix} \varepsilon_n \\ \gamma_{nv} \\ \gamma_{ns} \end{Bmatrix} \tag{4-3}$$

The above reduced 3x3 **qn** matrix is used in following procedures to define the laminate stiffness matrices. So the stresses plotted in the next figures of the chapter are the $\boldsymbol{\sigma_n}$ and $\boldsymbol{\sigma_{ns}}$, and the $\boldsymbol{\sigma_{nv}}$ is also used for the calculation of the Tsai-Hahn criterion.

In the absence of rotation, the 3x3 $\mathbf{q_n}$ matrix is expressed in terms of the material properties as follows:

$$q_n = \begin{bmatrix} E11^2 \ / \left(E11 - \nu 12^2 E22\right) & 0 & 0 \\ 0 & G_{13} & 0 \\ 0 & 0 & G_{12} \end{bmatrix} \tag{4-4}$$

Suggesting that the q_{n11} term is stiffer than $E11$ itself. Although the above reduction is mathematically sound, the extra stiffening of q_{n11} due to the $E22$ is not reasonable as long as the laminates are not constrained in the transversal direction. In order to correct this, an alternative $\boldsymbol{q_n}$ matrix reduction is followed. The $\boldsymbol{S_n}$ matrix calculated from Eq.2 is first reduced to a 3x3 matrix $\boldsymbol{S_{nR}}$ by eliminating its second and third row and column and then inverted to $\boldsymbol{q_n}=\boldsymbol{S_{nR}}^{-1}$. When there is no no rotation, this alternative calculation yields $q_{n11}=E_{11}$.

Figure 24 shows the flowchart of the procedure for estimating the design loads, the deflections and the stresses, with varying blade material properties.

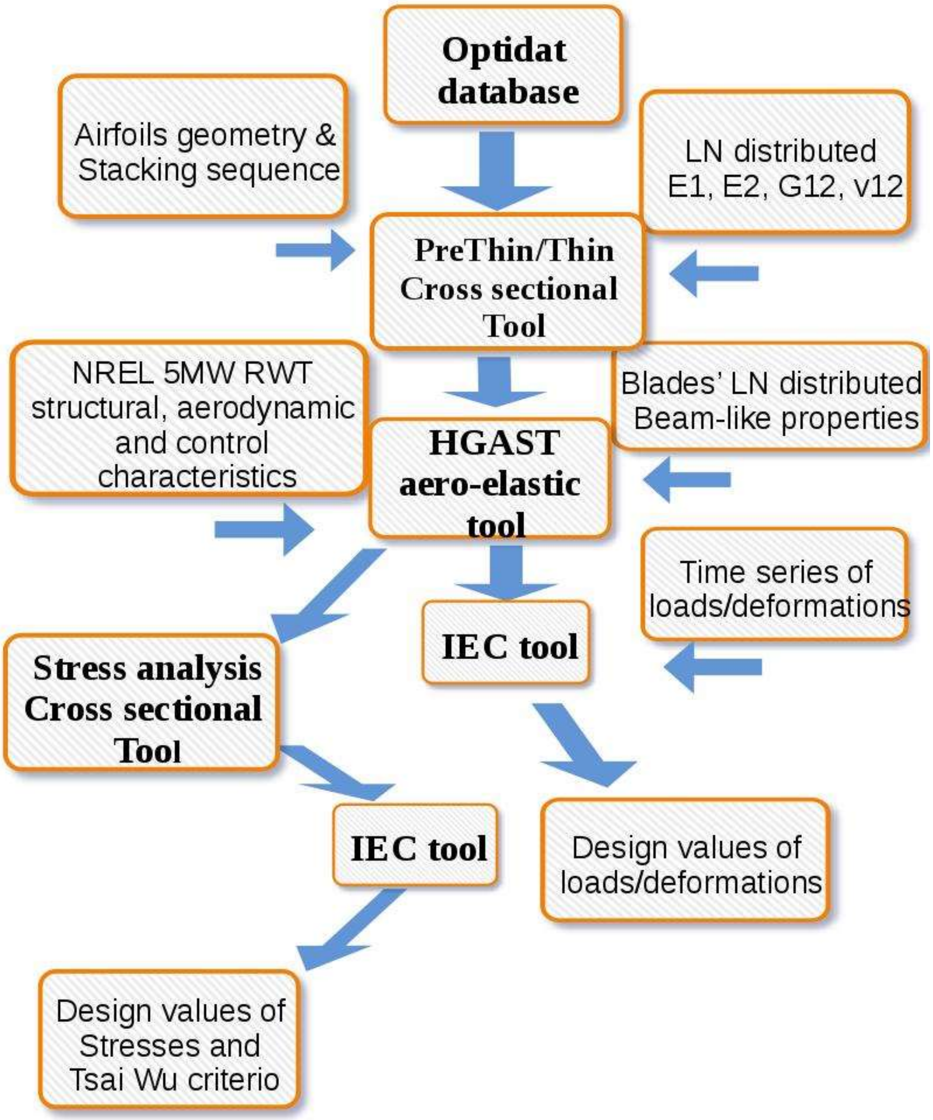

Figure 24. Flowchart illustrating the procedure for the estimation of the design loads/deflections/stresses with StoMP.

In order to assess the short-term blade tip deflection CoV, the flapwise moment CoV at r=14m and the stress assessment CoV in connection to blade material properties, the following short-term analysis is presented. The fitted CDF curves for the flapwise deflection and moment with StoMP are shown in Figure 25 and compared to the CDF curve obtained for the RefMP. The predicted values of the extreme deflection for the RefMP and StoMP will be substantially different. On the contrary, the CDF curves for the maximum flapwise moments show much smaller variations. Specifically, the CoV of the forecasts for the blade tip flapwise deflections at 1e-4 exceedance probability is 7.7% and for the flapwise moment at r=14m is 0.6%.

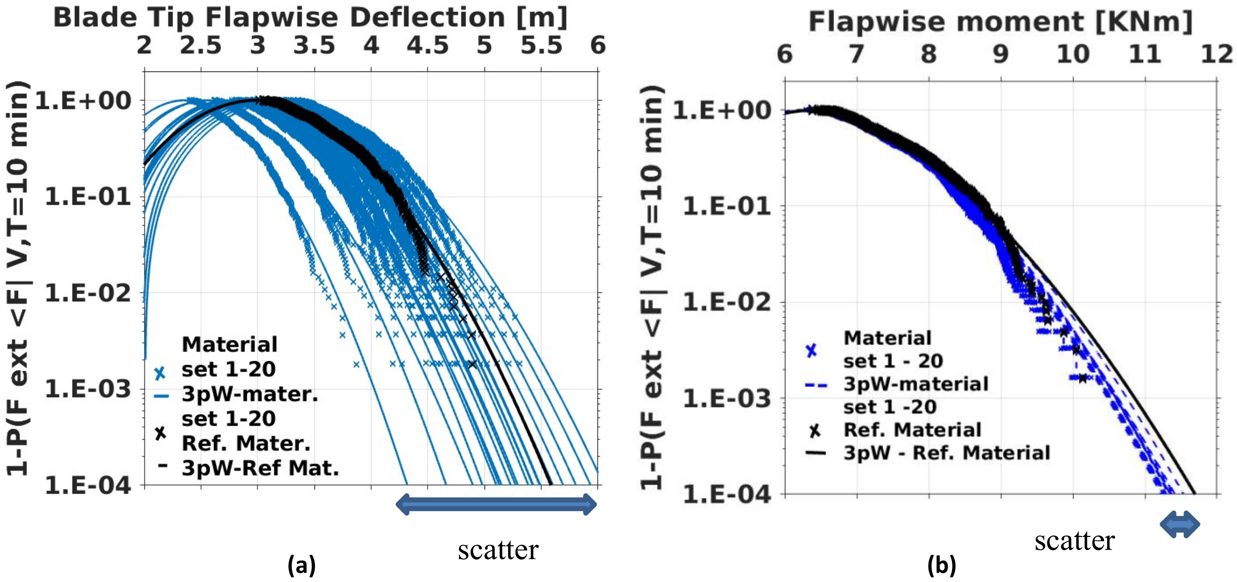

(a) **(b)**

Figure 25. Short term probability of the flapwise blade tip deflection (a) and the flapwise moment at r=14m (b) at wind speed of 14 m/s, for the reference blade data (black continues line) and 20 log normally distributed blade properties (blue dash line).

The average, minimum and maximum extreme flapwise deflection at the tip and flapwise moment at r=14m of the 24 simulations per material set are shown in Figure 26. The deviations amongst the different material sets are important as regards flapwise deflection, but much less pronounced as regards flapwise moments. The lines in Figure 26 indicate the reference blade data statistics.

Next, stress distributions and values of the Tsai-Hahn failure criterion are calculated over different cross sections along the span of the blade. Calculation of stresses is based on the cross-sectional analysis tool [56]. Input to the tool is the set of three resultant forces and moments per cross section. In this stress analysis, the input set of resultant loads that provide the design stress values of the section, includes: the global maximum of the flapwise bending moment per simulation of the blade along with the concurrent forces and moments in all other directions.

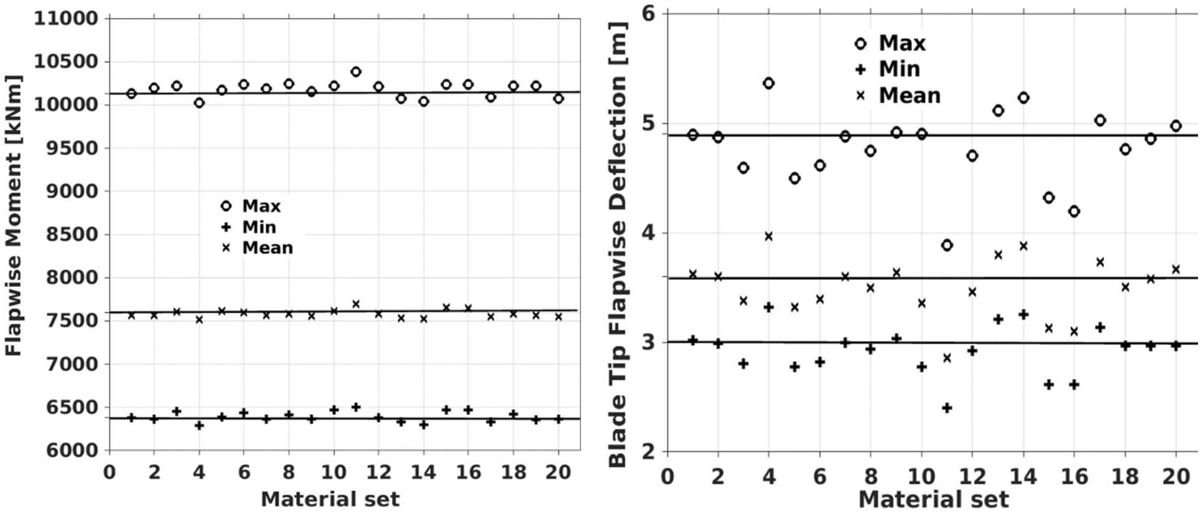

a)

b)

Figure 26: Statistics of maximum peak values of the flapwise moment (left) at r=14m and the flapwise blade tip deflection (right), at wind speed of 14 m/s, for the reference blade data and 20 random material properties with 24 wind data sets per material, considering the POT method.

Figure 27 presents the results of the stress analysis for the reference blade at r=22m. As discussed next, this is the station at which maximum stresses are obtained. Figure 27(a), illustrates the mean line along the skin of the section. Extreme values of stresses are recorded at nodes No95 and No100, which are both close to the spar cup on the suction side of the blade and indicated by arrows. In Figure 27(b) and (c) the normal (to the cross-section plane) and shear stresses (over the cross-section plane) along the skin of the section are shown for the different ply sequences. They correspond to six different laminate plies constructed by Tri-axial and UD material. The extreme normal stress appears at node No100 and it is equal to 85 MPa. The extreme shear stress is obtained at node No95 and is equal to -16MPa. For the failure criterion the lowest value is obtained at node No100 (point closer to failure) and it is equal to 2.39 (see Figure 27(d)).

In Figure 28 (a), fitted CDFs of the normal stresses of the blades with StoMP at r=14m (section where flapwise moments are analyzed) are compared to the CFD of the reference blade. The CoV of the extreme (ultimate) normal stress corresponding of the blades with stochastic properties is 2%. In Figure 28 (b) the minimum Tsai-Wu criterion at r=14m is shown for the different wind realizations (24 simulations) and for the different material properties. It is obvious that the difference between strength ratios of the criterio for the different blades due to variation to the material properties might be higher than 50% for any random wind simulation.

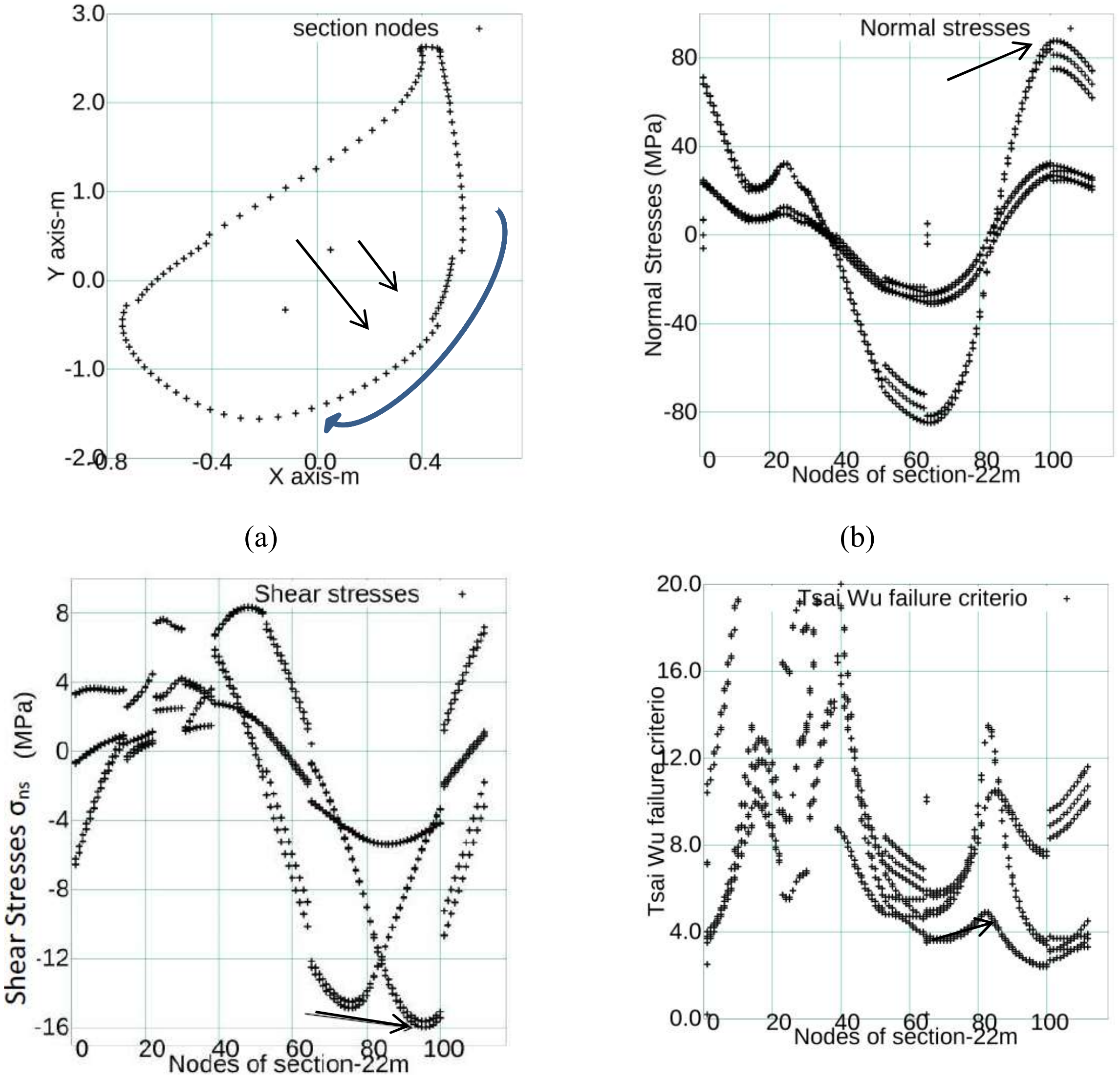

(a) (b)

(c) (d)

Figure 27. Stress analysis and failure criterion for the blade section at 22m for the Wind speed of 14 m/s. (a) The symbols correspond to the nodes of the mean surface of the section skin. Numbering is clockwise (b) shows the distribution of the normal stresses at the different nodes (c) the same for the shear stresses (d) the same for the Tsai-Wu failure criterion.

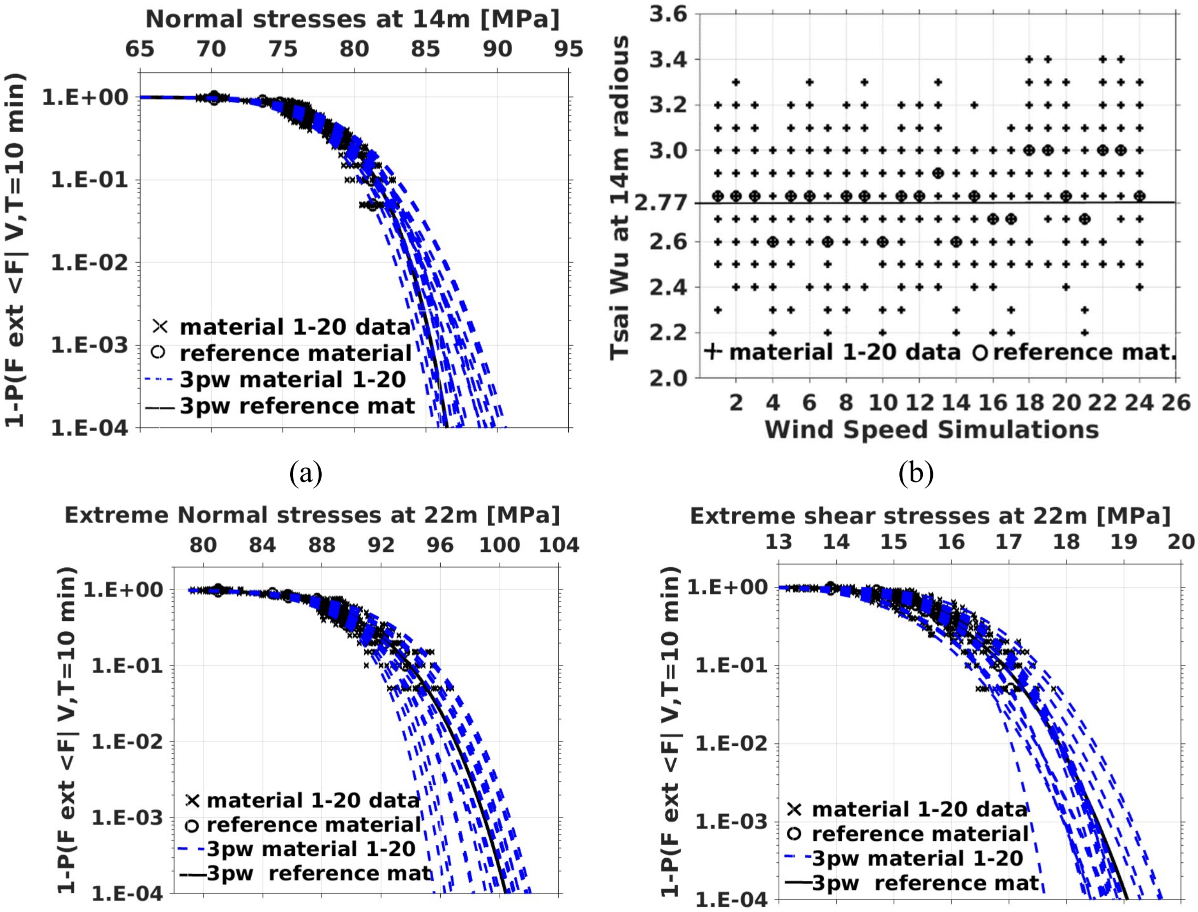

(a) (b)

(c) (d)

Figure 28. (a) Short term probability of the extreme normal stresses at r=14m, (b) Tsai-Wu failure criterion values at r=14m, (c) the extreme normal at r=22m, (d) the extreme shear stresses at r=22m, for the reference blade data (black continues line) and 20 log-normally distributed (blue dash lines). Wind speed 14m/s.

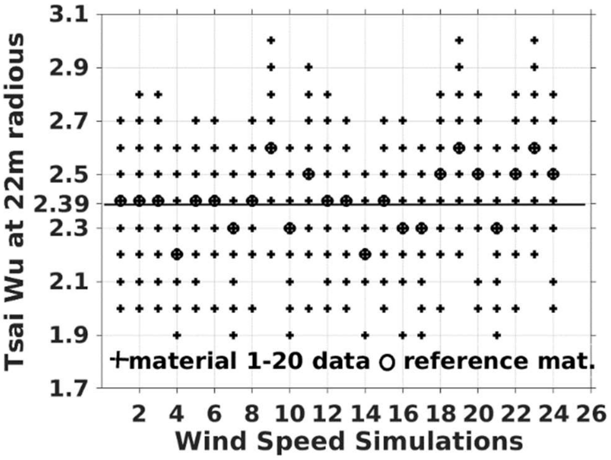

Figure 29: Tsai-Wu failure criterion values at r=22m, for the reference blade data (circles) and the 20 StoMP (cross dots). Wind speed 14m/s.

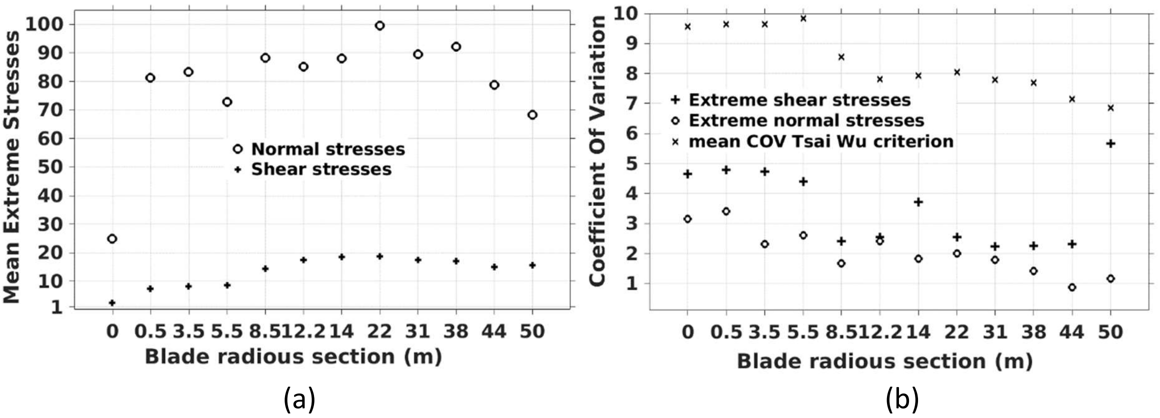

Figure 30. (a) Mean values of the extreme normal (circles) and shear stresses (crosses) and (b) CoV of the extreme normal and shear stresses and of the Tsai-Wu criterion, along the blade span at the wind speed of 14 m/s, for the StoMP.

The CoV of the criterion value for the reference blade (due to the different wind seeds) is 5%. The CoV of the criterion value for the blades with StoMP is 8%. The solid line in the plot corresponds to the mean of the reference blade (criterion value equal to 2.77).

In Figure 28 (c) and (d), the fitted CDF curves for the normal and the shear stresses of the blades with StoMP at r=22m (section where maximum stresses are obtained) are compared to the CDF of the reference blade. The CDF curves for the maximum normal stresses show smaller variation as compared to those of the shear stresses. Specifically, the CoV of the shear stresses is 2.5% and of the normal stresses is 1.8%.

In Figure 29, the minimum values of the Tsai-Wu failure criterion are shown for the section at r=22m. The CoV of the criterion values of the reference blade and the blades with stochastic properties remain 5% and 8% respectively, as at r=14m.

In Figure 30 (a), the distribution along the blade span of the mean ultimate normal and shear stresses (probability 1e-4) of the different blade sets with stochastic properties are shown. The values of the mean normal stresses range between 68 and 100 MPa, except at the blade root where a significantly lower stress is obtained (25MPa). The root section is cylindrical made of 177 composite laminates which results in lower stress resultants per laminate. The values of the mean extreme shear stresses range between 8 and 20 MPa. As already noted, maximum stresses (normal and shear) are obtained at r=22m. In Figure 30 (b), the radial distributions of the CoV of the mean Tsai-Wu value and the extreme normal and shear stresses, due to the material variation are shown. The CoV of the criterion lies in the range of 7 to 10%. The CoV of the extreme stresses is lower, i.e. 2% to 5.5% for the normal and 1% to 3.5% for the shear. It is noted that in the calculation of the Tsai-Wu criterion the variation in the yield properties for the different material sets is taken into account which explains the higher values of the CoV.

4.2 Long term fitting and comparisons for all moments - loads at r=14 m and for the blade tip deflections with both blade data inputs

4.2.1 Flapwise moment at r=14 m and blade tip flapwise deflection

In this section, long term fitting and 50-year design load are presented for the flapwise moment and the blade tip flapwise deflection based on 96 data sets per wind speed bin for the reference and the stochastic blade data input.

The 3pW probability distribution function is used for the reliability calculations as it was earlier proven to be the most appropriate distribution function to fit to short term data. In Figure 31 the long-term exceedance probability of the extreme loads is plotted for a return period of 50-years for the resultant flapwise moment at r=14 m for both sets of data using the POT peak method. The long-term exceedance probability forecasts the extreme value over a period of 50 years life time with all the wind speed bins included. In all plots the extreme load data points exhibit a rather smooth behavior at high cumulative probability values, while they are less smooth towards the tail of the distribution. In particular, at very low probability values, a change of slope appears in the flapwise moment results at about 10MNm. This “knee” is the same in the results from both blade data sets. Such a behavior of the low probability extremes is usually related to high wind speed conditions, in which turbulent content is high and therefore small variations for example in wind direction or pitch angle can result in high variations of the loads. It is noted that variability of the tail extreme loads is high for the flapwise bending moment as its variations are directly associated to wind variations. This is also expected for the edgewise moment at above rated wind conditions as a result of the thrust contribution to the edgewise bending direction when the blade is pitched.

In Figure 32 the long-term exceedance probability of the blade tip flapwise deflection is presented for a return period of 50-years, for the stochastic blade data set using the POT peak method. In the plots the deflection data points exhibit a rather smooth behavior at high cumulative probability values, while they are less smooth towards the tail of the distribution. In particular, at very low probability values a change of slope appears as close to 5m deflection.

In Figure 32 the long-term exceedance probability of extreme flapwise tip deflections is presented. According to Table 8, deflection attains a maximum difference higher than 4% while for this particular case the estimation based on RefMP is conservative (predicts higher extreme deflections). The flapwise bending moment results remain almost the same. The same holds for the bending moment confidence range and the design values presented in Table 7.

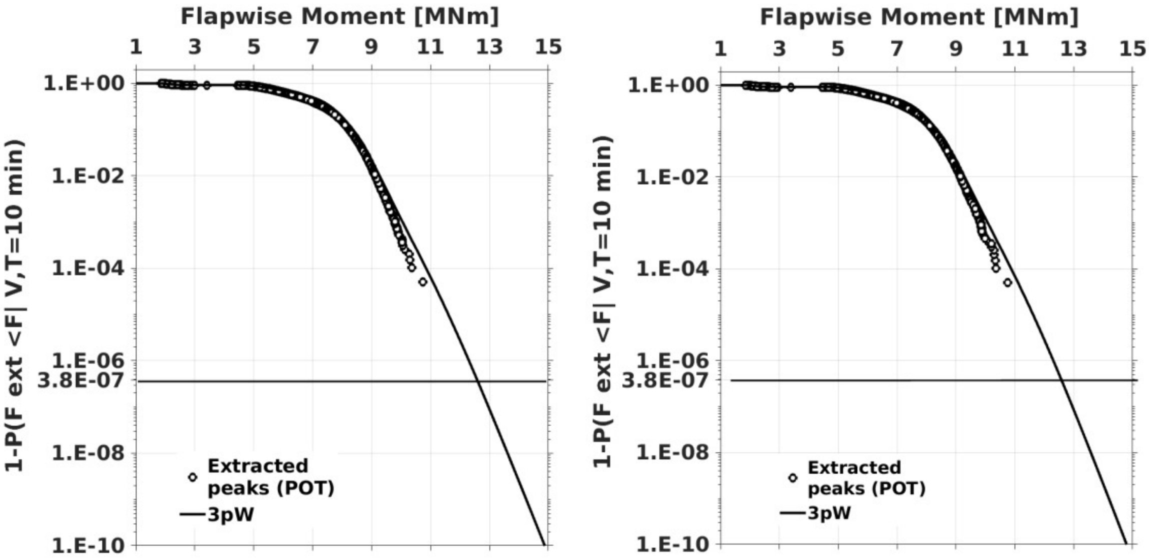

Reference blade properties **Log normally distributed blade properties**

Figure 31: Long term 50 years design load base target for the Flapwise moment, based on 96 10min simulations per wind speed bin. The reference (upper) and log normally distributed (lower) blade properties are presented using the POT method and the 3pW CDF, (Software Matlab R2012b used to illustrate figure and collect data).

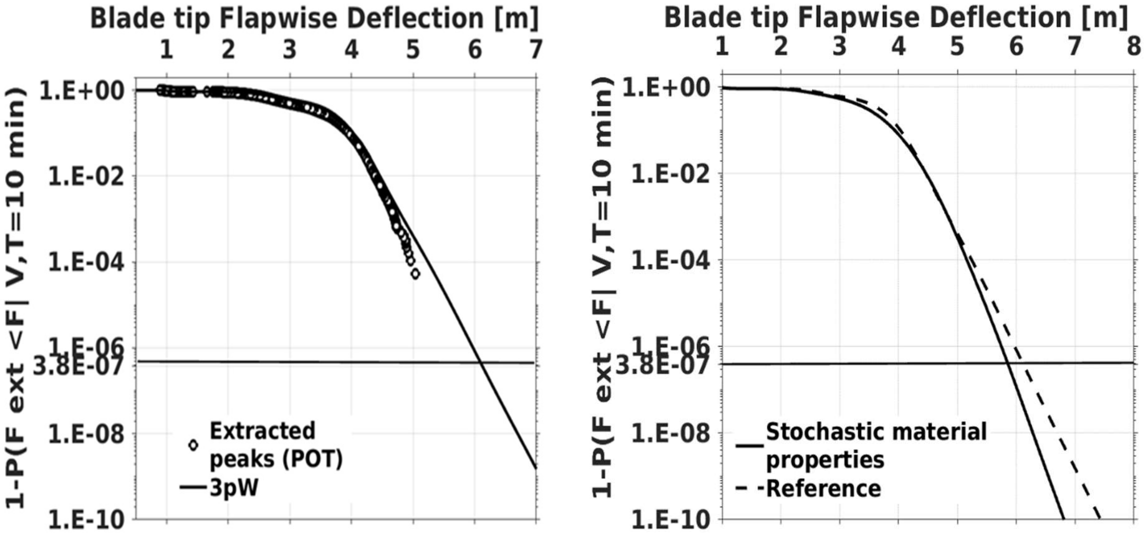

a) b)

Figure 32: Long term 50 years design load base target for the reference blade properties (left) and comparison between reference and stochastic (right) blade tip flapwise deflection, based on 96 10min simulations per wind speed bin. The results presented, are using the POT method and the 3pW CDF.

Flapwise moment (kNm)	Design value 5% conf. bound	Variation GM – POT	Design value	Variation GM - POT	Design value 95% conf. bound	Variation GM - POT	90% confidence range
GM-96-RefMP	10962		11652		12848		1886
POT-96-RefMP	12386	+13%	**12589**	8%	12786	-0,5%	400
GM-96-StoMP	11099		11750		12777		1678
POT-96-StoMP	12385	+11,6%	12584	+7,1%	12778	0%	393

Table 7: Long term fifty years design load base target and confidence bounds 5%-95% for flapwise moment, Number of data sets: 96, Blade data: Reference and stochastic, Comparison between Peak Methods GM and POT.

Blade tip flapwise deflection (m)	Design value 5% conf. bound	Variation GM – POT	Design value	Variation GM - POT	Design value 95% conf. bound	Variation GM - POT	90% conf. range
GM-96-RefMP	5.26		5.55		5.95		0.69
POT-96-RefMP	6.00	14%	6.12	10.3%	6.23	4.7%	0.23
GM-96-StoMP	5.76		6.16		6.51		0.75
POT-96-StoMP	5.7	-1%	5.86 (-4,2%) to RefMP	-5,8%	6.01	-7,6%	0.31

Table 8: Long term fifty years design load base target and confidence bounds 5%-95% for blade tip flapwise deflection Number of data sets: 96, Blade data: Reference and stochastic, Comparison between Peak Methods GM and POT.

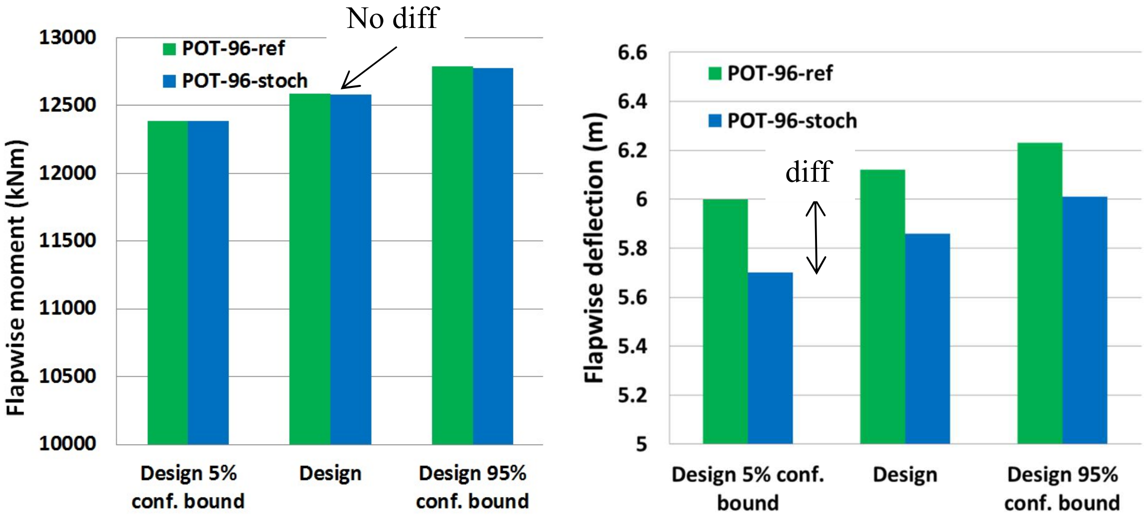

Figure 33: Fifty (50) years long term design base target and confidence bounds 5%-95% for the flapwise moment at r=14m (left) and the blade tip flapwise deflection (right), using 96 simulations per wind speed bin, the POT method and the 3pW distribution function. The reference and the log normally distributed (Stochastic) blade properties are compared, (Software windows excel used to illustrate figure and collect data).

In addition to the already discussed Table 7 and Table 8, in Figure 33, Figure 34, the design values of flapwise moments remain unchanged. The confidence bounds for the RefMP and the StoMP are almost identical, while the confidence interval is high, which is in line with the IEC convergence criterion. On the other hand, for the present case study, higher design deflection values are obtained for the reference blade data as compared to the stochastic ones, while the confidence interval is high for both data sets and consistently follows the difference in the design value. As for the POT method, the design deflections are lower for the stochastic blade data sets, but the range of the 90% confidence interval is wider.

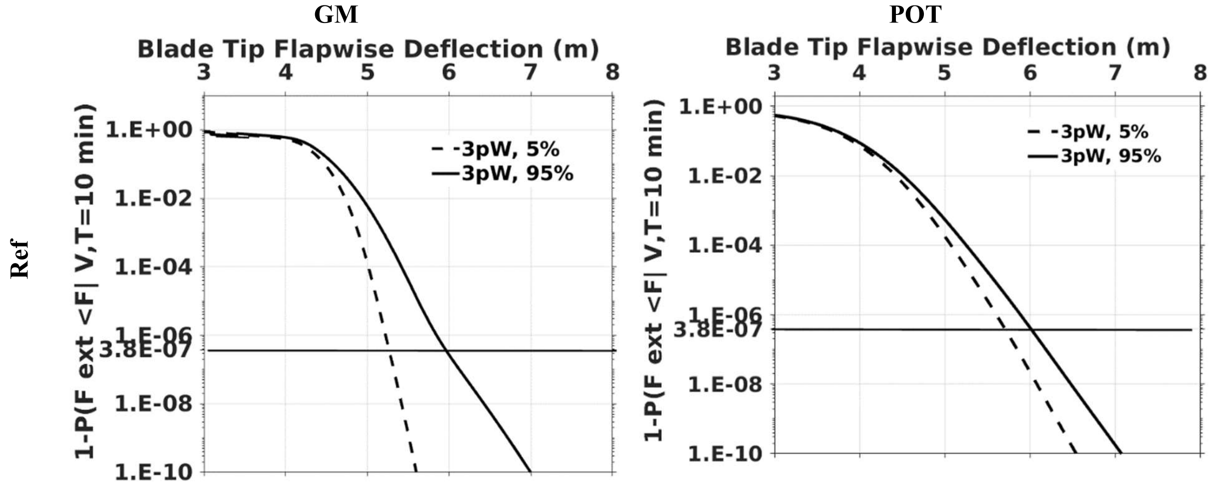

(a) **(b)**

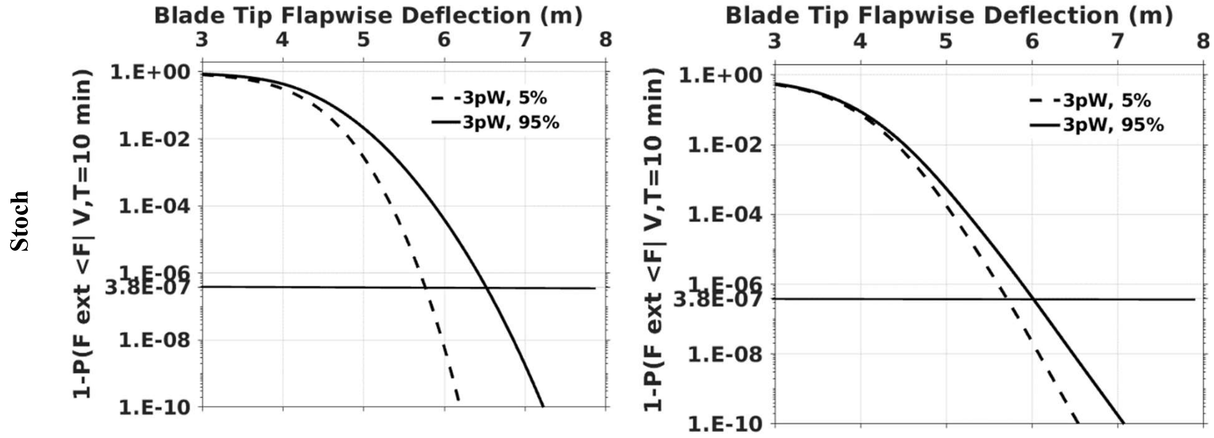

(c) **(d)**

Figure 34: Long term 90% confidence interval for the Flapwise deflections at tip, based on 96 10min simulations per wind speed bin considering the POT extraction method (right) and GM method (left) for the 3pW CDF. The solid lines correspond to the results for the 95% confidence interval, while the dashed to the 5% confidence interval. The log normally distributed blade properties illustrated to lower row and the reference to the upper row.

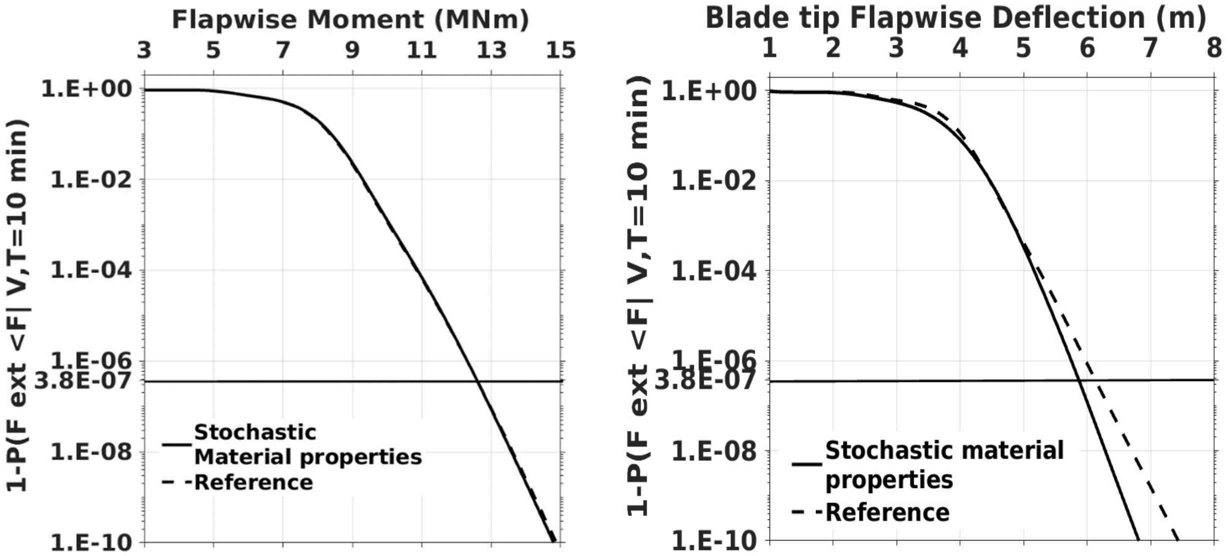

(a) **(b)**

Figure 35: Long term fifty years design load base target for flapwise moment (left) and blade tip flapwise deflection (right), Blade data: stochastic distributed and reference, Peak Method: POT.

The long-term exceedance probability of extreme flapwise moment and flapwise blade tip deflections are presented in Figure 35 for the POT method. Out of the two, the flapwise deflection attains the bigger difference, while for this particular case the estimation based on the reference blade data is conservative. The diff between the two sets of blade data is 11%, with respect to the reference blade.

4.2.2 Edgewise moment at section 7 (r=14m) and blade tip edgewise deflection

The long-term empirical exceedance distribution and the fifty years design load base target are calculated and presented also for the edgewise moment and the blade tip edgewise deflection, with the 3 parameter Weibull CDF, for both GM and POT methods.

In Figure 36 the long-term exceedance probability of extreme edgewise moment at blade section with r=14m and edgewise blade tip deflections are presented. While extreme moments remain almost unaffected, the same does not hold for the blade tip deflections. Out of the two, the deflection attains the difference, while for this particular case the estimation based on the reference blade data is conservative.

In Table 9 and Table 10, the 50-year extreme load resultants at r=14 m are provided. Results for the reference blade data are compared to those of the blades with StoMP. Also the long term 50-years design value and its confidence bounds 5% and 95% are presented for the edgewise moment at r=14m and the edgewise deflection at the tip, for both blade data sets, using the GM and the POT method with the 3pW distribution function and a set of 96 simulations per wind speed bin. The confidence bounds for the POT method and the StoMP are higher compared to the reference properties. The uncertainty of the material properties affects mainly the 50-years design blade tip edgewise deflection. Higher design deflection values are obtained for the RefMP, compared to the StoMP ones, while the confidence interval is higher for the StoMP sets of results.

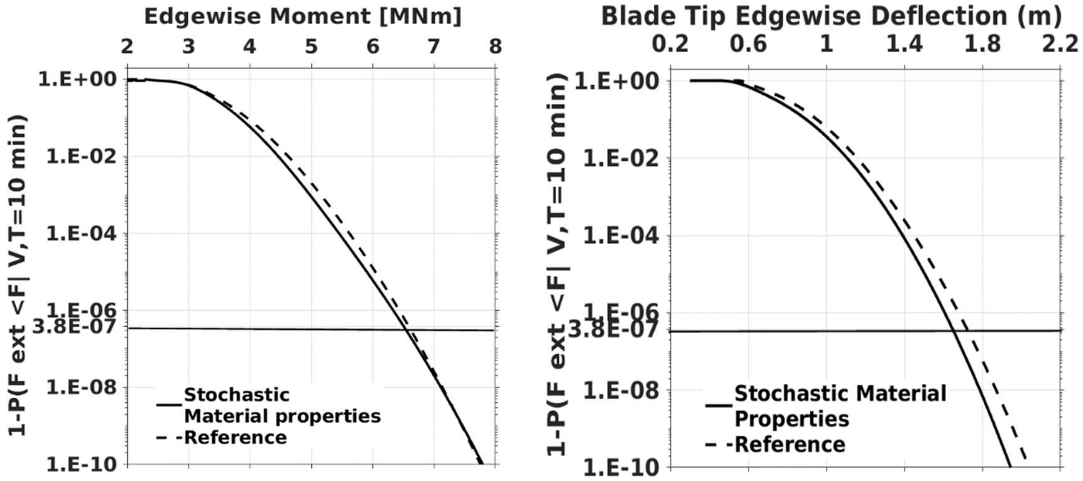

a) b)

Figure 36 : Long term 50 years design base target for the edgewise moment (left) and Edgewise deflections at the blade tip (right), based on 96 10min simulations per wind speed bin considering the POT extraction method and the 3pW CDF. The solid lines correspond to the results for the log normally distributed ones while the dashed to the reference blade properties.

Also, in Table 9 and Figure 37 a) like in Figure 36 a), the edgewise design moment calculated with POT method, is almost the same (6506, 6587), indicating a 1.2% reduction, when StoMP are used instead of RefMP. On the other hand, the long term 50-year edgewise design moment with GM method decreased by 4.8%. In Table 10 and Figure 37 b) like in Figure 36 b), the blade tip edgewise deflection decreased from 1.72m to 1.64m, giving a 4.6% reduction for the POT method. Concerning the choice between GM and POT for the edgewise design moment and the blade tip edgewise deflection; it is safer to use the POT method, as the confidence interval is shorter compared to the GM method.

Edgewise moment	Design value 5%	Diff. StoMP-RefMP	Design value	Diff. StoMP-RefMP	Design value 95%	Diff. StoMP-RefMP	Confidence 90% range (kNm)	Diff. blade data sets
GM-96-RefMP	6391		7081		7764		1373	
GM-96-StoMP	6304	-1.3%	6741	-4.8%	7238	-6.7%	934	-31%
POT-96-RefMP	6460		6587		6710		250	
POT-96-StoMP	6368	-1.4%	6506	-1.2%	6640	-1%	272	+8.8%

Table 9: Edgewise moment long term exceedance probability design values and 90% confidence interval with GM and POT method, for 96 data sets per wind speed bin, with 3pW CDF fitting, with reference and stochastic distributed blade data input

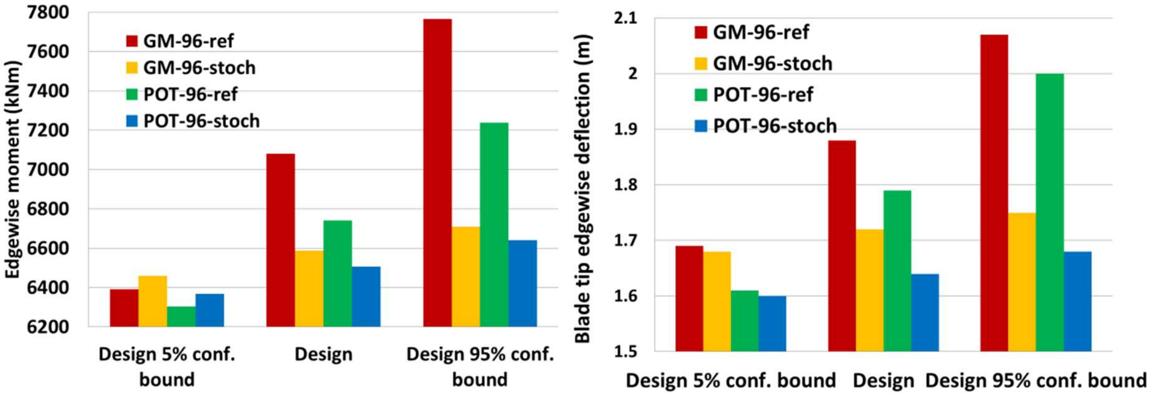

Figure 37: Long term exceedance probability design values and 90% confidence interval with GM and POT method, for 96 data sets per wind speed bin, with 3pW CDF fitting, with reference and stochastic distributed blade data input a) Edgewise moment, b) Blade tip edgewise deflection

Blade tip Edgewise deflection	Design value 5%	Diff. StoMP-RefMP	Design value	Diff. StoMP-RefMP	Design value 95%	Diff. StoMP-RefMP	Confidence 90% range (m)	Diff. blade data sets
GM-96-RefMP	1.69		1.88		2.07		0.38	
GM-96-StoMP	1.61	-4.8%	1.79	-4.7%	2	-3.3%	0.39	2.5%
POT-96-RefMP	1.68		1.72		1.75		0.07	
POT-96-StoMP	1.6	-4.8%	1.64	-4.6%	1.68	-4%	0.08	14.3%

Table 10: Blade tip edgewise deflection long term exceedance probability design load and 90% confidence interval with GM and POT method, for 96 data sets per wind speed bin, with 3pW CDF fitting, for reference and stochastic distributed blade data input

4.2.3 Torsion moment stress resultant and blade tip twist angle

In the following Table 11 and Table 12, the extrapolated 50-year design values for torsion moment and the blade tip twist angle are presented with GM and POT methods according to IEC. Also, the 90% confidence interval of the extrapolated design values is presented. The variance between the different blade data sets for the GM and POT peak methods is illustrated.

The design torsion moment for section 7 at 14 m from the root, with the GM method is higher compared to POT method, with wider confidence interval. So, the POT method is selected, as it is indicated from the confidence interval in Table 11 and the IEC code guidelines. Concerning the stochastic blade data there is no difference between the design load based on the GM and the POT methods.

Torsion moment kNm	Design value 5%	Diff. StoMP-RefMP	Design value	Diff. StoMP-RefMP	Design value 95%	Diff. StoMP-RefMP
GM-96-RefMP	206		222		238	
GM-96-StoMP	206	0%	215	-3.1%	236	-0.8%
POT-96-RefMP	212		214		217	
POT-96-StoMP	213	+0.5%	215	+0.5%	218	+0.5%

Table 11: Long term fifty years design load base target and confidence bounds 5%-95% for torsion moment, Number of data sets: 96, Blade data: Reference and stochastic with GM and POT method, Comparison between different blade data sets

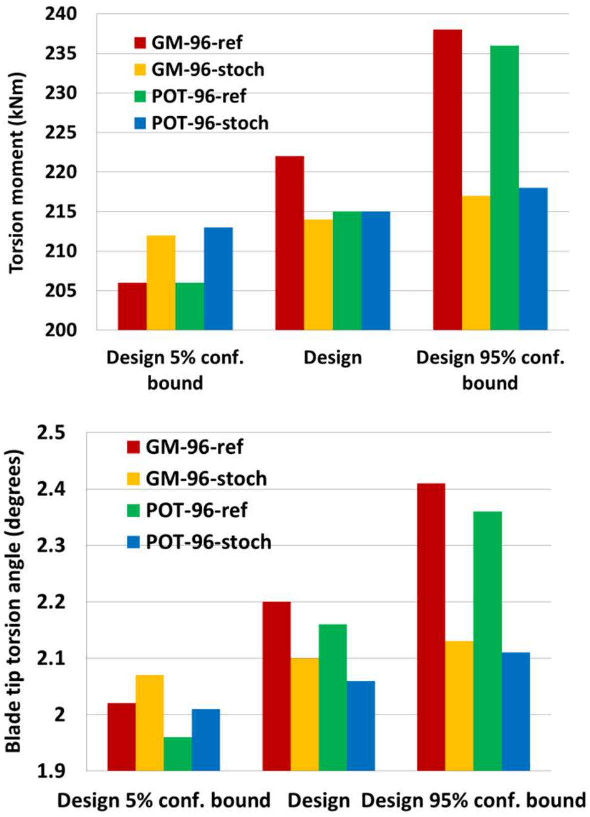

Figure 38: Long term exceedance probability design values and 90% confidence interval with GM and POT method, for 96 data sets per wind speed bin, with 3pW CDF fitting, with reference and stochastic distributed blade data input a) Torsion moment, b) Blade tip torsion angle

It is noted that in Table 11, the torsion moment design value remains almost the same when StoMP and RefMP are considered. The POT confidence bounds for the RefMP and StoMP are almost identical, while the confidence interval is high being in line with the IEC convergence criterion. On the other hand, the uncertainty of the material properties affects the 50-years design blade tip torsion angle in Table 12. For the present case study, higher design deflection values are obtained for the RefMP as compared to the StoMP ones, while the confidence interval is higher for stochastic data sets.

Blade tip Torsion angle (degrees)	Design value 5%	Diff. StoMP-RefMP	Design value	Diff. StoMP-RefMP	Design value 95%	Diff. StoMP-RefMP	Diff. 5-95%	Diff. StoMP-RefMP
GM-96-RefMP	2.02		2.20		2.41		0.39	
GM-96-StoMP	1.96	-3%	2.16	-1.8%	2.36	-2.1%	0.4	+2.5%
POT-96-RefMP	2.07		2.10		2.13		0.06	

POT-96-StoMP	2.01	-2.9%	2.06	-1.9%	2.11	-0.9%	0.09	+50%

Table 12: Long term fifty years design load base target and confidence bounds 5%-95% for blade tip twist angle, Number of data sets: 96, Blade data: Reference and stochastic, Comparison between Peak Methods GM and POT, Comparison between blade data

The design torsion angle in Table 12 for the blade tip section, with the GM method and for the reference blade is 2.2 degrees. When the POT method is used the 50-year design value is reduced to 2.16 degrees. POT method is proven to forecast lower design deflection value compared to GM, with shorter confidence interval. Concerning the StoMP, the same difference between GM and POT method, from 2.16 degrees to 2.06 degrees respectively is observed.

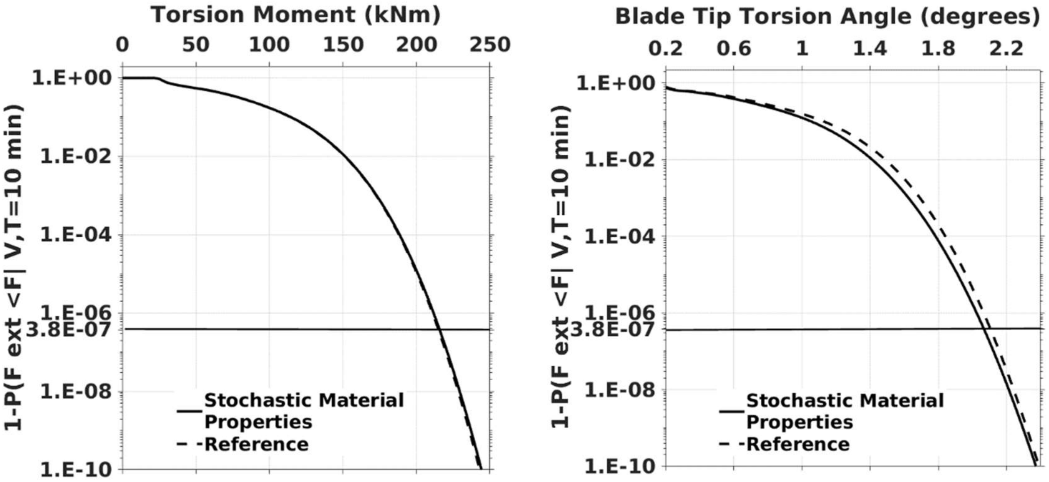

a) **b)**

Figure 39: Long term 50 years design base target for the torsion moment (left) and blade tip twist angle (right), based on 96 10min simulations per wind speed bin considering the POT extraction method and the 3pW CDF. The solid lines correspond to the results for the log normally distributed blade properties while the dashed to the reference ones.

The long-term empirical exceedance distribution for the POT case is plotted in Figure 39 for the torsion moment and the blade tip twist angle. The 3 parameter Weibull CDF suggests the most accurate fitting as proved from all short-term fittings visual inspection and the K-S test. The torsion deflection estimation based on the RefMP is conservative. The design torsion moment at section 7, 14 m from the root, with both blade data and POT methods are 215 kNm and 214 kNm. The conclusion is that torsion moment design load is not dependent on material properties, as the previously examined moments. However, the blade tip torsion angle design value is dependent on the material properties and the estimation based on the reference data is the conservative one. Concerning the choice between GM and POT for the torsion moment design base target, it is safer to use POT, as the confidence interval is shorter and therefore it is assumed a conservative choice.

4.2.4 Flapwise, edgewise and axial loads

In Figure 40, the long-term fitting for the flapwise and the edgewise fifty-year design load with POT method is displayed, with reference and stochastic blade data input, for 96 simulations per wind speed bin. The CDF that it is introduced is the 3pW distribution fitting. The fifty-year extreme flapwise load calculation is 519 kN, for the POT method and it is almost the same for both blade data sets. The variance between POT and GM method is 2.4% as mentioned in Table 13. The POT method suggests larger design values for the flapwise loads and is therefore on the conservative side.

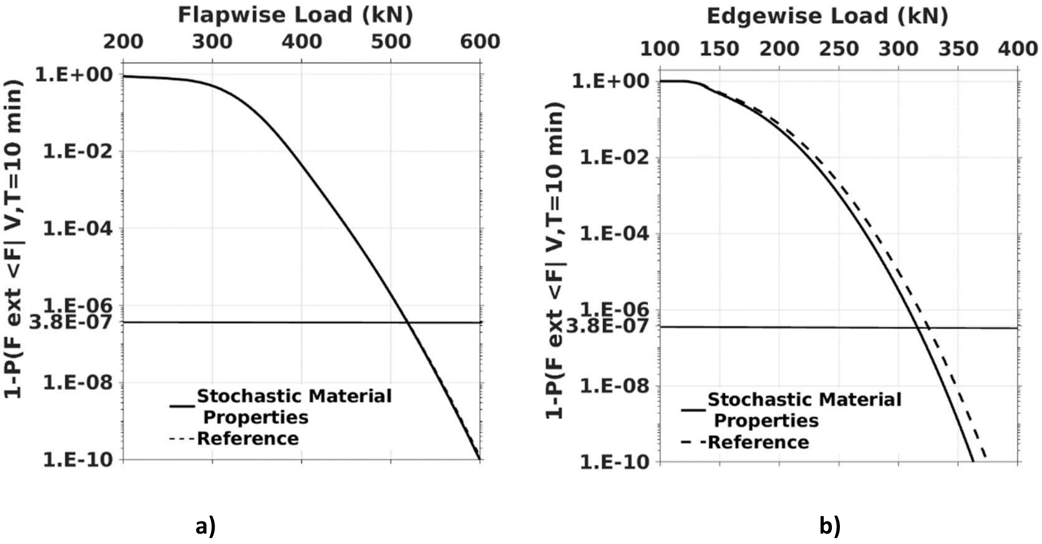

Figure 40: Flapwise and edgewise load long term fifty years design load base target, Blade data: RefMP (continuous lines) and StoMP (dash lines), Number of data sets: 96, Peak Method POT, a) Flapwise loads, b) edgewise load

In Table 13, the flapwise design load with the GM method is presented which is almost the same for both blade data sets. In Table 14, the long-term fitting for the edgewise load and the fifty year extreme load prediction with GM method is 375 kN while with POT is 325 kN for the reference and 315 kN for the stochastic blade data. So, the reduction of the design load values from GM to POT method is 13% for the RefMP and 16% for the StoMP.

Also, the relevant 90% confidence bounds were analyzed for both methods. It is concluded that the edgewise load is not dependent on material properties. Concerning the choice between GM and POT, the design loads provided by the GM method are higher, but the confidence interval is- much lower when the POT method used.

In Figure 41, Figure 42 and Table 15 the long-term fitting for axial loads and the extrapolated fifty-year design load with GM and POT methods are presented for reference and stochastic blade data input. The axial fifty-year extreme load prediction for the reference blade data is calculated at 1127 kN with GM method and 1143 kN with POT. In Figure 41, the difference between GM and POT methods and the relevant POT 90% confidence interval are illustrated, for the StoMP blade data input. So, the GM method gives 1098 kN 50 year extreme while the POT 1138 kN. The design load given by the POT method is +3.6% higher.

flapwise load (KN)	Design value 5%	Diff. StoMP-RefMP	Design value	Diff. StoMP-RefMP	Design value 95%	Diff. StoMP-RefMP	Diff. 5-95%	Diff. StoMP-RefMP
GM-96-RefMP	470		507		553		83	
GM-96-StoMP	469	-0.2%	505	-0.4 %	554	-0.2%	85	+2.4%
POT-96-RefMP	511		519		526		15	
POT-96-StoMP	510	-0.2%	518	-0.2 %	525	-0.2%	15	0%

Table 13: Long term fifty years design load base target and confidence bounds 5%-95% for flapwise load, Number of data sets: 96, Blade data: Reference and stochastic, Comparison between Peak Methods GM and POT, Comparison between blade data inputs.

edgewise load (KN)	Design value 5%	Diff. StoMP-RefMP	Design value	Diff. StoMP-RefMP	Design value 95%	Diff. StoMP-RefMP	Diff. 5-95%	Diff. StoMP-RefMP
GM-96-RefMP	333		375		403		70	
GM-96-StoMP	339	+1.8%	375	0 %	409	+1.5%	70	+0%
POT-96-RefMP	318		324		329		11	
POT-96-StoMP	309	-2.8%	315	-2.8%	321	-2.4%	12	+9%

Table 14: Long term fifty years design load base target and confidence bounds 5%-95% for edgewise load, Number of data sets: 96, Blade data: StoMP and RefMP, Comparison between Peak Methods GM and POT, Comparison between blade data sets

In Figure 41, Figure 42 and Table 15, the design predictions are presented with GM and POT methods. The design values are almost equal (-0.4%) for StoMP and RefMP blade data with the POT method. The same design axial loads have a difference of (-2.5%) between RefMP and StoMP when the GM is applied. Concerning the choice between GM and POT, it is safer to use POT, as the design loads are higher and therefore the choice is conservative. Also, the 90% confidence interval is minimized for the POT case in Figure 41 b).

axial load (KN)	Design value 5%	Diff. StoMP-RefMP	Design value	Diff. StoMP-RefMP	Design value 95%	Diff. StoMP-RefMP	Diff. 5-95%	Diff. StoMP-RefMP
GM-96-RefMP	1093		1127		1161		68	
GM-96-StoMP	1073	-1.8%	1098	-2.5 %	1124	-3.2%	51	+2.5%
POT-96-RefMP	1134		1143		1151		17	
POT-96-StoMP	1130	-0.35%	1138	-0.4 %	1146	-0.4%	16	+50%

Table 15: Long term fifty years design load base target and confidence bounds 5%-95% for axial load, Number of data sets: 96, Blade data: Reference and stochastic, Comparison between Peak Methods GM and POT, Comparison between blade

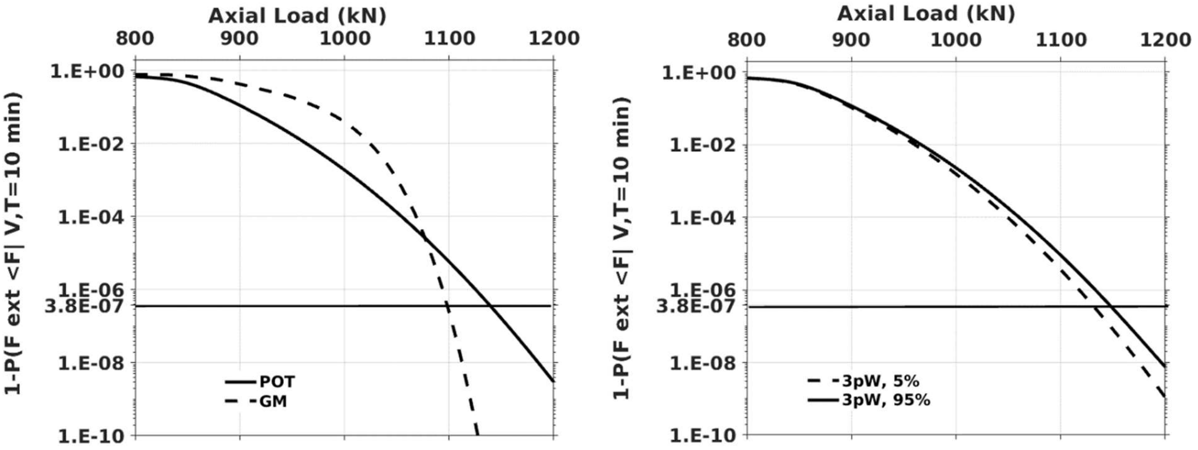

a)

b)

Figure 41: Long term fifty years axial design load base target, Number of data sets: 96, Blade data: StoMP, Peak Method: POT and GM, (a) Comparison between methods, (b) POT 90% confidence interval

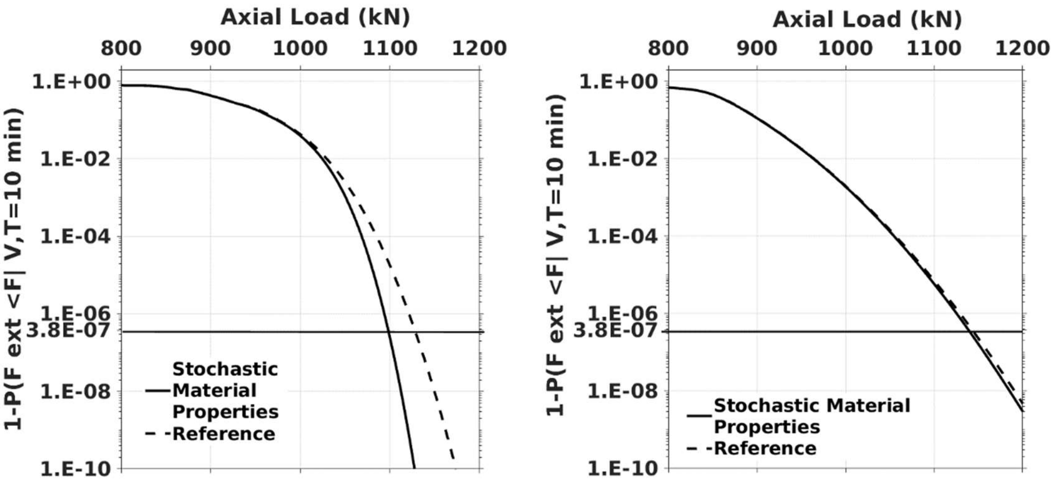

(a) **(b)**

Figure 42: Long term fifty years design load base target for axial load, Blade data: comparison between Stochastic distributed properties and reference blade data, Number of data sets: 96, Peak Method: (a) GM, (b) POT

4.3 Conclusions concerning certification process

The statistical estimation of the extreme loads of the NREL 5 MW reference W/T rotor has been detailed [66]. The process is based on 10 min simulated time series obtained through aero-elastic simulations in turbulent inflow conditions and carried out using a multi-body FEM based aero-elastic code. In addition to the stochastic wind inflow, the stochastic variability of the material properties due to manufacturing uncertainties is considered in the analyses. To this end, the blade material properties are varied according to existing composite coupon following a log-normal distribution. The estimated blade extreme load and deflection results, obtained for varying material properties, are compared to those produced for the RefMP. In addition, in order to better support the findings of the investigation on the uncertainty of the blade structural properties, the process for estimating the design values has been assessed in terms of its numerical implementation and the selection of appropriate peak extraction method and fitting cumulative distribution function.

With regard to the procedure for estimating the ultimate design values, it is concluded that the POT peak extraction method, with the threshold set at 1.4 times the STD, outperforms the GM method in terms of convergence, for the same number of simulations. The comparison of the convergence criterion values of the two methods is always in favour of the POT method, for all wind speed bins and regardless the number of simulations per bin (24, 48 and 96). Especially when running 24 simulations per bin, it appears that the convergence criterion of the GM method exceeds the 15% limit in several wind speed bins. Moreover, the P and H values of the K-S test always indicate better convergence of the POT method. It is worth noting that the use of POT method has no implications on computational cost since the same number of simulated samples as in the GM method are used but in a more efficient way.

The 3pW CDF outperforms the 2pW and LN in fitting the picked extreme values. The above conclusion is derived from the empirical short-term distributions of all load resultants (moments and forces) and tip deflections. The P values of the K-S test always indicate better convergence of the 3pW CDF. Moreover, application of POT method in conjunction with the 3pW CFD always leads to fulfilment of the K-S test. This is again due to the higher number of samples gathered by the POT method. With regard to the number of simulations, it is shown that it is preferable to use more simulations per wind speed bin. As the number of simulations increases from 24 to 48 and finally to 96 the IEC converge criterion decreases by about 40% and 60% respectively (always below the 6% obtained with 96 simulations per bin). The IEC convergence criterion suggests raising the number of simulations to 96, at which the range of confidence interval between 5% and 95% is also shorter.

Regarding the stochastic variability of the blades structural properties, the results indicate that the extreme loads are marginally affected. This holds for all three blade moments (flapwise, edgewise and torsion), which are mainly driven by gravitational and aerodynamic loads and remain almost unaffected by the variability of the blade structural properties. It is noted that aerodynamic loads mainly depend on the inflow conditions (effective angle of attack and effective velocity). So, any difference in the blade structural properties with respect to the reference set would only have an indirect effect related to the changes in the effective angle of attack or inflow velocity that the variability of blade properties would induce. For the levels of CoV of the material properties considered in the present work, neither torsion angle differences nor changes in the blade bending velocities result in any significant deviations of the angle of attack or the effective velocity and in turn of the blade loads. On the contrary, maximum deflections are substantially affected. This is expected since different material properties lead to changes in the overall blade stiffness properties and therefore different deflections are obtained for the same load. The analysis does not indicate that by neglecting the variability of the blade properties, the designer is on the safe side with respect to extreme blade deflections. In fact, a scatter of ~8% has been obtained around the value corresponding to the reference blade when considering the close to rated wind speed bin of 14m/s.

The stress analysis follows the pattern of ultimate structural loads, but the Tsai-Wu criterion, which is directly affected by the material properties, exhibits a similar variability as that of the material properties [67]. The conclusion concerning stress analysis is almost the same for all blade sections. For the levels of the CoV of the material properties considered, the extreme stresses and the Tsai-Wu criterion CoVs are in the order of 2% and 8% respectively.

So, in summary, the variability of the blade structural properties primarily affects the blade deflections and the Tsai-Wu failure criterion and less the extreme normal and shear stresses. As for the long term flapwise moment forecast, it is even less affected by the variability of the material properties.

5. Reduced Order Model formulation

5.1 Introduction to ROM formulation

In the design and certification of WTs the targets of maintaining high accuracy and reduced computational cost are interconflicting. A consistent and effective way to bridge the two is by decomposing the turbine dynamic response into modal contributions, which is part of the present thesis.

Modal analysis decomposes a small-amplitude free response to perturbations about a reference state into modal contributions. Every contribution is characterized by its amplitude modal frequency, modal damping, and a mode shape. These results, which are defined in the frequency domain, show if the reference state equilibrium is stable or not and can explain the load spectra obtained from time simulations.

Modal analysis consists of three steps:

1. Selection of a reference state.
2. Linearization of the equations of motion about this reference state.
3. Modal decomposition of the linearized system providing modal frequencies, modal damping, and mode shapes.

The nature of the reference state depends on the characteristics of the rotor and of the external conditions. We can distinguish between homogeneous and disparate situations. Homogeneous external conditions consist of a uniform and steady wind inflow that is aligned in tilt and yaw with the rotor axis, without gravity. A homogeneous rotor is defined as being polar symmetric and balanced. These homogeneous conditions result in a reference state and produce constant deflections on all turbine members.

Linearization of the equations of motion about the reference state is necessary in order to proceed with (linear) modal decomposition. It can be done analytically or approximately by considering small perturbations about the reference state, as suggested in [43].

The equations of motion for a W/T around the reference state have periodic coefficients caused by rotor rotation. In order to generate an equivalent set of equations with constant coefficients, a coordinate transformation is performed. In homogeneous conditions for both the wind inflow and rotor, this would either lead to a time – invariant system or a periodic one, due to rotation. Under such conditions the Coleman transformation is used that eliminates the periodic terms caused by the rotor rotation.

In the general case of disparate external conditions, or for a disparate rotor, the resulting reference state is periodic and so are the deflections of the turbine members, all having as period, that of the rotor rotation. Non-periodic effects like turbulence are in any case not included in the reference state.

In disparate conditions that end up in giving a set of periodic equations, Floquet's general method is used which also transforms the original equations. The resulting periodic mode shapes lead to a more complex motion that may contain an infinite number of harmonics for the supporting structure and the blades. As previously, modal analysis predicts the stability around a reference state.

A number of papers and reviews address the issue of modal analysis of W/T in homogeneous and disparate operating conditions from different perspectives.

Skjoldan and Hansen in [44] analyze the Coleman and the Lyapunov–Floquet (L–F) transformation approaches for rotor equipped systems. The Coleman transformation is proved to be a special case of Lyapunov–Floquet (L–F) transformation. At first, the Coleman transformed equations of motion are formulated with respect to the inertial frame. Then, the eigenvalue problem is solved into the time invariant context using the Floquet analysis for the periodic equations of a homogeneous rotor. Then, the uncertainty in modal characterization is resolved by requiring that the periodic mode shapes from the L–F approach are similar to the modes from the Coleman method. For disparate rotors the Floquet analysis results in periodic mode shapes that contain harmonics of integer multiples of the rotor speed and so this approach provides a way of identification.

In [45] modal analysis is performed on a homogeneous W/T that is structurally modelled with a few DOFs (flap-hinges for the three blades, tilt and yaw angles at the top of the tower). The rotor is assumed to be mass balanced and gravity is neglected, whereby the model can be linearized around equilibrium at constant rotor speed with zero angles. Modal analysis results in periodic mode shapes with up to three harmonic components. Next, stiffness difference is introduced that renders the disparate rotor. The stiffness asymmetry consists of an increase by 10 % for blade 1 and a decrease of 5% for blades 2 and 3 so that the mean stiffness is the same as on the homogeneous rotor. The comparison of the two sets of modal results shows for the disparate rotor additional harmonic components in the periodic mode shape and thus in the response. The amplitude of the additional harmonic components for the blades is up to a few percent of the blade amplitudes in the homogeneous case. The appearance of additional harmonic components in the response of the turbine with a disparate rotor is mostly interesting for the blade DOF, as this additional motion can introduce couplings with the unsteady aerodynamics in an aeroelastic model. Quoting the discussion in [45], the authors say that: "*It seems that the anisotropy affects the whirling modes the most, which is evidenced both by the change in damping and by the magnitude of the additional harmonic terms in the mode shape. However, it could also be that the least damped modes are affected most. It is difficult to draw conclusions from a model with only five modes, therefore further work must be done to apply these methods to a more complex model"* and add that "*It will also be interesting to see, whether quantitatively similar results are obtained from other sources of anisotropy such as rotor mass unbalance, gravity, non-uniform inflow*".

In [46] the aeroelastic code BHawC is used in order to calculate the dynamic response of a W/T with a nonlinear finite element formulation. Most W/T stability tools are based on linearized models. In [46] a method is presented that extracts the linear structural model for modal analysis from the FEM tool when the structure is in equilibrium. The analysis of the periodic system operating in homogeneous conditions, is performed by means of eigenvalue analysis after applying Coleman's transformation. For general disparate systems the implicit Floquet analysis is used to extract the least damped modes. Both methods are applied to the 2.3 MW Siemens W/T model.

One way of reducing the computation time is to use implicit Floquet analysis where the lowest damped modes can be extracted after a limited number of integrations. The method is computationally less intensive than the classical Floquet analysis. The implicit Floquet analysis provides the response of a single mode, that contains multiple harmonic components differing in frequency by the rotor speed. The implicit Floquet results converge to the results from the Coleman approach with the deviation in frequency and damping roughly proportional to the square of the integration time step, which increases with modal frequency. This finding shows the importance of precise time integration in implicit Floquet analysis. An analysis applied to a disparate system with one blade covered with ice shows a decrease in frequency up to 3% and changes in damping within 17%. It also reveals multiple harmonic components in the response of a single mode which will show up in measurements.

In [47] the contribution of wind shear to fatigue loads of wind turbines is considered. Shear causes an azimuthal variation in the angle of attack that affects aerodynamic damping. A linearized model of a W/T is used to assess the effect of wind shear on the modal damping. In homogeneous conditions, the modal properties are extracted using the Coleman transformation. In sheared conditions an implicit Floquet analysis is used for the modal analysis. The methods are applied to the 2.3MW Siemens W/T showing the difference in damping between homogeneous and extreme shear conditions at rated wind speed. The first longitudinal tower mode appears with lower damping while the first flapwise backward whirling and symmetric modes have higher damping. This difference is caused by the interaction between the periodic blade mode shapes and the azimuth-dependent local aerodynamic damping in sheared conditions.

In [48] a methodology to evaluate modal parameters of complex nonlinear systems is thoroughly analyzed. The method combines four different tools: the Coleman post-processing, the *partial* Floquet analysis, the moving window analysis and the signal synthesis algorithm. The partial Floquet analysis has been developed by (Bauchau and Wang, 2008) [49] and consists of applying Floquet analysis to a limited number of time signals of the free response obtained over relatively short time to perturbations about a periodic steady state., The method provides a robust estimation of linearized modal parameters and qualitative information on the nonlinear behavior of the system. The method is implemented on one or multiple discrete time signals and deals with both time-invariant and periodic systems. The process is computationally inexpensive and it can be used also with experimental data. It is validated using a simple, four degree of freedom model of a wind turbine. The predictions for the linear system are validated against the exact solution of the problem. Concerning the nonlinear system, qualitative information about the system behavior is obtained. Finally, the nonlinear behavior of a realistic, three-bladed horizontal axis W/T model is investigated. Nonlinear effects were found to be very mild for this specific wind turbine. For larger wind turbines to be built in the near future, nonlinear effects could become more pronounced due to increased flexibility of the blades.

[50] examines operating modes of a two-bladed teetered rotor W/T structural model. Because of gyroscopic asymmetry of its rotor, the dynamics of this turbine can be quite distinct from that of a turbine with three or more blades. The governing system equations bring out the time-periodic terms expected from a two-bladed turbine, whose dynamic interactions undergo a periodic variation in every rotor revolution. Due to lack of symmetry in a two-bladed rotor, a multi-blade coordinate transformation does not provide a time-invariant system, as with a turbine with three or more blades. A conventional eigenvalue analysis applied to the periodic equations yields erroneous results. Therefore, this asymmetry leads to system equations with periodic coefficients that must be solved with the Floquet approach in order to extract the correct modal parameters. The discussion starts with a single-degree-of-freedom system and progresses to a model with seven degrees-of-freedom. The DOFs that are examined include: the tower fore-aft and side-to-side

bending, the tower twist, the nacelle yaw, the hub teeter and the flapwise bending of every blade. The results illustrate how the turbine modes are dominated by centrifugal and gyroscopic effects as the rotor speed increases. Parametric studies are performed varying the precone angle, the teeter and yaw stiffnesses and damping properties. Below a certain level of yaw stiffness or damping, the gyroscopic coupling may cause yaw and teeter mode coalescence that result in self-excited dynamic instabilities. Teeter damping is the only parameter found to be able to strictly stabilize the turbine model.

5.2 General description

In Hamiltonian dynamics, the behaviour of mechanical systems is described by the Lagrange equations. To this end, appropriate generalized co-ordinates or DOFs q_j are defined that fully determine the position of any material point r and so the kinetic energy is readily obtained. Depending on the assumptions made regarding the flexibility of the system, the definition of the position will also include DOFs that describe the motions of the components due to flexibility and therefore the potential or internal energy can be defined. Finally all external loading is introduced through the virtual work this loading is contributing. The Lagrangian equations have the following form:

$$\frac{d}{dt}\left(\frac{\partial L}{\partial q'_j}\right)-\left(\frac{\partial L}{\partial q_j}\right)=Q_j=\sum_{i=1}^{n}\frac{\partial\left(\vec{f}_i.\vec{r}_i\right)}{\partial q_j} \qquad (5\text{-}1)$$

Where $'L = T - U'$ denotes the Lagrangian of the system, $'T'$ its kinetic energy, $'U'$ its internal energy and $'Q_j'$ the generalized loads corresponding to the external point loads $'f_i'$. In the proposed formulation the system has as components the blades, the drive train, the nacelle, the tower and the floating platform.

5.3 Aerodynamic modeling

In Blade Element Momentum theory, the aerodynamic forces are defined through the induction coefficients that specify the effective angle of attack $\boldsymbol{\alpha}$ and effective relative velocity along the blade. The local aerodynamic loads Cn and Ct are expressed as follows:

$$\text{Cn:}\quad Nq.(C_L\cos\varphi + C_D\sin\varphi).c(r) = 8.\pi.x.a.(1-a).r \qquad (5\text{-}2)$$

$$\text{Ct:}\quad Nq.(C_L\sin\varphi - C_D\cos(\varphi).c(r).r = 8.\pi.x.a'.(1-a).r^2$$

where,

c(r) is the local blade chord,

N denotes the number of blades,

$q = \frac{\rho}{2}.U_{\text{eff}}^2$ with U_{eff} the local effecting velocity

a, a' are the wake induction factors

$$x = \left(\frac{Uw}{Ur}\right)^2 \quad , \tan\varphi = \frac{U_W(1-a)+\delta U\alpha}{\Omega r(1+a')+\delta Uc}$$

C_L, C_D are the lift and drag coefficients given as functions of the angle of attack

$$\alpha = \varphi - (\theta_t + \beta_p)$$

θ_t, β_p denote the torsion and pitch angles while $\delta U_a, \delta U_c$ denote variations in the velocity components that are due to flexibility and/or turbulence (Figure 43)

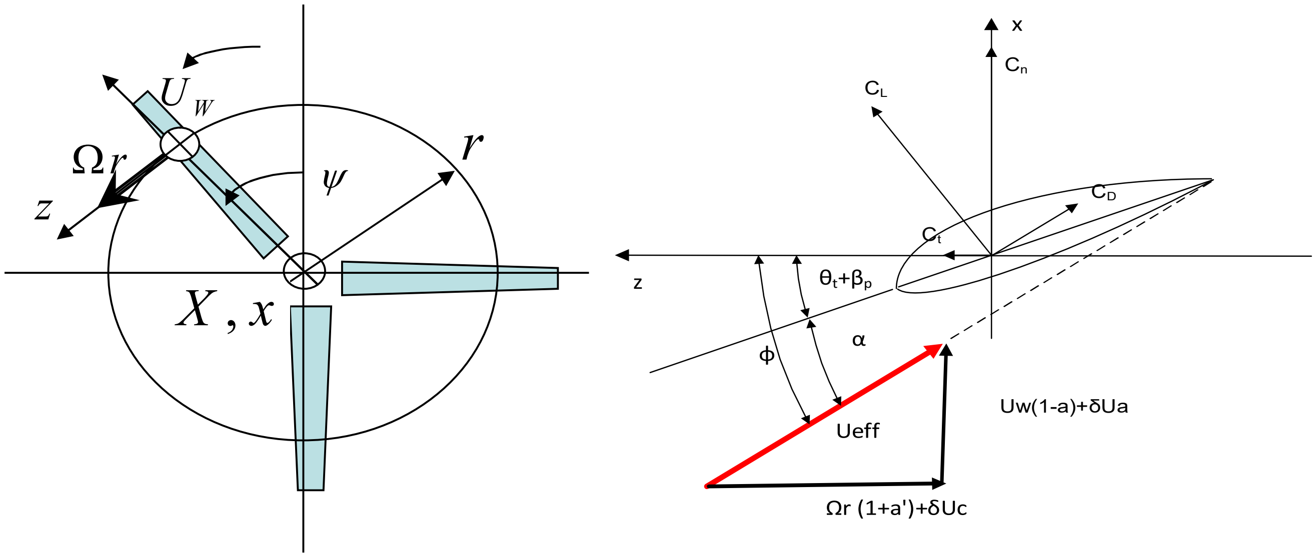

Figure 43: The rotor flow characteristics

The equations for a, a' are non-linear by definition and should be solved in fully coupled mode with the rest of the dynamic equations, namely: the structural equations of the complete system as well as any control equations. It is however possible to linearize the problem assuming a given reference state with respect to which all additional perturbations are considered small. The level of linearization depends on the kind of analysis we are interested in.

5.4 Dynamic definition of the mechanical system

The mechanical system of a wind turbine, comprises as components the blades, the drive train, the nacelle, the tower and the floater. More elaborate compositions can be defined by for example splitting one of the above components into several ones.

In the ROM context, every component is considered as a point “mass”. Mass as well as structural properties can be locally integrated in which case concentrated properties are introduced. For example, the blade can be considered as a point mass placed at the mass centre of the blade. Concentrated properties are important for simplified modelling. However, care should be taken so that the dynamics of the concentrated properties introduced are equivalent to those of the full (distributed system). This for example entails that a point 'mass' is associated to a full 6x6 mass matrix. Similarly, structural properties can be concentrated in the form of linear or angular springs. In this case equivalence means accurate prediction of the first eigenvalues of the system. It is possible to reduce the order of structural modelling by keeping a limited number of modes per component starting from the lowest ones. The number of Eigen modes depends on the level of accuracy desired.

A static solution can be defined assuming that all components are rigid with all of their mass concentrated at their mass centre and are interconnected with rotational springs and dampers. The wind is uniform and of 0 yaw misalignment and that both the rotational speed and pitch are fixed. Among other, this static solution will correspond to a given aerodynamic loading distribution defined by a, a' and therefore a specific distribution of angles of attack.

In order to derive the equations for the wind turbine, we assume that rotor aerodynamics is not affected by other motions. This means that a, a' will keep their reference values, so that the perturbation of the aerodynamic loads will only derive from the change in angle of attack due to $'\delta U_{a,c}'$ which will be linearized so that any load Q, admits the following expansion:

$$Q=Q_0+\partial_q Q_0 \cdot q_{fl}+\partial_{\dot{q}} Q_0 \cdot \dot{q}_{fl}+\partial_{\ddot{q}} Q_0 \cdot \ddot{q}_{fl} \qquad (5\text{-}3)$$

Where $q_{fl}, \dot{q}_{fl}, \ddot{q}_{fl}$ are the DOFs of the reduced order structural model of the W/T and their time derivatives. $\partial_* Q_0$ denotes the derivatives of Q with respect to $q_{fl}, \dot{q}_{fl}, \ddot{q}_{fl}$ and depend on the static position as well as the reference operation conditions of the rotor i.e. the wind speed.

The terms $\partial_* Q_0$ define in fact the stiffness, the damping and the mass matrices that are induced in the equations by the external forcing which includes aerodynamics. The aerodynamic damping is mainly determined by the direction of blade motion and the slope of the lift curve which is constant for the angles of attack experienced in most of the normal operating conditions. In the reviews mentioned above [44] - [48], the issue of aerodynamic damping is explained thoroughly. Edgewise motion results in low aerodynamic damping, hence the first lateral tower mode and first edgewise modes have low modal damping. Flapwise motion at the low angles of attack experienced in normal operations, results in a high aerodynamic damping for the flapwise modes. The change in pitch angle above W/T rated speed introduces flapwise motion to the first lateral tower mode, that increases damping, and conversely reduces flapwise motion for the flapwise modes, that slightly decreases damping. The damping of the first lateral tower mode and the first drivetrain mode do not precisely represent that of the real turbine because of the speed controller, which affects the damping of these modes, is not included in the modal analysis.

5.5 Linearization procedure of the aerodynamic effects

Let $\alpha_0(r)$ denote the effective angle of attack (a.o.a.) for the reference state at a specific radial position 'r'. For this angle, the lift coefficient $C_{L0}(r)$ and its slope ∂C_{L0} can be obtained from the tabulated polar input. Similarly for the drag and moment coefficients $C_{D0}(r)$, $\partial C_{D0}(r)$ and $C_{M0}(r)$, $\partial C_{M0}(r)$ are obtained:

$$C_*\left(r,a\right)=C_{*0}\left(r\right)+\partial C_{*0}.\left(\delta\alpha-\alpha_0\right),\quad *=L,D,M \tag{5-4}$$

$\delta\alpha=\delta\alpha\left(q_{fl},\dot{q}_{fl}\right)$ defines a (small) perturbation of the a.o.a. due to other motions e.g. defined by q_{fl},q'_{fl} that correspond to the displacements and rotations of the floater as well as of its velocities

Linearization of $\delta\alpha\left(q_{fl},\dot{q}_{fl}\right)$ results in:

$$\delta\alpha\left(q_{fl},\dot{q}_{fl}\right)=\overline{\delta\alpha_q}.q_{fl}+\overline{\delta\alpha_{dq}}.\dot{q}_{fl} \tag{5-5}$$

In which the over-barred terms correspond to derivatives with respect to q_{fl}, $\dot{q}_{fl}$.

Similarly, for the effective relative velocity,

$$\delta U_*\left(q_{fl},\dot{q}_{fl}\right)=\overline{\delta U_{*,q}}.q_{fl}+\overline{\delta U_{*,dq}}.\dot{q}_{fl} \tag{5-6}$$

By introducing the above expressions in (5-2) and eliminating higher order terms, the aerodynamic loading is projected to the turbine DOFs. Finally, by integrating along the blade span, the loads are expressed in the general coordinate system.

6. Simple model with twenty-two (22) degrees of freedom (DOFs) of an offshore W/T

6.1 General description of the model

A simple model that still represents the essential dynamics of a W/T is very useful for obtaining an understanding of the dynamics and for testing different solution methods with a minimum of implementation effort and computation time. Table 16 depicts such a model consisted of 22 DOFs together with the associated mass, the stiffness and the damping concentrated properties. The rest of the concentrated properties for the ROM are detailed in Appendix 6.

The bodies are modelled as rigid bodies with all of their mass concentrated at their mass centre and are interconnected with rotational springs and dampers. The model is purely structural, and is presented in Figure 44.

DOF Identity	DOF Symbol	DOF explanation
DOF 1.	$\beta 1$	flap-wise deflection angle of blade 1
DOF 2.	$\xi 1$	edge-wise deflection angle of blade 1
DOF 3.	q_{p1}	pitch angle of blade 1
DOF 4.	$\beta 2$	flap-wise deflection angle of blade 2
DOF 5.	$\xi 2$	edge-wise deflection angle of blade 2
DOF 6.	q_{p2}	pitch angle of blade 2
DOF 7.	$\beta 3$	flap-wise deflection angle of blade 3
DOF 8.	$\xi 3$	edge-wise deflection angle of blade 3
DOF 9.	q_{p3}	pitch angle of blade 3
DOF 10.	$\Delta\Psi$	edgewise torsion angle of rotor shaft
DOF 11.	Ψ_g	rotation angle of rotor shaft to the edgewise direction of the generator position angle $\dot{\Psi}_g = \omega(rad / sec)$
DOF 12.	q_{roll}	roll angle deflection to the vertical plain of the tower (side to side motion)
DOF 13.	q_{yaw}	yaw angle deflection of the tower
DOF 14.	q_{tilt}	tilt angle deflection to the vertical plain of the tower (for aft motion)
DOF 15.	q_f	displacement of the tower and nacelle to the horizontal plain to the for aft direction
DOF 16.	q_l	displacement of the tower and nacelle to the horizontal plain to the side to side direction
DOF 17.	x_{fr}	roll angle deflection to axis X of the floater
DOF 18.	y_{fp}	pitch angle deflection to axis Y of the floater
DOF 19.	z_{fy}	yaw angle deflection to axis Z of the floater
DOF 20.	x_{fsu}	surge displacement along axis X of the floater
DOF 21.	y_{fsw}	sway displacement along axis Y of the floater
DOF 22.	z_{fhe}	heave displacement along axis Z of the floater

Mass concentrated properties explanation	**Mass Symbol**	**Mass values property**
Mass of the blade	Mblade	17740 kg
Mass of hub	Mhub	56780 kg
Mass of the nacelle	Mnac	240000 kg
Mass of tower	Mtow	249720 kg
Mass of floater	Mfloat	13473000 kg

Stiffness property explanation	**Stiffness Symbol**	**Stiffness values properties**
Stiffness of the blade 1,2,3 to flap direction	Kbi	2.183 d8 Nm/rad
Stiffness of the blade 1,2,3 to edge direction	Kxi	5.436 d8 Nm/rad
Stiffness of shaft to torsion around X axis	Ksh	8.67 d8 Nm/rad
Stiffness of tower to roll motion around X axis	Kroll	1.42 d10 Nm/rad
Stiffness of tower to yaw motion around Y axis	Kyaw	4.3 d9 Nm/rad
Stiffness of tower to pitch motion around Z axis	Ktilt	1.8 d10 Nm/rad
Stiffness of floater to tilt around X axis	K11 – KXfloatROLL	1.4881 d9 Nm/rad
Stiffness of floater around Z axis, yaw motion	K33 - KZfloatYAW	1.1700 d8 Nm/rad
Stiffness of floater to sway direction because of roll motion	K51	1.08 d5 Nm/rad
Stiffness of floater to surge direction because of pitch motion	K42	1.08 d5 Nm/rad
Stiffness of floater to surge motion, on X axis	K44 - KXfloatSURGE	7.510 d4 Nm/rad
Stiffness of floater to heave motion, on Z axis	K66 – KZfloatHEAVE	3.8551 d6 Nm/rad
Stiffness of floater to tilt around Y axis, pitch motion	K22 - KYfloatPITCH	1.4881 d9 Nm/rad
Stiffness of floater to sway motion, on Y axis	K55 - KYfloatSWAY	7.510 d4 Nm/rad

Dumping property explanation	**Dumping Symbol**	**Dumping values properties**
Dumping of the blade 1,2,3 to flap direction	ACbi	483019.6 Nm/rad
Dumping of the blade 1,2,3 to edge direction	ACxi	762243.3 Nm/rad
Dumping of shaft to torsion around X axis	ACsh	1.0d8 Nm/rad
Dumping of tower to roll motion around X axis	ACroll	2223865 Nm/rad
Dumping of tower to yaw motion around Y axis	ACyaw	2501322 Nm/rad
Dumping of tower to pitch motion around Z axis	ACtilt	2503805 Nm/rad
Dumping of tower to front - back motion	ACfrontback	13145.34 Nm/rad
Dumping of tower to lateral motion	AClateral	13145.34 Nm/rad
Dumping of floater to tilt around X axis	AC11–floatROLL	1.0 d8 Nm/rad
Dumping of floater around Z axis, yaw motion	AC33 - KZfloatYAW	1.0 d8 Nm/rad
Dumping of floater to surge motion, on X axis	AC44 - KXfloatSURGE	5.0 d5 Nm/rad
Dumping of floater to heave motion, on Z axis	AC66 – KZfloatHEAVE	5.0 d5 Nm/rad

Dumping of floater to tilt around Y axis, pitch motion	AC22 - KYfloatPITCH	1.0 d8 Nm/rad
Dumping of floater to sway motion, on Y axis	AC55 - KYfloatSWAY	5.0 d5 Nm/rad

Table 16: ROM of a floating W/T with 22 DOFs: associated mass, stiffness and damping concentrated properties

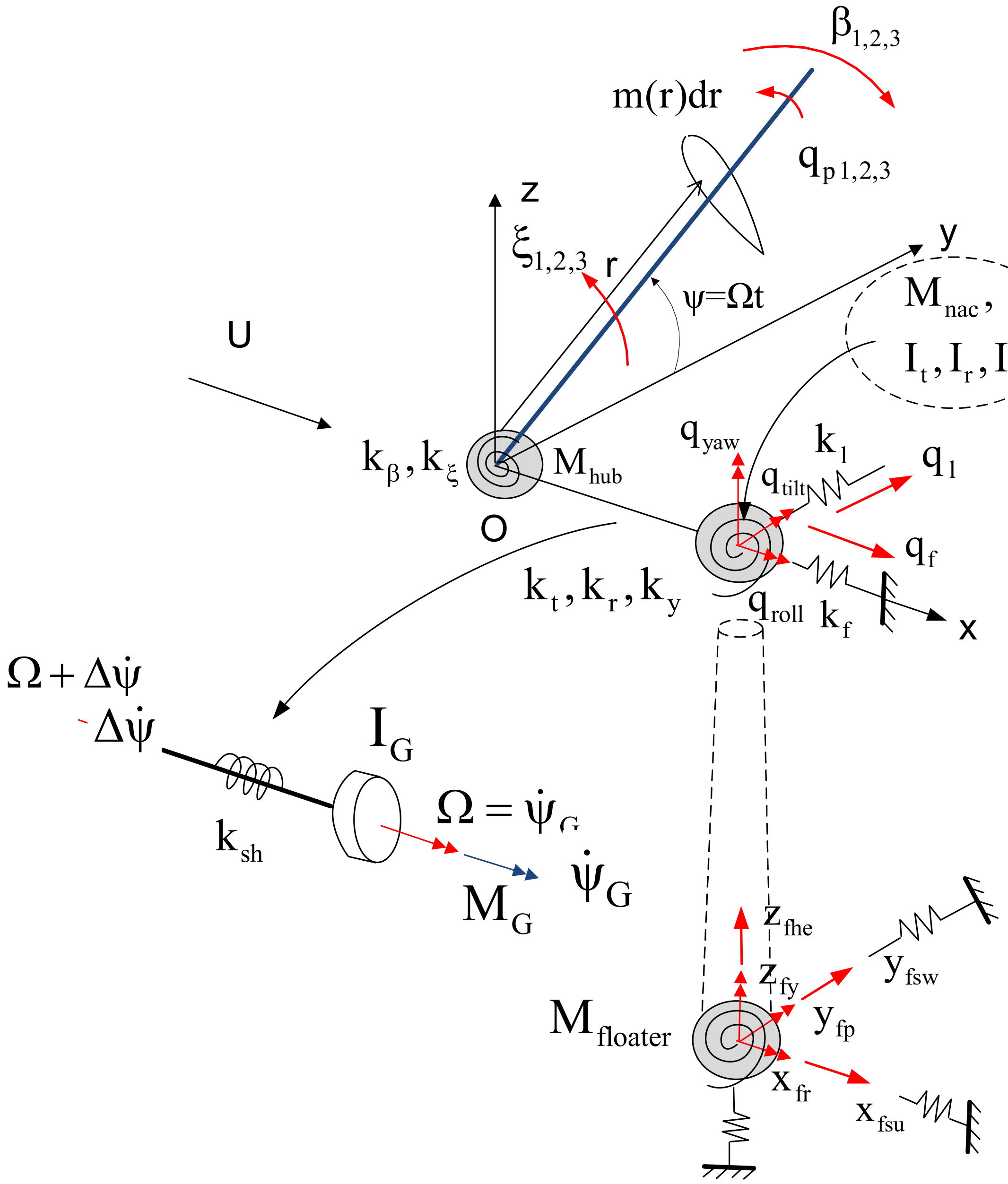

Figure 44: ROM of a floating W/T with 22 DOFs: View with DOFs and masses

6.2 The aero-elastic tool Stab-code

The nonlinear aero-elastic tool Stab-code has been developed at NTUA. In Appendix 8 the flow diagram and its subroutines are included. Its main purpose is to simulate the dynamic response and to calculate the displacements, the velocities and the accelerations on a three-bladed wind turbine.

The formulation corresponds to the Lagrange equations for the DOFs (as described in section 5.1). The equations, for all the DOFs (22) are produced as follows:

$$\frac{d}{dt}\left(\frac{\partial L}{\partial \dot{q}_j}\right)-\left(\frac{\partial L}{\partial q_j}\right)=Q_j=\sum_{i=1}^{n}\frac{\partial\left(f_i.r_i\right)}{\partial q_j} \tag{6-1}$$

with L=T-U, T: the kinetic energy, U: the dynamic energy and n=22. Processing of the different terms gives the system of the dynamic equations in the following form (overdot denote time derivation):

$$M.\ddot{q}+C.\dot{q}+K.q=Q \tag{6-2}$$

Linearization of the aerodynamic loads produces additional mass, damping and stiffness contributions. So, if the aerodynamic loading influence is added to equation (6-2), the following form is obtained:

$$\left(M+M_{aer}\right).\ddot{q}+\left(C+C_{aer}\right).\dot{q}+\left(K+K_{aer}\right).q=Q \tag{6-3}$$

Where ‘Q’ stands for the forcing term and contains gravity as well as the mean (static) aerodynamic forcing (*which can be easily eliminated).* In fact, because the aerodynamic loads depend on the d.o.f., it follows that

$$\begin{aligned}Q=Q_0&+\left(\frac{\partial Q}{\partial\left(d.o.f.\right)}\right).d\left(d.o.f.\right)\\&+\left(\frac{\partial Q}{\partial\left(Fn,Ft\right)}\right).d\left(Fn,Ft\right)\end{aligned} \tag{6-4}$$

From this point it is possible to procced with Stability analysis which is also connected to modal analysis. This kind of analysis deals with the characterization of the response of a dynamic system to external excitations. From linear theory it is known that the response of a dynamic system to an impulsive excitation will trigger all its eigenmodes. If the system can damp all eigenmodal responses then the system is stable. The ability of a system to damp external excitations as well as the level of damping plays a critical role in reliability and safety. As the level of damping decreases, the amplitudes of the loading increase and therefore the lifetime decreases.

Symbol DOF stands for the global coordinate's system DOFs. So, in state matrix form (because X is the state variable), the system of equations (6-3) takes the form:

$$\begin{bmatrix} M & 0 \\ 0 & I \end{bmatrix} . \begin{Bmatrix} \ddot{q} \\ \dot{q} \end{Bmatrix} + \begin{bmatrix} C & K \\ -I & 0 \end{bmatrix} . \begin{Bmatrix} \dot{q} \\ q \end{Bmatrix} = \begin{Bmatrix} Q \\ 0 \end{Bmatrix} \qquad (6\text{-}5)$$

or $\left[\tilde{M}\right].\dot{X} + \left[\tilde{K}\right].X = \left[\tilde{Q}\right]$ with $X = \left(\dot{q}^T, q^T\right)$

or

$$\dot{X}=A.X+B \text{ with} \left[A\right]= -\left[\tilde{M}\right]^{-1}\left[\tilde{K}\right], \left[B\right]= \left[\tilde{M}\right]^{-1}\left[\tilde{Q}\right] \qquad (6\text{-}6)$$

The eigenvalues of A

$$\det(A-\lambda_i I)=0 \qquad (6\text{-}7)$$

and eigenvectors of **A** (left and right) characterize the system.

The results of (6-7) provide the damping ratio 'ζ' which is usually given as logarithmic decrement 'd' and the natural undamped rotational frequency 'ω_n' for any eigenindex 'n':

$$d=2.\pi.\frac{\zeta}{\sqrt{1-\zeta^2}} \quad \text{and} \quad \lambda=-\zeta.\omega_n \pm i.\omega_n\sqrt{1-\zeta^2} \qquad (6\text{-}8)$$

6.3 Validation tests

6.3.1 Eigenvalue Analysis

The first validation checks the eigenvalues of the whole coupled system. Only the structural part (mass, damping and stiffness) is considered, excluding any other external loading (gravity, wind). The eigenvalues are calculated with Stab-code and with the verification code hGAST. The results are compared in Table 17 agreement in the low/medium range of frequencies is good, while the higher frequencies cannot be predicted using Stab-code, because of the limited number of DOFs.

Description	hGAST	Stab-code, ROM
floater surge	0.01092	0.01127
floater sway	0.01092	0.01127
floater yaw	0.01543	0.01551
floater roll	0.05745	0.05760
floater pitch	0.05755	0.05763
floater heave	0.08325	0.08325
tower side-side	0.45763	0.43392
tower fore aft	0.47435	0.44157
drive train torsion	0.64071	0.66143
1st blade asymmetric flapwise yaw	0.67688	0.68093
1st blade asymmetric flapwise pitch	0.72005	0.73664
1st blade collective flap	1.08565	1.08299
1st blade asymmetric edgewise pitch	1.10349	1.11109
1st blade asymmetric edgewise yaw	1.75557	1.7711

Table 17: Natural frequencies values comparison for the offshore W/T of NREL 5MW.

6.3.2 Time domain simulations

Time domain simulations using Stab-code and hGAST are compared, for wind speeds of 5 m/s, 7 m/s, 9 m/s, 11 m/s, 13 m/s, 15 m/s, 17 m/s, 19 m/s, 21 m/s, 23 m/s and 25 m/s without incoming waves. Only the hydrostatics are considered. The aerodynamic loading is calculated using the blade element momentum theory (BEM). Dynamic stall and dynamic inflow are disabled in both tools. In Stab-code the induction factors are calculated only once at the beginning and then assumed constant, while in hGAST they are updated in every time step. The mooring lines are modelled as a linear 6x6 stiffness matrix. The controller is disabled, so the W/T operates with fixed rotational speed and blade pitch angle.

In Table 3, the specifications are mentioned for the time simulations with hGAST and Stab-code, where ‘Y=yes’ and ‘N=No’

Preconditions for Time simulations	hGAST	Reduced order model
Without incoming waves	Y	Y
Only hydrostatics considered	Y	Y
Aerodynamic loading calculated using blade element momentum theory (BEM)	Y	Y
The induction factors calculated and updated every time step	Y	N
The mooring lines are modelled as a linear 6x6 matrix	Y	Y
Dynamic stall and dynamic inflow in the calculations.	N	N
Wake effects	N	N
The controller is disabled, so the W/T operates with fixed rotational speed and fixed degrees for blade pitch angle	Y	Y

Table 18: Specifications for time simulations with Stab-code and hGAST codes.

In Figure 45, the two simulation tools are compared in terms of flapwise and edgewise bending response moments. Results at 5 m/s, 13 m/s and 21 m/s are presented. The agreement between the two is acceptable. The flapwise bending moment at blade section 7 is the same at low wind speeds, and slightly different at higher ones. This variance appears because in Stab-code the induction factors **a** and **a’** are assumed constant. It is important that the ROM tool does not contain dynamic stall and dynamic inflow calculations as well as wake effects. Concerning edgewise bending moment, it is the same at all wind speeds and the mean value is zero in both codes. For all wind speeds above 8 m/s, Stab-code uses a fixed pitch, which is calculated by the hGAST controller. Finally, regarding the platform and tower results, they are almost the same at all wind speeds.

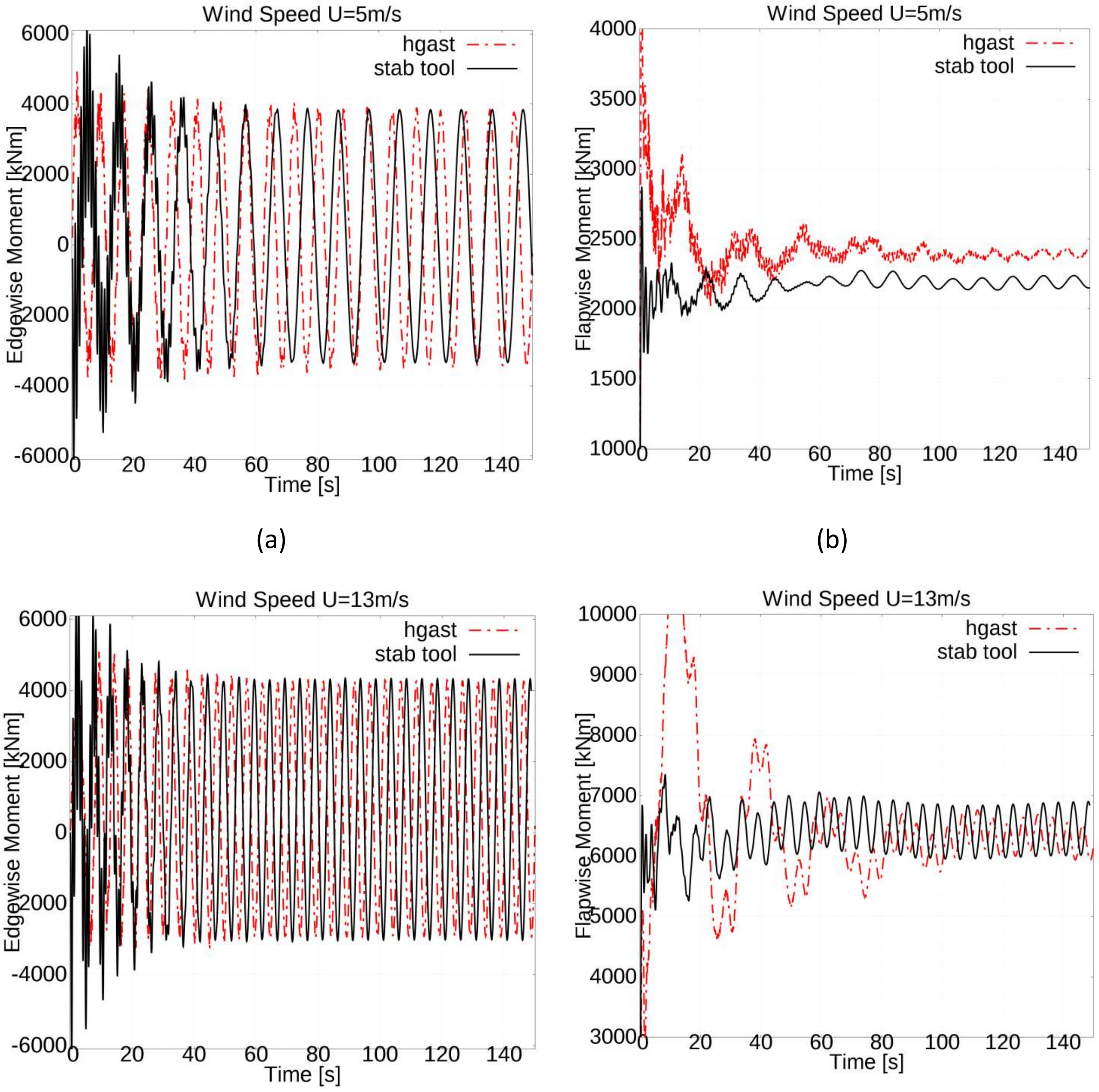

(a) (b)

(c) (d)

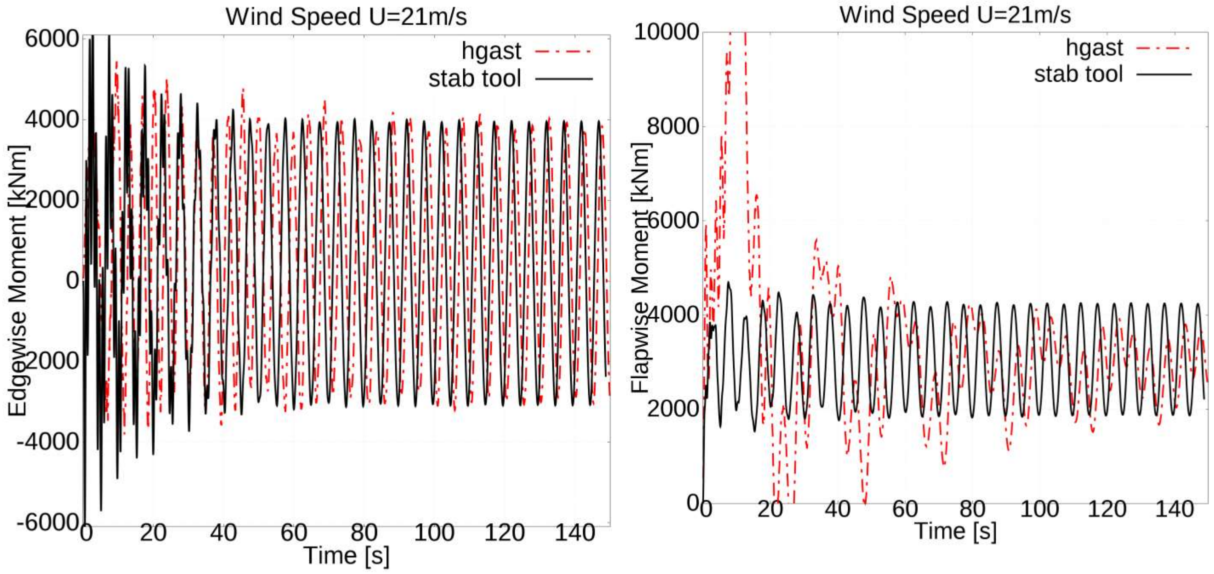

(e) (f)

Figure 45: Time domain simulations comparison between ROM Stab-code and hGAST, edgewise bending moment (left column) and flapwise bending moment (right column) for the wind speed bins: (a)-(b) 5m/s, (c)-(d) 13m/s and (e)-(f) 21m/s

In Figure 46 , the two simulations tools ROM Stab-code and hGAST are compared in terms over the last 50 seconds of the time domain simulations that the two codes converge from the whole time period of Figure 45. The blade root edgewise and flapwise bending moment for 5, 13 and 21 m/sec compared for the transient first period of timeseries in Figure 45 and for the last part of the simulations in Figure 46. It is mentioned, concerning the time step of 0.082 sec for the simulations, that the eigenfrequencies that are higher than 4.960 Hz cannot be seen from the figure analysis. So the frequencies that can be observed, due to the time step resolve are diminissed. The rest of the eigenfrequencies, although calculated from the hGAST tool, it is impossible to be presented in the figure analysis.

Regarding the transient part of timeseries in Figure 45, the two codes produce similar ranges for both the edgewise and flapwise loads. At 5m/s there is a level difference that is due to the effect of the rotational speed controller that is was not activated in the stab-tool results. Then as regards the vibratory part of the signals, again because of the controller there main frequency is different.

The comparison of the converged periodic state in Figure 46 gives better insight. Plots a) and b) correspond to the low speed case in which the rotational speed varies. The stab-tool simulations is at fixed speed (nominal at this wind speed), resulting a small sliding of the edgewise signal and signal and a small level difference in the flapwise signal (the edgewise signal is dominated by the weight, so quantitative difference is not expected). At 13m/s and 21m/s, the controller varies the pitch, and so there are differences in ranges but not infrequency. In the hgast results a lower frequency is present which is triggered by the more detailed representation of the wind turbine in hgast, and requires more time to fade out.

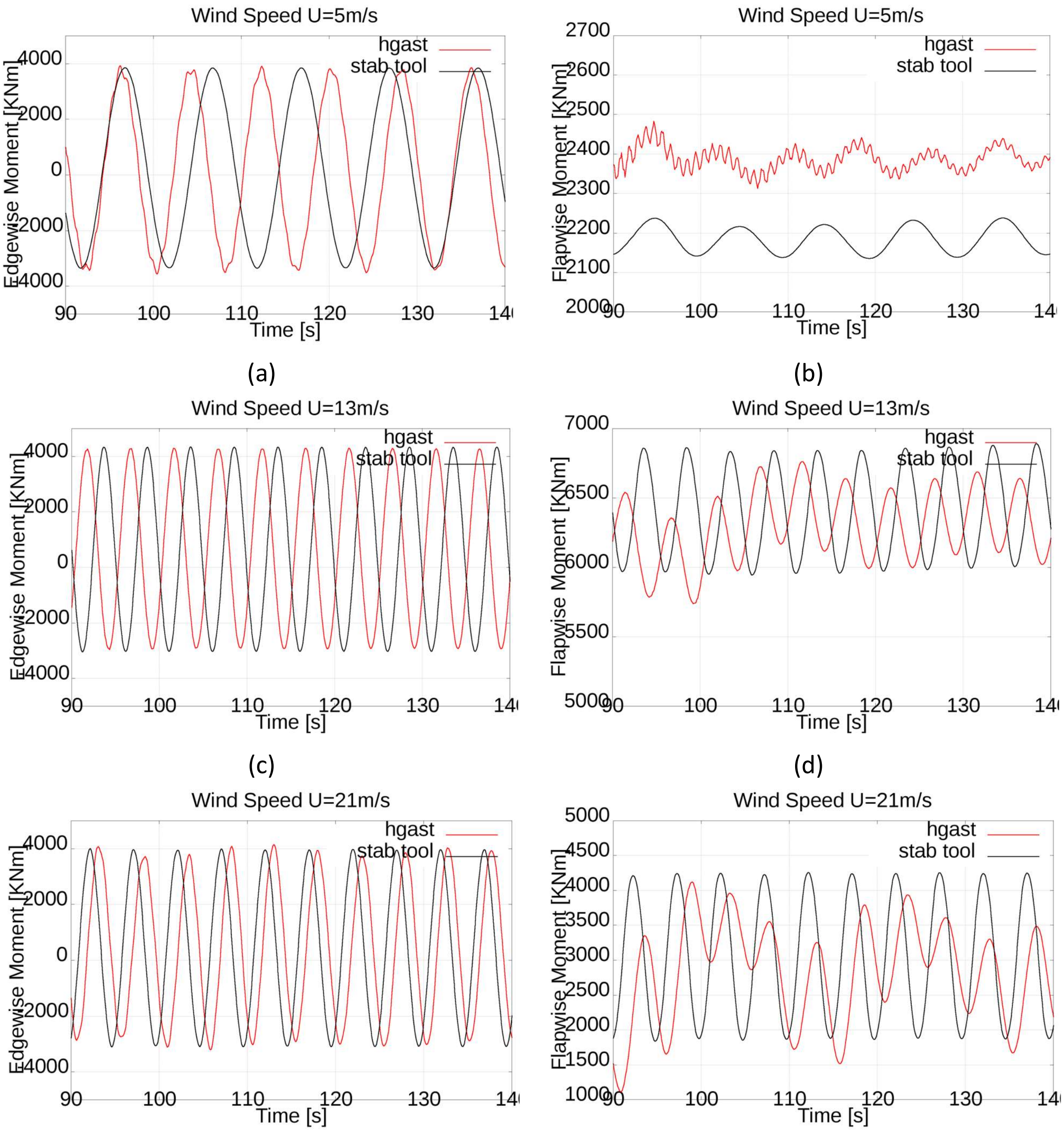

(a) (b)

(c) (d)

(e) (f)

Figure 46: Time domain simulations comparison between ROM Stab-code and hGAST for the last 50 sec , edgewise bending moment (left column) and flapwise bending moment (right column) for the wind speed bins: (a)-(b) 5m/s, (c)-(d) 13m/s and (e)-(f) 21m/s

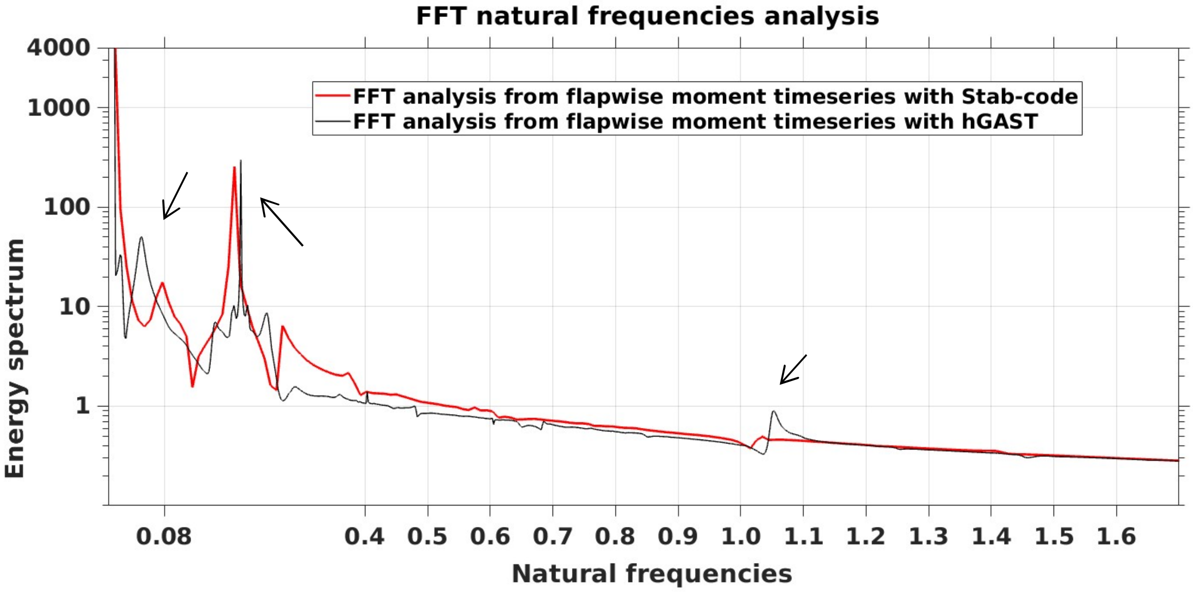

(a)

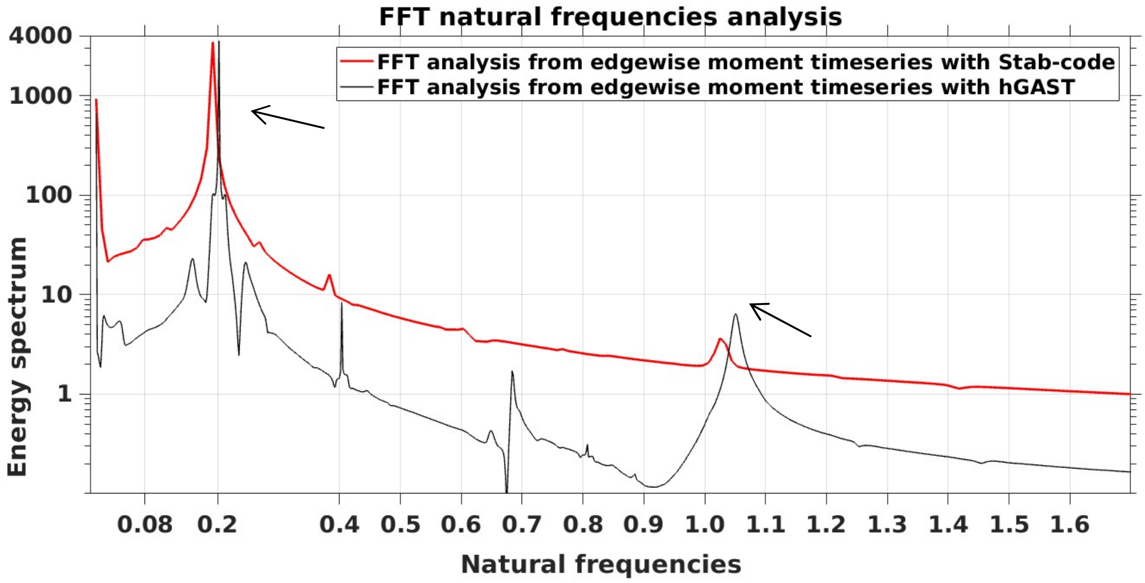

(b)

Figure 47: Comparison of the spectra obtained from the Stab code and hGAST analysis for the a) flap-wise and b) edgewise moments at blade root. The analysis concerns the wind speed bin of 12 m/s

Comparisons in terms of spectra are shown in Figure 47 with respect to the flap-wise and edgewise signals fromwhich the initial (transient) part has been removed. There is good comparison. The rotational frequence is at 0.2HZ with Stab-tool giving a slightly smaller value (again because of the controller) while there is agreement in the basic eigenfrequencies. The excitations of the tower (0.45, 0.47Hz) and the drive train modes (0.64Hz) that appear in the transient part are quickly damped. As for the heving mode at 0.08Hz, the response in Stab-tool remains, which could be due to the lack of aerodynamic damping (in Stab-tool the aerodynamic performance is not subjected to the dynamics of the system).

In conclusion, the proposed ROM is a fast-running tool for floating wind turbines of acceptable accuracy, despite the discrepancies in the flapwise bending moment signal especially at lower wind speeds, compared to hGAST FEM tool.

6.4 Coleman transformation of homogeneous rotating systems

Coleman's transformation is a multi-blade transformation [51] and [52] that eliminates the periodic terms in the equations for rotors that are equipped with identical blades and rotate at Ω. This transformation changes the rotating DOFs and equations into the non-rotating frame of reference. Periodic coefficients are still obtained, even after applying the transformation, when for instance gravity loads are taken into account. In such cases, Jonhson [53] suggested that if the equations are only weakly periodic, there is some constant coefficient system that closely represents the behaviour of the true system. It is necessary to establish the best way to construct such a constant coefficient approximation and to determine its range of validity. The constant coefficient system can be constructed by retaining only the mean values of the original periodic coefficients.

Based on the above considerations, in the case of weakly periodic coefficients system the following approach is used. First, a periodic solution is obtained, about which servo aeroelastic equations of motion are linearized. This is done by integrating the non-linear equations in time, until a periodic response (with respect to the rotor speed) is reached. The non-linear solution can be obtained by iteratively solving the system of equations within the time step of the computation, until convergence. Integration in time is carried out using Newmark's method [37]. Through this iterative procedure, the resulting reference solution 'y^0' is the solution of the non-linear system.

Then the multi-blade transformation is performed to the rotating DOFs and the equations of the system. This co-ordinate transformation is based on the polar symmetry of rotors with identical blades. The equations for the case of a three bladed rotor are given in (6-9):

$$\begin{aligned}
x_m &= x_0 + x_c.\cos\psi_m + x_s.\sin\psi_m \\
\dot{x}_m &= \dot{x}_0 + \left(\dot{x}_c + x_s.\Omega\right).\cos\psi_m + \left(\dot{x}_s - x_c.\Omega\right).\sin\psi_m \\
\ddot{x}_m &= \ddot{x}_0 + \left(\ddot{x}_c + 2.\dot{x}_s.\Omega - x_c.\Omega^2\right).\cos\psi_m \\
&+\left(\ddot{x}_s - 2.\dot{x}_c.\Omega - x_s.\Omega^2\right).\sin\psi_m
\end{aligned} \tag{6-9}$$

Where x_m is any rotating DOF of the m-th blade being at an azimuth position $\psi_m=\Omega t + (2\pi/N).(m-1)$, with m =1,2,3, N = 3. Symbols x_0, x_c and x_s are the transformed coordinates referred to as collective, cyclic cosine and cyclic sine, respectively. They are referenced to the non-rotating frame, and Ω is the mean rotational speed of the rotor. It is assumed that $\Omega'=0$, so, only perturbations of the rotational acceleration are allowed.

As rotating DOFs are transformed in the non-rotating frame, the same applies to the blade equations. To this end, the following operators are applied to the blade equations:

$$\begin{aligned}
&(\text{non - rotating equation})_1 = \frac{1}{N}\sum_{m=1}^{N}(\text{rotating equation})_m \\
&(\text{non - rotating equation})_2 = \frac{2}{N}\sum_{m=1}^{N}(\text{rotating equation})_m \cos\psi_m \qquad (6\text{-}10) \\
&(\text{non - rotating equation})_3 = \frac{2}{N}.\sum_{m=1}^{N}(\text{rotating equation})_m \sin\psi_m
\end{aligned}$$

Since the system of the transformed equations still contains periodic coefficients, they should be eliminated. Based on Jonhson's assumption, the mass, the damping and the stiffness matrices are computed over one period and then averaged. The whole procedure of the Coleman transformation to the non-rotating frame is described in [Appendix 7]. The final system is transformed into first order form (6-6). Finally, the eigenvalues of the corresponding matrix contain the aero elastic natural frequencies and damping characteristics of the W/T for the case of a constant coefficient system with reference to the non-rotating frame.

The Campbell diagrams of natural frequencies and the respective logarithmic damping are presented together for the natural frequencies in Figure 48 for the most important modes: the first 6 coupled modes of the floater, the first 4 coupled modes of the tower, the first 3 coupled flap modes and the first 2 coupled lead-lag modes of the rotor and finally the drive train torsion of the shaft for the 5MW NREL W/T.

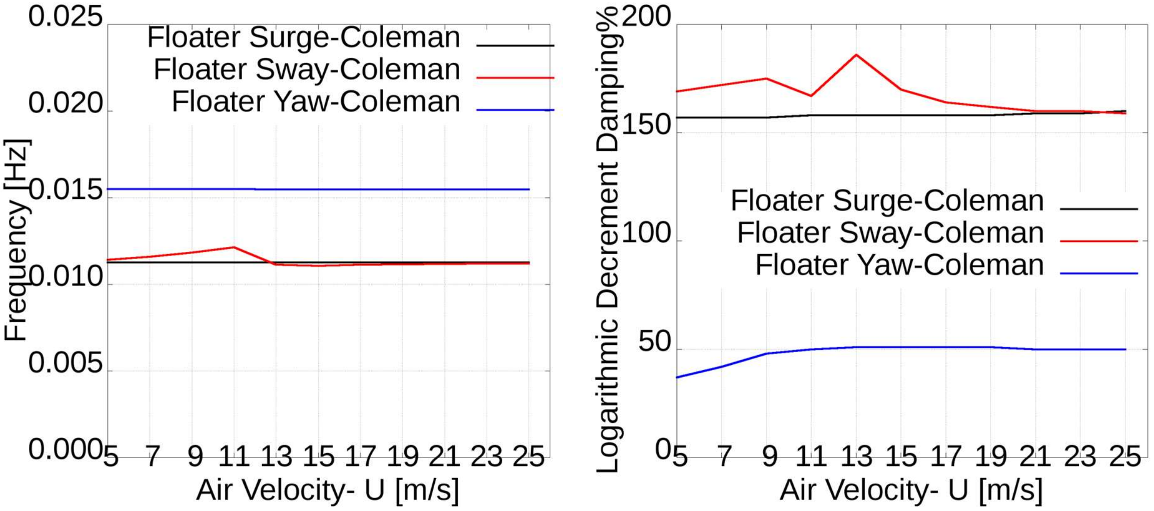

(a) (b)

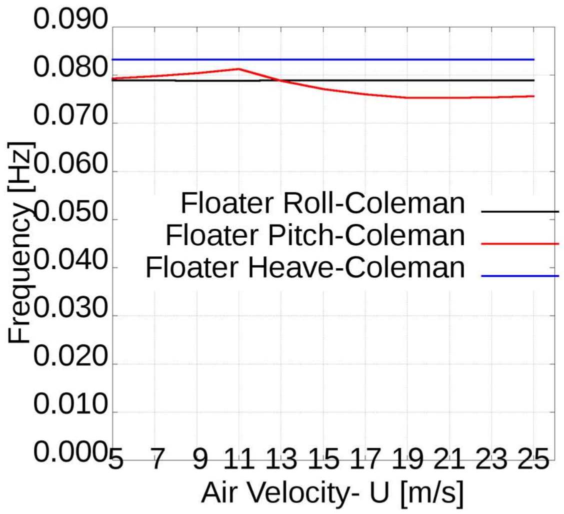
0.090
0.080
0.070
0.060
0.050
0.040
0.030
0.020
0.010
0.000
Frequency [Hz]
Floater Roll-Coleman
Floater Pitch-Coleman
Floater Heave-Coleman
5 7 9 11 13 15 17 19 21 23 25
Air Velocity- U [m/s]

(c)

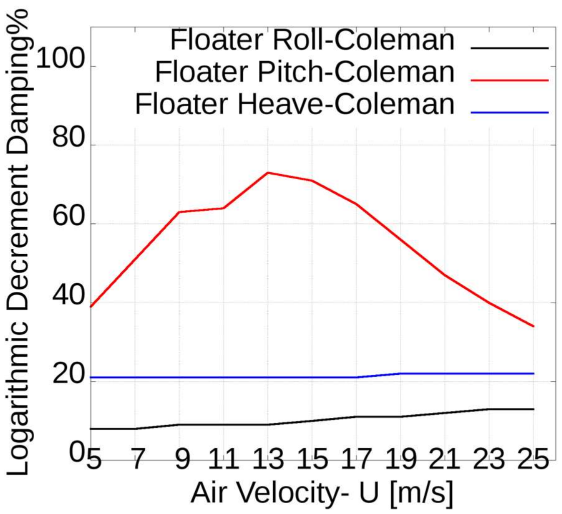
100
80
60
40
20
0
Logarithmic Decrement Damping%
Floater Roll-Coleman
Floater Pitch-Coleman
Floater Heave-Coleman
5 7 9 11 13 15 17 19 21 23 25
Air Velocity- U [m/s]

(d)

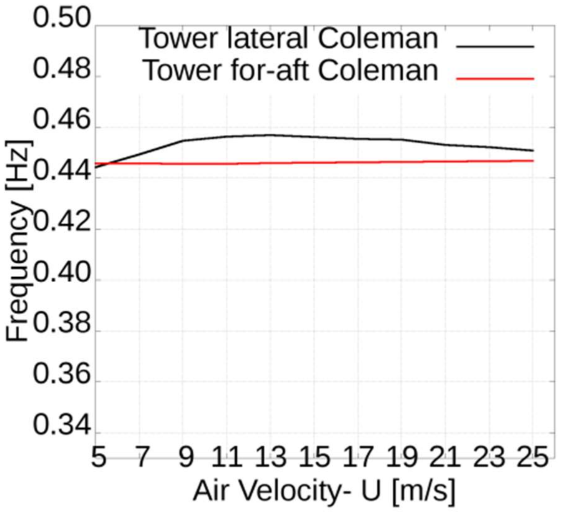
0.50
0.48
0.46
0.44
0.42
0.40
0.38
0.36
0.34
Frequency [Hz]
Tower lateral Coleman
Tower for-aft Coleman
5 7 9 11 13 15 17 19 21 23 25
Air Velocity- U [m/s]

(e)

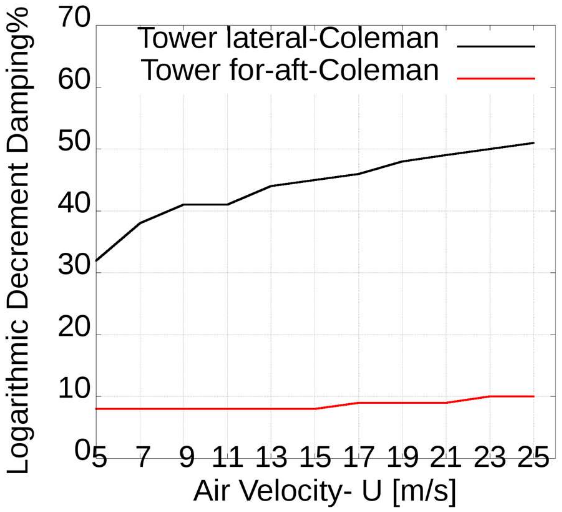
70
60
50
40
30
20
10
0
Logarithmic Decrement Damping%
Tower lateral-Coleman
Tower for-aft-Coleman
5 7 9 11 13 15 17 19 21 23 25
Air Velocity- U [m/s]

(f)

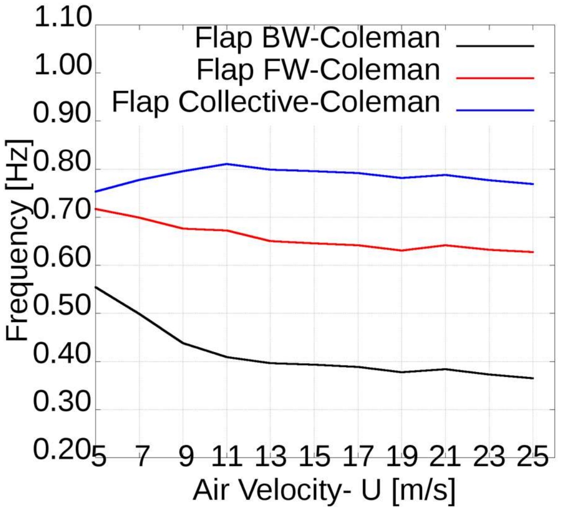
1.10
1.00
0.90
0.80
0.70
0.60
0.50
0.40
0.30
0.20
Frequency [Hz]
Flap BW-Coleman
Flap FW-Coleman
Flap Collective-Coleman
5 7 9 11 13 15 17 19 21 23 25
Air Velocity- U [m/s]

(g)

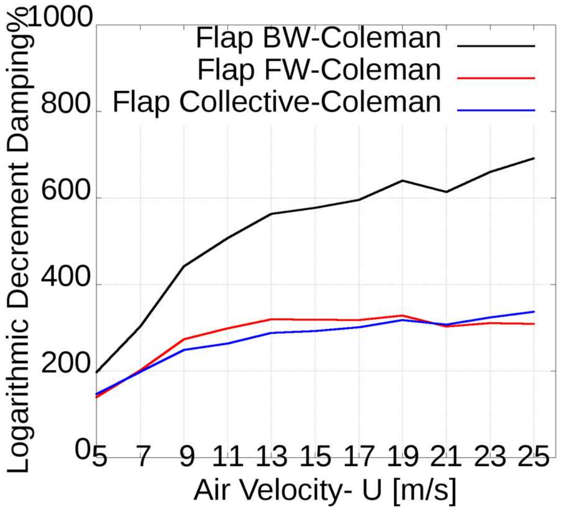
1000
800
600
400
200
0
Logarithmic Decrement Damping%
Flap BW-Coleman
Flap FW-Coleman
Flap Collective-Coleman
5 7 9 11 13 15 17 19 21 23 25
Air Velocity- U [m/s]

(h)

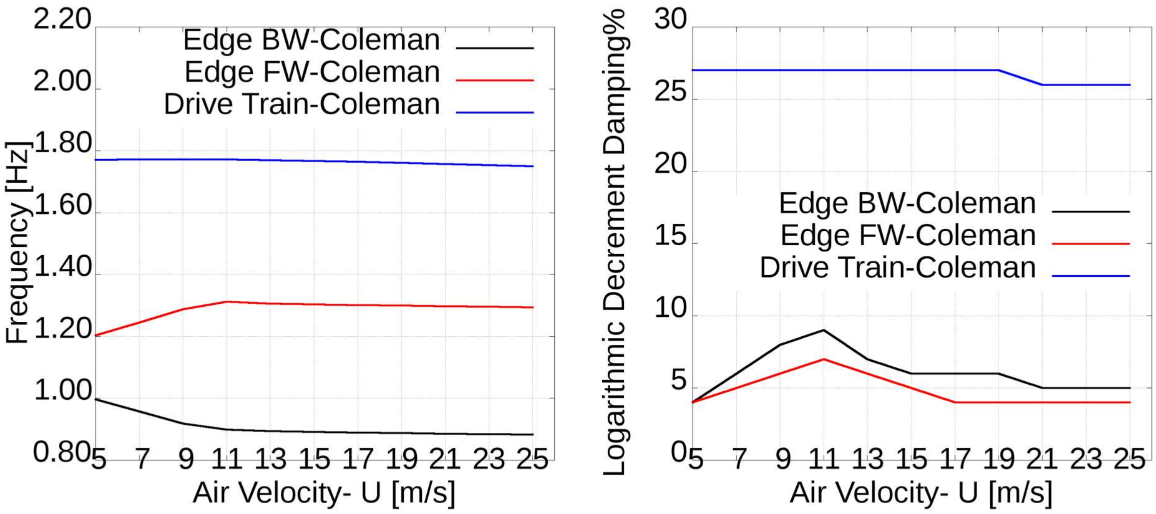

(i) (j)

Figure 48: Campbell diagrams with all natural frequencies and the respective logarithmic damping, (a), (b), (c) and (d) surge, sway, yaw, roll, pitch and heave floater frequencies, (e) and (f) tower side, tower for aft, (g) and (h) blade flap frequencies and (i), (j) blade edge frequencies

6.5 Anisotropy effects on wind turbines

This section describes the effects of anisotropy on the steady state and modal dynamics of a wind turbine. Anisotropy is caused by either the rotor or the external conditions. Rotor anisotropy can be caused by a mass or stiffness unbalance from production irregularity or material deposition such as ice or by a pitch misalignment from production or from a fault in the control system. Disparate external conditions arise from gravity forces or asymmetric wind flow caused by wind shear, nacelle tilt, terrain slope, yaw error, or tower shadow. .

In disparate conditions, the steady state is periodic and the response of a single mode contains an infinite number of harmonics making the modal analysis more complex than that described in section 6.4. At standstill, modal analysis of a disparate system can be performed using standard eigenvalue analysis. But once the rotor rotates, anisotropy causes unbalanced couplings between the rotor and the support structure such that a time-invariant system cannot be obtained by a simple physically based coordinate transformation. In such conditions, the required transformation applies Floquet analysis.

The frequency spectrum of a steady state due to a disparate rotor contains all multiples of the rotor speed, which is realized from a Fourier expansion of the forcing on the blades which is periodic with the rotor period. This approach for modal analysis of disparate systems is followed in the next sections.

6.6 Floquet theory and implementation

The first order system of the dynamic equations (6-6) has time depending coefficients A and B. In the special case that the system is periodic, linear stability analysis is possible based on Floquet's theory [54].

For the disparate cases considered, the cases of different masses for the blades and the 20 degrees wind yaw effect case, the equations system with periodic terms is integrated over one period for every DOF separately as follows:

$$\varphi(t)=[\ \varphi_1(t)\ \varphi_2(t)\ ....\ \varphi_N(t)\ ],\ \dot{\varphi}(t)=A(t).\ \varphi(t) \qquad \text{(6-11)}$$

$$\begin{Bmatrix} \varphi_1^1 \\ \varphi_2^1 \\ \varphi_N^1 \end{Bmatrix}' = A.\begin{Bmatrix} \varphi_1^1 \\ \varphi_2^1 \\ \varphi_N^1 \end{Bmatrix},\ \begin{Bmatrix} \varphi_1^1(0) \\ \varphi_2^1(0) \\ \varphi_N^1(0) \end{Bmatrix} = \begin{Bmatrix} 1 \\ 0 \\ 0 \end{Bmatrix} \xrightarrow{\text{integrated from 0 to } 2\pi} \begin{Bmatrix} \varphi_1^1(2\pi) \\ \varphi_2^1(2\pi) \\ \varphi_N^1(2\pi) \end{Bmatrix}$$

$$\begin{Bmatrix} \varphi_1^2 \\ \varphi_2^2 \\ \varphi_N^2 \end{Bmatrix}' = A.\begin{Bmatrix} \varphi_1^2 \\ \varphi_2^2 \\ \varphi_N^2 \end{Bmatrix},\ \begin{Bmatrix} \varphi_1^2(0) \\ \varphi_2^2(0) \\ \varphi_N^2(0) \end{Bmatrix} = \begin{Bmatrix} 0 \\ 1 \\ 0 \end{Bmatrix} \xrightarrow{\text{integrated from 0 to } 2\pi} \begin{Bmatrix} \varphi_1^2(2\pi) \\ \varphi_2^2(2\pi) \\ \varphi_N^2(2\pi) \end{Bmatrix} \qquad \text{(6-12)}$$

$$\begin{Bmatrix} \varphi_1^N \\ \varphi_2^N \\ \varphi_N^N \end{Bmatrix}' = A.\begin{Bmatrix} \varphi_1^N \\ \varphi_2^N \\ \varphi_N^N \end{Bmatrix},\ \begin{Bmatrix} \varphi_1^N(0) \\ \varphi_2^N(0) \\ \varphi_N^N(0) \end{Bmatrix} = \begin{Bmatrix} 0 \\ 0 \\ 1 \end{Bmatrix} \xrightarrow{\text{integrated from 0 to } 2\pi} \begin{Bmatrix} \varphi_1^N(2\pi) \\ \varphi_2^N(2\pi) \\ \varphi_N^N(2\pi) \end{Bmatrix}$$

The above is carried out directly without elimination of the periodic coefficients. The modal matrix solutions $\phi_k(t)$ are collected to the columns of the N×N state transition matrix, or the system fundamental matrix:

$$\text{FTM}=\begin{Bmatrix} \varphi_1^1(2\pi) & \varphi_1^2(2\pi) & \varphi_1^N(2\pi) \\ \varphi_2^1(2\pi) & \varphi_2^2(2\pi) & \varphi_2^N(2\pi) \\ \varphi_N^1(2\pi) & \varphi_N^2(2\pi) & \varphi_N^N(2\pi) \end{Bmatrix} \qquad \text{(6-13)}$$

The eigenvalue analysis of $\Phi(2\pi)$ (FTM) provides the stability characteristics of the system. The cost of the Floquet method is proportional to the number of DOFs and also depends on time resolution. So, depending on the size of the system and the accuracy of the integration method, this process can become computationally time consuming.

6.7 Resolving the indeterminacy of the modal frequencies in Stab–code

The eigenvalues of FTM are given by the complex logarithm:

$$\begin{aligned}\lambda_{p,k}=\sigma_k+i\omega_{p,k}&=\frac{1}{T}\ln\left|\rho_k\right|+i\frac{1}{T}\left(\arg\left(\rho_k\right)+J_k2\pi\right),J_k\in A\\&=\frac{1}{T}\ln\left|\rho_k\right|+i\left(\frac{\arg\left(\rho_k\right)}{T}+J_k\Omega\right),J_k\in A\left(\text{integer number}\right)\end{aligned}\qquad(6\text{-}14)$$

Where, σ_κ and $\omega_{p,\kappa}$ are the modal damping and principal frequencies of $\lambda_{p,\kappa}$ respectively. The integers J_k in the imaginary parts are undetermined and so the modal frequencies $\omega_{p,\kappa}$ are not uniquely determined. This indeterminacy is resolved by defining modal frequencies that are observed in the frequency responses, and measured in the inertial frame of reference.

Since $\arg\left(\rho_k\right)\in[-\pi,+\pi]$, modal frequency ω_k is within an integer multiple of the rotor speed:

$$\omega_k=\omega_{p,k}+J_k\Omega\qquad(6\text{-}15)$$

One way to specify the frequencies is to require that the mean value of the eigenvector has the largest magnitude; then the harmonic of largest magnitude of the eigenvector corresponding to the principal value of the eigenvalue gives the frequency. According to the eigenvalue identification method analysed in [44], the maximum value corresponds to that of the measure of A_{pk} (Appendix 9) for j=-10:+10, with $A_{p,k}$ the amplitudes of harmonic components in the principal periodic mode shape.

In Figure 49 the results of the identification method described in [44] are presented for the tower for aft and the blade symmetric flapwise eigenvalues. An alternative but less accurate identification method, has been presented by Nagabhushanam and Gaonkar in [55] which is called "automatic method". In this the integer factor of the frequency is determined by the ratio of the velocity over the displacement:

$$\text{ratio}=\frac{\text{derivative of displacement}\left(\text{velocity}\right)}{\text{displacement}}=\frac{\dot{b}}{b}=\frac{\dot{\text{dof}}}{\text{dof}}\qquad(6\text{-}16)$$

The imaginary part of this ratio is the right frequency and because of that it is called "automatic method".

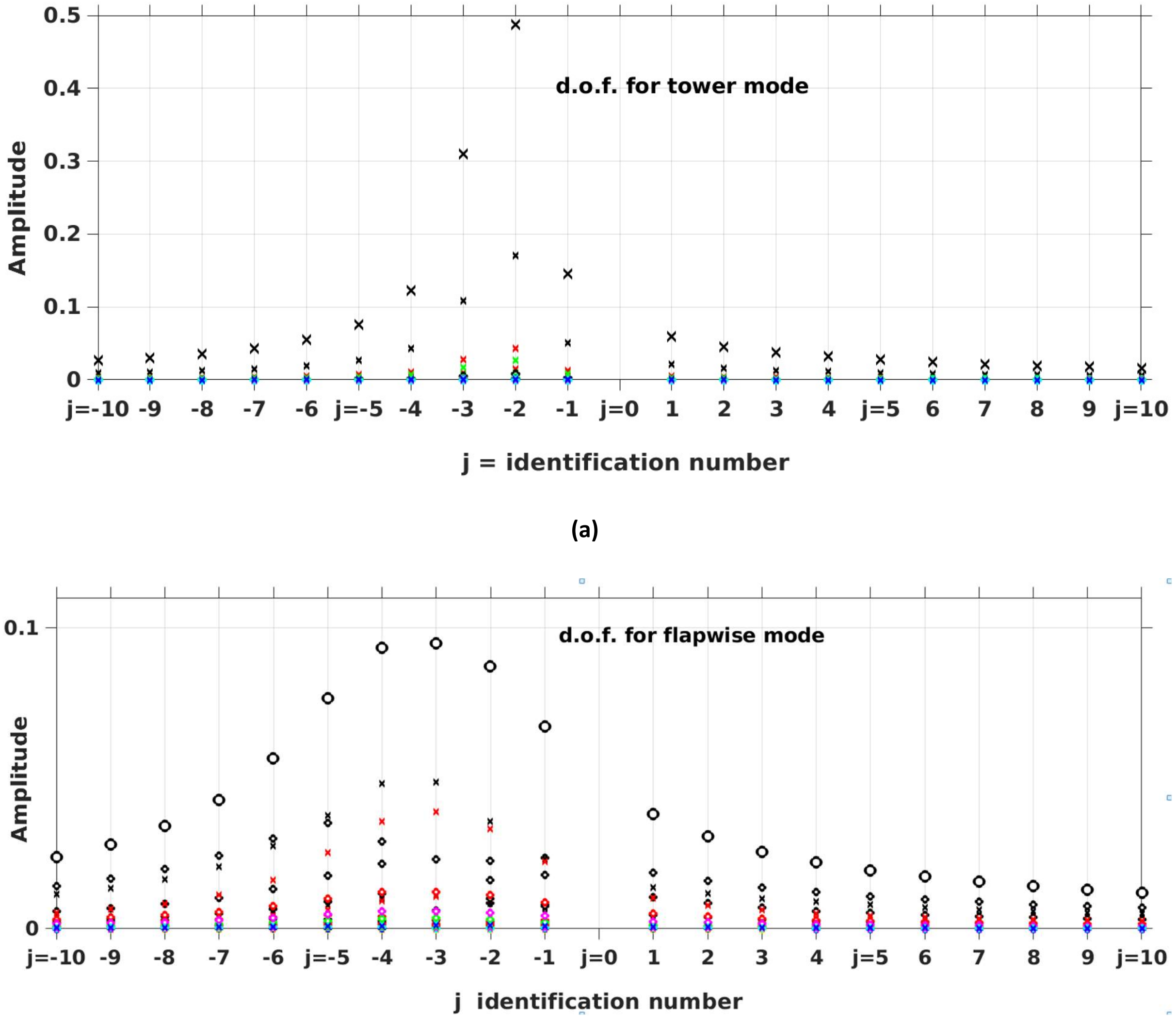

(a)

(b)

Figure 49: Identification method used, $A_{p,k}$ the amplitudes of harmonic components in the principal periodic mode shape versus identification number (a) tower for aft eigenvalue, (b) blade flapwise symmetric eigenvalue

6.8 ROM code results applying Floquet analysis, with and without disparate effects

In this section the effects of anisotropy on the dynamics of a wind turbine are considered. Two comparisons are made. First the Coleman and Floquet methods are compared in homogeneous conditions in terms of frequencies and damping which serves as validation of the present Floquet implementation. Then two specific examples of disparate conditions are discussed: one referring to mass imbalance and the second to yaw misalignment.

The results for the first comparison concern the NREL 5 MW W/T. In the Floquet calculations, 2880 time steps per period. With respect to time resolution and according to [44], convergence in the Floquet results is proportional to Δt^2 while the error itself increases with the modal frequency. The specific publication, finally suggests 512 steps per period as a compromise between precision and computation cost. In the present work, tests were carried out with lower time resolution (360, 720, 1440 and finally 2880 time steps per period). These tests proved that convergence of the specific implementation is achieved in between the two higher resolutions and so, the highest was chosen for safety.

The results of the first comparison (homogeneous conditions) are given in Figure 50. Specifically, the modes from the Floquet analysis were identified by means of the eigenvalue identification method [44] (see section 6.7). The agreement is good between the two methods.

Next the case of blade mass imbalance is considered and results are given in Figure 51. The first blade has mass exactly equal to the mean value 17.740 kgr, the second blade has mass +5% and the last one -5% of the mean value. The disparate case is presented with lines while the balanced one with dots. The comparison indicates that natural frequencies and damping are not substantially affected.

Figure 52 presents the results in the case of a 20 degrees yaw misalignment. The ROM code results are illustrated with Floquet transformation analysis for both cases of W/T with and without yaw periodic effect. The disparate effect case is presented with lines and the yaw periodic effect case with simple dots. The comparison shows that the flapwise forward FW and backward BW asymmetric eigenvalues slightly increase while damping decreases accordingly. The same effect appears also in the tower side-to-side mode.

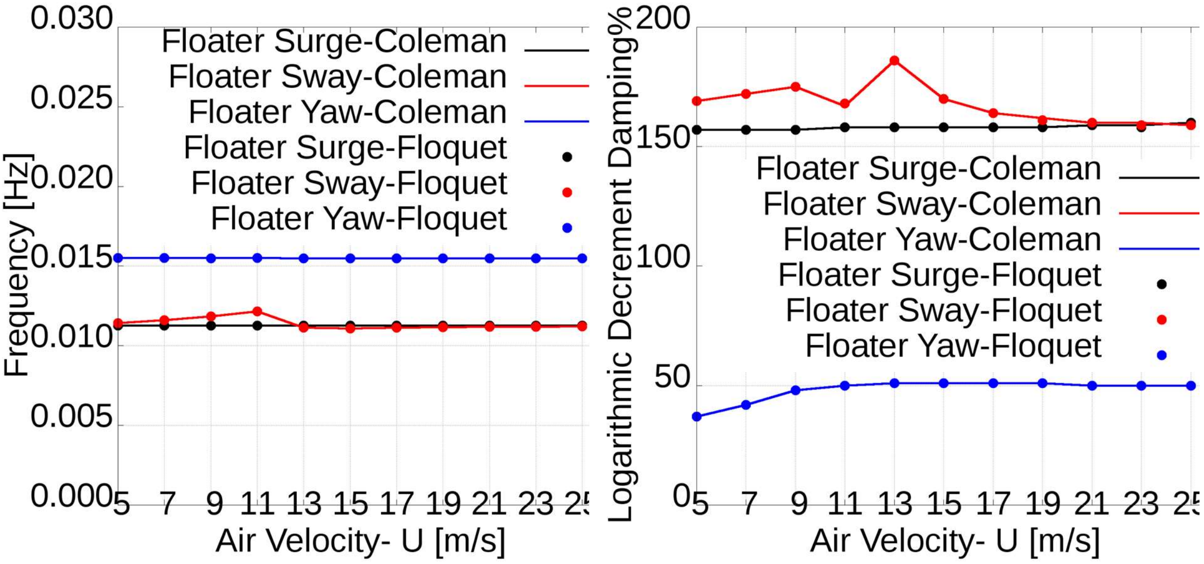

(a) **(b)**

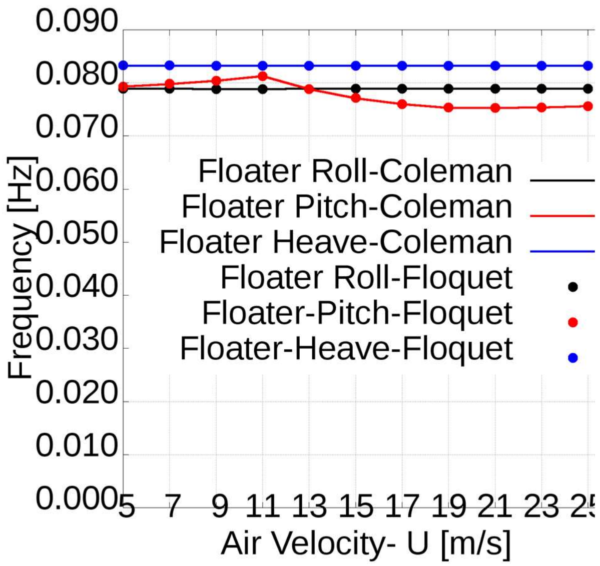
0.090
0.080
0.070
0.060
0.050
0.040
0.030
0.020
0.010
0.000
Frequency [Hz]
5 7 9 11 13 15 17 19 21 23 25
Air Velocity- U [m/s]
Floater Roll-Coleman
Floater Pitch-Coleman
Floater Heave-Coleman
Floater Roll-Floquet
Floater-Pitch-Floquet
Floater-Heave-Floquet

(c)

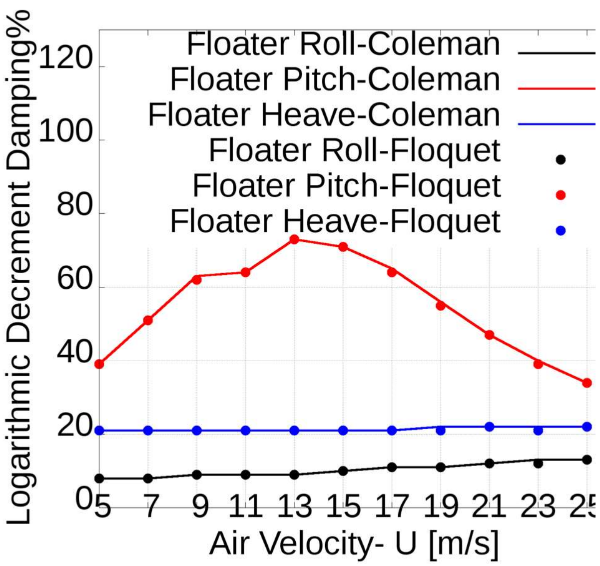
120
100
80
60
40
20
0
Logarithmic Decrement Damping%
5 7 9 11 13 15 17 19 21 23 25
Air Velocity- U [m/s]
Floater Roll-Coleman
Floater Pitch-Coleman
Floater Heave-Coleman
Floater Roll-Floquet
Floater Pitch-Floquet
Floater Heave-Floquet

(d)

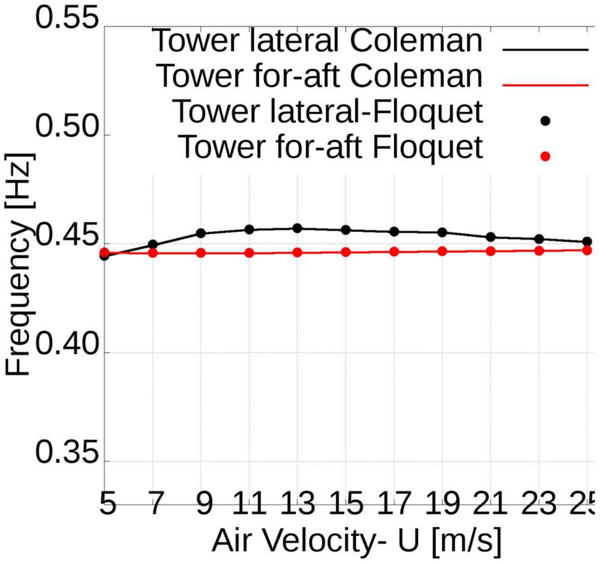
0.55
0.50
0.45
0.40
0.35
Frequency [Hz]
5 7 9 11 13 15 17 19 21 23 25
Air Velocity- U [m/s]
Tower lateral Coleman
Tower for-aft Coleman
Tower lateral-Floquet
Tower for-aft Floquet

(e)

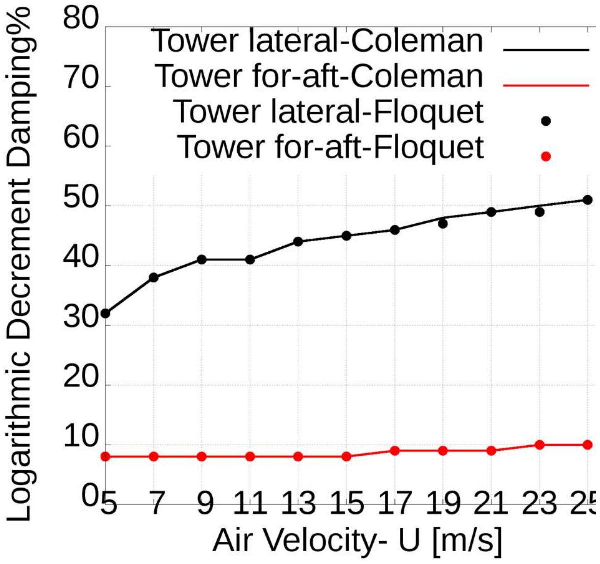
80
70
60
50
40
30
20
10
0
Logarithmic Decrement Damping%
5 7 9 11 13 15 17 19 21 23 25
Air Velocity- U [m/s]
Tower lateral-Coleman
Tower for-aft-Coleman
Tower lateral-Floquet
Tower for-aft-Floquet

(f)

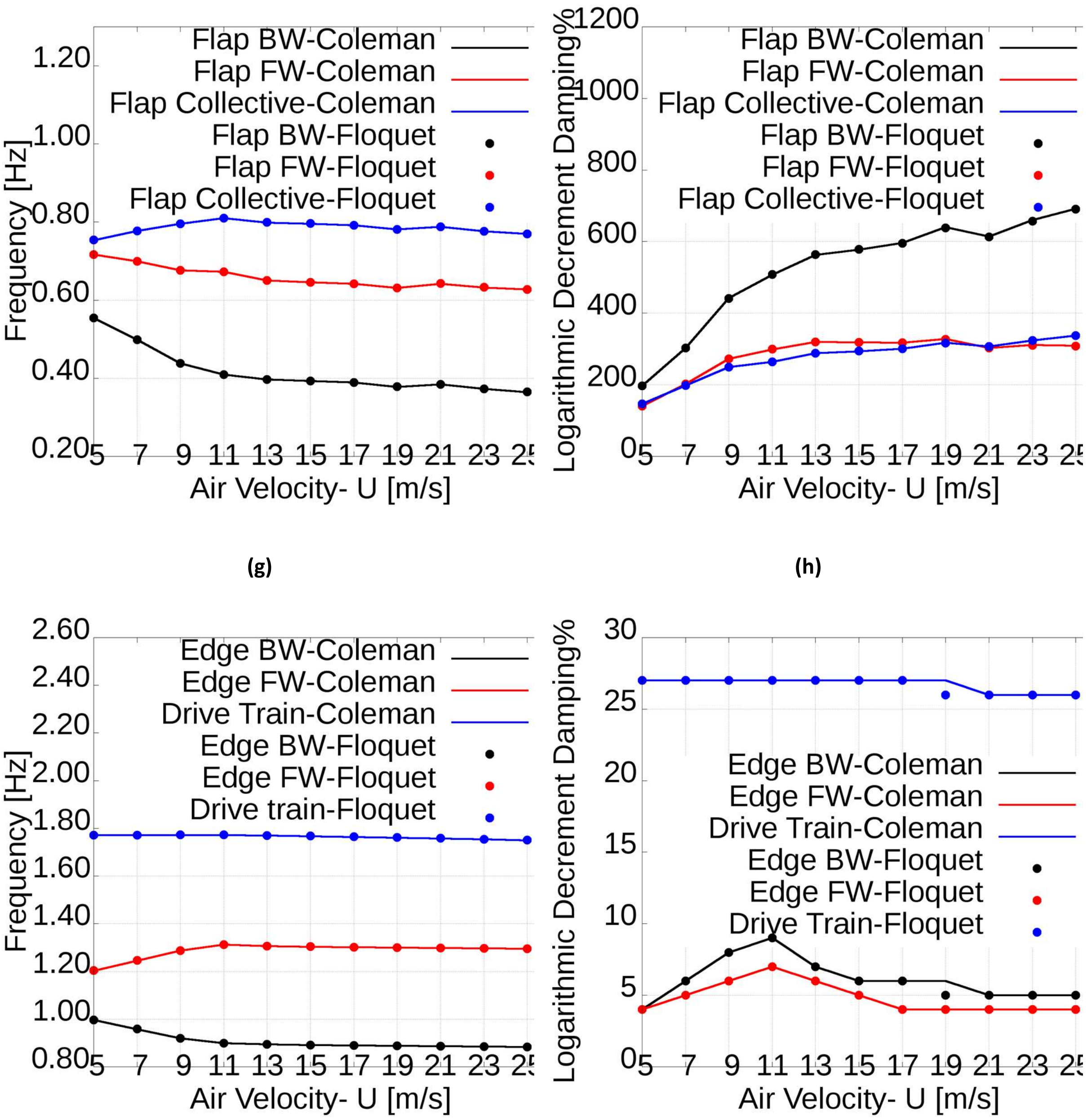

(g)

(h)

(i)

(j)

Figure 50: Campbell diagrams and comparison between Coleman and Floquet methods with all natural frequencies and respective logarithmic damping, (a), (b), (c) and (d) surge, sway, yaw, roll, pitch and heave floater frequencies, (e) and (f) tower side, tower for aft, (g) and (h) blade flap frequencies and (i) - (j) blade edge frequencies

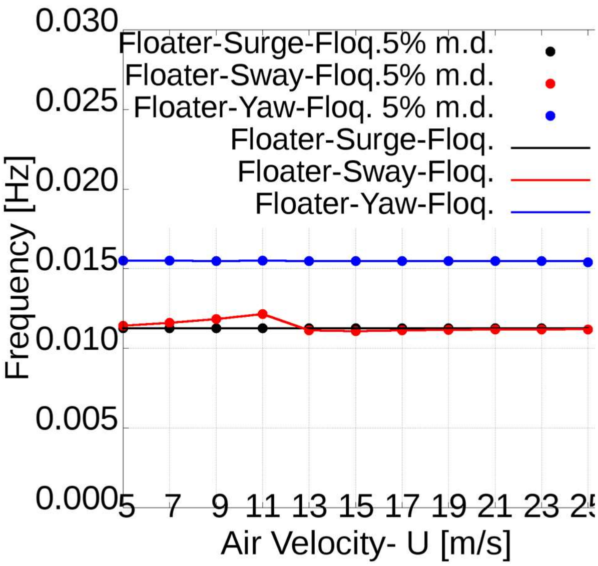
0.030
0.025
0.020
0.015
0.010
0.005
0.000
Frequency [Hz]
5 7 9 11 13 15 17 19 21 23
Air Velocity- U [m/s]
Floater-Surge-Floq.5% m.d.
Floater-Sway-Floq.5% m.d.
Floater-Yaw-Floq. 5% m.d.
Floater-Surge-Floq.
Floater-Sway-Floq.
Floater-Yaw-Floq.

(a)

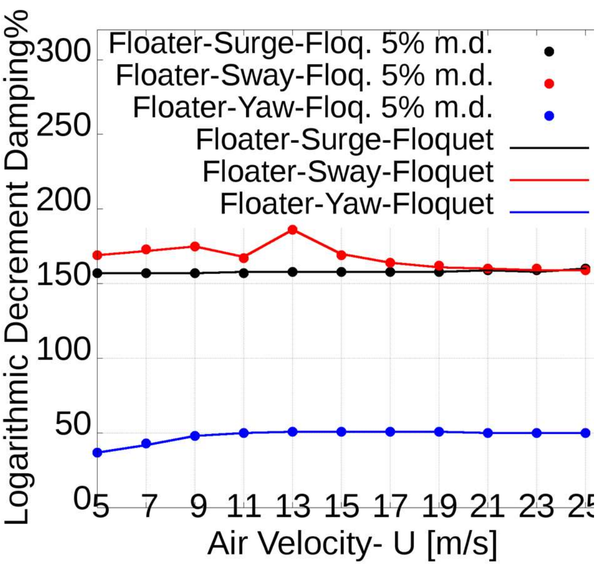
300
250
200
150
100
50
0
Logarithmic Decrement Damping%
5 7 9 11 13 15 17 19 21 23
Air Velocity- U [m/s]
Floater-Surge-Floq. 5% m.d.
Floater-Sway-Floq. 5% m.d.
Floater-Yaw-Floq. 5% m.d.
Floater-Surge-Floquet
Floater-Sway-Floquet
Floater-Yaw-Floquet

(b)

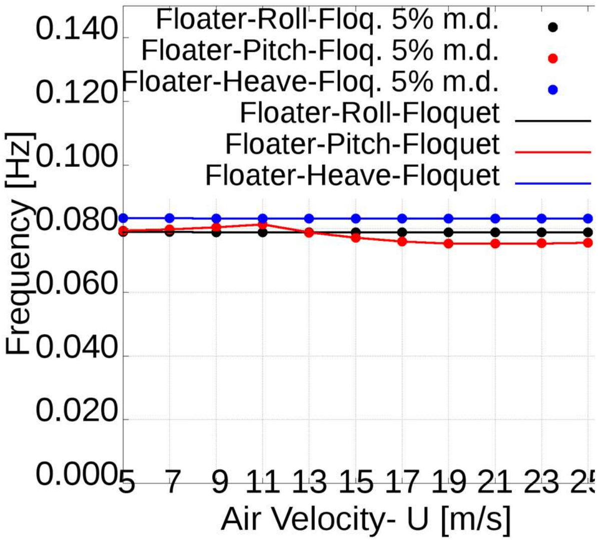
0.140
0.120
0.100
0.080
0.060
0.040
0.020
0.000
Frequency [Hz]
5 7 9 11 13 15 17 19 21 23
Air Velocity- U [m/s]
Floater-Roll-Floq. 5% m.d.
Floater-Pitch-Floq. 5% m.d.
Floater-Heave-Floq. 5% m.d.
Floater-Roll-Floquet
Floater-Pitch-Floquet
Floater-Heave-Floquet

(c)

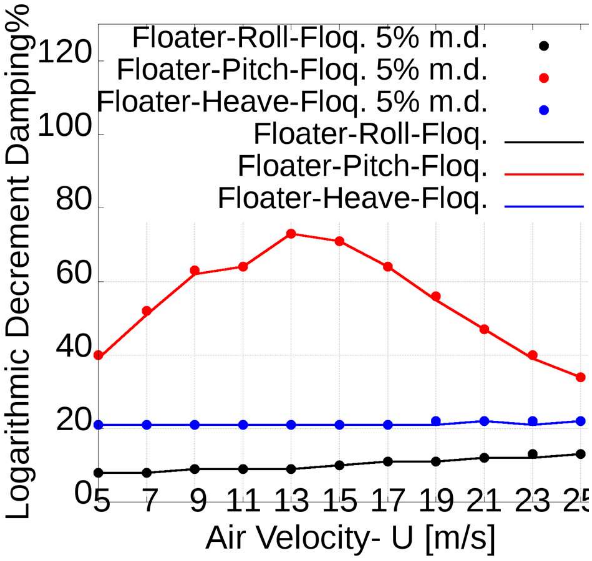
120
100
80
60
40
20
0
Logarithmic Decrement Damping%
5 7 9 11 13 15 17 19 21 23
Air Velocity- U [m/s]
Floater-Roll-Floq. 5% m.d.
Floater-Pitch-Floq. 5% m.d.
Floater-Heave-Floq. 5% m.d.
Floater-Roll-Floq.
Floater-Pitch-Floq.
Floater-Heave-Floq.

(d)

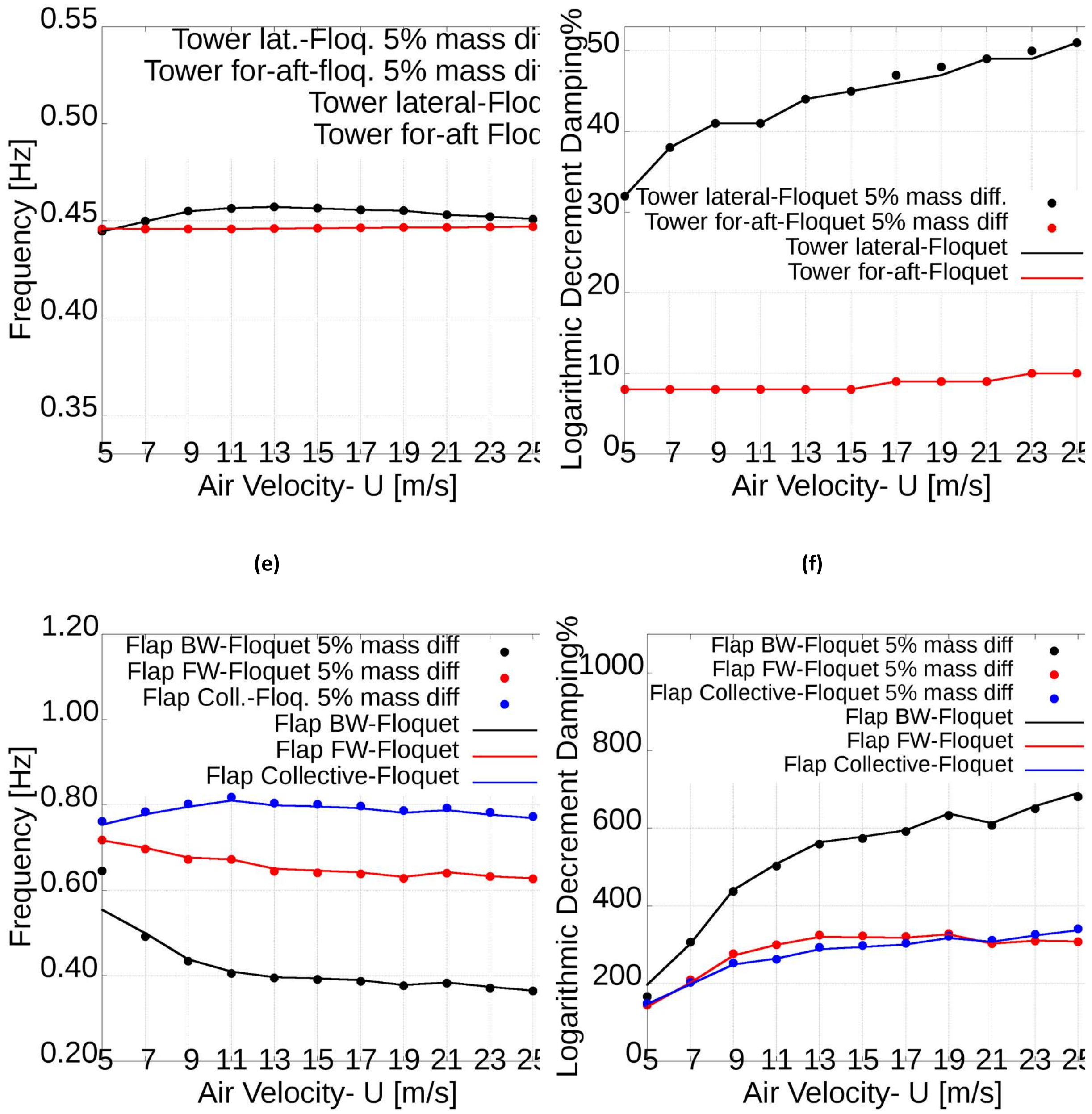
Tower lat.-Floq. 5% mass di
Tower for-aft-floq. 5% mass di
Tower lateral-Floc
Tower for-aft Floc
Frequency [Hz]
0.55
0.50
0.45
0.40
0.35
5 7 9 11 13 15 17 19 21 23 25
Air Velocity- U [m/s]
Logarithmic Decrement Damping%
50
40
30
20
10
0
Tower lateral-Floquet 5% mass diff.
Tower for-aft-Floquet 5% mass diff
Tower lateral-Floquet
Tower for-aft-Floquet
5 7 9 11 13 15 17 19 21 23 25
Air Velocity- U [m/s]
Flap BW-Floquet 5% mass diff
Flap FW-Floquet 5% mass diff
Flap Coll.-Floq. 5% mass diff
Flap BW-Floquet
Flap FW-Floquet
Flap Collective-Floquet
Frequency [Hz]
1.20
1.00
0.80
0.60
0.40
0.20
5 7 9 11 13 15 17 19 21 23 25
Air Velocity- U [m/s]
Flap BW-Floquet 5% mass diff
Flap FW-Floquet 5% mass diff
Flap Collective-Floquet 5% mass diff
Flap BW-Floquet
Flap FW-Floquet
Flap Collective-Floquet
Logarithmic Decrement Damping%
1000
800
600
400
200
0
5 7 9 11 13 15 17 19 21 23 25
Air Velocity- U [m/s]

(e)

(f)

(g)

(h)

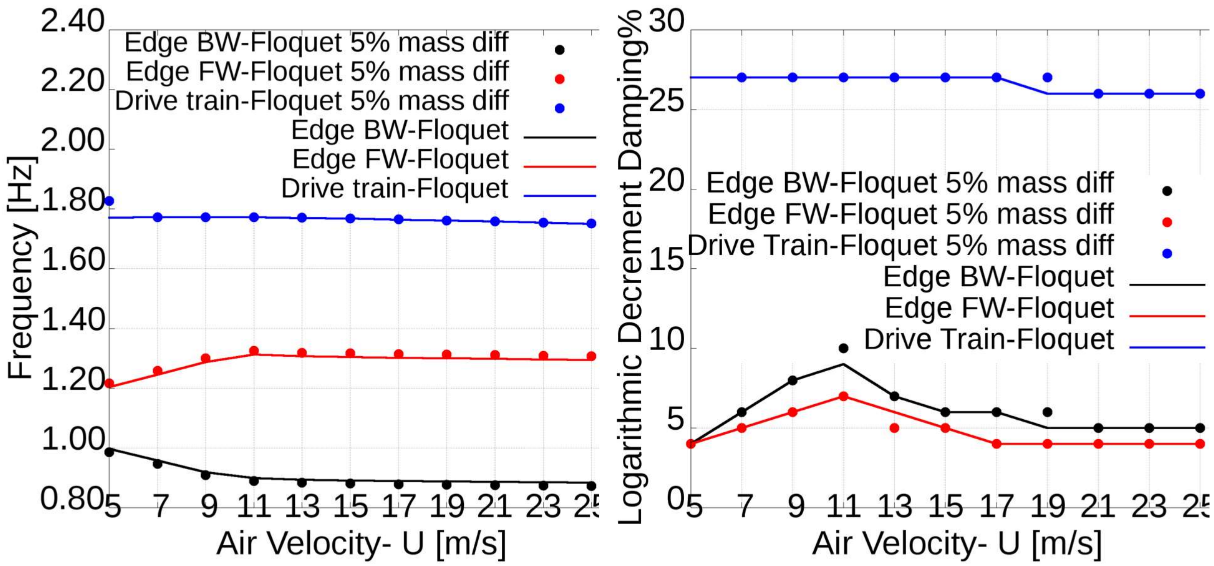

(i) **(j)**

Figure 51: Campbell diagrams and comparison between a W/T with mass difference 5% between blades and without this disparate effect, with all natural frequencies and respective logarithmic damping. (a), (b), (c) and (d) surge, sway, yaw, roll, pitch and heave floater frequencies, (e) and (f) tower side, tower for aft, (g) and (h) blade flap frequencies and (i) - (j) blade edge frequencies

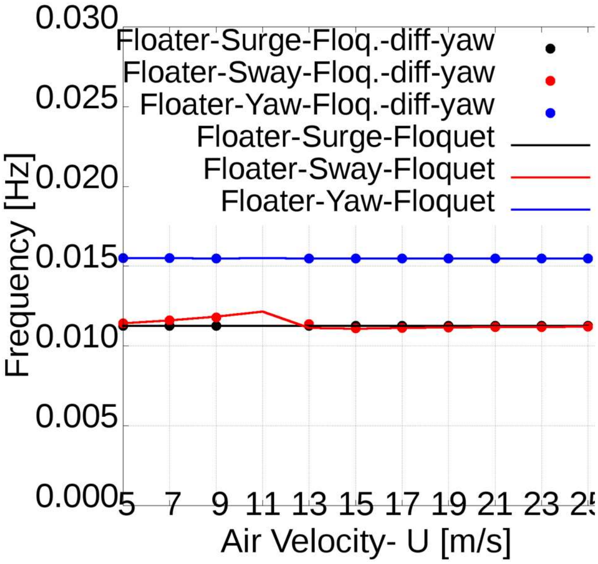
Frequency [Hz]
0.030
0.025
0.020
0.015
0.010
0.005
0.000
Floater-Surge-Floq.-diff-yaw
Floater-Sway-Floq.-diff-yaw
Floater-Yaw-Floq.-diff-yaw
Floater-Surge-Floquet
Floater-Sway-Floquet
Floater-Yaw-Floquet
5 7 9 11 13 15 17 19 21 23 2
Air Velocity- U [m/s]

(a)

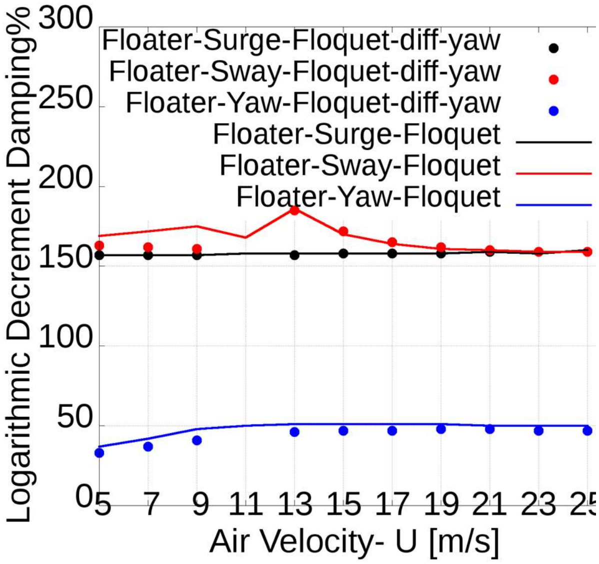
Logarithmic Decrement Damping%
300
250
200
150
100
50
0
Floater-Surge-Floquet-diff-yaw
Floater-Sway-Floquet-diff-yaw
Floater-Yaw-Floquet-diff-yaw
Floater-Surge-Floquet
Floater-Sway-Floquet
Floater-Yaw-Floquet
5 7 9 11 13 15 17 19 21 23 2
Air Velocity- U [m/s]

(b)

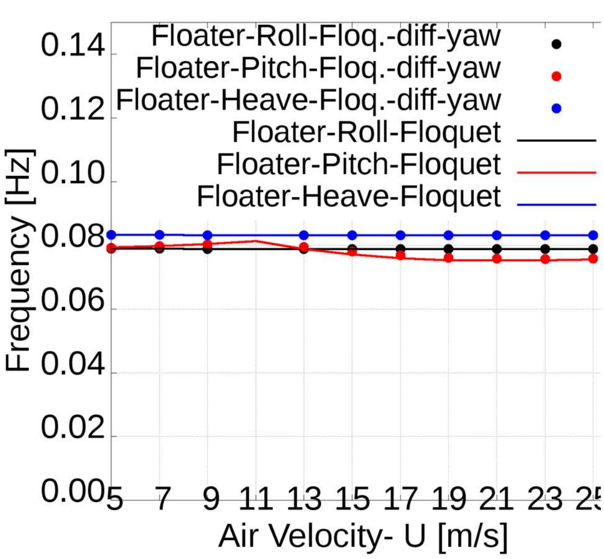
Frequency [Hz]
0.14
0.12
0.10
0.08
0.06
0.04
0.02
0.00
Floater-Roll-Floq.-diff-yaw
Floater-Pitch-Floq.-diff-yaw
Floater-Heave-Floq.-diff-yaw
Floater-Roll-Floquet
Floater-Pitch-Floquet
Floater-Heave-Floquet
5 7 9 11 13 15 17 19 21 23 2
Air Velocity- U [m/s]

(c)

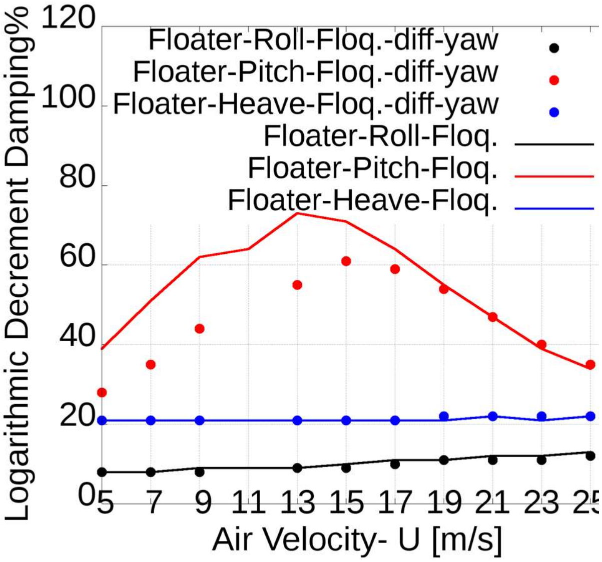
Logarithmic Decrement Damping%
120
100
80
60
40
20
0
Floater-Roll-Floq.-diff-yaw
Floater-Pitch-Floq.-diff-yaw
Floater-Heave-Floq.-diff-yaw
Floater-Roll-Floq.
Floater-Pitch-Floq.
Floater-Heave-Floq.
5 7 9 11 13 15 17 19 21 23 2
Air Velocity- U [m/s]

(d)

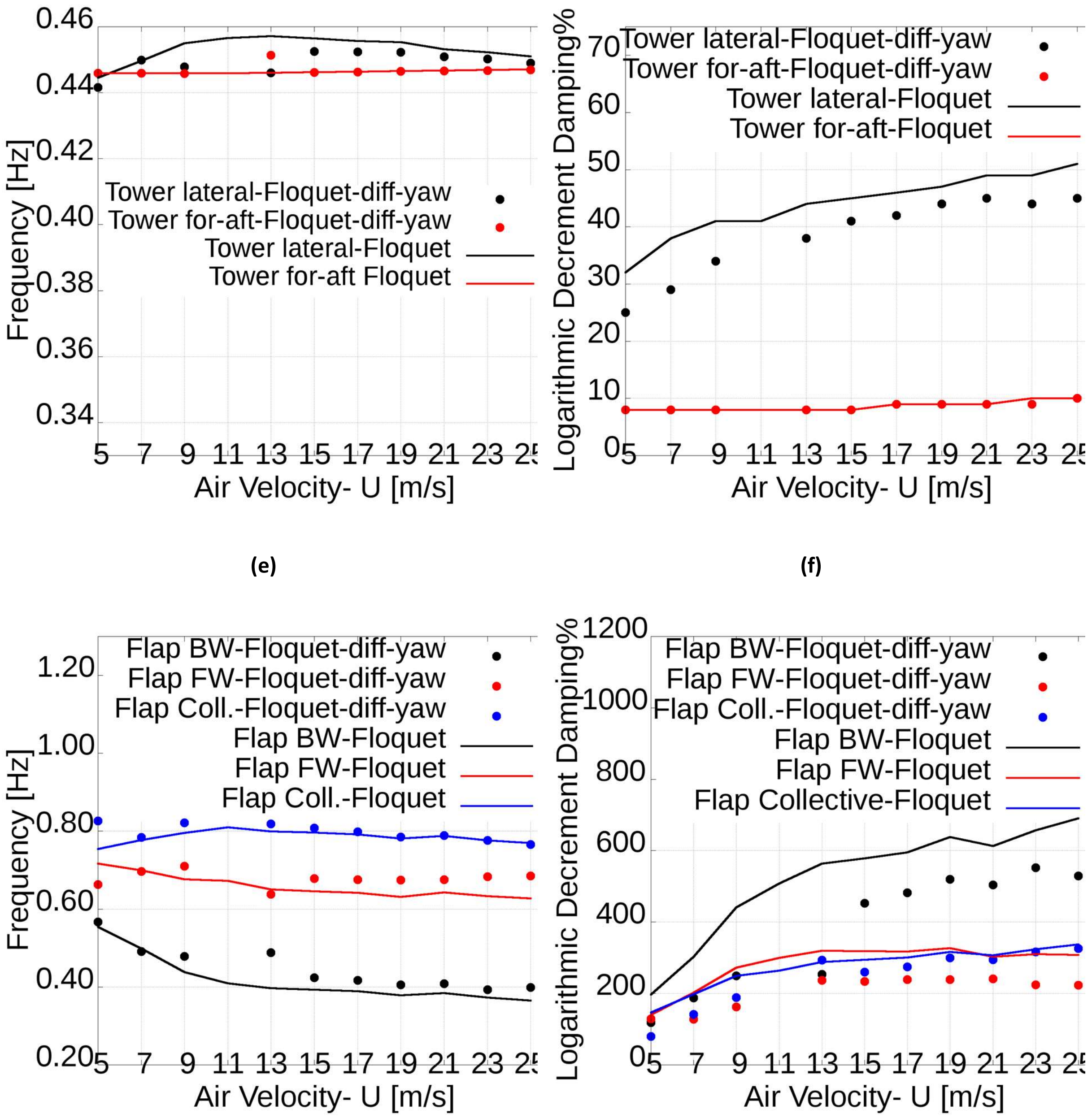
0.46
0.44
0.42
0.40
0.38
0.36
0.34
Frequency [Hz]
Tower lateral-Floquet-diff-yaw
Tower for-aft-Floquet-diff-yaw
Tower lateral-Floquet
Tower for-aft Floquet
5 7 9 11 13 15 17 19 21 23 25
Air Velocity- U [m/s]
70
60
50
40
30
20
10
0
Logarithmic Decrement Damping%
Tower lateral-Floquet-diff-yaw
Tower for-aft-Floquet-diff-yaw
Tower lateral-Floquet
Tower for-aft-Floquet
5 7 9 11 13 15 17 19 21 23 25
Air Velocity- U [m/s]
1.20
1.00
0.80
0.60
0.40
0.20
Frequency [Hz]
Flap BW-Floquet-diff-yaw
Flap FW-Floquet-diff-yaw
Flap Coll.-Floquet-diff-yaw
Flap BW-Floquet
Flap FW-Floquet
Flap Coll.-Floquet
5 7 9 11 13 15 17 19 21 23 25
Air Velocity- U [m/s]
1200
1000
800
600
400
200
0
Logarithmic Decrement Damping%
Flap BW-Floquet-diff-yaw
Flap FW-Floquet-diff-yaw
Flap Coll.-Floquet-diff-yaw
Flap BW-Floquet
Flap FW-Floquet
Flap Collective-Floquet
5 7 9 11 13 15 17 19 21 23 25
Air Velocity- U [m/s]

(e)

(f)

(g)

(h)

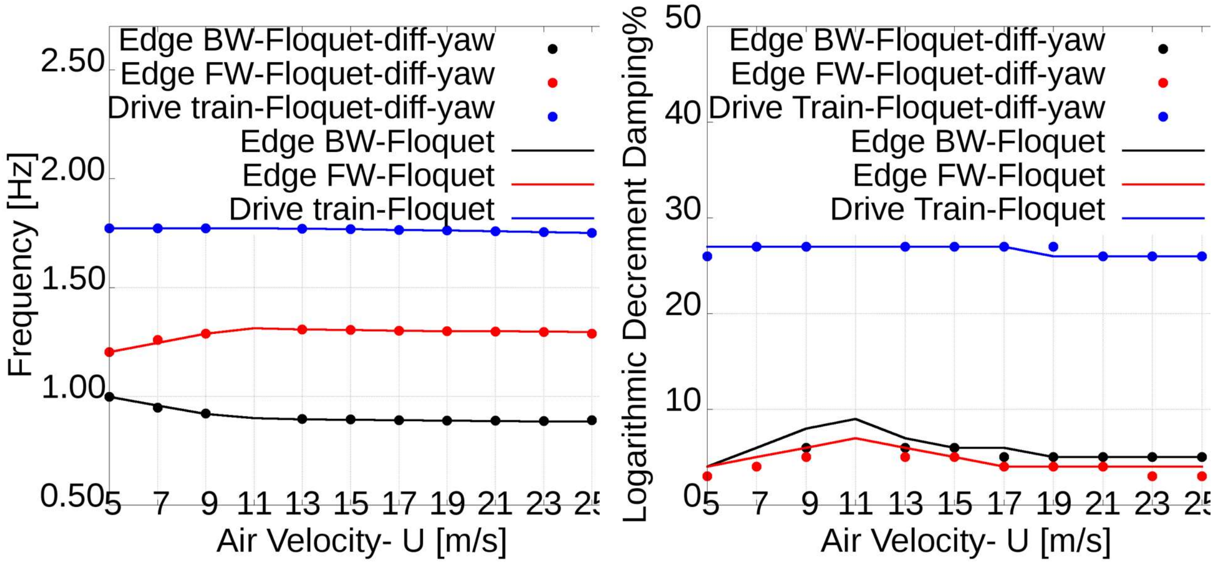

(i) **(j)**

Figure 52: Campbell diagrams and comparison between a W/T with 20 degrees angle 'yaw effect' to the wind speed and without this disparate effect. Natural frequencies and respective logarithmic damping, (a), (b), (c) and (d) surge, sway, yaw, roll, pitch and heave floater frequencies, (e) and (f) tower side, tower for aft, (g) and (h) blade flap frequencies and (i) - (j) blade edge frequencies

6.9 Conclusions for the aeroelastic tool Stab-code

A 22-DOF ROM model of a floating W/T has been implemented and validated in comparison to the FEM based code hGAST. To this model, the Coleman and Floquet modal methods have been implemented which allowed on one hand to verify the actual Floquet implementation and on the other to analyze the effects of anisotropies on stability. Mass imbalance of the rotor and yaw misalignment have been specifically addressed. In the mass unbalance scenario, the homogeneous results are not substantially changed while in the wind yaw scenario, there is slight change of the flapwise natural frequencies and the tower lateral frequency as well as of the corresponding damping [68].

7. General conclusions and suggestions for future research

7.1 Overview

In this work, stochastic variability of the material properties due to manufacturing uncertainties has been added to the inherent stochastic nature of wind in the process of estimating the extreme loads of the NREL 5 MW reference W/T. The estimated blade extreme load and deflection results, obtained for varying material properties, are compared to those produced for the reference ones. In order to better support the findings of the investigation on the uncertainty of the blade structural properties, the process for estimating the design values has been assessed in terms of its numerical implementation and selection of appropriate peak extraction method and fitting cumulative distribution function.

In this context, the OptiDAT database of composite materials has been used. The tensile modulus of elasticity E_1 along the direction of the fibers, the tensile modulus of elasticity E_2 vertical to the direction of the fibers, the major Poisson ratio ν_{12} and the in-plane shear modulus of elasticity G_{12}, are varied according to composite databases following a log-normal distribution. Also, the beam properties for the aeroelastic simulations are described by the LN function, since they depend on the material properties. The estimated blade extreme loads, the deflection results as well as the stress resultants obtained for the different material properties, are compared to those corresponding to the RefMP. The E_1, E_2, G_{12} and ν_{12} properties are varied with CoV 10% for all properties, while the laminate properties and the beam properties of the blade are varied with CoV between 5% and 9%.

The stochastic representation of extreme loads was presented for the UPWIND reference rotor blade. The methodology involves the statistical load extrapolation of the extreme loads derived from 10-min simulations. The respective simulations were based on aeroelastic calculations. The analysis showed that a number of issues that are related to load extrapolation techniques should be carefully considered for establishing the long-term distributions of the extremes. Two peak methods GM and POT are proposed by the IEC standard amendment to extract the maxima. Each one was shown to lead to a different long term exceedance distribution. Further, several parametric distributions (LN, W, 3pW) were fitted to the extracted maxima. It was found that specific recommendations for many aspects concerning the load extrapolation technique were missing from the IEC standard. The current study indicated the sensitivity of the load extrapolation technique on both the method used to extract the maxima and the selected probabilistic models to fit the collected data. A careless confrontation of these aspects may result in deviations up to 10% in the long-term distribution of the extremes.

With regard to the procedure for estimating ultimate design values, it is concluded that the POT peak extraction method, with the threshold set at 1.4 times the STD, outperforms the GM method in terms of convergence, for the same number of simulations. The comparison of the values of the convergence criterion for the two methods is always in favor of the POT method, for all wind speed bins and number of simulations per bin (24, 48 and 96). The 3pW CDF outperforms the 2pW and LN in fitting the peaked extreme values. The above conclusion is derived from the empirical short-term distributions of all load resultants (moments and forces) and tip deflections. Moreover, application of the POT method in conjunction with the 3pW CFD always leads to fulfilment of the K-S test. The IEC convergence criterion suggests raising the number of simulations to 96, at which the range of confidence interval between 5% and 95% is also shorter.

Regarding the stochastic variability of the blade structural properties, the results indicate that the extreme loads are marginally affected. This holds for all three blade moments (flapwise, edgewise and torsion), which are mainly driven by gravitational and aerodynamic loads and remain almost unaffected by the variability of the blade structural properties. On the contrary, maximum deflections are substantially affected. This is expected since different material properties lead to changes in the overall blade stiffness properties and therefore different deflections are obtained for the same load. The analysis does not indicate that by neglecting the variability of the blade properties the designer is on the safe side with respect to extreme blade deflections. In fact, a scatter of ~8% has been obtained around the value corresponding to the reference blade when considering the close to rated wind speed bin of 14m/s.

Stress analysis follows the pattern of ultimate structural loads, but the Tsai-Wu criterion, which is directly affected by the material properties, exhibits a similar variability as that of the material properties. The conclusion concerning stress analysis is almost the same for all blade sections. For the levels of the CoV of the material properties considered, the extreme stresses and the Tsai-Wu criterion CoVs are in the order of 2% and 8% respectively.

In addition to the certification aspects in the design, in many cases the need for fast aeroelastic codes has been identified and a ROM, Stab-code has been developed that allows analysing the most important modal dynamics of a floating WT. In this respect, the main contributions of the work, are the application of the ROM to floating W/Ts as well as to a new insight into anisotropy effects on modal dynamics. The ROM contains 22 DOFs and its formulation is based on Hamiltonian dynamics and has the option of carrying out modal analysis by implementing in this respect the Coleman and the Floquet options.

As a prediction tool, Stab-code has been verified against full FEM predictions using the hGAST software. In this verification structural as well aerodynamic predictions have been checked and found in relatively good agreement. The differences are attributed to two modeling simplifications introduced in Stab-code: on one hand structural properties are concentrated and on the other the induction factors '**a**' and '**à**' remain constant and correspond to the reference state considered.

In addition, by comparing the Coleman and Floquet modal results in homogeneous conditions the specific implementation of the Floquet theory has been verified on the floating NREL 5MW model wind turbine. Then with respect to disparate conditions, it is shown that a 5% mass imbalance does not change neither the frequencies nor the compared to the homogeneous W/T case, while a 20^0 yaw misalignment slightly changes the blade flapwise and tower side-to-side modal characteristics.

7.2 General conclusions

With respect to the estimation of extreme loads the recommendation is to use the combination of POT as peak selection method, with the 3pW probability distribution function and an extended set of 96 simulations per wind speed bin [66].

With respect to the variability of the blade structural properties, it primarily affects the blade deflections and the Tsai-Wu failure criterion and less the extreme normal and shear stresses. As for the long-term flapwise moment forecast, it is even less affected by the material properties [67].

With respect to modal analysis Floquet theory has been successfully implemented and specific non-axisymmetric operation conditions have been checked based on the ROM model [68].

7.3 Suggestions for future research

With respect to the first part of the present work, that addresses extreme load estimation, one topic for future research, consists of using ROM estimations in obtaining the raw load data. Having lower cost and provided that its accuracy is confirmed and eventually improved, ROM modeling will allow to cover the load spectrum with more realizations than 96 and for a wider variability (>10% CoV) of the material properties.

With respect to the second part of the present work, it is proposed to extend the ROM model in the aerodynamic aspects of the full hydro-aero-elastic simulations. This part would specifically include dynamic stall and dynamic inflow. A further step could also include the hydrodynamic effect of incoming waves and eventually currents. Finally, it would be vital to include the controller in Stab-code so that to enable rotor speed and pitch variations.

References

1. Lekou DJ, Philippidis TP. PRE-and POST_THIN: A Tool for the Probabilistic Design and Analysis of Composite Rotor Blade Strength. Wind Energy 2009; 12: 676-91.

2. Philippidis TP, Vassilopoulos AP, Katopis KG, Voutsinas SG. THIN-PROBEAM: software for fatigue design and analysis of composite rotor blades. Wind Engineering 1996;20(5); 349-362

3. Philippidis TP, Eliopoulos EN, Bacharoudis KC, Masmanidis IT, Assimakopoulou TT. Test results of in-plane mechanical properties for modeling complex stress states. D.3.3.6 UPWIND project, 2011, www.upwind.eu/publications/3-rotor-structure-and-materials.aspx.
4. Toft HS, Branner K, Mishnaevski L, Sørensen JD. Uncertainty modelling and code calibration for composite materials. J. of Compos. Mater. 2012; 0:1-19.

5. Lekou DJ, Philippidis TP. (2008) Mechanical property variability in FRP laminates and its effect on failure prediction, Composites: Part B, 39, 1247-1256Philippidis TP, Lekou DJ, Bacharoudis KC. Assessment of failure probability under uni-axial and multi-axial static and fatigue load. OB_TG2_R035, 2006.www.wmc.eu/public_docs/10372_000.pdf.

6. Philippidis TP, Lekou DJ, Bacharoudis KC. Assessment of failure probability under uni-axial and multi-axial static and fatigue load. OB_TG2_R035, 2006.www.wmc.eu/public_docs/10372_000.pdf.

7. Philippidis TP, Assimakopoulou TT, Passipoularidis V, Antoniou AE. Static and fatigue tests on ISO Standard ±45° coupons, main test phase I. OB_TG2_R020, 2004. www.wmc.eu/public_docs/index.htm.

8. Moriarty PJ, Holley WE, Butterfield SP. Extrapolation of extreme and fatigue loads using probabilistic methods. Technical report NREL/TP-500-34421, NREL, Golden, Colorado, USA, November 2004.
9. Joint Committee on Structural Safety. Probabilistic Model Code, 2001.
10. DNV-OS-J102. Design and Manufacture of Wind Turbine Blades, Det Norske Veritas, Working draft, 2005.

11. Smirnov N (1948). "Table for estimating the goodness of fit of empirical distributions". Annals of Mathematical Statistics. 19: 279–281. doi:10.1214/aoms

12. Toft HS, Sørensen JD. Reliability-Based design of wind turbine blades. Struct. Saf. 2011; 33:333-42.
13. Bacharoudis, Konstantinos (2014, *University of Patras*), [http://www.didaktorika.gr/eadd/handle/10442/39848]
14. A probabilistic approach for strength and stability evaluation of wind turbine rotor blades in ultimate loading, K. C. Bacharoudis, T.P.Philippidis, Structural Safety 40(2012)31-38
15. Estimating design reliability of composite rotor blades under ultimate loading, K. C. Bacharoudis, T.P.Philippidis, Wind Energy 18(2015)783-796

16. Philippidis TP, Antoniou AE, Passipoularidis V, Assimakopoulou TT. Static tests on the standard OB unidirectional coupon, main test phase I (static tensile tests). OB_TG2_R018, 2004. www.wmc.eu/public_docs/index.htm.
17. IEC 61400-1, Wind Turbines- PART 1: Design requirements, 3rd ed.; 2005.
18. IEC 61400-1, Wind Turbines- PART 1: Design requirements-Amendment 1, 3rd ed.; 2009.
19. Ragan P, Manuel L. Statistical extrapolation methods for estimating wind turbines extreme loads. AIAA 2007, January 8-11: 2007, 14553-71.
20. Peeringa J. Comparison of extreme load extrapolations using measured and calculated loads of a MW wind turbine. EWEC 2009, March 16-19: 2009.
21. Cheng PW, Bussel GJW, Kuik GAM, Vugts JH. Reliability-based design methods to determine the extreme response distribution of offshore wind turbines. Wind Energy 2003; 6: 1-22.
22. Toft HS, Sørensen JD, Veldkamp D. Assessment of load extrapolation methods for wind turbines. AIAA 2010, January 4-7: 2010, 1581-92.
23. Rice, S. O., "Mathematical analysis of random noise," Bell System Technical Journal, Vol. 23, 1944, pp. 282-332.
24. Fitzwater LM. Estimation of fatigue and extreme load distributions from limited data with application to wind energy systems. Technical report SAND 2004-0001, SANDIA, USA, January 2004.
25. Saranyasoontorn K, Manuel L. Design loads for wind turbines using the environmental contour method. J of Sol. Energy Eng. incl. Wind Energy and Build. Energy Conserv. 2006; 128: 554-61.
26. Fogle J, Agarwal P, Manuel L. Towards an improved understanding of statistical extrapolation for wind turbine extreme loads. Wind Energy 2008; 11: 613-35.
27. Freudenreich K, Argyriadis K. Wind turbine load level based on extrapolation and simplified methods. Wind Energy 2008; 11: 589-600.
28. Barone M., Paquette J., Resor B., Lance M. and Nguyen H., Simulating the entire life of an offshore wind turbine', Scandia national Laboratories, University Of Texas.
29. Abdallah, I.; Natarajan, A.; Sørensen, J. D. Impact of uncertainty in airfoil characteristics on wind turbine extreme loads, Renewable Energy, Vol. 75, 2015, p. 283-300.
30. Abdallah, I.; Natarajan, A.; Sørensen, J. D. Influence of the control system on wind turbine loads in power production in extreme turbulence: structural reliability, Renewable Energy, 2014, J. Phys.: Conf. Series, 524, 012069.
31. Jonkman, J.M., S. Butterfield, W. Musial, and G. Scott, *Definition of a 5-MW reference wind turbine for offshore system development*. 2009: National Renewable Energy Laboratory Golden, CO.
32. Patrick Moriarty, 'Database for validation of design load extrapolation techniques', NREL, Wind Energy 2008; 11: 559-576
33. Riziotis V.A. and Voutsinas S.G., "GAST: A general aerodynamic and structural prediction tool for wind turbines", EWEC 97, October 6-9:1997, 448-52.

34. Riziotis VA, Voutsinas SG, Politis ES, Chaviaropoulos PK, Hansen AM, Madsen, H.A., Rasmussen, F., "Identification of structural non-linearities due to large deflections on a 5MW wind turbine blade," Proc. of EWEC'2008, Brussels, Belgium
35. Belessis, M.A., Chassapoyiannis, P.I., Voutsinas S.G., Free-wake modelling of rotor aerodynamics: Recent developments and future perspectives'', Proc. Of EWEC'2001, Copenhagen, Denmark.
36. Petot, D.,"Differential equation modeling of dynamic stall", Recherche Aerospatiale, paper no. 5,(1989).
37. Newmark, N.M. (1959) 'A method of computation for structural dynamics', Journal of Engineering Mechanics, ASCE, 85(EM3) 67-94.
38. J.C. Kaimal, J.C. Wyngaard, Y. Izumi, and O.R. Cote, "Spectral characteristics of surface-layer turbulence," *Q.J.R. Meteorol. Soc.*, v. 98, 1972, pp. 563-598.
39. Manolas, D.I., Riziotis, V.A., Voutsinas, S.G., "Assessing the importance of geometric non-linear effects in the prediction of wind turbine blade loads", Computational and Nonlinear Dynamics Journal, Vol. 10, 041008, July 2015.
40. Nijssen R, de Winkel GD, Peeringa JM. UPWIND reference blade for WP 3, project report, December 2007.
41. Cousineau, D. (2009) 'Fitting the Three-Parameter Weibull Distribution: Review and Evaluation of Existing and New Methods. IEEE Transactions on Dielectrics and Electrical Insulations', 16(1), 281-288. [(31)].
42. Matlab. The Language of Technical Computing. Version R2011b (7.13.0.564), 2011.
43. Riziotis, V.A., Politis, E.S., (2010) "Methods for linearizing servo-aero-elastic equations of the full wind turbine, "appendix F, page 81"
44. P.F. Skjoldan, M.H. Hansen. "On the similarity of the Coleman and Lyapunov - Floquet transformations for modal analysis of bladed rotor structures", Siemens Wind Power A/S, Denmark National Laboratory for Sustainable Energy, Risø – Technical University of Denmark, 14 August 2009. *Journal of Sound and Vibration*, 327:424–439, 2009.
45. P.F. Skjoldan. Modal Dynamics of wind turbines with anisotropic rotors. In *Proceedings of 47th AIAA Aerospace Sciences Meeting*, Orlando FL, USA, 2009.
46. P.F. Skjoldan, M.H. Hansen. Implicit Floquet analysis of wind turbines using tangent matrices of a nonlinear aeroelastic code. *Wind Energy*. Accepted for publication, delivered to production 15th February 2011.
47. P.F. Skjoldan, M.H. Hansen. Effects of extreme wind shear on aeroelastic modal damping of wind turbines. *Wind Energy*. Accepted for publication, submitted in revised form 28th February 2011.
48. P.F. Skjoldan, O.A. Bauchau. Determination of modal parameters in complex nonlinear systems. *Journal of Nonlinear and Computational Dynamics*, 6(3):031017, 2011.

49. O.A. Bauchau and J. Wang. Efficient and robust approaches to the stability analysis of large multibody systems. Journal of Computational and Nonlinear Dynamics, 3, 2008. DOI:10.1115/1.2397690

50. Karl Stol, Mark Balas, Gunjit Bir, Floquet Modal Analysis of a Teetered-Rotor Wind Turbine, Journal of solar energy engineering, November 2002. DOI: 10.1115/1.1504846.

51. Coleman, R.P. and Feingold, A.M., (1957), ‘Theory of self-excited mechanical oscillations of helicopter rotors with hinged blades’, NASA TN 3844

52. R.P. Coleman, Theory of self-excited mechanical oscillations of hinged rotor blades, Technical Report NACA-WR-L-308, Langley Research Center, 1943, available from 〈ntrs.nasa.gov〉 .

53. Johnson, W., Helicopter Theory, Princeton University Press: Princeton, NJ, 1980.

54. Floquet, G., 1883, “Sur les équations différentielles linéaires à coefficients périodiques,” Ann. Sci. Ec. Normale Super., 12, pp. 47–88.

55. J. Nagabhushanam, G.H. Gaonkar, Automatic identification of modal damping from Floquet analysis, Journal of the American Helicopter Society, 40 (2) (1995), April, Vol & No 40, 2. pp. 39–42.

56. Saravanos DA, Varelis D, Plagianakos TS and Chrysochoidis N 2006 A shear beam finite element for the damping analysis of tubular laminated composite beams. *Journal of Sound and Vibration* **291** 802–23 (doi: 10.1016/j.jsv.2005.06.045).

57. Tsai SW and Wu EM 1971 A General Theory of Strength for Anisotropic Materials. Journal of Composite Materials, vol **5**, 58-80, (doi: 10.1177/002199837100500106).

58. Polymer matrix composites: Guidelines for characterization of structural materials. Composite materials handbook, vol. 1. Washington (DC): Department of Defence; 2002 DOD-MIL-HDBK-17-1F.

59. Philippidis TP, Lekou DJ, Aggelis DG. Mechanical property distribution of CFRP filament wound composites. Compos. Struct. 1999; 45: 41-50.

60. Jeong HK, Shenoi RA. Probabilistic strength analysis of rectangular FRP plates using Monte Carlo simulation. Comput Struct. 2000; 76: 219-35.

61. Zureick AH, Bennett RM, Ellingwood BR. Statistical characterization of fiber-reinforced polymer composite material properties for structural design. J. Struct. Eng. ASCE 2006; 132: 1320–7.

62. Sriramula S, Chryssanthopoulos MK. Probabilistic models for spatially varying mechanical properties of in-service GFRP cladding panels. J. Compos. Construct. ASCE 2009; 13: 159-67.

63. Shaw A, Sriramula S, Gosling PD, Chryssanthopoulos MK. A critical reliability evaluation of fibre reinforced composite materials based on probabilistic micro and macro-mechanical analysis. Compos. Part B: Engineer. 2010; 41: 446-53.

64. Toft HS, Branner K, Mishnaevski L, Sørensen JD. Uncertainty modelling and code calibration for composite materials. J. of Compos. Mater. 2012; 0:1-19.

65. Toft HS, Branner K, Berring P, Sørensen JD. Defect distribution and reliability assessment of wind turbine blades. Eng. Struct. 2011; 33: 171-80.
66. P Schinas, D Manolas, V Riziotis, T Philippidis, S Voutsinas, Statistical extrapolation methods for estimating extreme loads on wind turbine blades under turbulent wind conditions and stochastic material properties, Wind Engineering, Sage publications, July 2020, https://doi.org/10.1177/0309524X20936201
67. P Schinas, G Serafeim, D Manolas, V Riziotis, T Philippidis, S Voutsinas, P Chaviaropoulos, Assessment of extreme stresses and deflections on wind turbine blades with stochastic material properties using statistical extrapolation method, 2020 J. Phys.: Conf. Ser. 1618 052029
68. P Schinas, D Manolas, V Riziotis, S Voutsinas, Aeroelastic modal dynamics of floating wind turbines in anisotropic conditioning based on Floquet analysis, Torque Conference 2022
69. Evans, M., N. Hastings, and B. Peacock. Statistical Distributions. Hoboken, NJ: Wiley-Interscience, 2000. pp. 102–105.

APPENDIXES

Appendix 1: OptiDAT database material properties

E_1 [Gpa]	E_2 [GPa]	v_{12}	G_{12} [GPa]	XT [MPa]	XC [MPa]	YT [MPa]	YC [MPa]	S [MPa]
36.74	13.54	0.240	4.03	695.03	480.82	49.58	148.98	54.04
37.26	13.60	0.244	4.03	698.83	488.99	50.31	157.20	54.35
37.74	13.66	0.244	4.07	703.94	489.89	51.11	159.87	54.77
37.85	13.74	0.263	4.15	731.37	507.89	51.13	161.40	54.99
38.02	13.78	0.267	4.17	736.79	508.00	51.69	162.01	55.06
38.05	13.84	0.272	4.19	752.70	508.38	51.73	162.58	55.17
38.14	13.88	0.272	4.20	764.42	510.78	52.17	163.41	55.27
38.58	13.88	0.273	4.21	765.39	514.38	52.24	163.42	55.47
38.66	13.90	0.279	4.22	765.50	519.40	52.29	164.01	55.50
38.72	13.93	0.279	4.22	769.16	521.30	52.32	164.19	55.55
38.75	14.00	0.279	4.23	772.41	522.98	52.54	164.23	55.56
38.90	14.01	0.280	4.24	774.16	524.56	52.85	164.43	55.66
38.94	14.02	0.282	4.25	774.84	524.60	53.18	164.85	55.83
39.00	14.07	0.283	4.27	777.33	529.16	53.74	165.34	55.89
39.03	14.09	0.285	4.27	781.34	529.46	53.90	165.86	56.01
39.10	14.16	0.289	4.28	782.48	529.53	54.08	165.90	56.02
39.20	14.17	0.291	4.28	784.90	529.59	54.21	166.46	56.33
39.28	14.19	0.297	4.29	787.57	531.15	54.67	167.75	56.91
39.31	14.29	0.302	4.32	793.25	531.65	55.82	167.77	57.02
39.38	14.35	0.302	4.34	796.99	533.04	56.05	168.30	57.24
39.59	14.39	0.307	4.35	798.23	535.40	56.76	168.36	57.25
39.70	14.42	0.309	4.36	800.76	537.14	56.76	169.88	57.41
39.73	14.60	0.314	4.37	801.78	538.04	56.92	170.66	57.46
39.80	14.69	0.318	4.40	801.81	539.69	57.07	170.78	57.63
40.08	14.73	0.320		803.13	539.97	57.44	170.78	57.72
40.11		0.327		818.65	541.58	59.92	171.69	57.81
40.18		0.329		824.23				
40.99		0.333		825.40				
41.38		0.346		836.03				

Table 19: OptiDAT database, material properties extracted from experimental data

Appendix 2: Definitions and notations for descriptive statistics

Observations (Obs.)	n
Minimum (min)	$\min x_i$
Maximum (max)	$\max x_i$
Arithmetic mean (mean)	$\text{mean}=\sum_{i=1}^{n} x_i / n$
Standard deviation (STD) (σ)	$\sqrt{(1/n-1)\sum_{i=1}^{n}(x_i-\text{mean})^2}$
Coefficient of variation (CoV)	σ / mean
Skewness	$(1/n)\sum_{i=1}^{n}(x_i-\text{mean})^3 / \left(\sqrt{(1/n)\sum_{i=1}^{n}(x_i-\text{mean})^2}\right)^3$
Kurtosis	$(1/n)\sum_{i=1}^{n}(x_i-\text{mean})^4 / \left(\sqrt{(1/n)\sum_{i=1}^{n}(x_i-\text{mean})^2}\right)^2$

Table 20: Definitions and notations for descriptive statistics

Appendix 3: Descriptive statistics for the OptiDAT database

	E_1 [GPa]	E_2 [Gpa]	v_{12}	G_{12} [Gpa]	XT [Mpa]	XC [Mpa]	YT [MPa]	YC [MPa]	S [MPa]
Obs.	29	25	29	24	29	26	26	26	26
min	36.740	13.54	0.240	4.032	695.027	480.817	49.583	148.984	54.040
max	41.380	14.73	0.346	4.396	836.033	541.576	59.916	171.686	57.810
mean	39.042	14.077	0.291	4.239	776.497	521.820	53.865	165.004	56.071
CoV [%]	2.644	2.307	9.339	2.340	4.655	3.162	4.756	2.938	1.961
Skewness	0.018	0.392	0.054	-0.562	-0.740	-1.014	0.462	-1.331	0.096
kurtosis	3.099	2.428	2.443	2.803	3.120	3.210	2.471	5.779	1.905

Table 21: Descriptive statistics for the OptiDAT database

Material properties / distributions fitting	N	LN	W
K-S, E_1	0.98	0.96	0.80
K-S, E_2	0.97	0.98	0.64
K-S, G_{12}	0.98	0.95	0.97
K-S, v_{12}	0.93	0.98	0.70

Table 22: p-values of the K-S test (OptiDAT)

Appendix 4: NREL 5-MW Reference Wind Turbine

Rated Power	5 MW
Rotor Orientation, Configuration	Upwind, 3 Blades
Control	Variable Speed / Collective Pitch
Drivetrain	High Speed, Multiple-Stage Gearbox
Rotor, Hub Diameter	126 m, 3 m
Hub Height	90 m
Cut-In, Rated, Cut-Out Wind Speed	3 m/s, 11.4 m/s, 25 m/s
Cut-In, Rated Rotor Speed	6.9 rpm, 12.1 rpm
Optimum tip speed ratio λ, Optimum power coefficient c_p	7.55, 0.482
Rotor Mass	110.00 tn
Nacelle Mass	240.00 tn
Tower Mass	347.46 tn

Table 23: Main properties of the NREL 5-MW Reference Wind Turbine

Appendix 5: Conclusions and results for the visual criterion

Conclusions and results regarding the visual criterion method and the selection of the short term fitting distribution function are included in this appendix. The data listed below are for the flapwise moment, and refer to all wind speed bins. The fitting accuracy for the body and the tail of data are mentioned below in the table as follows: Precise='Prec', Underestimated='Under', Over-estimated='Over', Conservative (between Overestimated and Precise)= 'Cons'.

Peak method and blade data/ CDF	**LN**	**2pW**	**3pW**
Reference blade, GM method			
u=4 m/s	Prec / Under	Over/ Under	Prec / Under
u=8 m/s	Prec/ Prec	Over/ Under	Prec/ Prec
u=10 m/s	Prec/ Under	Over/ Under	Prec/ Prec
u=12 m/s	Prec/ Under	Over/ Under	Prec/ Under
u=14 m/s	Prec/ Under	Over/ Under	Prec/ Under
u=17 m/s	Prec/ Prec	Over/ Under	Prec/ Prec
u=21 m/s	Prec/ Under	Over/ Under	Prec/ Under
u=25 m/s	Prec/ Prec	Over/ Under	Prec/ Prec
Stochastic material blade., GM method			
u=4 m/s	Prec/ Under	Over/ Under	Prec/ Under
u=8 m/s	Prec/ Under	Over/ Under	Prec/ Under
u=10 m/s	Prec/ Prec	Over/ Under	Prec/ Prec
u=12 m/s	Prec/ Under	Over/ Under	Prec/ Prec
u=14 m/s	Prec/ Under	Over/ Under	Prec/ Under
u=17 m/s	Prec/ Prec	Over/ Under	Prec/ Prec
u=21 m/s	Prec/ Under	Over/ Under	Prec/ Under
u=25 m/s	Prec/ Under	Over/ Under	Prec/ Under
Reference blade, POT method			
u=4 m/s	Under / Under	Under / Under	Prec/ Cons
u=8 m/s	Under / Under	Over/ Under	Prec/ Prec
u=10 m/s	Prec/ Prec	Over/ Under	Prec/ Cons
u=12 m/s	Prec/ Under	Over/ Under	Prec/ Prec
u=14 m/s	Prec/ Prec	Over/ Under	Prec/ Cons
u=17 m/s	Prec/ Under	Over/ Under	Prec/ Cons
u=21 m/s	Prec/ Prec	Over/ Under	Prec/ Cons
u=25 m/s	Prec/ Cons	Over/ Under	Prec/ Cons
Stochastic material blade., POT method			

u=4 m/s	Under / Under	Under / Under	Prec/ Cons
u=8 m/s	Prec/ Under	Over/ Under	Prec/ Prec
u=10 m/s	Prec/ Prec	Over/ Under	Prec/ Cons
u=12 m/s	Prec/ Under	Over/ Under	Prec/ Prec
u=14 m/s	Prec/ Under	Over/ Under	Prec/ Cons
u=17 m/s	Prec/ Under	Over/ Under	Prec/ Cons
u=21 m/s	Prec/ Under	Over/ Under	Prec/ Cons
u=25 m/s	Prec/ Under	Over/ Under	Prec/ Cons

Table 24: Observations of the visual criterion method for all wind speed bins, both blades reference and stochastic, both peak methods GM and POT

Appendix 6: Concentrated properties for the reduced order model (R.O.M.)

The concentrated properties of the reduced order model and the initial conditions are described in the following Table 25 up to Table 28.

Description	Symbol	Value
Initial reference roll angle of the floater around X axis (rad)	XfloatROLLref	0.0
Initial reference pitch angle of the floater around Y axis (rad)	YfloatPITCHref	0.0
Initial reference yaw angle of the floater around Z axis (rad)	ZfloatYAWref	0.0
Stiffness of the floater in tilt direction due to rolling	K11 – KXfloatROLL	1.4881 d9 Nm/rad
Stiffness of the floater in yaw direction due to yawing	K33 - KZfloatYAW	1.1700 d8 Nm/rad
Stiffness of the floater in sway direction due to rolling	K51	1.08 d5 Nm/rad
Stiffness of the floater in surge direction due to pitching	K42	1.08 d5 Nm/rad
Stiffness of the floater in surge direction due to yawing	K43	0 Nm/rad
Stiffness of the floater in surge direction due to surging	K44 - KXfloatSURGE	7.510 d4 Nm/rad
Stiffness of the floater in heave direction due to heaving	K66 – KZfloatHEAVE	3.8551 d6 Nm/rad
Stiffness of the floater in tilt direction due to pitching	K22 - KYfloatPITCH	1.4881 d9 Nm/rad
Stiffness of floater to sway direction motion, on Y axis due to swaying	K55 - KYfloatSWAY	7.510 d4 Nm/rad

Table 25: Concentrated properties for the floater of the (floating) reduced order model

Description	Symbol	Value
Distance from the floater to the bottom of tower	Hfltower	10 m
Total height of the tower	HtowALL	89.6 m
Mass of the tower	Mtow	249720 kg
1st moment of inertia of the tower around X axis	Stowx	0
1st moment of inertia of the tower around Y axis	Stowy	8327661 kg.m
1st moment of inertia of the tower around Z axis	Stowz	0

2nd moment of inertia of the tower to X axis	Jtowxx	9.1 d5 kg.m^2
2nd moment of inertia of the tower to Y axis	Jtowyy	3.96 d8 kg.m^2
2nd moment of inertia of the tower to Z axis	Jtowzz	9.1 d5 kg.m^2
Stiffness of the tower in roll around X axis	Kroll	1.42 d10 Nm/rad
Stiffness of the tower in yaw around Y axis	Kyaw	4.3 d9 Nm/rad
Stiffness of the tower in pitch around Z axis	Ktilt	1.8 d10 Nm/rad
Length of the shaft	Hsh	5.0191 m
Offset of the shaft	Hoffsh	1.96 m
Mass of the nacelle	Mnac	240000 kg
2nd moment of inertia of the nacelle around X axis	Jnacx	8.707 d5 kg.m^2
2nd moment of inertia of the nacelle around Y axis	Jnacy	1.737 d6 kg.m^2
2nd moment of inertia of the nacelle around Z axis	Jnacz	2.607 d6 kg.m^2
Distance from the hub to blade	Hhub	1.5 m
Mass of the hub	Mhub	56780 kg

Table 26: Concentrated properties for the tower, nacelle and hub of the (floating) reduced order model

Description	Symbol	Value
2nd moment of inertia of the hub around X axis	Jhubx	1.1592 d5 kg.m^2
2nd moment of inertia of the hub around Y axis	Jhuby	1.1592 d5 kg.m^2
2nd moment of inertia of the hub around Z axis	Jhubz	1.1592 d5 kg.m^2
Stiffness of shaft to torsion around X axis	Ksh	8.67 d8 Nm/rad

Table 27: concentrated properties for the hub for the floating reduced order model

Description	Symbol	Value
Mass of the blade	Mblade	17740 kg
1st moment of inertia of the blade mass around axis X	Sb1	3.62979 d5 kg.m
1st moment of inertia of the blade mass around axis Y	Sb2	3.62979 d5 kg.m
1st moment of inertia of the blade mass around axis Z	Sb3	3.62979 d5 kg.m
2nd moment of inertia of the blade mass around axis X	Jb1	1.1743 d7 kg.m^2
2nd moment of inertia of the blade mass around axis Y	Jb2	1.1743 d7 kg.m^2
2nd moment of inertia of the blade mass around axis Z	Jb3	1.1743 d7 kg.m^2
Stiffness of the blade 1,2,3 into flap direction	Kbi	2.183 d8 Nm/rad
Stiffness of the blade 1,2,3 into edge direction	Kxi	5.436 d8 Nm/rad

Table 28: Concentrated properties of the blades of the (floating) reduced order model

Appendix 7: Stability and Eigenvalue analysis of linear systems with periodic coefficients matrices and peripheral symmetry –Coleman transformation.

This method is usually applied to systems with peripheral (azimuth) symmetry, like rotor systems with rotating identical blades and equal azimuth distance degrees between blades. It is based on the right coordinate's transformation Lyapunov-Floquet with which the system of periodic cooeficients transformed to another equal system with standard coefficients. Such a transformation that fits to rotor systems is the Coleman [51], [52] multi-blade coordinates transformation. This transformation takes advantage of the fact that the dynamic behavior of the rotor expressed with equations and degrees of freedom that refered to the rotational coordinates system, as well as to the fact that these systems described by pheripheral (azimuth) symmetry.

So for the isotropic rotor with 3 blades that rotates with standard angular speed Ω, each i degree of freedom, of the m blade $u_i^{(m)}$ (with u express the total number of the degrees of freedom to the second order differential equations system (6-2) or (6-6) that refered to the rotational coordinates system), it may be expressed as a function of coordinates (degrees of freedom), that refer to the total rotor system making reference to the non rotational inertial coordinate system. The coordinates to the non rotational system defined due to the transformation equations:

$$u_i^0 = \frac{1}{3}\sum_{m=1}^{3} u_i^{(m)}$$

$$u_i^c = \frac{2}{3}\sum_{m=1}^{3} u_i^{(m)} \cos(\psi_m) \tag{1}$$

$$u_i^s = \frac{2}{3}\sum_{m=1}^{3} u_i^{(m)} \sin(\psi_m)$$

And the degree of freedom $u_i^{(m)}$ it is written as a function of the new coordinates:

$$\begin{gathered} u_i^{(m)} = u_i^0 + u_i^c \cos(\psi_m) + u_i^s \sin(\psi_m) \\ m = 1,2,3\,, \quad i = 1, N_3 \end{gathered} \tag{2}$$

With N_3 the number of degrees of freedom for each rotor blade and $\psi_m = \psi + (m-1)\frac{2\pi}{3}$ the azimuth angle of m blade and $\psi = \Omega t$.

The transformation applies to the lines (equations) and the columns (DOFs) of the equations set. First the DOFs are transformed in the rotating context,

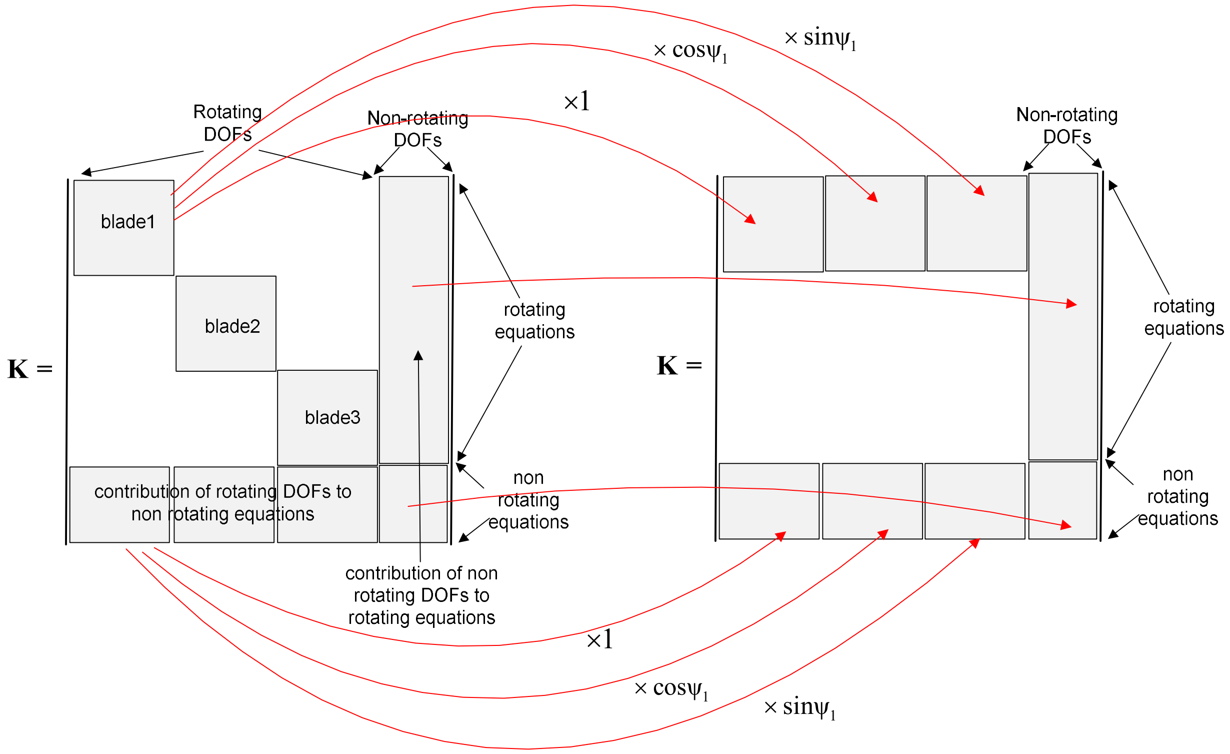

The above schematic shows the operations that concern the 1st blade

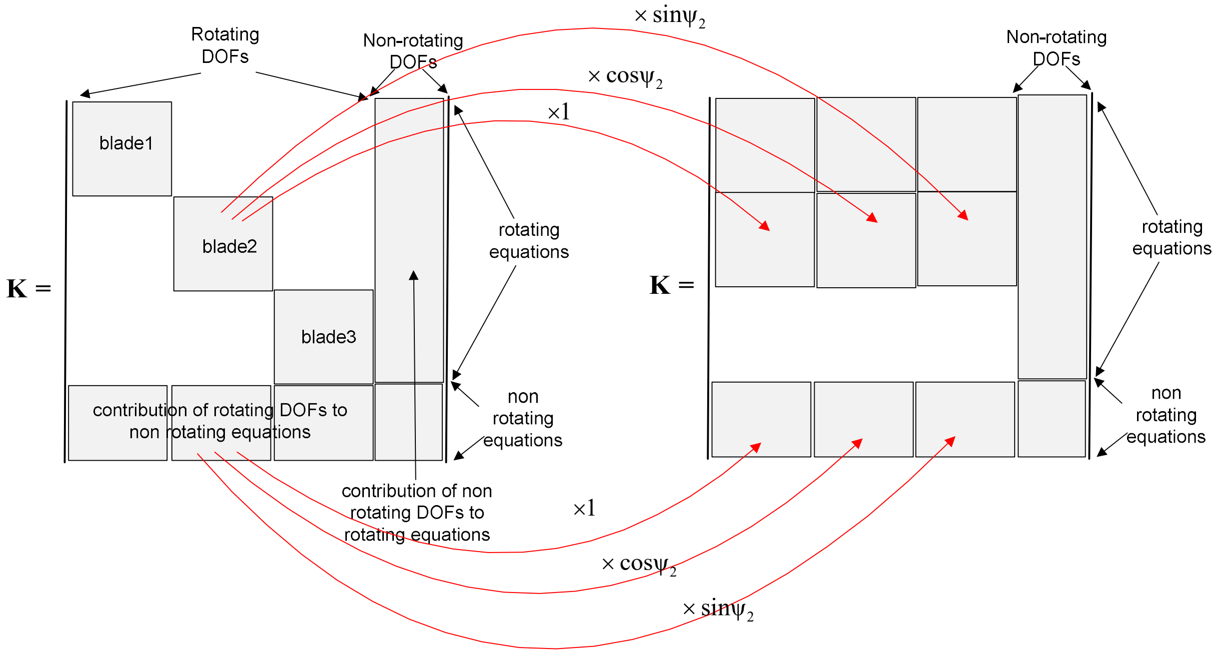

The above schematic shows the operations that concern the 2nd blade

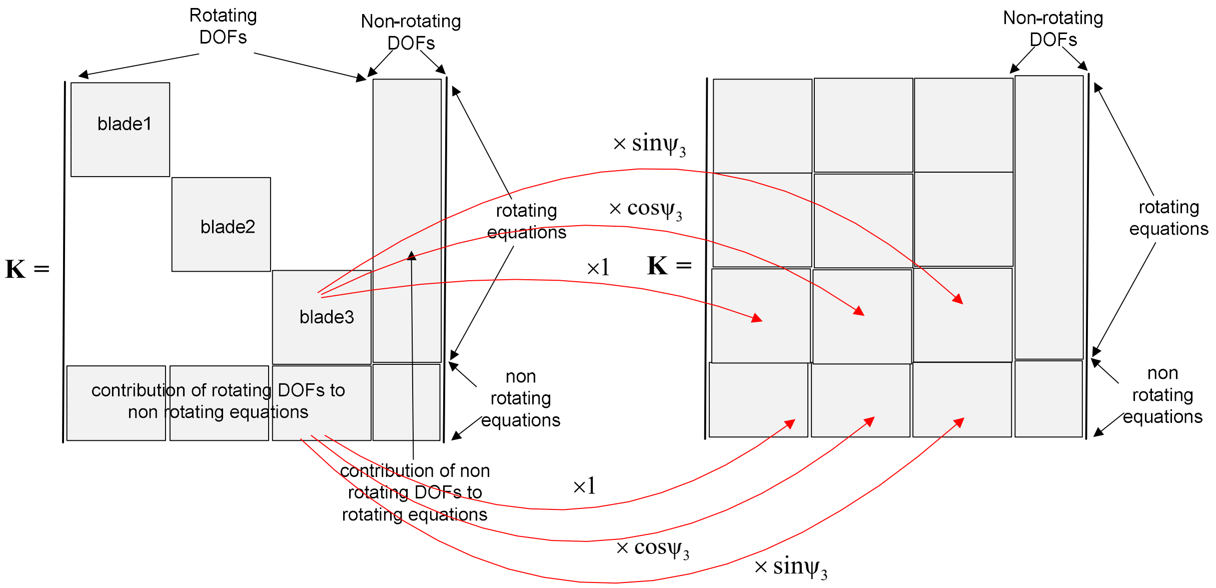

The above schematic shows the operations that concern the 3rd blade

The new coordinates (degrees of freedom) of the problem are time depended as well as the relevant initial degree of freedom of the blades to the rotational system and they are equal in number with them. Johnson [53] proves that these degrees of freedom are able to express the rotor behaviour with an equivalent way like the relevant degrees of freedom to the rotating system. The difference compared to the initial degrees of freedom to the rotating system is that they express the kinematic characteristics of the rotor as a whole. If for example $u^{(m)}$ is the displacement due to flapwise motion of the blade tip for the 3 blades to the rotational system, then the degree of freedom u^0 represent the cone angle of the rotor as a whole while the degrees of freedom u^c and u^s present the two angles that form the level of the deformed rotor (tip path plane angles) compared to the undeformed level. The first called total **collective** and the other two **cyclic**. The **collective** and the two **cyclic** are the most important degrees of freedom as far as it concerns the coupling of the rotating rotor with the non rotating elastic support structure and the relevant degrees of freedom that describe the system. For the axial flow these degrees are the only that interacts with the degrees of freedom of the non rotational elastic support structure.

The substitution to the second order differential equation system, of the degrees of freedom for the rotating blades, from those refered to the non rotating system, demands the calculation of the first and second order derivatives of $u_i^{(m)}$. These derivatives are given by the following relations:

$$\dot{u}_i^{(m)} = \dot{u}_i^0 + \left(\left[\dot{u}_i^c + \Omega\, u_i^s\right]\cos\left(\psi_m\right)\left[\dot{u}_i^s - \Omega\, u_i^c\right]\sin\left(\psi_m\right)\right)$$

$$\ddot{u}_i^{(m)} = \ddot{u}_i^0 + \left(\left[\ddot{u}_i^c + 2\Omega\, \dot{u}_i^s - \Omega^2 u_i^c\right]\cos\left(\psi_m\right)\left[\ddot{u}_i^s - 2\Omega\, \dot{u}_i^c - \Omega^2 u_i^s\right]\sin\left(\psi_m\right)\right) \tag{3}$$

And it is assumed that $\dot{\Omega} = 0$.

Finally, the implementation of the transformation, completed with the equation transformation of the rotating system to the relevant to the non rotating system. This is accomplished with the implementation of the following operators to all equations that presented to the local rotating system of the rotor blades:

$$\begin{aligned}
\left(\text{equation non rotating system}\right)_0 &= \frac{1}{3}\sum_{m=1}^{3}\left(\text{equation rotating system}\right)_m \\
\left(\text{equation non rotating system}\right)_c &= \frac{2}{3}\sum_{m=1}^{3}\left(\text{equation rotating system}\right)_m \cos(\psi_m) \\
\left(\text{equation non rotating system}\right)_s &= \frac{2}{3}\sum_{m=1}^{3}\left(\text{equation rotating system}\right)_m \sin(\psi_m)
\end{aligned} \tag{4}$$

After the implementation of the above mentioned transformations for the coordinates and the equations, for the general case, the periodic coefficients of the system matrices transformed to standard coefficients. So the eigenvalue analysis proceeds with the standard way.

Next to the figures, the equations are transformed into the rotating frame, leading to the collective and cyclic equations:

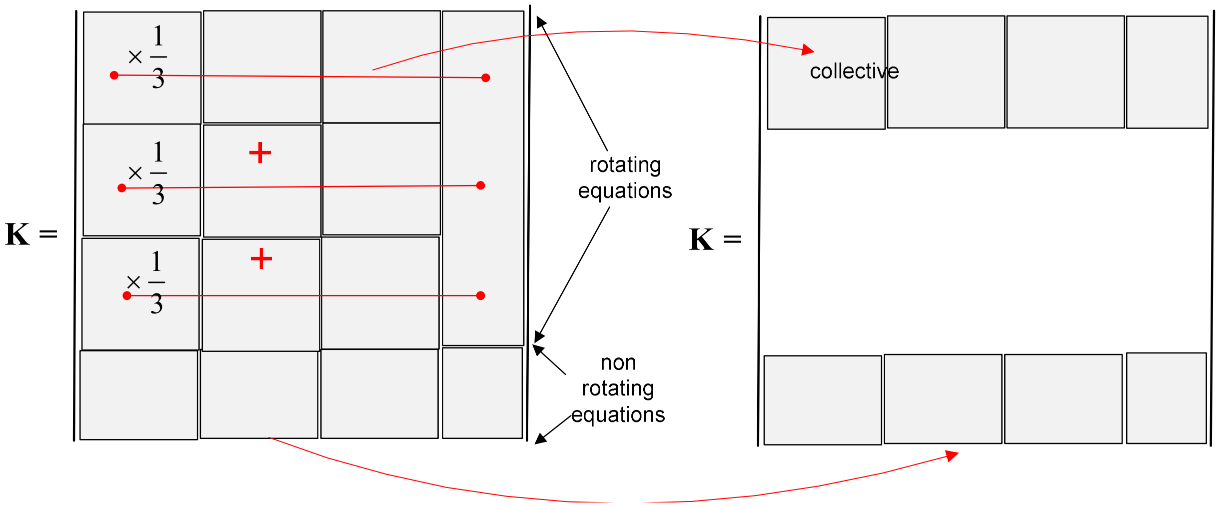

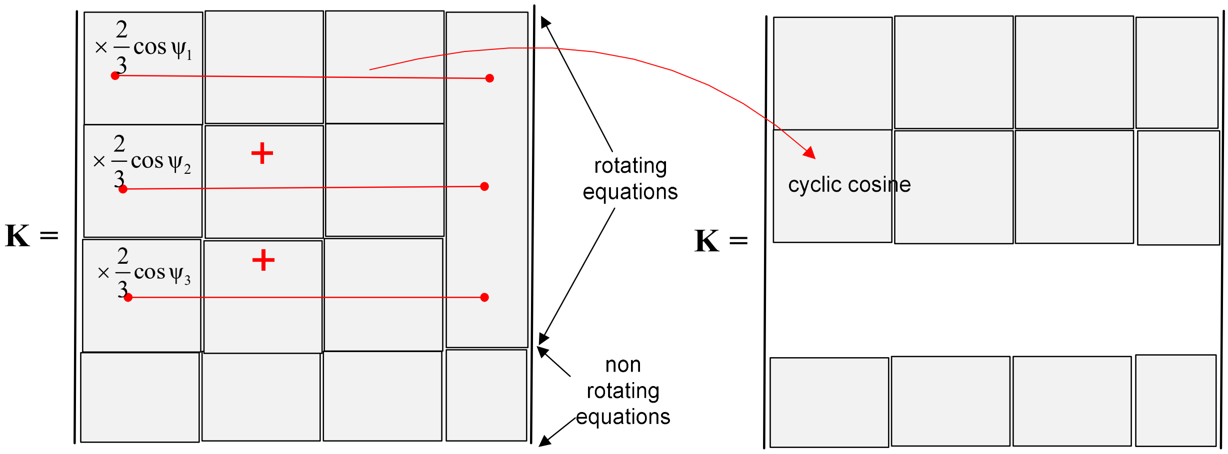

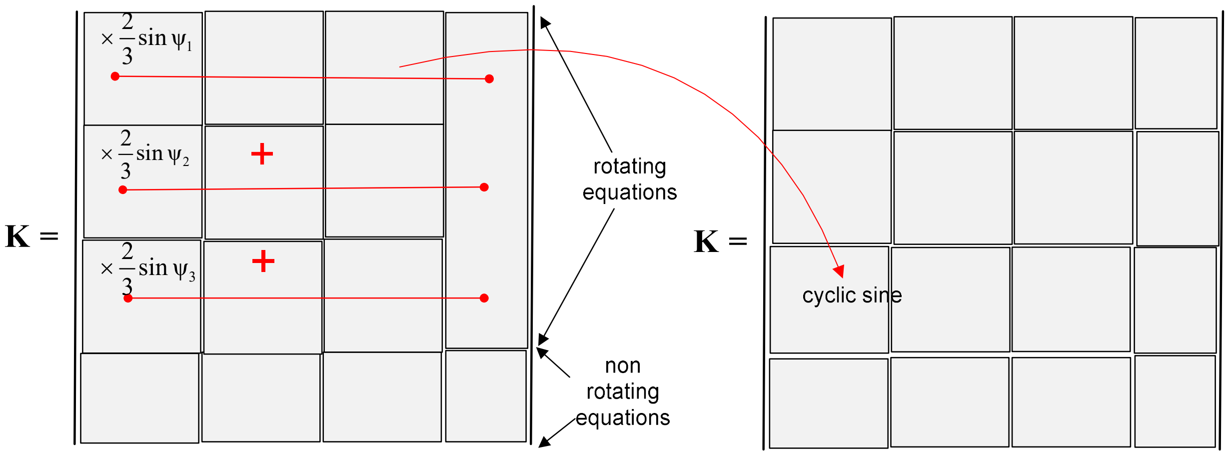

All the above coordinates' transformations may be expressed in a matrix form that enables the algorithmic problem solution of the eigenvalue analysis. For the system with periodic cooeficients (6-6), it is assumed that the state variables arranged for every blade (to the rotating system) and at the end those variables that refered to the standard non rotating system:

$$y=\left(\underbrace{u_1^{(1)},\ldots,u_{N_3}^{(1)}}_{u^{(1)}},\underbrace{u_1^{(2)},\ldots,u_{N_3}^{(2)}}_{u^{(2)}},\ldots,\underbrace{u_1^{(3)},\ldots,u_{N_3}^{(3)}}_{u^{(3)}},\underbrace{y_1^{(S)},\ldots,y_{N_S}^{(S)}}_{y^{(S)}}\right)^T \tag{5}$$

With $\mathbf{u}^{(m)}$, the vector of the degrees of freedom for every blade m (with $m=1,3$) to the rotating coordinates system, with number N_3 and $\mathbf{y}^{(S)}$ the vector of the degrees of freedom for the system refered to the non rotating coordinates system (which refered usually to the degrees of freedom of the elastic support structure), N_S in number. The total number of the state variables is the $N_{SS}=3N_3+N_S$. The corresponding way of thinking with the arrangement of the state variables, followed for the equations of the system. Firstly stated the equations that refered to the rotating system groupped together for each blade and at the end mentioned the equations refered to the non rotating system.

The Coleman transformation for the 3 blade rotor applied with the transformation matrix $\mathbf{T}(t)$:

$$\mathbf{T}(t)=\begin{bmatrix}\mathbf{I}_{N_3} & \mathbf{I}_{N_3}\cos\psi_1 & \mathbf{I}_{N_3}\sin\psi_1 & \cdots & \mathbf{I}_{N_3}\cos\left(\frac{1}{2}\psi_1\right) & \mathbf{I}_{N_3}\sin\left(\frac{1}{2}\psi_1\right) & \mathbf{0}\\ \mathbf{I}_{N_3} & \mathbf{I}_{N_3}\cos\psi_2 & \mathbf{I}_{N_3}\sin\psi_2 & \cdots & \mathbf{I}_{N_3}\cos\left(\frac{1}{2}\psi_2\right) & \mathbf{I}_{N_3}\sin\left(\frac{1}{2}\psi_2\right) & \mathbf{0}\\ \mathbf{I}_{N_3} & \mathbf{I}_{N_3}\cos\psi_3 & \mathbf{I}_{N_3}\sin\psi_3 & \cdots & \mathbf{I}_{N_3}\cos\left(\frac{1}{2}\psi_3\right) & \mathbf{I}_{N_3}\sin\left(\frac{1}{2}\psi_3\right) & \mathbf{0}\\ \\ \mathbf{0} & \mathbf{0} & \mathbf{0} & \mathbf{0} & \mathbf{0} & \mathbf{0} & \mathbf{I}_{N_S}\end{bmatrix} \tag{6}$$

And the transformation equation:

$$\mathbf{y} = \mathbf{T}(t)\cdot\mathbf{z} \tag{7}$$

With the unit matrix $\mathbf{I}_N$ with dimension $N \times N$. Additionally:

$$z = \Bigg(\underbrace{u_1^0,\ldots,u_{N_3}^0}_{u^0},\ \underbrace{u_1^c,\ldots,u_{N_3}^c}_{u^c},\ \underbrace{u_1^s,\ldots,u_{N_3}^s}_{u^s},\ \ldots,$$

$$\underbrace{u_1^{c-\frac{1}{2}},\ldots,u_{N_3}^{c-\frac{1}{2}}}_{u^{c-\frac{1}{2}}},\ \underbrace{u_1^{s-\frac{1}{2}},\ldots,u_{N_3}^{s-\frac{1}{2}}}_{u^{s-\frac{1}{2}}},\ \underbrace{u_1^{3/2},\ldots,u_{N_B}^{3/2}}_{u^{3/2}},\ \underbrace{y_1^{(S)},\ldots,y_{N_S}^{(S)}}_{y^{(S)}} \Bigg) \tag{8}$$

With $\mathbf{u}^0$ the vector of the total degrees of freedom, $\mathbf{u}^c$ and $\mathbf{u}^s$ the vectors of the cyclic degrees of freedom (cosine and sine) and $\mathbf{u}^{c-\frac{1}{2}}$, $u^{s-\frac{1}{2}}$, $\mathbf{u}^{3/2}$ the vectors of the **reactionless** degrees of freedom.

With substitution of (8) to the (6-6) and resulted to the homogenious system for the eigenvalue analysis to free vibration, we have the following relations:

$$\overset{\bullet}{\left(T(t)\cdot z\right)} = \dot{T}(t)\cdot z + T(t)\cdot\dot{z} = A\cdot T(t)\cdot z$$

or

$$\overset{\bullet}{\left(T(t)\cdot z\right)} = \dot{T}(t)\cdot z + T(t)\cdot\dot{z} = A\cdot T(t)\cdot z$$

or

$$\dot{z} = T^{-1}(t)\left(A\cdot T(t) - \dot{T}(t)\right)\cdot z = A_T\cdot z \tag{9}$$

with,

$$A_T = T^{-1}(t)\left(A\cdot T(t) - \dot{T}(t)\right) \tag{10}$$

The system (9) presents the transformed to the standard system coordinates equations, for the respective degrees of freedom $\mathbf{z}$ of the rotor. According to what mentioned above, the matrix $\mathbf{A}_T$ is a matrix of standard coefficients and concequently the eigenvalue analysis of equation (9) follows the standard procedure of the eigenvalue analysis.

Appendix 8: Stab – code tool with 22 DOFs, Flow chart diagram and subroutines

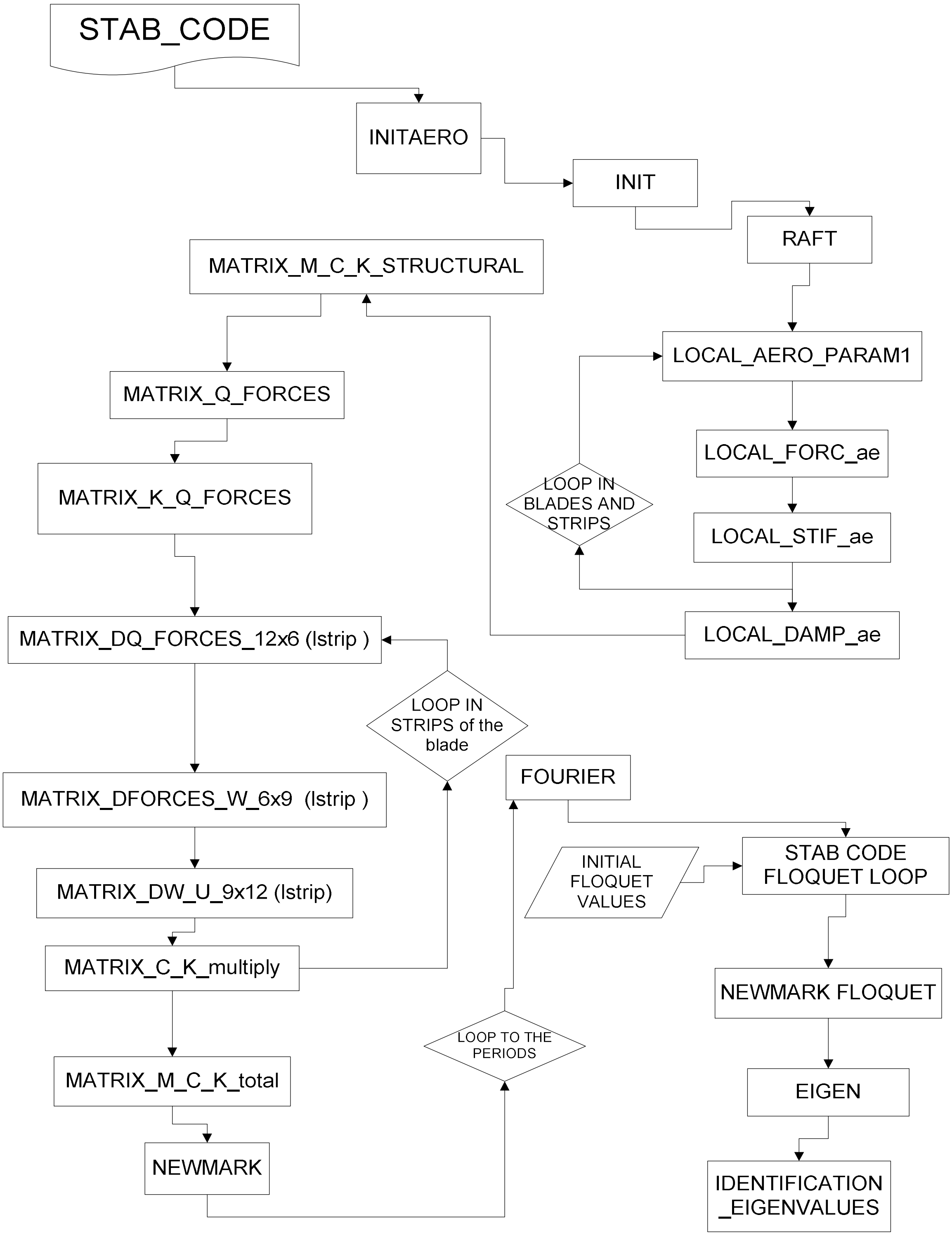

Input to 'initaero' (Table 29**) contains all the aerodynamic variables**

Input	Description
VELHUB	Wind speed
OMEGAG	Rotational speed
RTIP	Tip radial
AINI	Initial conditions for “a”
RHUB	Radial that aerodynamic part begins
AIRDEN	Air density
PITCH_COLL	Pitch angle
NSTRIP	Number of spanwise strips
APINI	Initial conditions for “a' “
IHUBLOS	Hub losses index
SSPEED	Speed of sound
RROOT	Blade root radial
ITIPLOS	Tip losses index
NBLADE	Number of blades

(a)

Input	Description
RCB1	Radial distance
TWTB	Twist
ZAERTB	Y aerodynamic coordinate
CHORDTB	Chord
XAERTB	X aerodynamic coordinate

(b)

Input	Description
NSPANB2	Aerodynamic parts of the blade
CLCDCMB	Aerodynamic characteristics CL , CD, CM
RCB2	Radial position
AATB	Angle of attack

(c)

Table 29: Stab code input, (a) subroutine ‘Initaero’, (b) geomp.inp, (c) Profilb.inp

Subroutine ‘Init’ is the preprocessor for the structural input data (Table 30).

INPUT	DESCRIPTION
NREV	Number of revolutions, for W/T engine to calculate.
NTIMEP	Time steps in one period
NTIMEPF	Floquet time steps in one period
Mbl1 , 2, 3	Blade masses 1,2,3
Sb1 , 2, 3	First (1st) moment of inertia of blade mass
Kf	Stiffness of the tower to forward - backward motion
Kl	Stiffness of the tower to lateral motion
GAMMA_el	γ coefficient
I_{blade}1, 2, 3	Second (2st) moment of inertia of blade mass
Kb1,2,3	Stiffness to the flapwise motion of the blade
Kxi1,2,3	Stiffness to the edgewise motion of the blade
Ishaft	First moment of inertia for the shaft
Ksh	Stiffness of the shaft to the torsion motion
Kt	Stiffness of the nacelle joint to the tilt motion
Kyaw	Stiffness of the nacelle joint to the yaw motion

Hoffset	Distance of nacelle mass center from hub mass center
Mn	Nacelle mass
Ini	Inertia of the nacelle mass in the tilt motion
Iyaw	Inertia of the nacelle mass in the yaw motion
Inl	Inertia of the nacelle mass in the lateral tilt motion
Ktl	Stiffness of the nacelle joint to the lateral tilt motion
BITA_el	β coefficient

Table 30: Input to subroutine 'init'

Subroutines 'Raft' and 'Blade' perform blade element aerodynamic calculations for each blade. Also subroutine 'Writeout' writes the results of the code. All variables are presented in Table 31 (a) as well as all necessary outputs from Stab-tool.

Subroutine 'Local_aero_param1' is used in Stab-code to set all local dependent parameters of every blade strip and these parameters are listed in Table 31(b).

Output	Description
VELHUB	Wind velocity to hub
TTHRUST	Thrust
RSTRIPEL	Radial position of the blade strip
WEFFZTB	Ueffz – local velocity in Z direction
FCP	Fnorm – flapwise force, Ftang – edgewise force
TSR	Lamda tip speed ratio
PITCH_COLL	Pitch
ALPHATB	Angle of attack
AINDTB	a- wake induction factor
POWER	Power
OMEGAG	Rotational velocity
WEFFXTB	Ueffx – local velocity in X direction
AINDPTB	a' - circumferential induction factor

(a)

Output	Description
Iblad	Number of blades
Lstrip	Number of strips
rloc	Radial position of the blade strip
UWINDX_ae	Ueffx – local velocity in X direction
UWINDZ_ae	Ueffz – local velocity in Z direction
AIND_ae	a - axial induction factor
AINDP_ae	a' - circumferential induction factor
TW_ae	Twist
CH_ae	Chord

(b)

Table 31: Stab code, variables for (a) subroutines 'Raft', 'Blade', 'Writeout', (b) subroutine Local_aero_param1

Subroutine 'Local_forc_ae' is used for the local forces calculations on the blade and Table 32 lists the output variables.

Input	Description
Iblad	Blade identification number
Lstrip	Strip identification number
rloc	Location – radial of the blade strip
UB	Local blade velocity in the edge direction
THY	Local blade pitch angle
UWINDX_ae	Ueffx – local wind velocity in the X direction
UWINDZ_ae	Ueffz – local wind velocity in the Z direction
AIND_ae	a axial induction factor
WB	Local blade velocity in the flap direction
TW_ae	Twist
CH_ae	Chord
AINDP_ae	a' - circumferential induction factor
output	**Description**
FTANG	Edgewise force
FNORM	Flapwise force

Table 32: Stab code, variables for subroutine 'Local_forc_ae'

Subroutine 'Local_stif_ae' provides the first derivative of the forces with respect to local blade pitch angle THY. The stiffness part results from with the same input values as above for 'Local_forc_ae' in Table 32. The main output variables are presented in Table 33.

Output	Description
FTANG_THY	First derivative of edgewise force with respect to THY pitch
FNORM_THY	First derivative of flapwise force with respect to THY pitch

Table 33: Stab code, subroutine 'Local_stif_ae'

Subroutine 'Local_damp_ae', outputs the first derivative of forces with respect to the local velocities Ub, Wb, at the blade strip under consideration. Damping results from $\frac{\partial FN}{\partial \dot{W}B}$, $\frac{\partial FN}{\partial \dot{U}B}$, $\frac{\partial FT}{\partial \dot{W}B}$, $\frac{\partial FT}{\partial \dot{U}B}$ with same input values as 'local_forc_ae'. The main output variables are presented in Table 34.

Output	**Description**
FTANG_DU	First derivative of edgewise force with respect to edgewise velocity Ub
FNORM_DW	First derivative of flapwise force with respect to flapwise velocity Wb

Table 34: Stab code, subroutine 'local_damp_ae'

Subroutine 'Local_aero_param2' is used to set local r to the blade and find the CL, CD, CM parameters, that are used in all of the above mentioned aerodynamic subroutines.

Subroutine 'Matrix_m_c_k_structural' calculates all the 22×22 elements of the mass matrix M, of the equation

$$M \times \ddot{q} + C \times \dot{q} + K = Q\,.$$

With $Q = Q_0 + \left(\partial Q / \partial dofs\right) .d\left(dof\right) + \left(\partial Q / \partial FnFt\right).\, d\left(FnFt\right)$.

Subroutine 'Matrix_q_forces' calculates the first of the forcing term Q_0 (steady term)

Subroutine 'Matrix_k_q_forces' calculates the matrix, corresponding to the first derivative of forces Q, with respect to the DOFs (2nd term in the RHS term of the dynamic equations)

Subroutine 'Matrix_dq_forces_22x6' calculates the matrix of the first derivatives of Q, with respect to the flapwise and edgewise forces: DQ/DFn,t.

Subroutine 'Matrix_dforces_w_6x9 (lstrip)' calculates the derivatives of forces $DQ_{fnf\,t}\_K\_el$ and $DQ_{fnft}\_C\_el$ with respect to the local blade velocities and pitch angle that are contained in the following expression equation

$$FN = FN_0 + DQ_{fnft}\_K\_el\,.\left[WB, UB, THY, ...\right] + DQ_{fnft}\_C\_el\,.\left[W\dot{B}, U\dot{B}, TH\dot{Y}, ...\right]$$

These are all the (6*9) elements of

$$d\left(Fn\,Ft\right) = +\partial\left(Fn\,Ft\right) / \partial\left(local\_dofs\_wu\right) .\ \partial\left(local\_dofs\_wu\right) / \partial\left(d.o.f.s.\right)$$

Subroutine 'Matrix_dw_u_9x22 (lstrip)' calculates the transformation from local to global DOFs of the matrices 'WB', 'UB' and 'THY' and their space derivatives 'WB'', 'UB'', 'DTHY'. The dimension of the matrices is 9×22 .

The subroutine 'Matrix_c_k_multiply' calculates the product of the above mentioned matrices and produces the following equation in a matrix form

$$\mathrm{Q} = \mathrm{Q}_0 + \left(\partial\mathrm{Q}/\partial\mathrm{dofs}\right).\mathrm{d}\left(\mathrm{dof}\right) + \left(\partial\mathrm{Q}/\partial\mathrm{FnFt}\right).\,\mathrm{d}\left(\mathrm{FnFt}\right)$$

Subroutine ‘Matrix_m_c_k_total’ summarize the above mentioned matrices and produce the following equation in a matrix form

$$\left(\mathrm{M}+\mathrm{M}_{\mathrm{aer}}\right)\times\ddot{\mathrm{X}}+\left(\mathrm{C}+\mathrm{C}_{\mathrm{aer}}\right)\times\dot{\mathrm{X}}+\left(\mathrm{K}+\mathrm{K}_{\mathrm{aer}}\right)\times\mathrm{X}=\mathrm{Q}$$

Subroutine ‘Newmark’ solves the final, above mentioned equation, which is transformed into:

$$\dot{X} = A.X \Rightarrow \mathbf{x}(\mathrm{t}) = \sum_i \mathrm{c}_{\mathrm{i}0}\mathrm{e}^{\lambda_{\mathrm{i}}\mathrm{t}}(\mathrm{t})\cdot\varphi_{\mathrm{i}}$$

So this equation calculates all displacements (values) and velocities (time derivatives) for all the DOFs, in every time step of the period.

Subroutine ‘Fourier’, at the end of every period and after the first 2 periods, transforms the time series of x(t) into Fourier time series that are used in the Floquet procedure.

Once the Fourier time series are obtained, the Floquet procedure starts in the ‘Nemark_floquet’ subroutine. Zero values are assumed for all displacements and velocities except one, for which a unit value is given. This is repeated for every DOF out of the 22. So the system of equations is solved with the known values from the Fourier time series, for a number of time steps (Floquet time steps) over one period. In this way, the Floquet transition matrix (F.T.M) is constructed. Subroutine ‘Eigen’ solves the eigenvalue problem of the F.T.M. and calculates eigenvalues and eigenmodes. These results are written in files 'Eigen.dat' and 'Mode_shapes.dat'.

Appendix 9: Floquet theory and resolving the indeterminacy of the modal frequencies

The theory is applied to system with periodic coefficients, of the form:

$$\dot{y} = A(t).y + B \text{ with } A(t+T) = A(t) \qquad (1)$$

Matrix A is the periodic $A(t+T) = A(t)$ with period T=2π/Ω, here connected to the nominal rotor speed Ω. In this form 2nd order dynamic systems of the usual form,

$$M.\ddot{x} + C.\dot{x} + K.x = Q \qquad (2)$$

Having mass/inertia, damping and stiffness, can be easily reformulated by doubling the dimension of the system. So if N denotes the number of DOF's of the physical system, then the dimension of y, A, B is N_{ss}= 2.N

The fundamental solution of (1), i.e. the solution of the homogenous problem,

$$\dot{\Psi}(t) = A(t).\Psi(t) \qquad (3)$$

Is written as a linear combination of the initial conditions,

$$y(t) = \Psi(t).\left(\Psi^{-1}(0).y(0)\right) \qquad (4)$$

Matrix $\Psi(t)$ is a N_{ss} x N_{ss} matrix called the fundamental state matrix, which for consistency with (4), $\Psi(0) = I$. Then for the complete solution,

$$y(t) = \Psi(t).y(0) + \int_0^t \Psi(t).B(\tau).d\tau \qquad (5)$$

$\Psi(t)$ can be formed by the N_{ss} column independent solutions over one period $t \in [0,T]$:

$$\Psi(t) = [\psi_1(t), \psi_2(t), \ldots, \psi_K(t), \ldots, \psi_{Nss}(t)] \qquad (6)$$

So for every column/solution **k**,

$$\dot{\psi}_\kappa(t) = A(t).\psi_\kappa(t) \qquad (7)$$

With N_{ss} initial independent conditions

$$\psi_k(0)=(0,0,\dots,1,0,\dots 0)^T_{k-\text{term}} \qquad (8)$$

Because

$$\dot{\Psi}(t+T)=A(t+T).\Psi(t+T)=A(t).\Psi(t+T),$$

the fundamental $\Psi(t+T)$ and $\Psi(t)$ responses are expressed as solutions of the same system matrices and so the one should be proportional to the other and therefore expressed as a product with a steady matrix **C**, which is called monodromy matrix:

$$\Psi(t+T)=\Psi(t).C \to C=\Psi^{-1}(t).\Psi(t+T) \qquad (9)$$

Floquet theory states that there exists a transformation for matrix $\Psi(t)$, consisted of a periodic matrix $L(t)$ and a constant matrix for the exponential part:

$$\Psi(t)=L(t).e^{Rt}.L^{-1}(0).\Psi(0) \qquad (10)$$

Where **R** is a constant nonsingular matrix related to C:

$$C=e^{RT} \qquad (11)$$

So stability of a system matrix with periodic coefficients depends on the exponential part and is related to the eigenvalues of the steady matrix R. The solution of the periodic system matrix is the product of the exponential term and the periodic matrix $L(t)$. This $L(t)$ is called Lyapunov – Floquet matrix and defines the transformation of the original coordinates **y** as follows:

$$y=L(t).z \qquad (12)$$

This transformation of the original coordinates **y** renders the periodic system (1) time invariant with constant coefficients:

$$\dot{z}=L^{-1}(t).\left(A.L(t)-\dot{L}(t)\right).z=A_L.z \qquad (13)$$

$$A_L=L^{-1}(0).\Psi(0)\ .\ R\ .\ (\ L^{-1}(0).\Psi(0)\ )^{-1} \qquad (14)$$

At **t=0**, equation (9) is written as

$$e^{RT}=C=\Psi^{-1}(0).\Psi(T)=\Psi(T) \qquad (15)$$

and so the monodromy matrix **C** and matrix **R,** for the initial condition $\Psi(0)=\mathrm{I}$, is calculated from the fundamental matrix $\Psi(t)$ at the end of the period: at **t=T**.

Eigenvalue decomposition of **C**,

$$C=V\;.\;\Theta\;.\;V^{-1},\quad \Theta=e^{\Lambda T} \tag{16}$$

is defined in terms of its eigenvalues contained in the diagonal matrix **Λ** and eigenmodes **V** of matrix **R,**

$$R=V\;.\;\Lambda\;.\;V^{-1} \tag{17}$$

So that

$$\Lambda=\frac{1}{T}.\ln\Theta \tag{18}$$

$$\lambda_\kappa=\sigma_\kappa+i.\omega_\kappa=\frac{1}{T}\ln(|\rho_\kappa|)+i.\frac{1}{T}(\arg(\rho_\kappa)+j_k 2\pi)\;,\;\; j_k\in Z \tag{19}$$

For every mode k, the integer $\mathbf{j_k}$ is undetermined and so the modal frequencies $\boldsymbol{\omega_\kappa}$ are not uniquely defined but may contain any multiple of the rotor speed.

The next step for the foundamental solution, is to write the fundamental response of the system as follows:

$$\begin{gathered}y(t)=\Psi(t).y(0)=L(t)\;e^{Rt}\;L^{-1}(0)\;y(0)=\\ \underbrace{L(t)\;V\quad e^{\Lambda t}}_{\Phi(t)}\;\;\underbrace{V^{-1}\;L^{-1}(0)\;y(0)}_{c_L}\end{gathered} \tag{20}$$

Equation (20) states that the fundamental response is the product of the periodic eigenmodes **Φ(t)** with exponential terms that include the eigenvalues and the corresponding dumping, multiplied by constant terms related to (and defined by) the initial conditions.

It is reminded that when equation (1) has constant coefficients, the solution of the free response vibration is of the form

$$y=\Phi\;.\;e^{\Lambda.t}.\;c \tag{21}$$

Which is exactly like the form of equation (20) with **Φ** being the eigenmodes matrix, $\mathbf{e^{\Lambda t}}$ the exponential eigenvalues diagonal matrix and **c** the vector of steady solutions calculated by the initial conditions for the DOFs and their corresponding derivatives.

So the solution for the free response of a system with periodic coefficients, like the system with constant coefficients, is written as:

$$y= \sum_{\kappa=1}^{N} (\varphi_k(t) . c_k . e^{\lambda_\kappa .t} + \varphi^c{}_k(t) . c^c{}_k . e^{\lambda^c{}_\kappa .t})=$$

$$\sum_{\kappa=1}^{N} (L(t) . V . c_k . e^{\lambda_\kappa .t} + L(t)\, V^c . c^c{}_k . e^{\lambda^c{}_\kappa .t}) \tag{22}$$

With $c_k = V^{-1} L^{-1}(0)\, y(0)$ as stated above in equation (20) and **λ_k, $\lambda^c{}_k$** the pairs of conjugate eigenvalues **k=1,N**. In the same way the eigenmodes **φ_k** and the steady terms **c_k** are introduced in conjugate numbers too.

Alternatively, equation (22) can be written in another form as:

$$y= \sum_{\kappa=1}^{N} u_k(t).e^{\lambda_\kappa .t}.q_k(0) \tag{23}$$

With $u_k(t)= L(t) . L^{-1}(0) . \varphi(0) . V_K$ is a periodic mode shape of mode **k** in the original coordinates and **$q_k(0)$** is its modal content in the initial condition.

In order to separate the undeterminacy in the Floquet eigenvalues, let,

$$\omega_\kappa=\omega_{p,\kappa}+ j_k\Omega \qquad (24]$$

and $\lambda_{p,\kappa}= \sigma_\kappa + i.\omega_{p,\kappa}$ define the principal Floquet exponents and integer **j_k** introduces the undeterminacy. The transient response to a pure excitation of mode **k** (obtainable by setting **$q_k(0)$ =1** and all other initial modal components equal to zero) can be thereby written as

$$y_k(t)= u_k(t).e^{(\lambda_{p,\kappa} + i\, j_\kappa\, \Omega)\, t} \tag{25}$$

$$u_k(t)=L(t).L^{-1}(0).\varphi(0).v_k.e^{-(\lambda_{p,\kappa}+i\,j_\kappa\,\Omega)\,t} \\ =\varphi(t).v_k.e^{-(\lambda_{p,\kappa}+i\,j_\kappa\,\Omega)\,t}=u_{p,k}(t)\;e^{-i\,j_\kappa\,\Omega\,t} \qquad (26)$$

where $u_{p,k}(t)=\varphi(t).v_k.e^{-\lambda_{p,\kappa}.t}$ is the principal periodic mode shape. Both the periodic mode shape $\mathbf{u_k(t)}$ and the exponential term in the solution (25) depend on the chosen integers $\mathbf{j_k}$. As the exponent has different signs in (25) and (26), the contributions from $\mathbf{j_k}$ cancel, and the same transient solution is obtained independent of the values of $\mathbf{j_k}$. Hence, a modal frequency of mode number $\mathbf{k}$ can be defined freely within an integer multiple of $\mathbf{\Omega}$, a choice that also determines the observer's frame of reference. The observer of the modal frequencies (19) is placed in the inertial frame of reference, which makes the modal frequencies similar to those obtained with the Coleman transformation approach, where the periodic mode shapes are constant for the non-transformed inertial state variables. The objective of the approach suggested in the sequel, is to make the inertial state variables in the periodic mode shapes constant, and if not possible diminish the variability as much as possible.

The Fourier expansion of the principal periodic mode shape $u_{p,k}(t)$ contains only harmonics of an integer multiple of $\mathbf{\Omega}$ because $u_{p,k}(t)$ is T-periodic, and it can be expressed for state variable $\mathbf{i}$ as

$$u_{p,ik}(t)=\sum_{j=-\infty}^{\infty}u_{p,j,ik}.e^{i\;2\pi j\,t/T}=\sum_{j=-\infty}^{\infty}u_{p,j,ik}.e^{i\,j\,\Omega\,t} \qquad (27)$$

where $u_{p,j,ik}$ are the Fourier coefficients. Using (26) and (27), the periodic mode shape corresponding to the modal frequency (19) can be written as

$$u_{ik}(t)=\sum_{j=-\infty}^{\infty}u_{p,j,ik}.e^{i.\,(j-j_k)\,\Omega\,t} \qquad (28)$$

By selecting the undetermined integer $\mathbf{j_k}$ for mode $\mathbf{k}$ as the index of the largest Fourier coefficient

$$j_k = \left\{ j_k \in Z \mid u_{p,j_k,ik} \geq u_{p,j\ ,ik} \forall j \in Z \right\} \qquad (29)$$

the largest harmonic component in the periodic mode shape (28) is removed. Note that index $\mathbf{i}$ must correspond to a state variable in the inertial frame. In the case of a homogeneous rotor, $u_{p,j,ik}$ is non-zero only for one $\mathbf{j_k}$,and $\mathbf{u_{ik}}$ is constant for the inertial state variables. If the rotor has any kind of anisotropy, either internal or external, then $u_{p,j,ik}$ will have several non-zero components in the expressions of the inertial state variables, but by using (29) in order to select $\mathbf{j_k}$, the periodic mode shape $u_{ik}(t)$ is made to be as constant as possible.

Johnson [49, p. 374] describes the above method in the following way: ''*One way to mechanize this choice of frequencies is to require that the mean value of the eigenvector have the largest magnitude; then the harmonic of largest magnitude in the eigenvector corresponding to the principal value of the eigenvalue gives the frequency* ***n2π/T*** '', where ''eigenvector'' refers to the periodic mode shape and $\mathbf{n}$ is $\mathbf{j_k}$. The periodic mode shape has the largest mean value in time, when it is not oscillating. Johnson's statement is, however, in this context only valid when considering the inertial state variables, because the rotor state variable harmonics can be non-zero at other frequencies than the harmonics of the inertial state variables.

Finally, with respect to Stab-code, the equations that have been implemented for the real and imaginary part of the Fourier terms are given below,

$$u_{p,real}(t) = \sum_{j=-\infty}^{\infty} A_{Real,p,k,j} \cdot \left(\cos\left(j\Omega t \right) + i.\sin\left(j\Omega t \right) \right) \qquad (30)$$

$$\text{With } J = \left[-10, 10 \right]$$

$$u_{p,imaginary}(t) = \sum_{j=-\infty}^{\infty} A_{imaginary,p,k,j} \cdot \left(\cos\left(j\Omega t \right) + i.\sin\left(j\Omega t \right) \right) \qquad (31)$$

So $\mathbf{u_{p,k}(t)}$ is calculated as,

$$\begin{aligned} u_{p,k}(t) &= \sum_{j=-10}^{+10} \left(A_{\mathrm{Real},p,k,j} + i.A_{\mathrm{imaginary},p,k,j} \right)\left(\cos\left(j\Omega t\right) + i.\sin\left(j\Omega t\right) \right) \\ &= \sum_{j=-10}^{+10} \left(A_{\mathrm{Real},p,k,j} + i.A_{\mathrm{imaginary},p,k,j} \right) e^{ij\Omega t} \end{aligned} \tag{32}$$

With

$$A_{\mathrm{Real},p,k,j} = \frac{1}{2}\left(A_{\mathrm{Real},p} \cos\left(kj\right) - i.A_{\mathrm{Real},p} \sin\left(kj\right) \right), \tag{33}$$

$$j = 1,\ldots,10$$

$$A_{\mathrm{Real},p,k,j} = \frac{1}{2}\left(A_{\mathrm{Real},p} \cos\left(kj\right) + i.A_{\mathrm{Real},p} \sin\left(kj\right) \right), \tag{34}$$

and $j = -10,\ldots,-1$

$$A_{\mathrm{Real},p} \cos\left(kj\right) = \frac{1}{\pi}\int_{0}^{2\pi} u_{\mathrm{Real},p,k}\left(t\right)\cos\left(j\psi\right)d\psi \tag{35}$$

$$A_{\mathrm{Real},p} \sin\left(kj\right) = \frac{1}{\pi}\int_{0}^{2\pi} u_{\mathrm{Real},p,k}\left(t\right)\sin\left(j\psi\right)d\psi \tag{36}$$